UNIVERSITAT POLITÈCNICA
DE CATALUNYA
BARCELONATECH

Spatial Modulation Schemes and Modem Architectures For Millimeter Wave Radio Systems

Ph.D. Dissertation

Author

Ahmed Raafat

Advisors

Josep Vidal

Adrian Agustin

Signal Processing and Communications Group
Department of Signal Theory and Communications
Universitat Politecnica de Catalunya (UPC)

Barcelona, June 2020

The research leading to the results presented in this PhD dissertation has been funded by the European Union's Horizon 2020 research and innovation training network under the Marie Sklodowzka-Curie grant agreement No. 641985, the project 5G&B RUNNER-UPC (TEC2016-77148-C2-1-R (AEI/FEDER, UE)) and the Catalan Government (2017 SGR 578 - AGAUR).

Abstract

The rapid growth of wireless industry opens the door to several use cases such as internet of things and device to device communications which require boosting the reliability and the spectral efficiency (SE) of the wireless access network, while reducing the energy consumption at the terminals. The vast spectrum available in millimeter-wave (mmWave) frequency band is one of the most promising candidates to achieve high speed communications. However, the propagation of the radio signals at high carrier frequencies suffers from severe path-loss which reduces the coverage area. Fortunately, the small wavelengths of the mmWave signals allow packing a large number of antennas not only at the base station (BS) but also at the user terminal (UT). These massive antenna arrays can be exploited to attain high beamforming and combining gains and overcome the path-loss associated with the mmWave propagation. Conventional (fully digital) multiple-input-multiple-output (MIMO) transceivers, each antenna is connected to a specific radio-frequency (RF) chain and high resolution analog-to-digital-converter (ADC). Unfortunately, these devices are expensive and power hungry especially at mmWave frequency band and when operating in large bandwidths. Having this in mind, several novel modulation schemes and massive MIMO transceiver designs for mmWave systems are proposed in the PhD thesis with the purpose of reducing the hardware cost and the energy consumption with the challenge of maintaining a high SE as follows:

- We present a low cost and low power consumption receive spatial modulation (RSM) scheme based on a simple transceiver architecture. We propose a time-division-duplex (TDD) transmission protocol aimed to reduce the training overhead where the channel knowledge is required only at the BS. Simulation results presented show that the power consumption and the energy efficiency (EE) of the proposed RSM architecture outperform the hybrid and conventional MIMO systems.

- We consider the downlink (DL) of a massive MIMO single user transmission system operating in the mmWave outdoor narrowband channel environment. We propose

a novel RSM scheme aimed to reduce the power consumption at the user terminal, while attaining a significant throughput. The energy consumption saving is obtained through the use of analog devices (amplitude detector), and the reduction of number of RF chains and ADCs. The BS transmits spatial and modulation symbols per channel use. We show that the optimal spatial symbol detector is a threshold detector that can be implemented by using one bit ADC. We derive expressions for the average bit error probability in the presence and absence of the threshold estimation error showing that a small number of pilot symbols is needed. A performance comparison is done between the proposed system and fully digital (FD) MIMO showing that a suitable constellation selection can reduce the performance gap.

- In order to combat the poor scattering environment of mmWave propagation, RSM schemes demand a challenging receive antenna selection (RAS) procedure. Moreover, the power consumption at the transmitter side is high when a full digital precoder is envisioned. Thus, we consider the joint problem of RAS and precoder designs based low complexity hybrid architecture. For the sake of simplicity, we divide this problem into two subproblems. First, we design the RAS assuming FD precoder, and then, we design the hybrid precoder. We propose RAS methods based on convex optimization problems and RAS schemes based on fast sequential algorithms.

- We propose novel zero forcing (ZF) hybrid precoder based convex optimization that maximizes the received power. We prove that the proposed precoder is optimal when the channel is highly spatially sparse. The proposed designs have been compared with the best known methods in terms of average mutual information and EE showing significant improvements.

- Since SM schemes are designed to include ZF precoders, performance can be impaired in the presence of highly spatially correlated channels. Minimum mean square error (MMSE) precoding outperforms the ZF precoding in the spatially correlated MIMO channels [1]. However, extending the SM schemes for MMSE precoding is not trivial due to the hardware constraints of the energy efficient UT architecture. Specifically, we adapt the MMSE precoder to the low complexity RSM architecture and develop detection methods for the spatial and modulation symbols. The proposed MMSE RSM scheme with total and per-antenna power constraints have been compared with ZF RSM in terms of average and outage mutual information by simulations showing superior gain for mmWave channels.

- Wideband propagation of mmWave signals is a major player in attaining high data rates. Thus, we adapt the energy efficient RSM schemes for outdoor wideband mmWave massive MIMO systems. We consider the DL of a single user system

operating with single carrier RSM and design a low complexity time-domain finite impulse response pre-equalizer to combat the intersymbol interference caused by the wideband transmission. We show that RAS is necessary for attaining high SE and we suggest fast and efficient RAS algorithm. Simulation results show that the proposed RSM scheme achieves comparable SE to the FD orthogonal frequency division multiplexing MIMO system with superior EE.

- We propose novel transmit SM (TSM) and RSM schemes for UL and DL data transmission phases based on a novel energy efficient hybrid UT architecture. The analog circuitry of the proposed hybrid architecture is divided into two stages: phase shifters and analog switches. The phase shifting stage assures high gain and overcomes the severe path-loss caused by outdoor mmWave propagation. The analog switching stage smartly allocates the antennas to be used at the phase shifting stage and combats the spatial correlation. We provide the analysis of the SE of the UL and DL systems. Next, we propose a reduced complexity algorithm that jointly optimizes the analog beamformer and combiner design of the UL and DL circuitry to maximize the EE. Finally, we compare and evaluate the performance of the proposed algorithm in terms of the SE and EE assuming both stochastic and realistic channel models.

- For the sake of improving the SE, we propose a novel RSM scheme assuming multiple RF chains at the UT. First, we consider analog switches at the UT that control which antennas are active to ensure full rank channel. With the goal of minimizing the power consumption at the BS, we consider analog switches at the BS that control the ON/OFF status of RF chains. These switches are designed in such a way the EE (SE/power consumption at the BS) is maximized.

- We extend the SM concept to multiple users transmission. Specifically, we propose an algorithm for RSM broadcast channel and an algorithm for TSM multiple access channel. In the two algorithms, we optimize the number of users, set of antennas and the transmit power allocated to each user to maximize the sum SE. Simulation results show that SM outperforms conventional modulation in terms of spectral and energy efficiency. Moreover, the proposed algorithms tightly approach the exhaustive search and outperform the prior art in terms of SE performance and convergence.

Resum

El ràpid creixement de la indústria de les comunicacions sense fils obre les portes a diversos casos d'ús com ara l'Internet de coses i les comunicacions de dispositiu a dispositiu que requereixen augmentar la fiabilitat i l'eficiència espectral (SE) de la xarxa d'accés sense fils, alhora que reduir el consum d'energia als terminals. L'ampli espectre disponible en la banda de les ones mil.limètriques (mmWave) és un dels candidats més prometedors per aconseguir comunicacions d'alta velocitat. Tot i això, els senyals de ràdio a freqüències portadores elevades pateixen intenses pèrdues per atenuació que redueixen la superfície de cobertura. Per sort, les longituds d'ona petites dels senyals mmWave permeten empaquetar no només un gran nombre d'antenes a l'estació base (BS) sinó també als terminals d'usuari (UT). Aquestes agrupacions massives d'antenes es poden explotar per obtenir grans guanys i compensar les pèrdues associades a la propagació mmWave. En els transceptors totalment digitals MIMO (multi-input-multiple-output-output), cada antena està connectada a un cadena específica de radiofreqüència (RF) i a un convertidor analògic-digital (ADC) d'alta resolució. Malauradament, aquests dispositius són costosos i tenen un consum elevat de potència, especialment a la banda mmWave per operar amb grans amplades de banda. Tenint això en compte, a la tesi es proposen diversos nous esquemes de modulació i de transceptors MIMO massius per la banda mmWave amb el propósit de reduir costos d'implementació i el consum d'energia, amb el repte de mantenir un SE elevat:

- Es presenta una modulació espacial de baix consum (RSM) basada en una arquitectura de transceptor simple. Proposem un protocol de transmissió duplex (TDD) destinat a reduir l'entrenament general on el coneixement del canal només es requereix a la BS. Els resultats de simulació presentats mostren que el consum d'energia i l'eficiència energètica (EE) de la l'arquitectura RSM proposada supera els sistemes MIMO híbrids i convencionals.

- Considerem l'enllaç de baixada (DL) d'un sistema massiu de transmissió d'un sol usuari MIMO que funciona a l'entorn de canal de banda estreta mmWave a l'aire

lliure. Proposem un nou esquema de RSM per reduir el consum d'energia als terminals d'usuari, tot aconseguint un rendiment important. S'obté un estalvi en el consum d'energia mitjançant l'ús de dispositius analògics (detector d'amplitud) i la reducció del nombre de cadenes de radiofreqüència i ADC. Mostrem que el detector de símbols espacials òptim és un detector de llindar que es pot implementar mitjançant un ADC de 1 bit. En derivem expressions per a la probabilitat d'error de bit mitjana en preséncia i absència de l'error d'estimació del llindar que demostra que calen només un nombre reduït de símbols pilot. Es fa una comparació de rendiment entre el sistema proposat i un completament MIMO digital (FD) que mostra que una selecció de constel.lació adequada pot reduir la bretxa de rendiment.

- Per combatre el mal entorn de dispersió de la propagació de mmWave, els sistemes RSM requereixen un procediment de selecció de l'antena de recepciò (RAS). A més, el consum d'energia al costat del transmissor és elevat quan el precodificador es digital. Així, considerem el problema conjunt de RAS i precodificador basats en arquitectura híbrida de baixa complexitat. Per senzillesa, dividim aquest problema en dos subproblemes. Primer, dissenyem el RAS assumint la FD precodificador, i després, dissenyem el precodificador híbrid. Proposem mètodes RAS basat en problemes d'optimització convexe i esquemes RAS basats en algoritmes seqüencials ràpids.

- Proposem una optimització convexa basada en un precodificador híbrid de forçament zero (ZF) que maximitza el la potència rebuda. Demostrem que el precodificador proposat és óptim quan el canal és molt dispersiu espacialment. Els dissenys proposats s'han comparat amb els mètodes més coneguts en termes d'informació mútua mitjana i EE, mostrant millores importants.

- Com que els esquemes SM estan dissenyats per incloure precodificadors ZF, el rendiment es pot veure deteriorat en presència de canals espacialment correlats. La precodificació d'error quadrat mitjá mínim (MMSE) supera la precodificació ZF en aquests casos [1]. Tanmateix, ampliant els esquemes de SM per a MMSE, la precodificació no és trivial a causa de les restriccions del hardware de l'UT. Concretament, adaptem el precodificador MMSE per a tenir una arquitectura de poca complexitat RSM i desenvolupem mètodes de detecció de la modulació espacial de símbols. L'esquema MMSE RSM proposat es dissenya amb restriccions de potència total i per antena. S'han comparat amb ZF RSM en termes de mitjana i d'informació mútua mitjançant simulacions que mostren un guany superior per als canals de mmWave.

- Hem adaptat els esquemes de RSM energètics i eficients per als sistemes massius MIMO de banda ampla exteriors. Considerem l'enllaç DL d'un sistema d'un sol usuari operant amb RSM i dissenyem un preequaitzador en el domini temporal

de baixa complexitat per combatre la interferència causada per la transmissió de banda ampla. Mostrem que el RAS és necessari per assolir un SE elevat i us proposem un algorisme RAS ràpid i eficient. Els resultats de la simulació mostren que el l'esquema de RSM proposat aconsegueix una SE comparable a un esquema OFDM MIMO amb millor EE.

- Proposem nous esquemes de transmissió SM (TSM) i RSM per a dades UL i DL fases de transmissió basades en una nova arquitectura UT híbrida eficient i energètica. El circuit analògic de l'arquitectura híbrida proposada es divideix en dues etapes: commutadors de fase i commutadors analògics. La fase de canvi de fase garanteix un gran guany I supera la greu pérdua de ruta causada per la propagació mmWave exterior. L'analògic Etapa de commutació assigna de manera intel.ligent les antenes a utilitzar en el canvi de fase etapa i combat la correlació espacial. Proporcionem l'anàlisi del SE de els sistemes UL i DL. A continuació, proposem un algorisme de complexitat reduïda que optimitza conjuntament el disseny del formador i del combinador analógic de la UL i la DL circuits per maximitzar els EE. Finalment, comparem i avaluem el rendiment de l'algorisme proposat en termes de SE i EE, assumint tant estocàstica com models realistes de canals.

- Per millorar el SE, proposem un nou esquema de RSM múltiples cadenes de RF a la UT. Primer, considerem els commutadors analògics a l'UT que controlar quines antenes estan actives per assegurar el canal de rang complet. Amb l'objectiu de minimitzant el consum d'energia a la BS, considerem els interruptors analògics a la BS que controlen l'estat ON / OFF de les cadenes RF. Aquests interruptors estan dissenyats a d'aquesta manera es maximitza el consum d'EE (SE / energia elèctrica a la BS).

- Estenem el concepte SM a la transmissió de diversos usuaris. Concretament, proposem un algorisme per al canal de transmissió RSM i un algorisme d'accés múltiple TSM canal. En els dos algoritmes, optimitzem el nombre d'usuaris, conjunt d'antenes i la potència de transmissió assignada a cada usuari per maximitzar la suma SE. Simulació els resultats mostren que SM supera la modulació convencional en termes d'espectrals i eficiència energètica. D'altra banda, els algorismes proposats s'acosten estrictament a la cerca exhaustiva i la superació de la tècnica anterior en termes de rendiment de SE I convergència.

Acknowledgements

Special thanks to the Marie Sklodowzka-Curie H2020 European project for giving me the opportunity to improve the research and the soft skills through attending well-organized summer schools given by worldwide technology leaders.
Special thanks to my PhD supervisors Dr. Josep Vidal and Dr. Adrian Agustin, they are always helping me to convert the basic ideas into scientific papers published in tier one conferences and journals.
Special thanks to my wife, she did a lot of efforts with our kids while I was working day and night to make this work happens.
Special thanks to my mother, father and brothers for their continuous support.
Special thank to Merve, Eduard A. Jorswieck, Yoann Corre and Zahid for the successful collaboration, I learned a lot from them.
Special thanks to Alexios Aravanis who helped me to renew my residence permission in Spain, it was a very stressful period during my PhD.
Special thanks to Mostafa Hussien, thanks to his advise, I avoided a serious surgery in my back and I become more healthy.
Special thanks to my friends Mostafa Hussien, Diaa El-Wakel, Mostafa Imam, Abdul-Gawad, Mohamed Moamen and all the nice Egyptian guys in Stockholm, the good moments that we spent together are very important for me to keep progressing in the PhD dissertation.

List of Acronyms

ABEP	Average bit error probability
ADC	Analog-to-digital-converter
AD	Amplitude detector
APSK	Amplitude-phase-shift-keying
ARA	Active receive antennas
BAC	Binary asymmetric channel
BB	Baseband
BC	Broadcast channel
BS	Base station
BW	Bandwidth
CDF	Cumulative density function
CM	Conventional modulation
CSI	Channel state information
DAC	Digital-to-analog-converter
DC	Dependent combining
DFT	Discrete fourier-transform
DL	Downlink
EE	Energy efficiency
ERC	Equal ratio combiner
FDD	frequency-division-duplexing
FD	Fully digital
FIR	Finite impulse response
FP	Fractional programming
FRSM	Flexible RSM
GRSM	Generalized RSM
GSM	Generalized SM
GTSM	Generalized TSM
HRSM	Hybrid RSM
HSA	High SNR approximation

HTSM	Hybrid TSM
IC	Independent combining
LNA	Low noise amplifier
MAC	Multiple access channel
MIMO	Multiple-input-multiple-output
MISO	Multiple-input-single-output
ML	Maximum likelihood
MMSE	Minimum mean square error
MRF	Multiple RF
MSA	Moderate SNR approximation
NLoS	Non line-of-sight
OFDM	Orthogonal-frequency-division-multiplexing
PAPC	Per antenna power constraint
PA	Power amplifier
PDF	Probability density function
PSK	Phase-shift-keying
PS	Phase shifter
QAM	Quadrature-amplitude-modulation
RAS	Receive antenna selection
RF	Radio-frequency
RSM	Receive spatial modulation
SE	Spectral efficiency
SM	Spatial modulation
SNR	Signal-to-noise-ratio
SRF	Single RF
SVD	Singular value decomposition
TAG	Transmit antennas grouping
TAS	Transmit antenna selection
TDD	Time-division-duplex
TPC	Total power constraint
TSM	Transmit spatial modulation
UG	Uniform grouping
ULA	Uniform linear array
UL	Uplink
UT	User terminal
ZF	Zero forcing
i.i.d	Independent and identically distributed
mmWave	Millimeter-wave

Notation

x	Scalar
$\mathbf{x}$	Column vector
$\mathbf{X}$	Matrix
$\mathbf{I}$	Identity matrix
$\mathbf{0}$	Zero matrix
$\mathbf{X}^T$	Transpose of matrix $\mathbf{X}$
$\mathbf{X}^\star$	Conjugate of matrix $\mathbf{X}$
$\mathbf{X}^H$	Transpose the conjugate of matrix $\mathbf{X}$
$\mathbf{X}^\dagger$	Pseudo-inverse of matrix $\mathbf{X}$
$\mathrm{Tr}\{\mathbf{X}\}$	Trace of matrix $\mathbf{X}$
$\mathrm{E}[\mathbf{X}]$	Expectation of matrix $\mathbf{X}$
$\mathrm{diag}\{\mathbf{x}\}$	Diagonal matrix with elements of vector $\mathbf{x}$ on the diagonal
$\mathbf{X}^{(i)}$	The i^{th} column of matrix $\mathbf{X}$
$\mathbf{X}^{(i:j)}$	From the i^{th} to the j^{th} columns of matrix $\mathbf{X}$
$\mathbf{X}^{(i,j)}$	Entry at the i^{th} row and the j^{th} column of matrix $\mathbf{X}$
$\mathbf{X} \succeq \mathbf{0}$	Matrix $\mathbf{X}$ is positive semi-definite
$\mathrm{Rank}\ (\mathbf{X})$	Rank of Matrix $(\mathbf{X})$
$\|\mathbf{X}\|_F$	Frobenius norm of matrix $\mathbf{X}$
$\mathbf{X}\,(k,:)$	The k^{th} row of matrix $\mathbf{X}$
$\mathbf{V}_N\{\mathbf{X}\}$	Matrix contains the largest N eigenvectors of matrix $\mathbf{X}$
$\|\mathbf{x}\|_2$	The 2-norm of the vector $\mathbf{x}$
$\|x\|$	Absolute value of x
$\mathrm{Arg}(x)$	Phase of x
$\lfloor x \rfloor$	The floor of x
$\mathcal{X}$	Set
$\|\mathcal{X}\|$	Cardinality of the set

Contents

List of Figures

List of Tables

Chapter 1

Introduction

With the advances in communications technology and the new wireless-based applications and services such as internet of things and device to device communications [2], [3], it is forecasted that the number of connected devices will reach tens of billions by 2030 [2]. In addition, every device connected to the network will demand a minimum data rate which will add up to 1000x increase compared to today's networks. The shortage of bandwidth (BW) in low frequency bands has led to the consideration of migration to the higher frequencies to satisfy the vast increase in data rates [4]. Availability of spectrum in millimeter-wave (mmWave) band attracts research community as a way to deliver expected large traffic demands [5]. Thus, the vast spectrum available in the mmWave frequency band (28 to 300 GHz) compared to sub-6 GHz band(less than 6 GHz, for example, $3.4 - 3.6$ GHz) is one of the most promising candidates in achieving high data rate communications [6], [7], [8].

A shortcoming of the mmWave band is related to the radio signals propagation characteristics at these high frequencies which brings additional challenges to the network design [9]. Specifically, the propagation of the radio signals at high carrier frequencies suffers from severe path-loss which is a bottleneck in increasing the coverage area [10]. Moreover, the attenuation of the non-line-of-sight (NLOS) component in mmWave frequency band is much stronger with respect to the sub-6 GHz. One reason for that is the severe **penetration losses** of building materials. These losses lead to poorly reflective environment and thus, the short delay spread of wideband wireless channel is limited to a few taps [11]. At 28 GHz, the penetration loss due to a 3.8 cm thickness glass is 40 dB [12] while pane of glass at 2GHz leads to 13dB penetration loss [13]. A high thickness brick pillar leads to 28dB penetration loss at 28GHz [12] and 20 dB at 2.5 GHz [13]. As an illustrative example, Table 3.2 shows the path loss for LOS and NLOS scenarios at different frequencies and transmitter (TX)-receiver (RX) distances [9]-[14]. Also, mmWave propagation in urban cellular systems is very sensitive to the **blockage** caused by the human-body. At 28GHz and 50m TX-RX distance, a full blockage can occur with

Table 1.1: Path loss in dB [9]-[14]

Frequency (GHz) / Distance (m)	2.5 NLOS	28 NLOS	73 NLOS	2.5 LOS	28 LOS	73 LOS
50	90	122	128	75	95	105
100	100	130	138	80	100	110

Table 1.2: Possible number of antennas [16]

Carrier Frequency (GHz)	2.5	28	73
Base Station	8×8	16×16	40×40
Mobile Equipment	1	2×2	5×5

probability 60% [15]. The channel fluctuation is a limiting factor at high velocities. For example, at 60 Km/h and 60GHz, the channel **coherence time** is in order of hundreds of microseconds while for today's cellular systems it is in order of milliseconds [9]. Thus, the channel changes faster in mmWave communication.

Fortunately, the small wavelengths of mmWave signals permits packing large number of antennas elements in small area that enables using the massive antennas arrays at the base station (BS) and also at the user terminal (UT) to maintain high beamforming gain [16] as illustrated in Table 1.2. Thus, large-scale multiple-input multiple output (MIMO) technology is one of the promising candidates to combat these challenges [17]. These massive antennas can be exploited in attaining high beamforming and combining gains to overcome the path-loss associated with the mmWave propagation. By increasing the number of antennas, performance can be traded between antenna gain and additional degrees of freedom [18]. Linear precoding schemes can be employed to reduce the complexity of the system drastically [19]. Having accurate knowledge of the channel state information (CSI) is crucial in the design of the precoder that nulls out the unintended space-time-frequency dimensions. The downside is that a larger number of antennas comes together with an increased complexity and overhead, impacting in the throughput of the systems, to precisely acquire the CSI. A pilot-based channel estimation using polynomial expansion proposed in [20] and a low complexity adaptive compress sensing based algorithm proposed in [21] are two among the many low complexity methods proposed to estimate the CSI of large-scale MIMO systems.

1.1 Hardware Limitations, State of The Art Transceivers and Modulation Schemes

Fully digital (FD) architectures (conventional MIMO) such as block diagonalization algorithm in [22] have been proven to achieve high performance. However, implementation of a FD architecture at a terminal with large number of antennas is not practical due

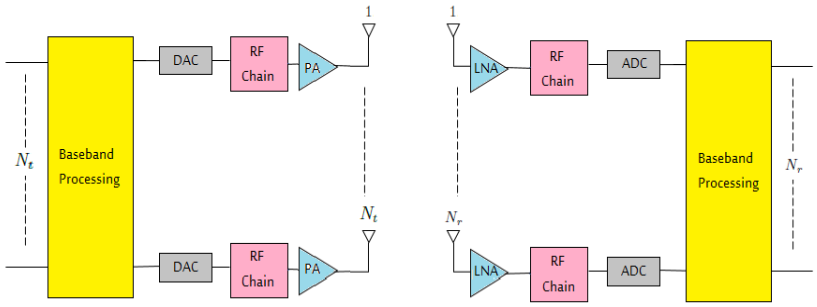

Power Consumption (mW)

Device\Frequency	2.5 GHz	28 GHz	73 GHz
LNA	5	10	30
RF Chain	10	40	60
ADC	50	200	300

Figure 1.1: Conventional MIMO transceiver.

to space limitations and energy consumption constraints. Specifically, in conventional MIMO, each antenna is connected to a specific radio-frequency (RF) chain and high resolution analog-to-digital-converter (ADC) as shown in Fig. 1.1. Unfortunately, these devices are expensive and power hungry especially at mmWave frequency band. Therefore, applying the conventional transceiver design (used for small-scale sub-6GHz MIMO systems [23]) to massive mmWave MIMO systems is challenging because its high cost and power consumption. For example, at $N_r = 16$, the receiver power consumption of the architecture in Fig. 1.1 equals 1 W at 2.5GHz and 6.2 W at 73 GHz in addition to the power consumption by the baseband (BB) processing. The previous example shows that the receiver power consumption at 73 GHz increase six times more than at 2 GHz. In the sequel, we present some alternate MIMO transceiver architectures that have been developed with the aim of reducing the cost and the power consumption.

1.1.1 Analog MIMO

Analog MIMO is the simplest transceiver design that can be applied to mmWave systems. In this system, each antenna element is connected to analog phase shifter and all phase shifters (PSs) are connected to a single RF (SRF) chain as shown in Fig. 1.2. The PSs weights are digitally controlled according to the beamformers design. Analog precoding can support single-user and single-stream transmission and it is usually used for beam steering [24]-[25]-[23].

1.1.2 Hybrid MIMO

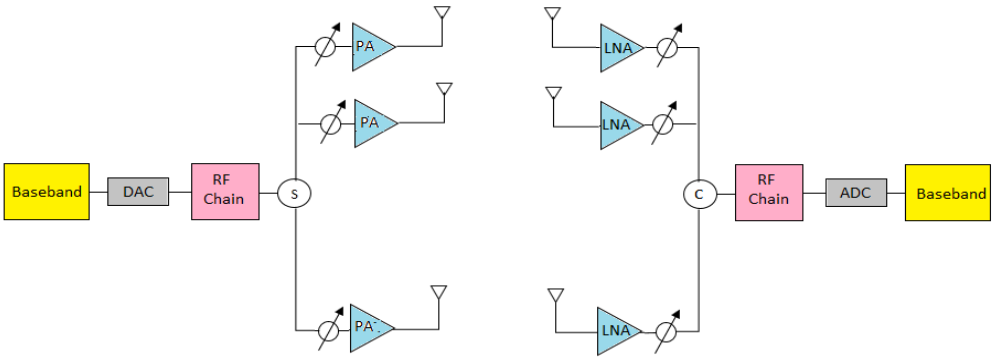

Figure 1.2: Analog MIMO transceiver.

Hybrid MIMO [23] is an extension to the analog MIMO where multiple RF (MRF) chains are deployed at the transceiver and thus, it supports multiple stream and multiple users transmissions. As shown in Fig. 1.3, the beamforming process of the hybrid architecture is divided between analog and digital domains with number of RF chains smaller than number of antennas where it allows multi-user transmission [23]. In [26], the hybrid architecture is introduced for centimeter-wave frequencies. The design algorithms described in this paper can be used for mmWave frequencies. However, they did not consider the properties of mmWave propagation in designing the precoders and combiners. In [27], the spatially sparse nature of mmWave propagation (explained in Sec. 2.4.2) is

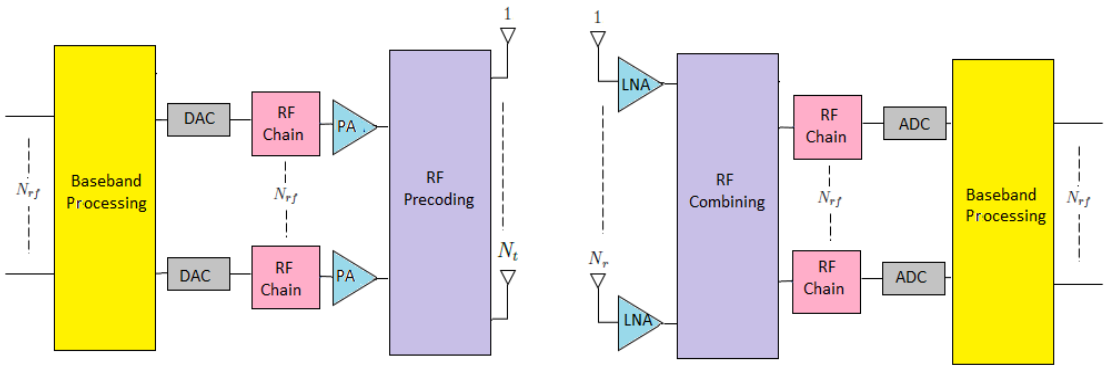

Figure 1.3: Hybrid MIMO transceiver.

leveraged to simplify the hybrid transceiver design. The spectral efficiency (SE) of the fully connected hybrid architecture approaches the FD MIMO with a reduced number of RF chains [28]. However, each RF chain has to be connected to a number of PSs that equals the number of receive antennas. Thus, the number of PSs increases rapidly by increasing the number of RF chains. Consequently, although a single PS has a small power consumption, many PSs could consume greater power than RF chains and ADCs. In [28], many low complexity hybrid systems have been studied based on PSs and switches but their (SE) gap with respect conventional MIMO is large. Partially connected hybrid

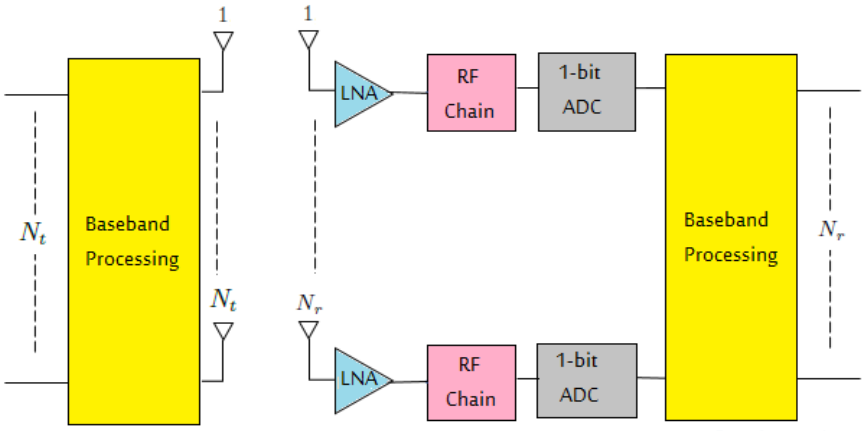

Figure 1.4: MIMO with Low Precision ADCs transceiver.

architectures [29], [30], [31] have been proposed to improve the energy efficiency (EE) of the fully connected transceivers by reducing the number of analog devices. However, improving the EE entails a degradation in the (SE).

1.1.3 MIMO Based on 1-bit ADC

The high resolution ADC at mmWave frequencies is the most power consuming device [23]. The ADC power consumption increases exponentially with its quantization bits and linearly with the transmission BW [23]. Thus, the MIMO receiver design based low precision ADCs as shown in Fig. 1.4 is an alternative technique to reduce the power consumption. For example, the 1-bit ADC at sampling rate 240GS/s consumes 10mW [32]. Nonetheless, the use of low bit ADCs hamper the availability of perfect channel knowledge and entails a reduction of the (SE) .

1.2 Advantages of Spatial Modulation for 5G Cellular Systems

Spatial modulation (SM) is a powerful tool that can be exploited to simplify the MIMO transceiver design and attain high SE [33]. SM techniques have been initially introduced for sub-6 GHz with the aim of reducing number of RF chains and minimizing the hardware cost and power consumption [34]. Moreover, SM schemes are able to attain significant SE values by exploiting the spatial dimension. The concept of spatial transmission can be applied at the transmitter (transmit SM (TSM)) [34] or at the receive (receive SM (RSM)) [35]. In the sequel, we illustrate TSM and RSM methods.

1.2.1 Transmit Spatial Modulation

In TSM, one antenna is active during the transmission and the remaining are silent and thus, only one RF chain is needed. Part of the input data bits is mapped into the index of the active transmit antenna and the other part is mapped into M-ary modulation symbol to be transmitted from the active antenna. After that, the receiver applies maximum likelihood (ML) detector to jointly detect the index of the active transmit antenna and the M-ary symbol assuming that the CSI is available at the receiver. For the sake of improving the SE, generalized SM (GSM) techniques have been developed to enable activating a set of transmit antennas instead of one transmit antenna for the TSM systems [36]. However, TSM schemes suffer from low antenna gain because most of the transmit antennas are silent which is an impairment at higher frequencies (e.g. 28 GHz) where large beamforming gain is needed to combat the severe path-loss. Hybrid TSM (HTSM) schemes have been reported in [37], [38] to exploit the PSs in attaining high beamforming gain where SM bits are mapped into group of antennas each connected to PS instead of single antenna of TSM. Outdoor propagation of mmWave signals suffers from rank deficient channel matrices as explained in Fig. 10 in [39]. Thus, the performance of HTSM schemes in [37], [38] can be highly degraded if the receiver cannot distinguish between correlated PSs groups.

1.2.2 Receive Spatial Modulation

In RSM, a subset of receive antennas is active during a transmission. In contrast to the previous case, the SM bits are devoted to indicate the active receive antennas (ARA) whilst the other bits are mapped into M-ary symbol [35]. In RSM, the transmitter applies zero forcing (ZF) precoding assuming CSI knowledge in transmission and the receiver applies the ML principle to jointly detect the index of the ARA set and the M-ary symbol. However, conventional RSM systems adopt FD MIMO architectures and thus exhibit high power consumption, which is especially worrying when operating at mmWave band. Moreover, ZF precoders suffer from performance degradation in rank deficient MIMO channels. In [40], the authors developed an RSM scheme for indoor propagation of mmWave signals where they control the inter antenna spacing to ensure orthogonal MIMO channel. However, the proposal is not practical in outdoor scenarios as the large transmitter-receiver separation requires large inter antenna spacing.

1.3 Challenges addressed in this PhD dissertation

Challenge 1: Developing novel modulation schemes (in Chapter 2.2) based on energy efficient UT architecture for massive and mmWave MIMO systems operating in outdoor propagation environment.

The prior art in RSM mostly assumes sub-6 GHz communications and full dimension MIMO systems which is not suitable for mmWave systems. In [41], we developed downlink (DL) RSM scheme based on energy efficient UT architecture for the outdoor propagation of the mmWave signals assuming ZF precoding at the BS.

Challenge 2: Developing mmWave RSM schemes based on ZF precoding in Chapter 3.3.1.1 and extending the design to minimum mean square error (MMSE) precoding in Chapter 3.3.1.6 by considering total power constraint (TPC) and the more practical per antenna power constraint (PAPC).

Adapting the RSM scheme in [41] to minimum mean square error (MMSE) precoding is not straightforward due to the UT hardware constraints and the unavailability of CSI at the UT. In ZF RSM, no CSI is needed at the UT for phase compensation to the modulation symbol [41]. In contrast, the UT for MMSE RSM needs partial channel knowledge for modulation symbol phase compensation that could increase the training overhead.

Challenge 3: Developing reduced computational complexity receive antenna selection (RAS) algorithms to overcome the spatial correlation associated with outdoor propagation of the mmWave signals in Chapter 3.3.2.

ZF precoding is challenging if the channel is spatially correlated: badly conditioned solutions and low signal-to-noise-ration (SNR) at the receiver are obtained. Thus, efficient RAS algorithms based ZF precoding have been developed in [42] to enhance the RSM performance in the spatially correlated channels.

Challenge 4: Extending the proposed energy efficient modulation scheme for wideband propagation in Chapter 3.3.3.

Single carrier with channel equalization and orthogonal-frequency-division-multiplexing (OFDM) are two methods to combat the frequency selectivity of the wideband transmission. OFDM schemes have been considered as the art of the DL communications, however, the large BWs and the use of RSM schemes make single carrier transmission more attractive. The reason is that in RSM schemes [43]-[41], it is possible to transmit one spatial symbol per channel use, thus symbols with shorter duration (single carrier) allow transmitting more spatial symbols and attaining higher SE than symbols with longer duration (OFDM). On the other hand, single carrier systems require some sort of equalization. In [44], we proposed a wideband single carrier RSM scheme based on a time-domain finite impulse response (FIR) pre-equalizer [45] and RAS.

Challenge 5: Exploiting the channel reciprocity to provide a joint design for the uplink (UL) TSM and the DL RSM schemes based on energy efficient UT architecture in Chapter 3.4. The joint design of UL TSM and the DL RSM systems is a novel approach that aims at reducing the computational complexity by exploiting the channel reciprocity. In [46], [47], we developed novel transmit and receive SM schemes for UL and DL data transmission phases based on novel energy efficient hybrid UT architecture.

Challenge 6: Extending the DL RSM and the UL TSM schemes for multi-user systems in Chapter 4.

The joint scheduling of multiple users, power allocation and antenna selection for broadcast and multiple access channels are novel problems for SM systems. In [48], we proposed a RSM scheme for the DL of multi-user (MU) MIMO system based on novel and energy efficient flexible UT architecture that works with RSM or conventional modulation (CM) transmissions. We proposed novel algorithms to jointly schedule users, allocate the power and selecting the UT antennas. Moreover, in this PhD thesis, we propose optimization algorithms to jointly schedule the UL users and selecting the UT antennas assuming TSM schemes in the multiple access transmission.

1.4 Research Contributions

1.4.1 Publications of Journal and Conference Papers

The research contributions published in flagship journals and conferences are detailed in the chapters of this Ph.D. dissertation as follows

Chapter 2

The main result in this chapter is the development of a novel and energy efficient UT Massive MIMO architecture based on RSM scheme for the outdoor propagation of the mmWave signals. The work has been published in one conference paper:

[C1] **A. Raafat**, A. Agustin and J. Vidal, " Energy-Efficient Architecture for Receive Spatial Modulation in Large MIMO Systems ", *International Symposium on Wireless Communication Systems (ISWCS)*, Bologna (Italy), August 2017.

Chapter 3

The main results in this chapter are developing single user DL RSM schemes for single and MRF chains at the UT, FD and hybrid BS architectures, ZF and MMSE precoding, narrowband and wideband transmissions. After that, we extend to UL-DL massive MIMO systems based on hybrid UT architecture. The work has published in one journal paper and five conference papers:

[J1] **A. Raafat**, M. Yuzgecciogl u, A. Agustin, J. Vidal, E. Jorswieck and Y. Corre, "Energy Efficient Transmit-Receive Hybrid Spatial Modulation for

Large-Scale MIMO Systems", *in IEEE Trans. on Communications,* vol. 68, pp. 1448 - 1463, March 2020.

[**C2**] **A. Raafat**, A. Agustin and J. Vidal, "Receive Spatial Modulation for Massive MIMO Systems", *IEEE Global Communications Conference (GLOBECOM)*, Singapore, December 2017.

[**C3**] **A. Raafat**, A. Agustin and J. Vidal, "Receive Antenna Selection and Hybrid Precoding for Receive Spatial Modulation in Massive MIMO Systems", *in IEEE International ITG Workshop on Smart Antennas (WSA)*, Bochum (Germany), March 2018.

[**C4**] **A. Raafat**, A. Agustin, and J. Vidal, "MMSE precoding for receive spatial modulation in large MIMO systems," in IEEE International Workshop on Signal Processing Advances in Wireless Communications (SPAWC), June 2018.

[**C5**] **A. Raafat**, M. Yuzgeccioglu, M. Z. Aslam, A. Agustin, J. Vidal, E. Jorswieck and Y. Corre, "Energy Efficient Transmit-Receive Spatial Modulation for Uplink-Downlink Large-scale MIMO Systems", *in the proceedings of IEEE Global Communications Conference (GLOBECOM)*, Abu Dhabi (UAE), Dec. 2018.

[**C6**] **A. Raafat**, A. Agustin, and J. Vidal, "Wideband Receive Spatial Modulation with Time Domain Pre-Equalizer for Large MIMO Systems," *in the proceedings of IEEE Global Communications Conference (GLOBECOM)*, Abu Dhabi (UAE), Dec. 2018.

Chapter 4

The main results in this chapter are developing MU power allocation, antenna selection and user selection for the broadcast channel (BC) using RSM transmission scheme and for the multiple access channel (MAC) using TSM scheme. The results have been published in one journal paper:

[**J2**] **A. Raafat**, A. Agustin and J. Vidal, "Downlink Multi-User Massive MIMO Transmission using Receive Spatial Modulation", *Accepted with minor revision in IEEE Trans. on Wireless Communications.*

1.4.2 Contribution to the 5GWireless Project

The results obtained in Chapters 2-3-4 of this Ph.D. dissertation have been major contributions to the multi-partner European Training Network (ETN) project

(5GWireless) within the framework of the H2020 Marie Sklodowska-Curie Innovative Training Networks (ITNs) with grant number 641985 (August 2016 to July 2019). 5Gwireless is a fully-integrated and multi-disciplinary network of 15 Early Stage Researchers (ESRs) working in 10 research institutions distributed in 6 European countries. The consortium is formed by 4 Universities, 1 Research Center and 5 Private Companies. 5Gwireless offers a cross-sectoral environment to 15 ESRs, in order to shape their long-term research view and to allow them to get fundamental methodological tools on various research fields and novel concepts, such as, cellless/device-centric architectures, ultra-dense networks and mmW communications. This is the project website "`http://www.h2020-msca-etn-5gwireless.eu/`".

1.4.3 Research Appointments

SIRADEL

From February to July 2018, the author stayed five months as a research secondment at SIRADEL company in Rennes, France. In that period, the author had the opportunity to evaluate the performance of the developed signal processing algorithms in his PhD thesis using realistic VOLCANO channel simulator provided by SIRADEL to validate the theoretical work in real life small cells deployments at 28 GHz carrier frequency. Parts of the conference paper [**C5**] and the journal paper [**J1**] presented in Chapter 3 of this doctoral thesis are results of this collaboration.

Technische Universitat Dresden

From October to November 2018, the author stayed one month as a research appointment in Technische Universitat Dresden in a collaboration with Prof. Eduard Jorswieck in the topic of "Energy efficient transmit-receive hybrid spatial modulation for uplink-downlink large-scale MIMO systems". Parts of the conference paper [**C5**] and the journal paper [**J1**] presented in Chapter 3 of this doctoral thesis are results of this collaboration.

1.5 Mathematical Tools and Required Prior Knowledge

The novel signal processing algorithms and the modulation schemes developed in this PhD thesis require some background on fundamental mathematical tools and wireless communications summarized as follows

- **Linear Algebra**: In chapters 2, 3 and 4 the author used the linear algebra principles to develop the MIMO system model that composed of linear matrices. Moreover, the author applied the advanced linear algebra decompositions such as singular value decomposition (SVD) [49] and QR decomposition [50]

to develop efficient signal processing algorithms for mmWave Massive MIMO systems.

- **Detection and Estimation Theory**: In chapters 3 and 4, the author applied the detection and estimation techniques [51] such as matched filter, zero forcing, least squares, minimum-mean-square, and ML for MIMO detection and parameters estimation.
- **Digital Signal Processing (DSP)**: In chapter 3 the author applied the DSP methods [52] such as convolution and FIR filtering for equalizing the MIMO wideband multi-tap channel.
- **Digital Modulation**: In chapters 3 and 4 the author considered various digital modulation schemes [53] such as M-quadrature-amplitude-modulation (QAM), M-phase-shift-keying (PSK), spatial modulation, OFDM and single carrier modulated signals.
- **Information Theory**: In chapters 3 and 4 the author applied the information theory [54] to derive closed form expressions to the mutual information of the transmit and receive SM schemes.
- **Optimization Theory** : In chapters 3 and 4, the author applied the convex and non-convex optimization techniques [55] to solve problems such as antenna selection in Massive MIMO systems and multi-user power allocation. Moreover, the user used the CVX simulator [56] to solve the convex optimization problems.

1.6 Organization

The organization of this PhD thesis is described as follows

- We address challenge one in chapter 2. First, we mathematically describe the state of the art of the SM and highlight the main challenges with these schemes when applied at mmWave frequency band. Next, we propose a novel SM scheme specifically designed for mmWave massive MIMO systems. After that, we illustrate how the concept of the SM can be exploited in attaining energy efficient UT architecture. Finally, we present the channel model, systems assumptions and the transceiver devices power consumption model.
- We address challenges two, three, four and five in chapter 3. We consider single user SM system. First, we propose DL RSM scheme where the UT can be implemented with single or MRF chains and the BS can be FD or hybrid

architecture. Moreover, we consider different precoders at the BS and propose low complexity and efficient antenna selection schemes for narrowband and wideband transmissions. After that, we propose joint UL-DL SM scheme where we consider RSM in the DL and TSM in the UL based on energy efficient hybrid UT architecture.

- We address challenge six in chapter 4. We extend the SM system to the multi-user case. Specifically, we develop joint multi-user power allocation, user selection and antenna selection algorithms for the broadcast and the multiple access channels. We propose novel alternating optimization technique for solving non-convex optimization problems.

- Chapter 5 is presented for proposing future research directions.

Chapter 2

Spatial Modulation Architecture for Massive MIMO Systems

2.1 State of the Art on Spatial Modulation

SM techniques have been introduced for sub-6 GHz communications with the aim of reducing number of RF chains and minimizing the cost and the power consumption of the MIMO transceiver. The SM concept is to activate set of antennas based on the information bits. If those active antennas are at the transmitter, the scheme called TSM. If the active antennas are at the receiver, the scheme called RSM. Let us consider a single user MIMO system with N_t transmit antennas and N_r receive antennas. In TSM [34], one transmit antenna out of N_t is activated according to the input spatial bit stream and thus the possible number of the spatially modulated bits is $\lfloor \log_2 \binom{N_t}{1} \rfloor$. Since the active antenna provides information about the spatially modulated symbol, we can also transmit conventionally modulated symbol $x \in M$-ary constellation from the active antenna. Hence, the number of conventionally modulated bits is $\log_2 M$ and the total number of transmitted bits is

$$n_{\text{TSM}} = \left\lfloor \log_2 \binom{N_t}{1} \right\rfloor + \log_2 M \tag{2.1}$$

The transmit signal of the TSM scheme can be expressed as

$$\mathbf{x}_{\text{TSM}} = \sqrt{P_t}\mathbf{s}x \tag{2.2}$$

where $x \in \mathbb{C}^{1\times 1}$, $\mathbf{s} \in \mathbb{R}^{N_t \times 1}$ with i-th entry $s_i \in \{0, 1\}$, the vector $\mathbf{s}$ includes single one and the other entries are zeros such that $\mathbf{s}^T\mathbf{s} = 1$ and P_t is the transmit power.

The received signal can be expressed as

$$\mathbf{y}_{\text{TSM}} = \sqrt{P_t}\mathbf{H}\mathbf{s}x + \mathbf{n} = \sqrt{P_t}\mathbf{h}_i x + \mathbf{n}$$

where the MIMO channel matrix $\mathbf{H} \in \mathbb{C}^{N_r \times N_t}$ and $\mathbf{n} \in \mathbb{C}^{N_r \times 1}$ is the generated noise vector where its coefficients are independent and identically distributed (i.i.d) zero mean circularly symmetric complex Gaussian random variables. The multiplication $\mathbf{Hs}$ results in the channel vector $\mathbf{h}_i$ between the i-th active antenna at the transmitter and all the antennas at the receiver. After that, assuming frequency-division duplexing (FDD) communications and the CSI is available at the receiver that applies a joint ML detector to the spatially modulated and conventionally modulated symbols as

$$[\mathbf{s}^\star, x^\star] = \min_{\substack{i=1,\cdots,N_t \\ j=1,\cdots,\log_2 M}} \|\mathbf{y}/P_t - \mathbf{h}_i x_j\|_2 \tag{2.3}$$

The computational complexity is in order of $N_t \times \log_2 M$ search points. With the aim of improving the SE, GTSM schemes [36] have been developed where a set of transmit antennas are active simultaneously and transmit the same conventionally modulated symbol x. In the GTSM scheme, the spatial symbol $\mathbf{s}$ contains N ones (number of active antennas at the transmitter) and $N_t - N$ zeros. Thus, the number of spatially modulated bits increase from $\lfloor \log_2 \binom{N_t}{1} \rfloor$ to $\lfloor \log_2 \binom{N_t}{N} \rfloor$. However, GTSM schemes lead to an increased detection computational complexity at the ML receiver, as the search points increase from $\lfloor \log_2 \binom{N_t}{1} \rfloor \log_2 M$ to $\lfloor \log_2 \binom{N_t}{N} \rfloor \log_2 M$.

Applying these schemes to the mmWave frequency band is challenging especially in outdoor propagation scenario for many reasons

- First, mmWave propagation suffers from severe path-loss and thus, high beamforming gain is needed. However, in TSM and GTSM not all the transmit antennas are active simultaneously that reduces the antenna gain. Fortunately, large-scale MIMO systems supports very high beamforming gains so it is a key technology for mmWave because of its potential to overcome the path-loss. HTSM schemes have been reported in [37], [38] to exploit PSs in attaining high beamforming gain where SM bits are mapped into a group of antennas each connected to a PS instead of a single active antenna, as in TSM. However, outdoor propagation of mmWave signals exhibits poor scattering which entails spatially sparse and rank deficient channel matrices as explained in Fig. 10 in [39]. Thus, the performance of HTSM schemes in [37], [38] can be highly degraded if the receiver cannot distinguish between correlated PSs groups.

- Second, the large scale MIMO makes the FD transceiver expensive and power consuming [23]. The TSM and GTSM have been introduced for FD receivers (second challenge when we go to mmWave).

- Third, the ML detectors of the TSM and the GTSM have high computational complexity that are not suitable for the very rapid communications of mmWave signals.

As we highlighted at the beginning of this section, SM techniques can be applied at the receiver (RSM). In RSM [35], the transmitter applies ZF or MMSE precoding in such a way that a subset of antennas (N_s antennas) receive conventionally modulated symbols and the complementary set ($N_r - N_s$ antennas) are silent. These sets are selected according to the spatially modulated symbol. In this scheme, the total number of transmit bits are

$$n_{\mathrm{RSM}} = \left\lfloor \log_2 \binom{N_r}{N_s} \right\rfloor + \log_2 M \tag{2.4}$$

In RSM, the transmitter applies ZF precoding assuming CSI knowledge and the receiver applies the ML principle to jointly detect the index of the ARA set and the M-ary symbol. In the literature, RSM systems adopt fully digital MIMO architectures and thus exhibit high power consumption especially for systems operating at mmWave band. Moreover, ZF precoders suffer from performance degradation in rank deficient MIMO channels. In [46], the authors developed HTSM in the UL and RSM in the DL assuming outdoor propagation of mmWave signals. However, they do not consider a hybrid structure for the RSM in DL and rely on a rigid hybrid architecture for the UL TSM. In [57], [58], the authors developed HTSM based on partially connected hybrid transmitter and FD receiver. In [59], a DL multi-user RSM scheme has been proposed; however, a high energy consuming FD UT architecture is considered. In [60], the authors evaluated the performance of the RSM scheme assuming MIMO BC and FD transceivers; however, they did not consider power control and the transmit power is equally split among the users.

2.2 Proposed Energy Efficient User Terminal Architectures

In order to overcome the cost and power consumption problems in mmWave massive MIMO systems, we exploit the SM concept to propose several energy efficient UE architectures as follows

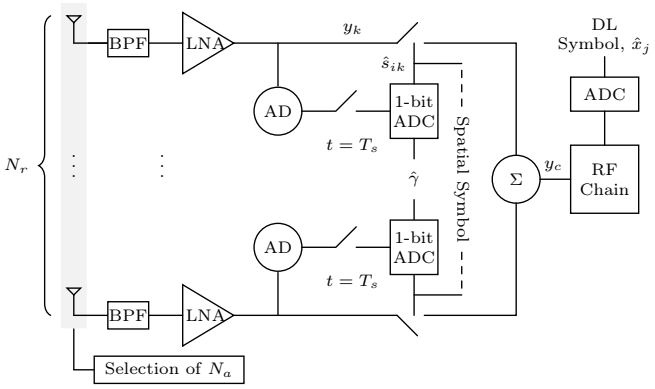

Figure 2.1: Single RF RSM Large MIMO transceiver architecture [41]

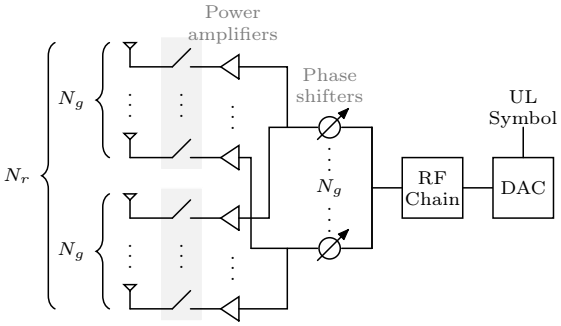

(a) Transmit UL circuitry - uniform grouping

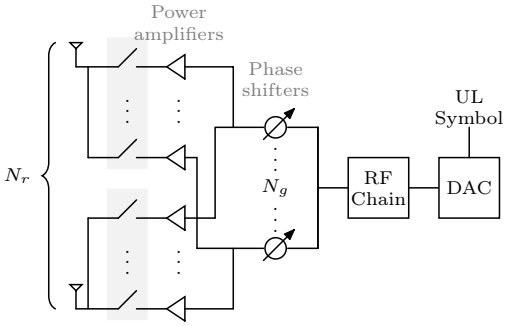

(b) Transmit UL circuitry - transmit antenna grouping

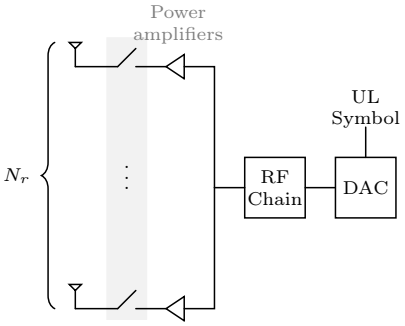

(c) Transmit UL circuitry - transmit antenna selection

Figure 2.2: Low complexity circuitries for single RF TSM scheme [46]

2.2.1 Single RF RSM

The proposed UT architecture for SRF RSM scheme in Fig. 2.1 relies on energy-efficient devices that can be represented as follows:

- RF chain and high precision ADC: these devices are the most power consuming so we consider a SRF chain and a single high precision ADC with any number of antennas.

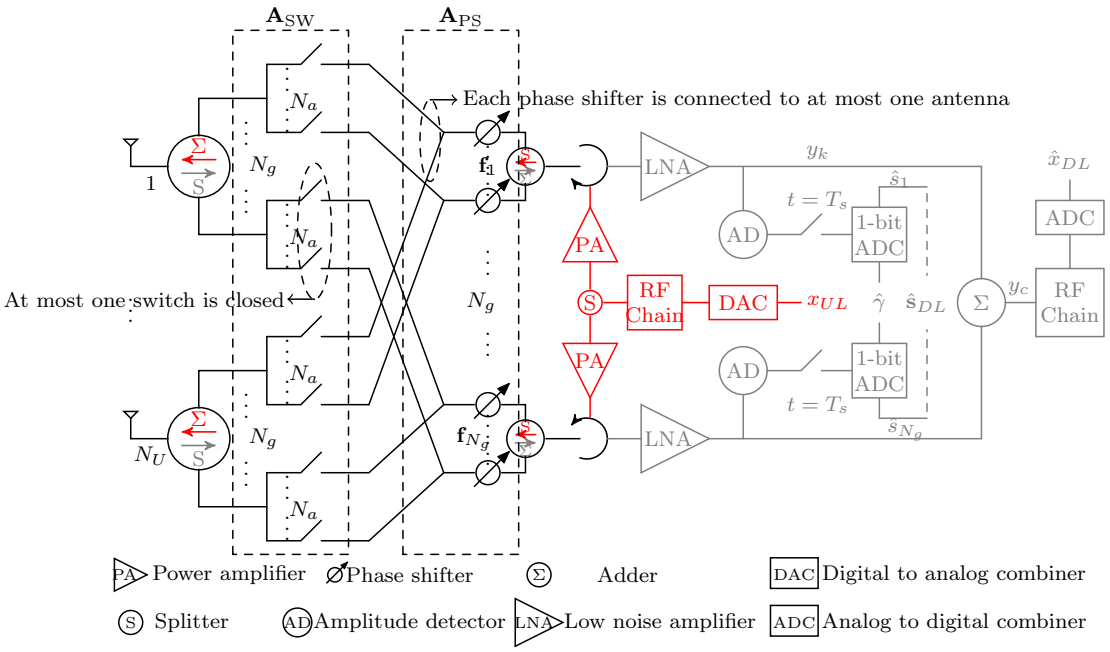

Figure 2.3: Block diagram at the user terminal, with transmit and receive circuitry in red and grey respectively. Black elements (like antennas or phase shitfers) are common using single RF chain.

- Amplitude detector (AD): it is a cheap analog device that detects the amplitude of the RF signal in absolute value and operates at high frequencies with high sensitivity and negligible power consumption [61]. TABLE I in [62] shows that the AD can operate at frequency range from (1GHz to 85GHz) with sensitivity from (-5dBm to -50dBm).

- 1-bit ADC: the power consumption of the ADC grows exponentially with number of quantization bits. We choose using single bit devices (or comparator).

2.2.2 Single RF TSM

In Fig. 2.2, we propose three low hardware complexity UT architectures for SRF TSM scheme as follows

- Uniform grouping (UG) shown in Fig. 2.2a: In this scheme, we consider $\frac{N_T}{N_g}$ phase shifting groups each containing N_g antennas. The name UG means that antennas are uniformly distributed among the phase shifting groups. For example, if we have four antennas and two groups, the first group comprises first and second antennas while the second group contains third and fourth antennas. At a given transmission, one group of antennas is active based on

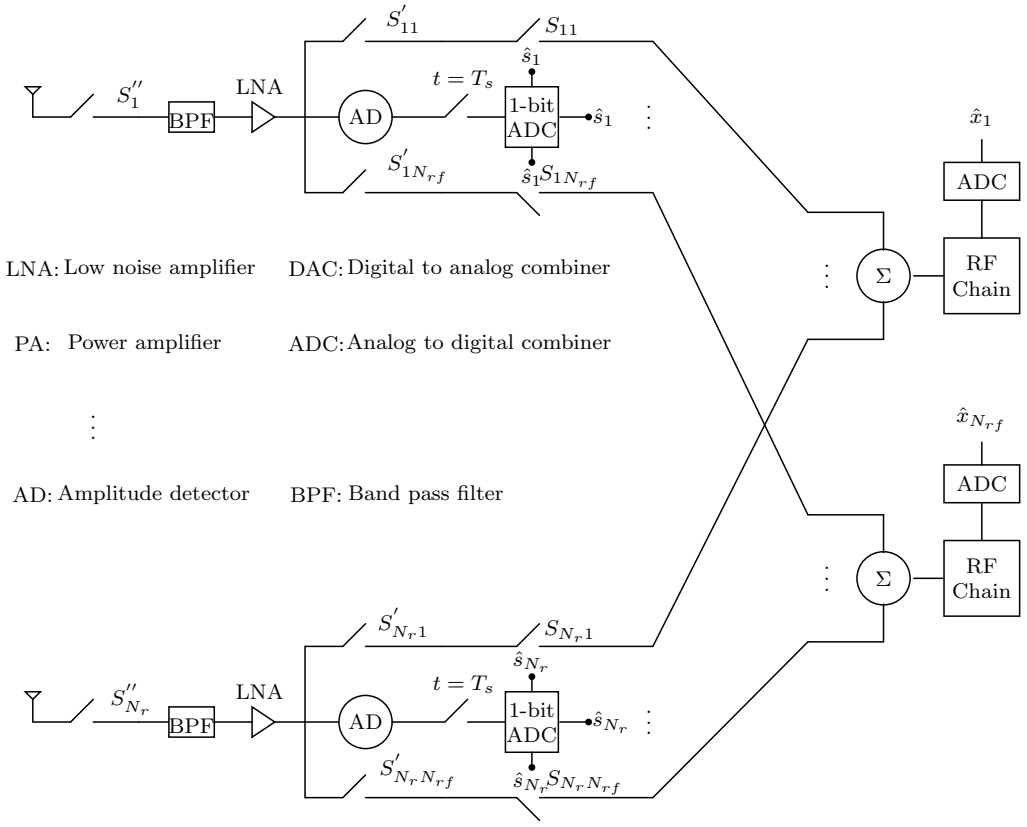

Figure 2.4: User terminal transceiver circuitries. The switch S''_k controls the ON/OFF status of the k-th antenna, S'_{ij} connects the i^{th} received symbol to the j^{th} RF chain. The switch status is determined according to an optimization algorithm. The switch S_{ij} controls the combining method at the UT.

the spatial information bits. This scheme has low computational complexity but it suffers from performance degradation in correlated channels.

- Transmit antenna grouping (TAG) shown in Fig. 2.2b: In this scheme, we consider $\frac{N_r}{N_g}$ phase shifting groups each contains N_g antennas. In this case, the set of antennas inside each group is optimized such that we obtain the most uncorrelated groups. At a given transmission, one group of antennas is active based on the spatial information bits. This scheme works well at the correlated channels but with higher computational complexity.
- Transmit antenna selection (TAS) shown in Fig. 2.2c: In this scheme, we do not consider PSs, however, the most uncorrelated N_g antennas are selected to be active. After that, at a given transmission, one antenna out of N_g antennas is active based on the spatial information bits. This scheme approaches the performance of TAG but with much lower computational complexity.

2.2.3 Single RF TRSM

As an extension to the circuitry proposed in Fig. 2.2b, we propose a hybrid UL and DL architecture at the UT in Fig. 2.3. The architecture in Fig. 2.3 consisting of two

analog stages. The phase shifting stage provides high transmit beamforming gain and high receive combining gain during UL and DL transmissions, respectively. The phase shifting architecture consists of N_g groups of linear antenna arrays where each group comprises N_a PSs. As we map the spatial bits into phase shifting groups, we have to include analog switches stage to obtain uncorrelated antenna groups. This can be achieved by smartly mapping the antennas among the phase shifting groups. Specifically, each antenna can be connected to any PS and hence $N_a N_g$ ($N_a^{\mathrm{UL}} N_g^{\mathrm{UL}}$ for the UL and $N_a^{\mathrm{DL}} N_g^{\mathrm{DL}}$ for the DL architectures) switches per antenna are required. The maximum number of groups is $N_g = C$ (around 7 in the realistic urban scenario) and the maximum number of PSs per group is $N_a = N_U$. Within a specific linear antenna array group, each PS is connected to a distinct antenna but different groups can share the same antenna. The number of active phase shifting groups $\{N_g^{\mathrm{UL}}, N_g^{\mathrm{DL}}\}$, antennas inside the groups and the number of active PSs per group $\{N_a^{\mathrm{UL}}, N_a^{\mathrm{DL}}\}$ are determined to maximize the EE at the beginning of each coherence time by employing the low complexity optimization algorithm as explained in Sec. 3.4.

2.2.4 Multiple RF RSM

In Fig. 2.4, for the sake of improving the SE, we propose a novel energy efficient UT circuitry that extends the architecture in Fig. 2.1 into MRF chains. In the proposed architecture, we consider energy efficient control switches. First, the switch $S_k^{''}$ controls the ON/OFF status of the k-th UT antenna. Second, only one of the switches $(S_{i1}^{'}, \cdots, S_{iN_{rf}}^{'})$ is ON to connect the i^{th} received signal to a specific RF chain. Finally, the switch S_{ij} can be always closed (independent combining (IC) scheme) or controlled by the received spatial symbol (dependent combining (DC) scheme). The switches status are determined according to optimization algorithms proposed in Chapter 4. The status of the switches remains fixed within the channel coherence time.

2.3 Circuitry Power Consumption

In this section, we present a power consumption model of the electronic devices used in the above circuitries. Hence, we evaluate the power consumption of each circuitry. The power consumed by UT devices at 28GHz, according to, [28]-[63] can be modelled as

$$P_{\mathrm{PS}} = P_{\mathrm{LNA}} = P_{\mathrm{ref}},\ P_{\mathrm{ADC}} = P_{\mathrm{DAC}} = \mathrm{FoM} \times f_s \times 2^n,$$

$$P_{\text{Switch}} = 0.25P_{\text{ref}},\ P_{\text{RF}} = 2P_{\text{ref}},\ P_{\text{BB}} = 10P_{\text{ref}},\ P_{\text{PA}} = \left(\frac{1}{\eta} - 1\right) P_t. \tag{2.5}$$

Therein, P_{LNA} refers to the power consumption of the low noise amplifier (LNA) and it is taken as the reference P_{ref} in the hardware circuitry. The power consumption of the remaining hardware elements such as PS, power amplifier (PA), ADC, digital-to-analog converter (DAC), RF chain and BB computation are defined by using the reference power consumption value P_{ref}, f_s is the sampling frequency that equals to twice the BW, n refers to number of ADC/DAC bits, FoM is the figure of merit that depends on the technology and takes value of 34.4 fJ/Conv.-step at $n = 12$ and $f_s = 600$-MS/s [64], η is the PA efficiency that takes value 40% at 28 GHz [65] and P_t is the transmit power. The power consumption of the AD is considered negligible. Given this model, the power consumption for each one of the circuitries proposed above is given by:

- The power consumption of the SRF RSM circuitry shown in Fig. 2.1 can be expressed as

$$P_{c,,\text{SRF-RSM}} = N_r \left(2P_{\text{LNA}} + P_{\text{PS}} + P_{\text{SW}}\right) + \left(P_{\text{RF chain}} + P_{\text{ADC}}\right) + P_{\text{BB}} \tag{2.6}$$

- The power consumption of the SRF TSM circuitries shown in Fig. 2.2 can be expressed as

$$\text{Fig. 2.2a: } P_{c,\text{UG}} = P_{\text{RF}} + P_{\text{DAC}} + N_g P_{\text{PS}} + N_r P_{\text{SW}} + P_{\text{BB}}, \tag{2.7}$$

$$\text{Fig. 2.2b: } P_{c,\text{TAG}} = P_{\text{RF}} + P_{\text{DAC}} + N_g P_{\text{PS}} + N_g N_r P_{\text{SW}} + P_{\text{BB}}, \tag{2.8}$$

$$\text{Fig. 2.2c: } P_{c,\text{TAS}} = P_{\text{RF}} + P_{\text{DAC}} + N_r P_{\text{SW}} + P_{\text{BB}}. \tag{2.9}$$

- The DL and UL power consumption of the SRF TRSM architectures shown in Fig. 2.3 can be expressed as

$$\begin{aligned} P_c^{\text{DL}} &= N_a^{\text{DL}} N_g^{\text{DL}} (P_{\text{SW}} + P_{\text{PS}}) + N_g^{\text{DL}} P_{\text{LNA}} + P_{\text{RF}} + P_{\text{ADC}} + P_{\text{BB}}, \\ P_c^{\text{UL}} &= N_a^{\text{UL}} N_g^{\text{UL}} (P_{\text{SW}} + P_{\text{PS}}) + N_g^{\text{UL}} P_{\text{PA}} + P_{\text{RF}} + P_{\text{DAC}} + P_{\text{BB}}, \end{aligned} \tag{2.10}$$

- The power consumption of the MRF RSM circuitry shown in Fig. 2.4 can be expressed as

$$P_{c,\text{MRF-RSM}} = N_a \left(3P_{\text{SW}} + P_{\text{LNA}}\right) + N_{\text{RF}} \left(P_{\text{RF}} + P_{\text{ADC}}\right) + P_{\text{BB}} \tag{2.11}$$

  where N_a represents number of active antennas.

2.4 System Assumptions and Channel Models [11], [39]

2.4.1 System Assumptions

The duplexing protocol is assumed to be time-division duplex (TDD) where the CSI is needed only at the BS and the channel reciprocity is assumed. The BS can acquire the CSI during the UL training phase by any method, for instance the authors in [21] exploit the spatially sparse nature of the outdoor mmWave channel in developing low complexity adaptive compress sensing based algorithms. Imperfect CSI at the BS with ZF precoder can be accurately modelled as an increase in the noise power [66]. The BS informs the UT about the results of the optimization algorithm during the DL training phase. Since the information required by the UT is limited, the DL training phase entails low overhead. Moreover, the BS applies the ZF precoder and the combiner to employ during DL and UL transmissions, respectively using a FD or hybrid architecture like the one proposed in [67].

2.4.2 Outdoor mmWabe Narrowband Channel Model

In the mmWave band, the number of scatterers is typically assumed to be a few, as a result of the severe path-loss of the waves traveling at high frequencies. In order to take this effect into account in the system performance evaluation, we adopt a geometry-based channel model [39] whereby the UL channel matrix is given by

$$\mathbf{H} = \sqrt{\frac{N_{\mathrm{BS}} N_U}{P_l C}} \sum_{i=1}^{C} g_i \mathbf{v}_r\left(\theta_i\right) \mathbf{v}_t\left(\phi_i\right)^H . \tag{2.12}$$

Herein, P_l is the path-loss of the channel $\mathbf{H} \in \mathbb{C}^{N_U \times N_{\mathrm{BS}}}$ between the BS and the UT, g_i is the gain of the i-th path that follows a complex Gaussian distribution as $\mathcal{CN}(0,1)$, $\theta_i \sim \mathcal{U}[-\pi/6, \pi/6]$ and $\phi_i \sim \mathcal{U}[-\pi/2, \pi/2]$ represent the azimuth angles of arrival at the BS and departure from the UT. By assuming uniform linear array (ULA), transmit and receive array response vectors of the i-th path $\mathbf{v}_t(\phi_i)$ and $\mathbf{v}_r(\theta_i)$ are generated as $\mathbf{v}(\varphi) = 1/N \left[1, e^{jkd\sin(\varphi)}, ..., e^{j(N-1)kd\sin(\varphi)}\right]^T$, where φ is the angle of the considered path, N is the number of elements in the array, $k = \frac{2\pi}{\lambda}$ where λ is the signal wavelength and $d = \frac{\lambda}{2}$ is the inter-elements spacing. The channel model in (2.12) can be decomposed as $\mathbf{H} = \mathbf{A}_r \mathbf{D} \mathbf{A}_t^H$ where $\mathbf{A}_r \in \mathbb{C}^{N_U \times C}$ and $\mathbf{A}_t \in \mathbb{C}^{N_{\mathrm{BS}} \times C}$ comprise the array response vectors of all the paths $\mathbf{A}_r = [\mathbf{v}_r(\theta_1), \mathbf{v}_r(\theta_2), \ldots, \mathbf{v}_r(\theta_C)]$ and $\mathbf{A}_t = [\mathbf{v}_t(\phi_1), \mathbf{v}_t(\phi_2), \ldots, \mathbf{v}_t(\phi_C)]$. The diagonal matrix $\mathbf{D} \in \mathbb{C}^{C \times C}$ has the complex path gains and the path loss at the diagonal entries $\sqrt{N_{\mathrm{BS}} N_U / P_l C}[g_1, g_2, \ldots, g_C]$.

2.4.3 Outdoor mmWabe Wideband Channel Model

The severe path loss of mmWave propagation leads to limited scattering environment [68], so an accurate wideband channel model [11] is used in evaluating the proposed system performance. According to this model, the time domain delay-d MIMO channel matrix can be expressed as

$$\mathbf{H}[d]=\sqrt{\frac{N_t N_r}{CL}}\sum_{i=1}^{C}\sum_{l=1}^{L} g_{li}\mathrm{P}_{rc}\left(dT_s-\tau_{li}\right)\mathbf{v}_r(\theta_{li})\mathbf{v}_t(\phi_{li})^H \tag{2.13}$$

where $\mathbf{H}[d]\in\mathbb{C}^{N_r\times N_t}$, $d=0,\cdots,N_c-1$, C is the number of scattering clusters and each cluster contributes with L rays. Further analysis about the mmWave delay spread is presented in [69]. Each ray has delay τ_{li}, complex gain g_{li}, sampling time T_s and azimuth angles of departures and arrivals (ϕ_{li},θ_{li}), respectively. We consider ULA for the transmit and the receive array response vectors $(\mathbf{v}_t(\phi_{li}),\mathbf{v}_r(\theta_{li}))$ where the N-antennas array response vector can be expressed as

$$\mathbf{v}(\phi)=\frac{1}{\sqrt{N}}\left[1,e^{jkd_s\sin(\phi)},...,e^{j(N-1)kd_s\sin(\phi)}\right]^T \tag{2.14}$$

where d_s is the antennas spacing and $k=\frac{2\pi}{\lambda}$. The raised-cosine pulse shaping filter [70] can be expressed as

$$\mathrm{P}_{rc}(t)=\begin{cases}\frac{\pi}{4}\mathrm{sinc}\left(\frac{1}{2\beta}\right), & \text{if} \quad t=\pm\frac{T_s}{2\beta}\\ \mathrm{sinc}\left(\frac{t}{T_s}\right)\frac{\cos\left(\frac{\pi\beta t}{T_s}\right)}{1-\left(\frac{2\beta t}{T_s}\right)^2}, & \text{else,}\end{cases} \tag{2.15}$$

In the sequel, the matrix $\mathbf{H}_a[d]$ denotes the delay-d tap channel after selecting N_a antennas to be active at the UT. For comparison purposes of the proposed energy efficient single carrier RSM scheme with FD K-subcarriers OFDM MIMO, the channel matrix of the k^{th} subcarrier can be obtained by applying Discrete Fourier Transform (DFT) as follows

$$\mathbf{H}_f[k]=\sum_{d=0}^{N_c-1}\mathbf{H}[d]e^{-j\frac{2\pi k}{K}d} \tag{2.16}$$

Chapter 3

Single User Spatial Modulation

3.1 Contributions

In this chapter, we address challenges 2, 3, 4 and 5. The research contributions presented in this chapter are published in five flagship conferences ([**C2**], [**C3**], [**C4**], [**C5**], [**C6**]) and one IEEE Transactions on Communications [**J1**].

3.2 Introduction

Several low complexity MIMO transceiver designs have been developed in the literature. Hybrid analog and digital precoding techniques have been proposed with the aim of simplifying the architecture and reducing power consumption [27]. The spectral efficiency of the hybrid systems approach the FD MIMO [27]. Nevertheless, hybrid structures comprise a large number of PSs, power splitters and power combiners for analog signal processing. These analog devices consume a lot of power principally with large arrays [28].

MIMO transceivers based on low precision ADCs have been studied to reduce the cost and power consumption [71]. Nonetheless, the use of low bit ADCs hamper the availability of perfect channel knowledge at the receiver side and entails a reduction of the spectral efficiency.

SM schemes have been reported to reduce the number of RF chains and to achieve high spectral efficiency. In TSM, the transmit antennas are exploited in transmitting extra information where part of the input data bits are used to select the set of active transmit antennas and the UT detects this set [72]. However, SM techniques suffer from small antennas gain because most of the transmit antennas are silent. Further, the UT cannot detect the set of active transmit antennas precisely if the channel vectors are correlated.

In contrast, RSM techniques exploit the receive antennas to transmit more information [35]. Conventional RSM methods use FD receiver architecture and suffer from high performance degradation under low rank channel matrices. Thus, traditional SM/RSM methods are not convenient for mmWave systems. In [40], the authors developed an RSM scheme for indoor propagation of mmWave signals where they control the inter antenna spacing to ensure orthogonal MIMO channel. However, the proposal is not practical in outdoor scenarios as the large transmitter-receiver separation requires large inter antenna spacing. Unlike the previous RSM methods, this chapter focuses on designing a new and simple RSM receiver based on a novel spatial detection method aimed to exploit the spatial dimension to transmit additional data symbols reliably. Moreover, we show that the proposed RSM system works efficiently for outdoor narrowband mmWave channels assuming TDD transmission where the CSI is needed only at the transmitter side. In the sequel, we present the novelties and contributions of this chapter. In Sec. 3.3.1.1, we consider the ZF RSM design for narrowband transmission such that

- For the sake of minimizing the power consumption at the UT, we exploit the RSM concept to attain energy efficient UT architecture assuming ZF precoding.

- We consider UT architecture based on one bit ADC due to its low power consumption and hence, we show that the optimal spatial symbol detector is a threshold detector that can be implemented by using one bit ADC.

- For the sake of reducing the computational complexity, we derive closed form expressions for the ADC detection threshold at different SNR regions showing that a simple threshold can be obtained at high SNR and its performance approaches the exact threshold.

- To evaluate the performance of the proposed scheme, we derive expressions for the average bit error probability (ABEP) in the presence and absence of the threshold estimation error, and show that a small number of DL pilot symbols is needed.

The outdoor mmWave channels are spatially correlated and poorly conditioned and hence, MMSE precoding outperforms ZF precoding in such scenario. However, the extension of the proposed RSM scheme to MMSE precoding is not straightforward due to hardware limitations at the UT. Thus, in Sec. 3.3.1.6, we extend the RSM design to MMSE precoding with per antenna and total transmit power constraints, specifically,

- We derive semi-closed form expression for the ML spatial symbol detector that can be evaluated numerically and high SNR closed form expression.

- To tackle the UT hardware limitations and the absence of the CSI at the UT, we develop modulation symbol detection scheme such that blind phase compensation is performed at the UT.

- To maximize the SE, we perform RAS method based on exhaustive search and show that the RAS is needed for MMSE RSM system operating in spatially correlated channels.

We show that ZF RSM and MMSE RSM schemes require RAS to work properly in the poor conditions of the outdoor mmWave propagation. Our proposed schemes consider exhaustive search based algorithms for RAS which is computationally complex. Thus, in Sec. 3.3.2, we propose novel fast and efficient RAS algorithms. Our main contributions are

- We show that sequential algorithms for RAS outperform the convex optimization methods. This is due to the relaxing of the optimization problem to fit a convex standard form.

- We develop novel ZF hybrid precoder that has the same performance as the FD precoder when channel is highly spatially sparse and outperforms the design in [73] in achievable rates, EE and complexity.

Wideband transmission is essential for mmWave systems to exploit the vast bandwidths available. However, at these huge BWs, signals suffer from intersymbol interference. Therefore, in Sec. 3.3.3, we extend our narrowband design into wideband by applying ZF FIR pre-equalizer at the transmitter to convert the multi-tap delay MIMO channel into single tap channel, specifically

- We propose a wideband single carrier RSM scheme based on a low complexity ZF time-domain FIR pre-equalizer with optimized delay for the UT narrowband architecture in [41] and no CSI at the UT and imperfect CSI at the BS.

- We study the impact of the channel angular spread and the number of delay tap channels on the minimum number of FIR taps.

- We show that we can attain high SE by applying RAS and we provide fast and efficient RAS algorithm based on QR decomposition [74].

With the aim of further improving to SE, MRF chains can be deployed at the UT to support multiple streams transmission. However, extending the SRF UT architecture to MRF is not straightforward due to the power consumption constraints. Hence, in Sec. 3.3.4, we develop more general RSM scheme by considering MRF chains at the UT. Utilizing PSs at the UT improves the beamforming/combining gains which boost the coverage of mmWave communications. Optimizing number of needed PSs, optimal mapping between PSs and antennas introduce challenging optimization problems. Thus, in Sec. 3.4, we propose a joint design of HTSM for the UL transmission and hybrid RSM (HRSM) for the DL transmission. The main contributions can be summarized as follows

- We propose novel UT architectures consisting of two stages analog beamformer in the UL and combiner in the DL. We consider an analog PS stage to attain high gain and combat the severe path-loss, and apply the analog switches stage to perform antenna selection and grouping to maximize the EE at the UT.

- We exploit the SM principles to transmit two streams (spatially modulated stream and conventionally modulated stream) using a single RF chain. Specifically, in the UL, we propose an HTSM scheme and present the analytical system model followed by two detection schemes. First, we apply an ML detector and prove closed form expressions of the SE using the mutual information. After that, we propose a reduced complexity detector with two combiners (optimal and equal ratio). In DL, we propose an HRSM scheme with a reduced complexity detector that can be implemented using the energy efficient UT architecture proposed in Fig. 2.3 and then, we prove a closed form expression of its SE.

- For the sake of reducing the computational complexity, we propose optimization algorithm to jointly design the precoder for the UL transmission and the combiner for the DL transmission with the purpose of maximising the EE at the UT. Specifically, the proposed algorithm jointly optimises the number of ULA PSs groups, the set of selected antennas per group and the transmit powers for the spatial symbols both in UL and DL transmissions.

- We evaluate the system performance by adopting a theoretical channel model and a realistic ray-trace based channel model to validate the results in real world like scenarios. Moreover, we compare the proposed scheme with state of the art SM and hybrid precoding systems.

3.3 Receive Spatial Modulation for Downlink Massive MIMO Transmission

In this section we present a holistic view of RSM schemes in the DL and single user systems. First, we illustrate in details RSM schemes based on SRF UT and narrowband transmission. Next, we introduce several antenna selection techniques that are necessary for RSM schemes to operate properly in the outdoor environment of the mmWave propagation. After that, we illustrate how to extend the RSM architecture and the scheme for wideband transmission and for MRF chains.

3.3.1 Single Radio Frequency Chain UT at Narrowband Transmission

3.3.1.1 System Model of ZF precoding RSM scheme

In this section. we consider the DL of a large MIMO single user that operates in the mmWave outdoor narrowband channel environment. We present a RSM system where the BS transmits modulation symbol from M size constellation and spatial symbol per channel use. We show that the optimal spatial symbol detector is a threshold detector that can be implemented by using one bit ADC. We derive closed form expressions for the detection threshold at different SNR regions showing that a simple threshold can be obtained at high SNR and its performance approaches the exact threshold. We derive expressions for the ABEP in the presence and absence of the threshold estimation error, and show that a small number of DL pilot symbols is needed. Simulation results show that the performance of the proposed system with good constellation design approaches the FD MIMO system. The work presented in this section is published in **[C2]**

The BS and UT are equipped with N_t and N_r antennas respectively. Based on the properties of mmWave propagation, we consider reciprocal propagation environment. We exploit the channel reciprocity by considering TDD system where the CSI is needed only at the BS. In Fig. 2.1, displayed in red, we consider a low complexity UL UT circuit based on analog PSs. During the UL training, the UT sends pilot symbols so that the BS can acquire the CSI. This can be achieved, since the optimal training pilot symbols matrix for the least squares channel estimation can be selected as a DFT basis [75] that can be implemented by PSs. Since massive mmWave MIMO systems suffer from high path loss and antenna correlation, antenna selection at the receiver is necessary. The BS selects the most suitable N_a antennas based on the channel knowledge (assumed perfect). After that, the BS informs the UT by the N_a ARA. The BS transmits data vector to the ARA that comprises spatial and modulation symbols. The transmitted data

vector can be written as

$$\mathbf{x}_i^j = \sqrt{\alpha P}\mathbf{B}\mathbf{s}_i x_j \tag{3.1}$$

where the spatial symbol $\mathbf{s}_i \in \mathbb{R}^{N_a \times 1}$ contains N_a bits from the input data bits, $i \in \{1, ..., 2^{N_a} - 1\}$, we assume that the all-zeros spatial symbol is not allowed, the modulation symbol x_j is a symbol from certain constellation with size M, $j \in \{1, ..., M\}$, the number of transmitted bits per data vector are $(N_a + \log_2 M)$, $\mathbf{B} \in \mathbb{C}^{N_t \times N_a}$ is the precoding matrix, P is the average transmit power and we adjust the transmitted power by a normalization factor $\alpha \approx \left(\mathrm{Tr}\left\{\mathbf{B}^H\mathbf{B}\right\}\right)^{-1}$ where $\mathrm{Tr}\{.\}$ is the trace operator. The received signal vector is given by

$$\mathbf{y} = \sqrt{\alpha P}\mathbf{H}\mathbf{B}\mathbf{s}_i x_j + \mathbf{n} \tag{3.2}$$

where $\mathbf{H} \in \mathbb{C}^{N_r \times N_t}$ is the channel matrix and $\mathbf{n} \in \mathbb{C}^{N_r \times 1}$ is the generated noise vector where its coefficients are i.i.d zero mean circularly symmetric complex Gaussian random variables and each has variance σ^2. Let us define the matrix $\mathbf{H}_a$ as the channel matrix from the BS to the selected ARAs. In order to direct the data vector to the ARA, we design the precoding matrix $\mathbf{B}$ as a ZF precoder that can be expressed as

$$\mathbf{B} = \mathbf{H}_a^H \left(\mathbf{H}_a\mathbf{H}_a^H\right)^{-1} \tag{3.3}$$

The received signal by the k-th active antenna can be expressed as

$$y_k = \sqrt{\alpha P}s_{ik}x_j + n_k \tag{3.4}$$

where $s_{ik} \in \{0, 1\}$. For a given N_a, the BS selects the best N_a ARA such that the received power is maximized that is, α is maximized, where $\alpha^{-1} = \mathrm{Tr}\left\{(\mathbf{H}_a\mathbf{H}_a^H)^{-1}\right\}$. The maximization of α can be done through the exhaustive search. A simple method for solving a similar problem was mentioned in [76]. Low complexity algorithms that exploit the sparse nature of the outdoor mmWave channel to maximize α were left for future work. We assume that the UT can be successfully informed by the ARA through a control channel. Imperfect detection to the ARA at the UT is a topic for future research.

According to equation (3.4), all the ARA associated to a spatial bit $s_{ik} = 1$ receive the same modulation symbol. The k-th ARA is connected to RF switch that passes the signal only if the estimated spatial bit $\hat{s}_{ik} = 1$. All of the signals that pass through the switches are combined. After that, the combined signal passes through RF chain and a single ADC to detect the modulation symbol. The

combined signal can be given as

$$y_c = \sum_{k=1}^{N_a} s_{ik}\hat{s}_{ik}\sqrt{\alpha P}x_j + \hat{s}_{ik}n_k \tag{3.5}$$

where the optimal $\hat{s}_{ik}$ detection scheme is shown in section 3.3.1.2. In order to avoid the case $y_c = 0$, we assume that the all-zeros transmit spatial symbol is not allowed.

The DL circuit in Fig. 2.1 (displayed in black lines) shows that each receive antenna is connected to RF AD. The AD works efficiently with high sensitivity and negligible power consumption at mmWave frequencies [61]. The signal provided by the AD at the k-th active antenna is

$$a_k = \sqrt{\left(\sqrt{\alpha P}s_{ik}x_{jI} + n_{kI}\right)^2 + \left(\sqrt{\alpha P}s_{ik}x_{jQ} + n_{kQ}\right)^2} \tag{3.6}$$

where the indices I and Q represent the in-phase and quadrature components. The probability density function (PDF) of the received amplitude at the k-th active antenna follows either a Rice or Rayleigh distributions [77]. The PDF of the received amplitude can be expressed as

$$f(a_k) = \begin{cases} \frac{2a_k}{\sigma^2} e^{-\frac{a_k^2+\alpha P}{\sigma^2}} \mathrm{I}_0\left(\frac{2a_k\sqrt{\alpha P}}{\sigma^2}\right) & \text{if} \quad s_{ik} = 1 \\ \frac{2a_k}{\sigma^2} e^{-\frac{a_k^2}{\sigma^2}} & \text{if} \quad s_{ik} = 0 \end{cases} \tag{3.7}$$

where $\mathrm{I}_0(x)$ is the zero order modified Bessel function of the first kind.

Channel model: mmWave channels have limited scattering clusters due to the high path loss. Moreover, using large arrays increases the antennas correlation. Therefore, we choose the narrowband clustered channel model that is widely used for outdoor mmWave channels [27]. This channel model is illustrated in Sec. 2.4.2.

Power consumption: The power consumption of the significant UT circuit components can be expressed in terms of reference power [28] as

$$P_{\text{RF chain}} = 2P_{\text{ref}} \qquad P_{\text{ADC}} = 10P_{\text{ref}} \qquad P_{\text{SW}} = 0.25P_{\text{ref}}$$

$$P_{\text{LNA}} = P_{\text{ref}} \qquad P_{\text{BB}} = N_{\text{RF}}P_{\text{ref}} \qquad P_{\text{PS}} = 1.5P_{\text{ref}} \tag{3.8}$$

where N_{RF} is the number of the RF chains, P_{SW} and P_{BB} are the switch and the base band power consumption respectively. The UL and DL power consumption at the UT with the proposed system P_{P} and with FD MIMO P_{FD} can be expressed

as

$$\begin{aligned} P_{\mathrm{P}} =& N_r(2P_{\mathrm{LNA}} + P_{\mathrm{PS}} + P_{\mathrm{SW}}) + 2\left(P_{\text{RF chain}} + P_{\mathrm{ADC}}\right) + P_{\mathrm{BB}} \\ P_{\mathrm{FD}} =& 2N_r\left(P_{\mathrm{LNA}} + P_{\text{RF chain}} + P_{\mathrm{ADC}}\right) + P_{\mathrm{BB}} \end{aligned} \tag{3.9}$$

The power consumption ratio $P_{\mathrm{P}}/P_{\mathrm{FD}} \approx (0.14 + \frac{0.9}{N_r})$. At 60 GHz and 500 MHz BW systems, $P_{\text{ref}} = 20\text{mW}$ [28], $N_r = 16$, $P_{\mathrm{P}} = 1700\text{mW}$ and $P_{\mathrm{FD}} = 8640\text{mW}$, the hybrid MIMO architecture consumes 8000mW [28].

3.3.1.2 Symbol Detection

Spatial Symbol Detection

In order to recover the spatial symbol, each ARA is connected to AD and one bit ADC as illustrated in Fig. 2.1. The AD measures the amplitude of the received signal and it is compared to a predefined threshold at the ADC. Thus, the output signals from the ADCs represent the spatial symbol. In the spatial symbol detection, we will show that both per antenna detection and joint detection lead to the same results.

Separate Spatial Symbol Detection

We consider ML detector per ARA to decide if the received spatial bit is one or zero. The detection problem per the k^{th} antenna can be formulated as

$$f(a_k|s_{ik}=1) \underset{\hat{s}_{ik}=0}{\overset{\hat{s}_{ik}=1}{\gtrless}} f(a_k|s_{ik}=0) \tag{3.10}$$

$$\frac{2a_k}{\sigma^2} e^{-\frac{a_k^2+\alpha P}{\sigma^2}} \mathrm{I}_0\left(\frac{2a_k\sqrt{\alpha P}}{\sigma^2}\right) \underset{\hat{s}_{ik}=0}{\overset{\hat{s}_{ik}=1}{\gtrless}} \frac{2a_k}{\sigma^2} e^{-\frac{a_k^2}{\sigma^2}} \tag{3.11}$$

$$e^{-\frac{\alpha P}{\sigma^2}} \mathrm{I}_0\left(\frac{2a_k\sqrt{\alpha P}}{\sigma^2}\right) \underset{\hat{s}_{ik}=0}{\overset{\hat{s}_{ik}=1}{\gtrless}} 1 \tag{3.12}$$

According to the problem in (3.12), the estimated spatial bit for the k-th antenna can be expressed as

$$\hat{s}_{ik} = \begin{cases} 1 & \text{if } a_k > \gamma \\ 0 & \text{if } a_k < \gamma \end{cases} \tag{3.13}$$

where γ is a threshold that results from solution of the problem in (3.12). In the following, we present three ways to determine γ based on the received SNR.

Exact Threshold We can obtain the exact value of the threshold directly by solving (3.12) numerically. However, this solution will increase the UT circuit

complexity.

Moderate SNR Approximation (MSA) At moderate SNR, we can approximate $\mathrm{I}_0(x) \approx \frac{e^x}{\sqrt{2\pi x}}$ in problem (3.12) and calculate the threshold by solving the following equation

$$\frac{\sigma^2}{4\pi\gamma\sqrt{\alpha P}} e^{\frac{4\gamma\sqrt{\alpha P}-2\alpha P}{\sigma^2}} = 1 \tag{3.14}$$

putting it in the form $xe^x = c$ as

$$\frac{-4\gamma\sqrt{\alpha P}}{\sigma^2} e^{\frac{-4\gamma\sqrt{\alpha P}}{\sigma^2}} = -\frac{1}{\pi} e^{-\frac{2\alpha P}{\sigma^2}} \tag{3.15}$$

The solution of the equation in (3.15) can be given by

$$\gamma = \frac{-\sigma^2}{4\sqrt{\alpha P}} \mathrm{W}_{-1}\left(-\frac{1}{\pi} e^{-2\frac{\alpha P}{\sigma^2}}\right) \tag{3.16}$$

where $\mathrm{W}_{-1}(x)$ is one of the main branches of the Lambert W function [78]. Nevertheless, we have to calculate the threshold in (3.16) numerically and this leads to increase in the UT circuit complexity.

High SNR Approximation (HSA) At high SNR, the left hand side of equation (3.14) takes either infinity or zero values based on the sign of the term in the exponential power. Therefore, we can obtain a simple threshold that can be expressed as

$$\gamma = \frac{1}{2}\sqrt{\alpha P} \tag{3.17}$$

Since the received modulation symbol may come from non-constant amplitude constellation, the exact, MSA and HSA thresholds should be designed based on the minimum received constellation symbol amplitude. This can be achieved by replacing the average power P by the minimum power $P_{min} = \beta P$ in thresholds expressions where β depends on the constellation.

Joint Spatial Symbol Detection

In order to jointly detect the spatial symbol bits, we apply the ML detector based on the received amplitudes from all of the active antennas. Since the received amplitudes are i.i.d, their joint PDF can be expressed as

$$f(\mathbf{a}) = \prod_{k=1}^{N_a} f(a_k) \tag{3.18}$$

The joint ML detection problem can be formulated as

$$\hat{\mathbf{s}}_i = \arg\max_{\mathbf{s}_i}\{f(\mathbf{a}|\mathbf{s}_i)\} \tag{3.19}$$

For the sake of simplicity, let us consider the case when the number of the ARA is two. In this case, the joint ML detection problem can be expressed as

$$\hat{\mathbf{s}}_i = \arg\max\{f_{01}, f_{10}, f_{11}\} \tag{3.20}$$

where $f_{nm} = f_{\mathbf{A}}\left(\mathbf{a}|s_{i1} = n, s_{i2} = m\right)$.

As an illustrative example, we decide symbol $[0\ 1]^T$ if the following conditions are satisfied

$$f_{01} = f_{00}f_2 > f_{10} = f_{00}f_1 \tag{3.21}$$
$$f_{01} = f_{00}f_2 > f_{11} = f_{00}f_1f_2 \tag{3.22}$$

where f_k can be given by

$$f_k = e^{-\frac{\alpha P}{\sigma^2}}\mathrm{I}_0\left(\frac{2a_k}{\sigma^2}\sqrt{\alpha P}\right) \tag{3.23}$$

Inequalities in (3.21) and (3.22) imply that $a_1 < \gamma$ and $a_2 > \gamma$ respectively. See equations (3.12) and (3.13) for more illustration. The analysis of the joint detection can be extended for any number of ARA. Therefore, the joint detection results are same as per antenna detection.

3.3.1.3 Downlink Training

The BS sends pilot modulation symbols to allow the UT estimates the detection threshold. We consider that the entries of the transmitted spatial symbol are all ones.

Amplitude Estimation

In order to estimate the detection threshold, the UT estimates the average received signal amplitude and the noise level from the outputs of the ADs connected to the ARA. The joint PDF of the received amplitudes can be expressed as

$$f(\mathbf{a}|\mathbf{1}_a) = \prod_{k=1}^{N}\frac{2a_{k1}}{\sigma^2}e^{-\frac{a_{k1}^2+\vartheta^2}{\sigma^2}}\mathrm{I}_0\left(\frac{2a_{k1}\vartheta}{\sigma^2}\right) \tag{3.24}$$

where $\mathbf{1}_a$ is all-ones spatial symbol, $\vartheta = \sqrt{\alpha P}$, a_{k1} is the measured amplitude at the k-th active antenna according to $s_{ik} = 1$, $N = N_p N_a$ and N_p is the number of pilot symbols. We design the amplitude estimator $\hat{\vartheta}$ so as to maximize

$$\log f(\mathbf{a}|\mathbf{1}_a) = \sum_{k=1}^{N} \log\left(\frac{2a_{k1}}{\sigma^2}\right) - \frac{a_{k1}^2 + \vartheta^2}{\sigma^2} + \log \mathrm{I}_0\left(\frac{2a_{k1}\vartheta}{\sigma^2}\right) \tag{3.25}$$

By using the fact that $\mathrm{I}_0(x) = \frac{e^x}{\sqrt{2\pi x}}$ for large x, we can simplify equation (3.133) as

$$\log \mathrm{I}_0\left(\frac{2a_{k1}\vartheta}{\sigma^2}\right) = \frac{2a_{k1}\vartheta}{\sigma^2} - \frac{1}{2}\log\frac{4\pi a_{k1}\vartheta}{\sigma^2} \tag{3.26}$$

In order to find the ML amplitude estimator $\hat{\vartheta}_{ML}$, we solve the problem, $\frac{\partial}{\partial\vartheta}\log f(\mathbf{a}|\mathbf{1}_a) = 0$, that can be expressed as

$$\sum_{k=1}^{N}\left(\frac{-2\vartheta}{\sigma^2} + \frac{2a_{k1}}{\sigma^2} - \frac{1}{2\vartheta}\right) = 0 \tag{3.27}$$

From (3.27), the $\hat{\vartheta}_{ML}$ can be expressed as

$$\hat{\vartheta}_{ML} = \frac{\sum_{k=1}^{N} a_{k1}}{2N} + \frac{1}{2}\sqrt{\left(\frac{\sum_{k=1}^{N} a_{k1}}{N}\right)^2 - \sigma^2} \tag{3.28}$$

The ML estimator of the noise variance $\hat{\sigma}_{ML}^2$ can be obtained by solving $\frac{\partial}{\partial\sigma^2}\log f(\mathbf{a}|\mathbf{1}_a) = 0$ as

$$\hat{\sigma}_{ML}^2 = \frac{2}{N}\sum_{k=1}^{N}(a_{k1} - \vartheta)^2 \tag{3.29}$$

By solving the equations in (3.28,3.29) simultaneously, a closed form expression for the $\hat{\vartheta}_{ML}$ can be given as

$$\hat{\vartheta}_{ML} = \frac{2\sum_{k=1}^{N} a_{k1}}{3N} + \frac{1}{3}\sqrt{4\left(\frac{\sum_{k=1}^{N} a_{k1}}{N}\right)^2 - \frac{3}{N}\sum_{k=1}^{N} a_{k1}^2} \tag{3.30}$$

3.3.1.4 Error Analysis

We evaluate the proposed system performance based on the ABEP that can be expressed as

$$\text{ABEP} = \frac{N_a P_{es} + \log_2 M P_{em}}{N_a + \log_2 M} \tag{3.31}$$

where P_{es} and P_{em} are the spatial and modulation bit error probabilities respectively that can be given by

$$P_{es} = 0.5\,(P_1 + P_0) \tag{3.32}$$

where $P_1 = \Pr\,(a_{k1} < \gamma)$ and $P_0 = \Pr\,(a_{k0} > \gamma)$.

$$P_{em} = \sum_{i=1}^{2^{N_a}-1} \sum_{n=1}^{2^{N_a}} \mathrm{BEP}\,(x_j \in \mathcal{C}_M | \hat{\mathbf{s}}_n, \mathbf{s}_i)\,\Pr\,(\hat{\mathbf{s}}_n | \mathbf{s}_i)\,\Pr\,(\mathbf{s}_i) \tag{3.33}$$

where $\mathrm{BEP}\,(x_j \in \mathcal{C}_M)$ is the bit error probability of M-QAM, M-PSK or M-amplitude-phase-shift-keying (M-APSK) with rings ratio r [79]. The probabilities in equation (3.33) can be expressed as

$$\mathrm{BEP}\,(x_j \in \mathcal{C}_M | \hat{\mathbf{s}}_n, \mathbf{s}_i) = \mathrm{BEP}\,(x_j \in \mathcal{C}_M | \mathrm{SNR_c}) \tag{3.34}$$

$$\mathrm{SNR_c} = \frac{(b_{in}^{11})^2}{b_{in}^{11} + b_{in}^{01}} \frac{\alpha P}{\sigma^2} \tag{3.35}$$

$$\Pr\,(\hat{\mathbf{s}}_n | \mathbf{s}_i) = P_1^{b_{in}^{10}} (1 - P_1)^{b_{in}^{11}} P_0^{b_{in}^{01}} (1 - P_0)^{b_{in}^{00}} \tag{3.36}$$

$$\Pr\,(\mathbf{s}_i) = \frac{1}{2^{N_a} - 1} \tag{3.37}$$

where $b_{in}^{(m_1 m_2)}$ is the number of entries in $\mathbf{s}_i$ that each one of them equals m_1 and its corresponding entry in $\hat{\mathbf{s}}_n$ equals m_2 and $\sum_{m_1, m_2 \in \{0,1\}} b_{in}^{(m_1 m_2)} = N_a$.

Perfect Threshold

If the UT knows the threshold γ perfectly, the probabilities P_1 and P_0 can be expressed by the cumulative density function (CDF) of Rice and Rayleigh distributions [77] as

$$\begin{aligned} P_1 &= 1 - Q_1\left(\frac{1}{\sigma}\sqrt{2\alpha P}, \frac{1}{\sigma}\sqrt{2}\gamma\right) \\ P_0 &= e^{-\frac{\gamma^2}{\sigma^2}} \end{aligned} \tag{3.38}$$

where $Q_1(x)$ is the first order Marcum Q-function.

Estimated HSA Threshold

The ML estimator is asymptotically gaussian and we consider that the gaussianity is prevailed. The estimated HSA threshold $\hat{\gamma} \sim \mathcal{N}(\mu_{\hat{\gamma}}, \sigma_{\hat{\gamma}}^2)$ where $\mu_{\hat{\gamma}}$ and $\sigma_{\hat{\gamma}}^2$ are the mean and variance of $\hat{\gamma}$. Since the received amplitudes are positive, we can

express P_1 and P_0 as

$$\begin{aligned} P_1 &= \Pr\left(\frac{\hat{\gamma}}{a_{k1}} > 1\right) \\ P_0 &= \Pr\left(\frac{\hat{\gamma}}{a_{k0}} < 1\right) \end{aligned} \tag{3.39}$$

In order to find the probabilities in equation (3.39), we put it in the following form

$$\begin{aligned} P_1 &= \Pr\left(t_{\delta,n,l} > \frac{\sigma}{\sigma_{\hat{\gamma}}}\right) \\ P_0 &= \Pr\left(t_{\delta,n} < \frac{\sigma}{\sigma_{\hat{\gamma}}}\right) \end{aligned} \tag{3.40}$$

where $t_{\delta,n}$ is Non-central t distribution, $t_{\delta,n,l}$ is Doubly-non-central t distribution [80], n is the degrees of freedom, δ, l are the non-centrality parameters, $\delta = \frac{\mu_{\hat{\gamma}}}{\sigma_{\hat{\gamma}}}$, n=2 and $l = \frac{2\alpha P}{\sigma^2}$. A closed form expressions for P_1 and P_0 with threshold estimation error can be given as

$$\begin{aligned} P_1 &= 1 - T_{\delta,n,l}\left(\frac{\sigma}{\sigma_{\hat{\gamma}}}\right) \\ P_0 &= T_{\delta,n}\left(\frac{\sigma}{\sigma_{\hat{\gamma}}}\right) \end{aligned} \tag{3.41}$$

where $T_{\delta,n}$ and $T_{\delta,n,l}$ are the cumulative density functions of Non-central and Doubly-non-central t distributions [80].

In order to determine the probabilities in equation (3.41), we need the mean and the variance of $\hat{\gamma}$. The estimated HSA threshold $\hat{\gamma}$ can be expressed as

$$\hat{\gamma} = \frac{1}{2}\hat{\vartheta}_{ML} \tag{3.42}$$

From the asymptotic properties of the ML estimator [51], the mean and variance of $\hat{\gamma}$ can be expressed as

$$\mu_{\hat{\gamma}} = \frac{1}{2}\vartheta \tag{3.43}$$

$$\sigma^2_{\hat{\gamma}} = \frac{1}{4}\left[\mathbf{I}_\theta^{-1}\right]_{11} \tag{3.44}$$

where $\mathbf{I}_\theta$ is a 2×2 fisher information matrix [51] whose elements can be expressed as

$$[\mathbf{I}_\theta]_{11} = -\,\mathrm{E}\left[\frac{\partial^2 f(\mathbf{a}|\mathbf{1}_a)}{\partial \vartheta^2}\right] = \frac{2N}{\sigma^2} - \frac{N}{2\vartheta^2}$$

$$
\begin{aligned}
[\mathbf{I}_\theta]_{12} &= [\mathbf{I}_\theta]_{21} = -\,\mathrm{E}\left[\frac{\partial^2 f(\mathbf{a}|\mathbf{1}_a)}{\partial\vartheta\partial\sigma^2}\right] = \frac{2N}{\sigma^4}\left(\mu_1 - \vartheta\right) \\
[\mathbf{I}_\theta]_{22} &= -\,\mathrm{E}\left[\frac{\partial^2 f(\mathbf{a}|\mathbf{1}_a)}{\partial\sigma^2\partial\sigma^2}\right] \\
&= \frac{2N}{\sigma^6}\left(\mu_2 + \vartheta^2 - 2\vartheta\mu_1\right) - \frac{N}{2\sigma^4}
\end{aligned} \tag{3.45}
$$

where E[.] is the expectation operator, $\mu_1 = \mathrm{E}[a_{k1}]$ and $\mu_2 = \mathrm{E}[a_{k1}^2]$. The inverse of the fisher information matrix can be expressed as

$$
\mathbf{I}_\theta^{-1} = \frac{1}{[\mathbf{I}_\theta]_{11}[\mathbf{I}_\theta]_{22} - [\mathbf{I}_\theta]_{12}^2}\begin{bmatrix} [\mathbf{I}_\theta]_{22} & -[\mathbf{I}_\theta]_{12} \\ -[\mathbf{I}_\theta]_{21} & [\mathbf{I}_\theta]_{11} \end{bmatrix} \tag{3.46}
$$

From equations (3.44,3.46), the variance $\sigma_{\hat{\gamma}}^2$ can be given as

$$
\sigma_{\hat{\gamma}}^2 = \frac{1}{4}\frac{[\mathbf{I}_\theta]_{22}}{[\mathbf{I}_\theta]_{11}[\mathbf{I}_\theta]_{22} - [\mathbf{I}_\theta]_{12}^2} \tag{3.47}
$$

3.3.1.5 Simulation Results of ZF precoding RSM scheme

In this section, we present simulation results that show the performance of the proposed system. In simulation environment, we consider that g_{il} are i.i.d $\mathcal{CN}(0,\, \sigma_g^2)$ where σ_g^2 is designed such that $\mathrm{E}\left[\mathrm{Tr}\left\{\mathbf{H}^H\mathbf{H}\right\}\right] = N_t N_r$, $N_c = 8$, $N_y = 10$ [27], the elevation and azimuth angles (θ_{il}, ϕ_{il}) have Laplacian distributions with uniform random means (θ_i, ϕ_i) and angular spreads $\sigma_\theta = \sigma_\phi = 1$, SNR $= \frac{P}{\sigma^2}$, the width of the transmission angle is 50° and the user has omni-directional antenna array. We compare the performance of the proposed system with SVD based precoding and decoding of the FD MIMO system. We allocate the power at SVD such that all of the activated modes achieve the same received SNR [81]. Fig. 3.1 shows the ABEP of the proposed system with exact threshold compared to FD MIMO at 32×8 MIMO system. The performance of the proposed system without RAS is inferior to that with antenna selection. Moreover, the proposed system performance with constant amplitude constellation and 4 spatial bits approaches the FD MIMO. The optimal values of spatial, modulation bits and constellation design to minimize the ABEP are topics for future research.

Fig. 3.2 represents the ABEP of the proposed system at different thresholds and different numbers of receive antennas. Applying HSA threshold leads to the lowest complexity and the performance gap is less than 1 dB with respect to the exact threshold. The ABEP with threshold estimation error is very close to that with perfect threshold by using only one DL pilot symbol. Increasing the number

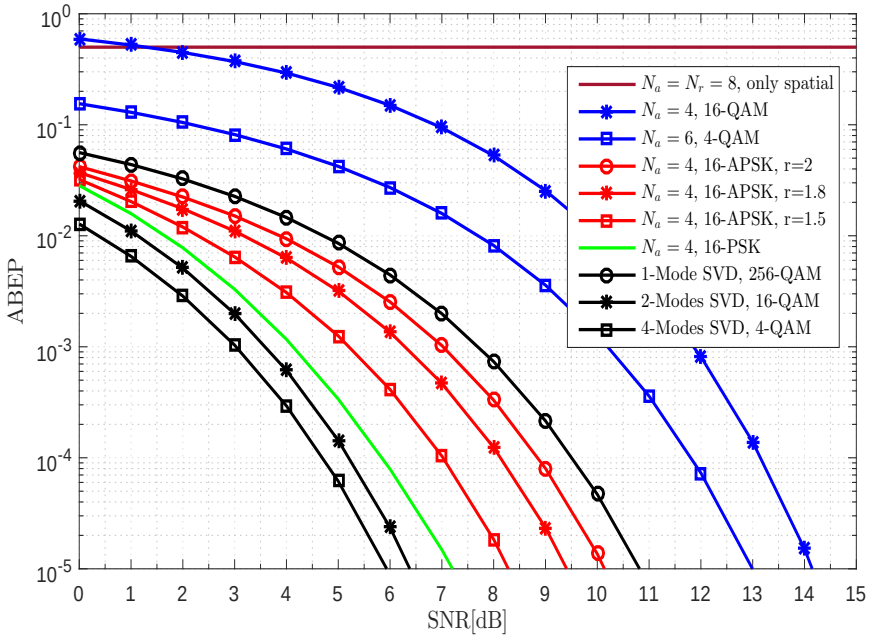

Figure 3.1: Average bit error probability of the proposed system and FD MIMO at different constellation designs and 8 transmit bits per data vector.

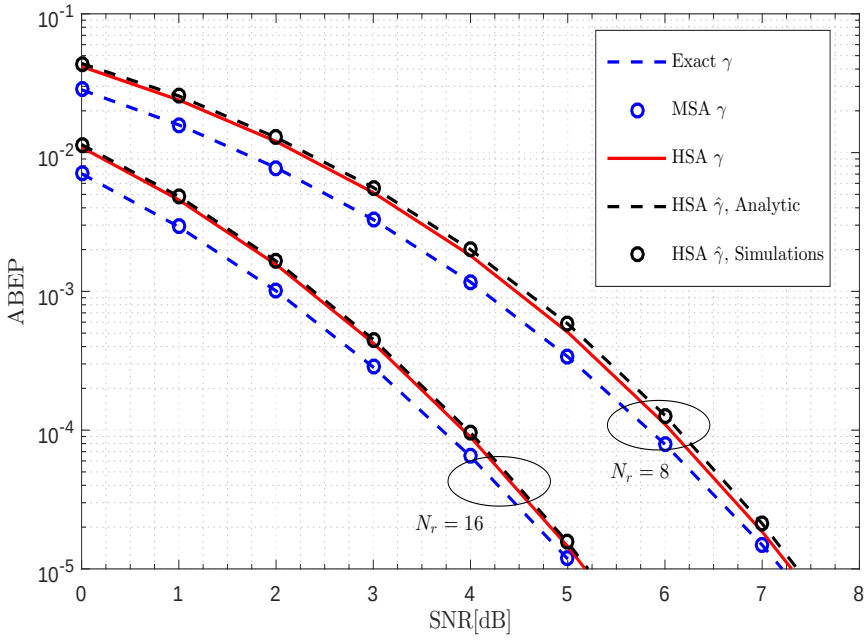

Figure 3.2: Average bit error probability of the proposed system at $N_t = 32$, $N_a = 4$, 16-PSK, perfect and estimated thresholds.

of receive antennas while N_a is fixed boosts the receive antennas gain and as a result the ABEP is improved.

3.3.1.6 MMSE Precoding RSM

MMSE precoding outperforms ZF precoding in correlated MIMO channels. However, extending the proposed architecture is not straightforward due to the hardware limitations and the absence of the CSI at the UT. Therefore, we propose a RSM scheme based on MMSE precoding considering total and per antenna (more practical) power constraints. The main contributions are published in **[C4]** and can be summarized as follows

- We derive semi-closed form expression for the ML spatial symbol detector that can be evaluated numerically and high SNR closed form expression.
- We develop modulation symbol detection scheme such that blind phase compensation is performed at the UT.
- We perform RAS method to maximize the mutual information based on exhaustive search and show that the RAS is needed for MMSE RSM system operating in spatially correlated channels.
- We show that the proposed MMSE RSM scheme with TPC and with PAPC at the BS outperforms the ZF RSM in terms of average and outage mutual information.

Bit to symbol mapping

In [41], the BS transmits two symbols per channel use, spatial symbol $\mathbf{s}_i \in \mathbb{R}^{N_r \times 1}$ comprises N_r input bits and modulation symbol x_j from M-ary constellation. The transmit vector at the precoder input is $(\mathbf{x}_i^j = \mathbf{s}_i x_j)$ where the number of transmit bits per channel use equal $(N_r + \log_2 M)$. According to this mapping, we lose x_j if $\mathbf{s}_i$ is all zeros vector. Hence, in [41], the authors assume that the all zeros $\mathbf{s}_i$ is not allowed. However, this assumption entails significant SE loss if N_r is small. Thus, we modify this mapping such that

$$\mathbf{x}_i^j = \begin{cases} \mathbf{s}_i x_j & \text{if} \quad \mathbf{s}_i \neq \mathbf{0}_{N_r} \\ \mathbf{s}_i & \text{if} \quad \mathbf{s}_i = \mathbf{0}_{N_r} \end{cases} \tag{3.48}$$

we consider the all zeros $\mathbf{s}_i$ but do not transmit x_j with it.

The received signal vector can be expressed as

$$\mathbf{y} = \mathbf{H}\mathbf{P}\mathbf{s}_i x_j + \mathbf{n} \tag{3.49}$$

where $\mathbf{n} \in \mathbb{C}^{N_a \times 1}$ is a noise vector has i.i.d $\mathcal{CN}(0, \sigma^2)$ entries, the precoding matrix

$\mathbf{P} \in \mathbb{C}^{N_t \times N_a}$ is fixed during the coherence time and satisfies

$$\mathrm{E}\big[\|\mathbf{P}\mathbf{s}_i x_j\|_2^2\big] = \mathrm{Tr}\left\{\mathbf{P}\mathbf{R}_{ss}\mathbf{P}^H\right\} = P_t. \tag{3.50}$$

where $\mathbf{R}_{ss} = \mathrm{E}\big[\mathbf{s}_i\mathbf{s}_i^H\big]$ and P_t is the transmit power.

In the sequel, we consider MMSE precoding with PAPC and TPC and develop the detection technique. Let us consider the MMSE precoding matrix ($\mathbf{P} = \tilde{\mathbf{P}}/\sqrt{\beta}$) where β is used for adjusting the transmit power at the BS and for scaling the desired signal at the UT [82]. The MSE can be expressed as

$$\mathrm{E}\left[\left\|\sqrt{\beta}\mathbf{y} - \mathbf{s}_i x_j\right\|_2^2\right] = \left\|(\mathbf{H}\tilde{\mathbf{P}} - \mathbf{I}_{N_r})\mathbf{R}_{ss}^{\frac{1}{2}}\right\|_F^2 + \sigma^2 N_r \beta \tag{3.51}$$

As it will be illustrated in section (3.3.1.7), the matrix $\mathbf{HP}$ has to be symmetric to allow blind phase compensation to the modulation symbol. Thus, the design problem of the MMSE precoder with PAPC (MMSEPAPC) can be expressed as

$$\text{(P1)} \begin{cases} \min\limits_{\tilde{\mathbf{P}},\beta} & \left\|(\mathbf{H}\tilde{\mathbf{P}} - \mathbf{I}_{N_r})\mathbf{R}_{ss}^{\frac{1}{2}}\right\|_F^2 + \sigma^2 N_r \beta \\ \text{s.t.} & \left[\tilde{\mathbf{P}}\mathbf{R}_{ss}^{\frac{1}{2}}\right]_{(k,:)}^H \left[\tilde{\mathbf{P}}\mathbf{R}_{ss}^{\frac{1}{2}}\right]_{(k,:)} \leqslant \beta\frac{P_t}{N_t}, \\ & \qquad\qquad\qquad\qquad k = 1, \cdots, N_t. \\ & \mathbf{H}\tilde{\mathbf{P}} = \tilde{\mathbf{P}}^H\mathbf{H}^H. \end{cases} \tag{3.52}$$

where problem (P1) is convex quadratic constrained quadratic program that can be solved by software packages like CVX [56].

A closed form expression of the MMSE precoder with TPC (MMSETPC) [82] can be obtained by replacing the PAPC in problem (P1) with a TPC ($\mathrm{Tr}\left\{\tilde{\mathbf{P}}\mathbf{R}_{ss}\tilde{\mathbf{P}}^H\right\} \leqslant \beta P_t$) and dropping the symmetry constraint ($\mathbf{H}\tilde{\mathbf{P}} = \tilde{\mathbf{P}}^H\mathbf{H}^H$) as follows

$$\begin{aligned} \tilde{\mathbf{P}} &= \mathbf{H}^H\left(\mathbf{H}\mathbf{H}^H + \frac{\sigma^2 N_r}{P_t}\mathbf{I}_{N_r}\right)^{-1} \\ \beta &= \mathrm{Tr}\left\{\tilde{\mathbf{P}}\mathbf{R}_{ss}\tilde{\mathbf{P}}^H\right\}/P_t \end{aligned} \tag{3.53}$$

Although we drop the symmetry constraint, the precoder in equation (3.53) satisfies the symmetric property ($\mathbf{H}\tilde{\mathbf{P}} = \tilde{\mathbf{P}}^H\mathbf{H}^H$) as illustrated in the sequel.

$$\begin{aligned} \mathbf{H}\tilde{\mathbf{P}} &= \mathbf{H}\mathbf{H}^H\left(\mathbf{H}\mathbf{H}^H + c\mathbf{I}_{N_r}\right)^{-1} \\ \tilde{\mathbf{P}}^H\mathbf{H}^H &= \left(\mathbf{H}\mathbf{H}^H + c\mathbf{I}_{N_r}\right)^{-1}\mathbf{H}\mathbf{H}^H \end{aligned} \tag{3.54}$$

According to the matrix inversion lemma [83]

$$\mathbf{A}\left(\mathbf{A}+c\mathbf{I}_{Nr}\right)^{-1}=\left(\mathbf{A}+c\mathbf{I}_{Nr}\right)^{-1}\mathbf{A} \tag{3.55}$$

equation (3.54) shows that $\mathbf{H}\tilde{\mathbf{P}}$ is symmetric.

3.3.1.7 MMSE Detection

The received signal by the k-th antenna can be expressed as

$$y_k=\underbrace{\left[\mathbf{HP}\right]_{k,k}s_{ik}x_j+\sum_{l\neq k}\left[\mathbf{HP}\right]_{k,l}s_{il}x_j}_{r_k}+n_k \tag{3.56}$$

where s_{ik} is the k-th bit of the spatial symbol $\mathbf{s}_i$.

The spatial symbol detection based on joint processing of the signals received by all antennas requires complex receiver architecture. For the sake of reducing the receiver hardware complexity, we consider per antenna spatial symbol detection where we can exploit energy efficient devices (amplitude detectors, 1-bit analog-to-digital-converters) represented in Fig. 2.1 in the spatial symbol detection. The output signal from the k-th AD can be expressed as

$$a_k=\left|y_k\right| \tag{3.57}$$

The PDF of the k-th received amplitude (a_k) given the k-th transmit spatial bit (s_{ik}) is

$$f(a_k\mid s_{ik}=m)=\sum_{i=1}^{2^{N_r-1}}f(a_k\mid s_{ik},\tilde{\mathbf{s}}_i)\Pr\left(\tilde{\mathbf{s}}_i\right) \tag{3.58}$$

where $\tilde{\mathbf{s}}_i\in\mathbb{R}^{N_r-1\times 1}$ equals $\mathbf{s}_i$ without s_{ik} and $m\in\{0,1\}$. Equation (3.58) is weighted sum of Rice distributions [77] and can be expressed as

$$f(a_k|s_{ik}=m)=\frac{1}{2^{N_r-1}}\sum_{i=1}^{2^{N_r-1}}\frac{2a_k}{\sigma^2}e^{-\frac{a_k^2+a_{m,ik}^2}{\sigma^2}}\mathrm{I}_0\left(\frac{2a_ka_{m,ik}}{\sigma^2}\right) \tag{3.59}$$

where $a_{m,ik}=\left|r_{k|s_{ik}=m}\right|$ and $\mathrm{I}_0\left(x\right)$ is the zero order modified bessel function of the first kind.

MMSE spatial symbol detection

The received spatial bit per antenna can be either one or zero, thus we can detect

it by applying ML detector per receive antenna as follows

$$f(a_k|s_{ik}=1) \underset{\hat{s}_{ik}=0}{\overset{\hat{s}_{ik}=1}{\gtrless}} f(a_k|s_{ik}=0) \tag{3.60}$$

$$\hat{s}_{ik} = \begin{cases} 1 & \text{if } a_k > \gamma_k \\ 0 & \text{if } a_k < \gamma_k \end{cases}, \gamma_k = \left\{ a_k \left| \frac{f(a_k|s_{ik}=1)}{f(a_k|s_{ik}=0)} = 1 \right. \right\} \tag{3.61}$$

$$\gamma_k = \left\{ a_k \left| \frac{\sum_{i=1}^{2^{N_r-1}} e^{-\frac{a_{1,ik}^2}{\sigma^2}} \mathrm{I}_0\left(\frac{2a_k a_{1,ik}}{\sigma^2}\right)}{\sum_{i=1}^{2^{N_r-1}} e^{-\frac{a_{0,ik}^2}{\sigma^2}} \mathrm{I}_0\left(\frac{2a_k a_{0,ik}}{\sigma^2}\right)} = 1 \right. \right\} \tag{3.62}$$

where equation (3.62) can be solved numerically at the BS to obtain γ_k, then the BS informs the UT about γ_k through low DL training overhead.

Approximate γ_k: with the aim of reducing the computational complexity at the BS, γ_k can be obtained in closed form by applying the high SNR assumption (HSA) ($\mathrm{I}_0(x) \approx \frac{e^x}{\sqrt{2\pi x}}$) to $f(a_k|s_{ik}=1)$ as follows

$$f(a_k|s_{ik}=1) \propto e^{-\frac{\min\left(a_{1,ik}^2\right) - 2\min\left(a_{1,ik}\right)\gamma_k}{\sigma^2}} \tag{3.63}$$

where at high SNR the exponential term in equation (3.63) tends to zero or infinity if the exponent is negative or positive, respectively. Thus, the HSA threshold can be expressed as

$$\gamma_k \approx \frac{1}{2}\min(a_{1,ik}) \tag{3.64}$$

MMSE modulation symbol detection

We consider one RF chain and one high precision ADC at the UT to detect the modulation symbol x_j. In order not to accumulate noise at the RF chain, $\hat{s}_{ik}$ controls switch in such a way that y_k goes to the RF chain only if $\hat{s}_{ik} = 1$. The combined signal y_c (shown in Fig. 2.1) can be expressed as

$$y_c = \sum_{k=1}^{N_r} \hat{s}_{ik} y_k = \alpha_i x_j + n_c \tag{3.65}$$

where α_i is a complex gain and n_c is the combined noise.

Worst case detection: In the worst case, we can detect the modulation symbol x_j only if the detected spatial symbol is error free ($\hat{s}_{ik} = s_{ik}$). In this case, we show that the phase of the modulation symbol does not change after combining and as a result no phase compensation is needed. From equations (3.56) and (3.128), α_i

without spatial errors, can be expressed as

$$\alpha_i = \sum_{k\in\{s_{ik}=1\}} [\mathbf{HP}]_{k,k} + \frac{1}{2} \sum_{\substack{k\in\{s_{ik}=1\} \\ l\in\{s_{ik}=1\}, l\neq k}} [\mathbf{HP}]_{k,l} + [\mathbf{HP}]_{l,k} \tag{3.66}$$

Thanks to the symmetry of the matrix **HP**, α_i in equation (3.66) becomes real positive gain, and therefore the phase of x_j in equation (3.128) does not change after combining.

Estimation of the detection thresholds for MMSE RSM

The UT needs the thresholds $(\gamma_1, \cdots, \gamma_{N_r})$ obtained in equation (3.62) for spatial symbol detection. During the DL training, the BS sends these thresholds to the UT. The accuracy of the estimated thresholds affect the system performance, thus the DL pilot symbols are designed in such a way that the k-th received signal vector can be expressed as

$$\mathbf{y}_{k,dl} = \gamma_k \mathbf{1}_{N_r} + \mathbf{n} \tag{3.67}$$

A closed form for the ML estimator $(\hat{\gamma}_k)$ has been proved in equation (33) in [41]. The number of needed pilot symbols is N_r to estimate N_r distinct thresholds.

From the asymptotic properties of the ML estimator, $\hat{\gamma}_k$ can be considered as a Gaussian random variable such that

$$\hat{\gamma}_k \sim \mathcal{N}(\gamma_k, \sigma_k^2), \quad \sigma_k^2 = [\mathbf{I}_\theta]_{k,k}^{-1} \tag{3.68}$$

where $\sigma_k^2 \propto \frac{1}{N_r}$ is the estimator variance and $\mathbf{I}_\theta$ is the fisher information matrix [51].

3.3.1.8 Mutual Information

In this section, we consider the mutual information as a performance metric to compare the proposed scheme with the state of the art. We show that the binary asymmetric channel (BAC) and the multiple-input-single-output (MISO) channel can be used to describe the mutual information of the spatial and modulation symbols, respectively. We provide expressions for the mutual information based on perfect and estimated thresholds. According to the mutual information of the RSM system in equation (22) in [42], the mutual information of the proposed scheme can similarly be expressed as

$$I(\mathbf{s}, x; \hat{\mathbf{s}}, y_c) = I(\mathbf{s}; \hat{\mathbf{s}}) + I(x; y_c|\hat{\mathbf{s}}, \mathbf{s}) \triangleq I_s + I_m \tag{3.69}$$

where I_s and I_m are the spatial and modulation mutual information, respectively.

Spatial symbol mutual information

As we consider independent per antenna spatial detection, the spatial mutual information can be expressed as

$$I_s = \sum_{k=1}^{N_r} I\left(s_k; \hat{s}_k\right) \tag{3.70}$$

where $I\left(s_k; \hat{s}_k\right)$ can be obtained using the BAC [84] as follows

$$\begin{aligned} I\left(s_k; \hat{s}_k\right) = &\mathcal{H}\left(p_1 P_{1k} + p_0(1 - P_{0k})\right) \\ &- p_1 \mathcal{H}\left(P_{1k}\right) - p_0 \mathcal{H}\left(1 - P_{0k}\right) \end{aligned} \tag{3.71}$$

where $\mathcal{H}(x)$ is the entropy function [85], $p_1 = \Pr(s_k = 1) = \frac{1}{2}$, $p_0 = \Pr(s_k = 0) = \frac{1}{2}$, and P_{mk} is the probability of the k-th antenna to receive $s_k = m$ that can be expressed as

$$P_{mk} = \sum_{i=1}^{2^{N_r - 1}} \Pr\left(a_k \underset{m=0}{\overset{m=1}{\gtrless}} \gamma_k \mid \tilde{\mathbf{s}}_i\right) \Pr\left(\tilde{\mathbf{s}}_i\right) \tag{3.72}$$

If γ_k is perfectly known at the UT, the probability $\Pr\left(a_k > \gamma_k \mid \tilde{\mathbf{s}}_i\right)$ can be computed using the CDF of Rice distribution [77] as follows

$$\Pr\left(a_k > \gamma_k \mid \tilde{\mathbf{s}}_i\right) = Q_1\left(\tfrac{\sqrt{2}|r_k|}{\sigma}, \tfrac{\sqrt{2}\gamma_k}{\sigma}\right) \tag{3.73}$$

The probability $\Pr\left(a_k > \hat{\gamma}_k \mid \tilde{\mathbf{s}}_i\right)$ by considering the estimated threshold in equation (3.68) can be expressed as

$$\Pr\left(a_k > \hat{\gamma}_k \mid \tilde{\mathbf{s}}_i\right) = \Pr\left(\tfrac{\hat{\gamma}_k}{a_k} < 1 \mid \tilde{\mathbf{s}}_i\right) = T_{\delta,n,l}\left(\tfrac{\sigma}{\sigma_k}\right) \tag{3.74}$$

where $T_{\delta,n,l}(\sigma/\sigma_k)$ is the CDF of doubly-non-central t distribution [80] with $\delta = \frac{\gamma_k}{\sigma_k}$, $n = 2$ and $l = \frac{2|r_k|^2}{\sigma^2}$.

Modulation symbol mutual information

Although we consider multiple antennas at the UT, the combined signal at the UT comprises only one modulation symbol that passes through a SRF chain as illustrated in equation (3.128). Therefore, I_m in equation (3.69) can be computed using the expression of the mutual information of MISO channel. In [41], the authors showed that the M-PSK constellation can achieve the best performance for the same RSM architecture. Thus, we consider the mutual information expression

based M-PSK symbols [86]. From equation (3.69), I_m can be expressed as

$$I_m = \sum_{i=1}^{2^{N_r}-1} \Pr(\mathbf{s}_i) \sum_{j=1}^{2^{N_r}} \Pr(\hat{\mathbf{s}}_j|\mathbf{s}_i)\, I_{m-\mathrm{MPSK}}(x; y_c)_{|_{\mathbf{s}_i,\hat{\mathbf{s}}_j}} \tag{3.75}$$

$$\Pr(\hat{\mathbf{s}}_j|\mathbf{s}_i) = \prod_{k=1}^{N_r} \Pr\left(a_k \underset{\hat{s}_{jk}=0}{\overset{\hat{s}_{jk}=1}{\gtrless}} \gamma_k \mid \mathbf{s}_i \right), \Pr(\mathbf{s}_i) = \frac{1}{2^{N_r}} \tag{3.76}$$

We consider the worst case detection such that

$$I_{m-\mathrm{MPSK}} = \begin{cases} 0 & \text{if } \hat{\mathbf{s}}_j \neq \mathbf{s}_i \\ \frac{1}{2}\log_2 \frac{4\pi}{\mathrm{e}} \frac{\alpha_i^2}{\left(\sum_{k=1}^{N_r} s_{ik}\right)\sigma^2} & \text{if } \hat{\mathbf{s}}_j = \mathbf{s}_i \end{cases} \tag{3.77}$$

In this case, I_m can be expressed as

$$I_m = \frac{1}{2^{N_r}} \sum_{i=1}^{2^{N_r}-1} \frac{1}{2}\log_2 \frac{4\pi}{\mathrm{e}} \frac{\alpha_i^2}{\left(\sum_{k=1}^{N_r} s_{ik}\right)\sigma^2} \Pr(\hat{\mathbf{s}}_i|\mathbf{s}_i) \tag{3.78}$$

3.3.1.9 Simulation Results of MMSE precoding RSM scheme

In this section, we compare the performance of the proposed MMSE RSM scheme with the state of the art (ZF RSM) under TPC and PAPC at the BS. A ZF RSM scheme based the energy efficient UT architecture in Fig. 2.1 has been developed in [41] under TPC and extending this scheme to PAPC can be easily obtained through convex second-order cone programming [87]. In simulations, we consider that $L = 16$, $\mathrm{SNR} = P_t/\sigma^2$, $(\phi_i \in [-\pi/6, \pi/6], \theta_i \in [-\pi, \pi])$ are uniformly distributed , $g_i \sim \mathcal{CN}(0, \sigma_g^2)$ and σ_g^2 satisfies $\mathrm{E}\left[\mathrm{Tr}\{\mathbf{H}^H\mathbf{H}\}\right] = N_t N_r$.

Fig. 3.3 shows the mutual information of the proposed MMSE RSM and the ZF RSM under TPC and PAPC at the BS. The achievable mutual information of the MMSE RSM outperforms that of the ZF RSM specifically at large N_r. This is because the received power in ZF precoding could reach zero when N_r approaches L. Thus, RSM systems with RAS are shown to achieve higher rates that not decrease with N_r. RAS is performed by exhaustive search to maximize its mutual information and updated per the coherence time.

Fig. 3.4 shows that the 10% outage mutual information of the MMSE RSM outperforms that of the ZF RSM assuming that RAS are performed. Further, at given SNR, there is a number of receive antennas that maximizes the mutual information.

Fig. 3.5 shows the spatial and modulation mutual information of the (MMSE/ZF)

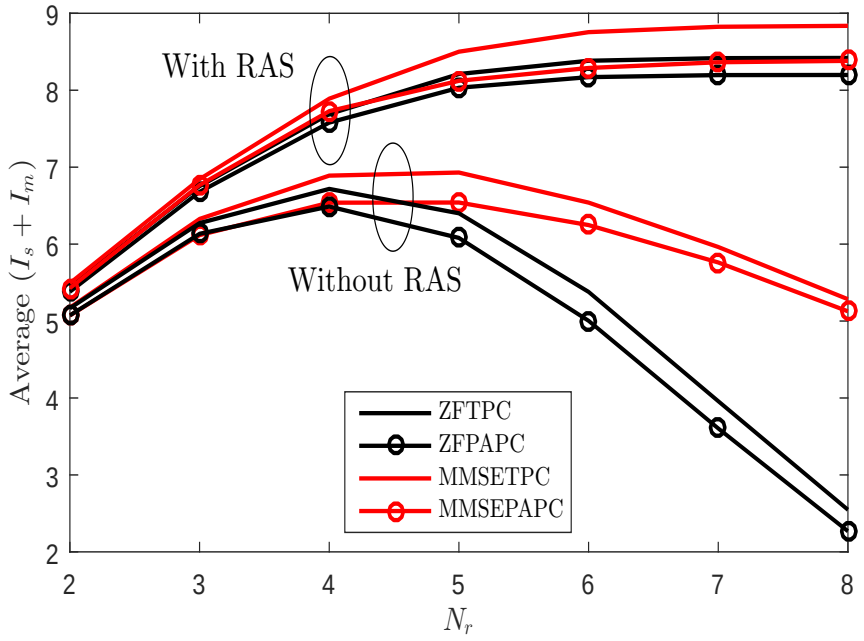

Figure 3.3: Mutual information at $L = 16$, $N_t = 32$, SNR $= 5$dB and (average over 1000 channel realizations).

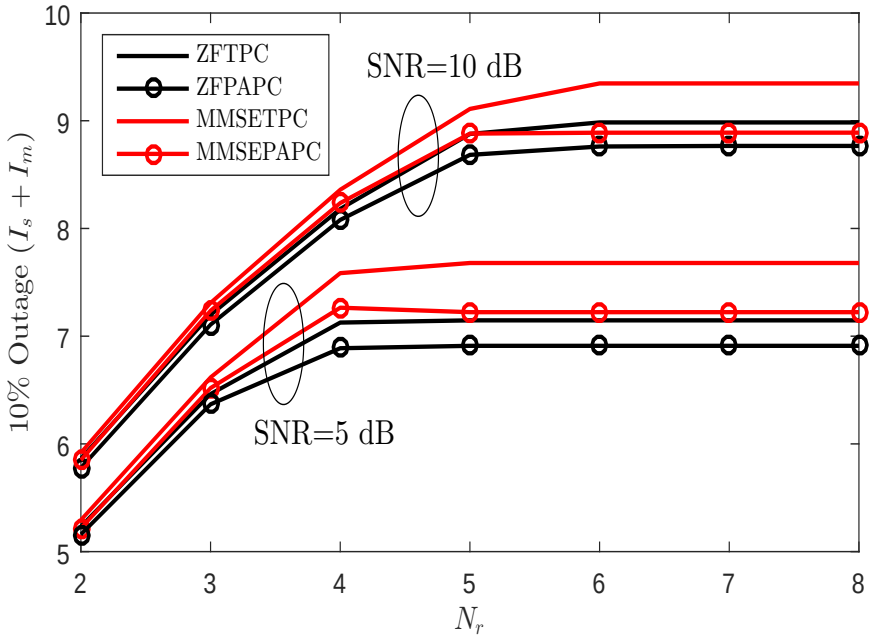

Figure 3.4: 10% Outage mutual information with RAS at $L = 16$, $N_t = 32$ and (evaluated over 1000 channel realizations).

RSM schemes under TPC and RAS assumptions. MMSE precoding achieve higher spatial rates due to its ability to combat the spatial correlation of the channel and

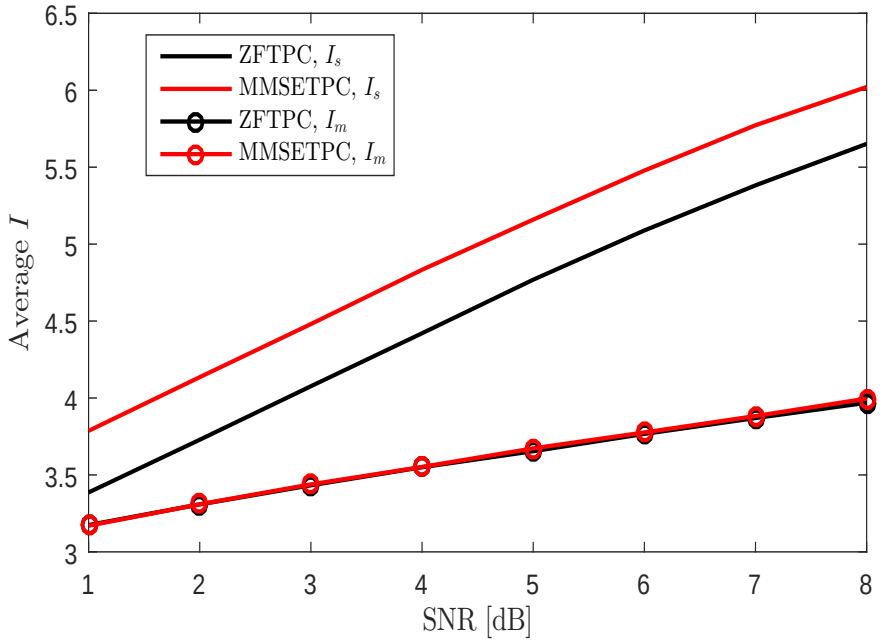

Figure 3.5: Mutual information with RAS at $L = 16$, $N_r = 7$, $N_t = 32$ and (average over 1000 channel realizations).

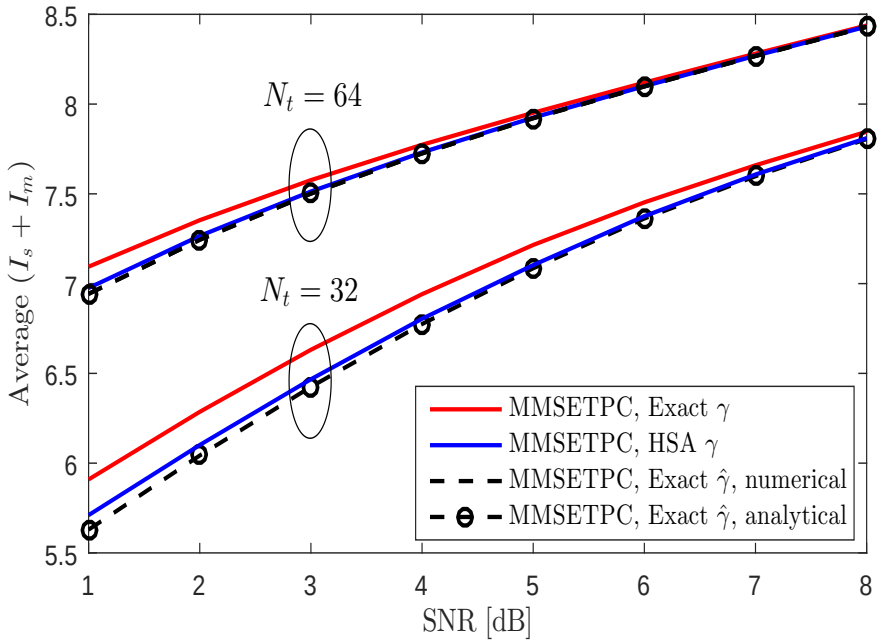

Figure 3.6: Mutual information with RAS at $L = 16$, $N_r = 4$ and (average over 1000 channel realizations).

hence a larger number of receive antennas can be activated. In MMSE precoding, we can activate more receive antennas than in ZF precoding but each active antenna receives lower power. Thus, the combined signal power in MMSE or ZF is

close which leads to similar modulation rates.

Fig. 3.6 represents the mutual information of the proposed MMSE RSM scheme with TPC and RAS under different thresholds. Not surprisingly, exact threshold is the best and the HSA threshold approaches the rates of the exact threshold with much lower computational complexity and performs well at low SNR. The gap between the perfect and the estimated threshold reduces when N_t or SNR increases.

3.3.2 Receive Antenna Selection

Recently, simple RSM MIMO transceiver and novel detection method have been introduced in [41] for outdoor narrowband mmWave communication. Nevertheless, the system in [41] relies on computationally complex receive antenna subset selection (RAS) algorithm and power hungry FD BS.

Inspired by fast algorithms [88] and by convex optimization [89], several RAS techniques have been studied to maximize MIMO channel spectral efficiency. However, these methods are not alleviating the problems associated to ZF precoding operating in rank deficient channels. ZF hybrid precoding has been studied in [90] to simplify MIMO BS, whereby signal processing is divided among digital processing at BB and analog processing at passband. In [73], the authors developed ZF hybrid precoder that can achieve data rates higher to those in [90]. However, the design in [73] is computationally complex and suboptimal.

In this section, we study the RAS problem and ZF hybrid precoder design. The major contributions are published in **[C3]** and can be summarized as as follows:

- We develop novel, fast and efficient RAS methods.
- We determine the optimal number of ARA by maximizing the mutual information using fast algorithm.
- We develop novel ZF hybrid precoder that has the same performance as the FD precoder when channel is highly spatially sparse and outperforms the design in [73] in achievable rates, EE and complexity.

Precoding and detection

The sparse nature of mmWave propagation leads to correlation among receive antennas. Therefore, the BS selects the best ($N_a \leq N_r$) receive antennas to be active and informs the UT about those antennas over a control channel. The received signal vector can be expressed as

$$\mathbf{y} = \sqrt{\alpha P}\mathbf{H}_a\mathbf{B}\mathbf{s}_i x_j + \mathbf{n} \tag{3.79}$$

where $x_j \sim \mathcal{CN}(0,1)$ is the modulation symbol, $\mathbf{s}_i \in \mathbb{R}^{N_a \times 1}$ is a binary spatial symbol conveying N_a data bits, $\mathbf{H}_a \in \mathbb{C}^{N_a \times N_t}$ is the channel between the BS and ARA of the UT, P is average transmit power, $\alpha \approx \left(\frac{1}{2} \times \mathrm{Tr}\left\{\mathbf{B}^H\mathbf{B}\right\}\right)^{-1}$ is a normalization factor that fixes the average transmit power, $\mathbf{n} \in \mathbb{C}^{N_a \times 1}$ noise vector whose entries are i.i.d. $\mathcal{CN}(0,\sigma^2)$ and $\mathbf{B} \in \mathbb{C}^{N_t \times N_a}$ is the ZF precoder that can be expressed as

$$\mathbf{B} = \mathbf{H}_a^H \left(\mathbf{H}_a\mathbf{H}_a^H\right)^{-1} \tag{3.80}$$

The received signal at the k-th antenna can be expressed as

$$y_k = \sqrt{\alpha P} s_{ik} x_j + n_k \tag{3.81}$$

where s_{ik} is the k-th element of $\mathbf{s}_i$.

RAS is necessary to perform ZF precoding in correlated mmWave massive MIMO channels. For a given N_a, ARA are selected to maximize per antenna received power as

$$\text{(P1)} \quad \min_{\mathbf{H}_a \subseteq \mathbf{H}} \quad \mathrm{Tr}\left\{\left(\mathbf{H}_a\mathbf{H}_a^H\right)^{-1}\right\} \tag{3.82}$$

The detection of spatial and modulation symbols can be recapitulated as follows [41]

- First, the output of the k-th AD is compared to $\hat{\gamma}$ to detect k-th spatial bit $\hat{s}_{ik} \in \{0,1\}$ [41].
- Then, the combined signal y_c passes through RF chain to enable detection of the modulation symbol x_j where

$$y_c = \sum_{k=1}^{N_a} \sqrt{\alpha P}\hat{s}_{ik} s_{ik} x_j + \hat{s}_{ik} n_k \tag{3.83}$$

Challenges and proposed solutions

Problem (P1) is solved by exhaustive search in [41] but this method entails considerable computational complexity especially in large MIMO systems. Besides, FD BS is expensive and power consuming particularly in mmWave massive MIMO systems.

In the sequel, we formulate the joint problem of designing low complexity ZF hybrid precoder and RAS. We divide this problem into two subproblems. First, we select the ARA assuming FD BS by using convex optimization and efficient algorithms to solve (P1). Then, in section 3.3.2.4 we consider those selected antennas in designing novel ZF hybrid precoder. We compare all the proposed designs with the best known.

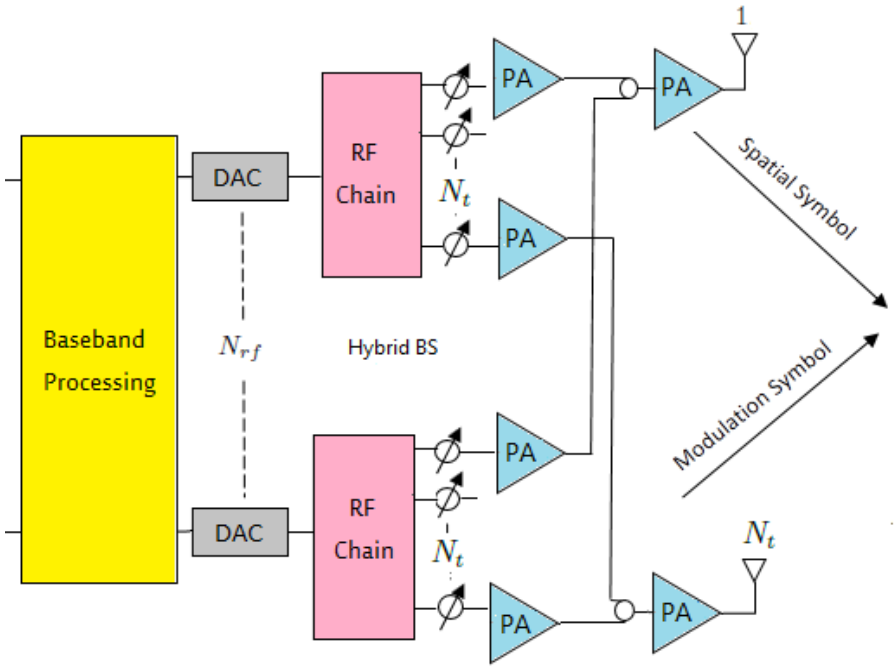

Figure 3.7: Fully connected hybrid base station [28].

subsubsectionJoint ZF hybrid precoder design and RAS At mmWave band, the cost and power consumption of RF chains and high resolution DACs are significant. In this section, we motivate the benefit of the hybrid architecture (Fig. 3.7) by comparing its power consumption with the FD and then we propose a joint problem of ZF hybrid precoder design and RAS.

Power consumption

With the goal of justifying the use of hybrid architectures, equation (3.84) shows the power consumption of P_{PA}, PS (P_{PS}), DAC (P_{DAC}) and RF chain (P_{RF}) in terms of reference power (P_{ref}) [28] as

$$P_{\mathrm{PA}} = P_{\mathrm{ref}}, P_{\mathrm{PS}} = 1.5P_{\mathrm{ref}}, P_{\mathrm{RF}} = 2P_{\mathrm{ref}}, P_{\mathrm{DAC}} = 10P_{\mathrm{ref}} \tag{3.84}$$

The hardware power consumption of FD BS (P_d) and the hybrid BS (P_h) in Fig. 3.7 can be expressed as

$$\begin{aligned} P_h &= N_f N_t \left(P_{\mathrm{PA}} + P_{\mathrm{PS}}\right) + N_f \left(P_{\mathrm{RF}} + P_{\mathrm{DAC}}\right) + P_{\mathrm{BB}} \\ P_d &= N_t \left(P_{\mathrm{PA}} + P_{\mathrm{RF}} + P_{\mathrm{DAC}}\right) + P_{\mathrm{BB}} \end{aligned} \tag{3.85}$$

where N_f is the number of RF chains and $P_{\mathrm{BB}} = 10P_{\mathrm{ref}}$ is the BB processing power consumption [28].

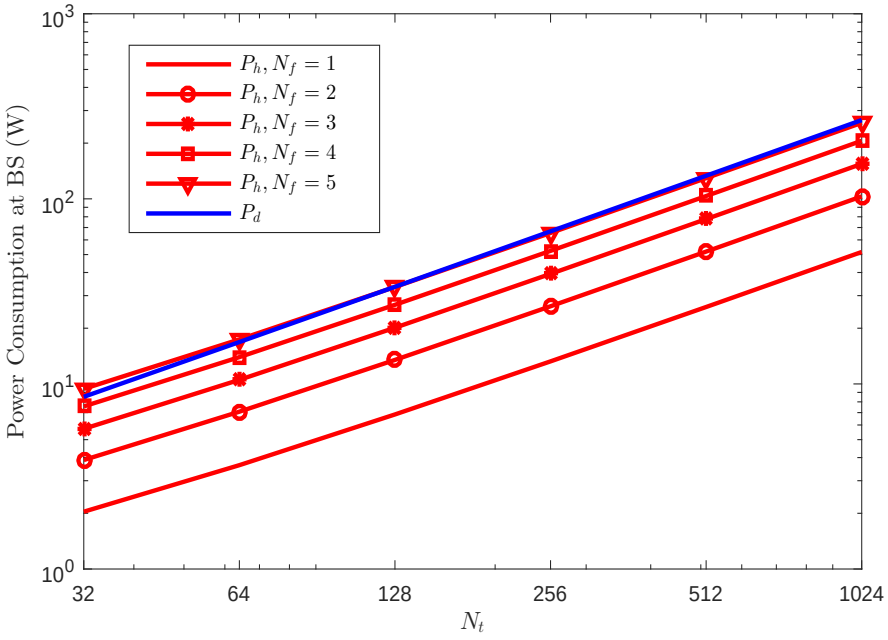

Figure 3.8: Hardware power consumption at BS versus N_t at $P_{\text{ref}} = 20\text{mW}$.

Fig. 3.8 shows hardware power consumption of FD BS and hybrid BS at different values of N_f. At low values of N_f, the hybrid architecture consumes much lower power than FD and the same power as FD at $N_f = 5$. Therefore, hybrid architecture is primness for highly spatially sparse mmWave massive MIMO channels that limited by few scattering clusters. **Joint design**
The hybrid precoder can be expressed as

$$\mathbf{B}_h = \sqrt{P_g}\mathbf{B}_{\text{RF}}\mathbf{B}_{\text{BB}} = \frac{1}{\parallel \mathbf{B}_{\text{RF}}\mathbf{B}_{\text{BB}} \parallel_F}\mathbf{B}_{\text{RF}}\mathbf{B}_{\text{BB}} \tag{3.86}$$

where $\mathbf{B}_{\text{RF}} \in \mathbb{C}^{N_t \times N_f}$ is the RF precoder that implemented by using PSs, $\mathbf{B}_{\text{BB}} \in \mathbb{C}^{N_f \times N_a}$ is the BB precoder and P_g is the precoder gain.

By considering the equivalent channel ($\mathbf{H}_{\text{eq}} = \mathbf{H}_a\mathbf{B}_{\text{RF}}$), the BB precoder is designed to zero force the equivalent channel $\left(\mathbf{B}_{\text{BB}} = \mathbf{H}_{\text{eq}}^H \left(\mathbf{H}_{\text{eq}}\mathbf{H}_{\text{eq}}^H\right)^{-1}, N_f \geq N_a\right)$. Hence, the ZF hybrid precoder can be expressed as

$$\mathbf{B}_h = \frac{\mathbf{B}_{\text{RF}}\mathbf{B}_{\text{BB}}}{\sqrt{\text{Tr}\left\{\left(\mathbf{H}_a\mathbf{B}_{\text{RF}}\mathbf{B}_{\text{RF}}^H\mathbf{H}_a^H\right)^{-2}\mathbf{H}_a\left(\mathbf{B}_{\text{RF}}\mathbf{B}_{\text{RF}}^H\right)^2\mathbf{H}_a^H\right\}}} \tag{3.87}$$

At large N_t, we can assume that $\left(\mathbf{B}_{\text{RF}}^H\mathbf{B}_{\text{RF}} = \mathbf{I}_{N_f}\right)$ and hence, $\mathbf{B}_h$ in equation

(3.87) can be expressed as

$$\mathbf{B}_h = \frac{\mathbf{B}_{\mathrm{RF}}\mathbf{B}_{\mathrm{BB}}}{\sqrt{\mathrm{Tr}\left\{\left(\mathbf{H}_a\mathbf{B}_{\mathrm{RF}}\mathbf{B}_{\mathrm{RF}}^H\mathbf{H}_a^H\right)^{-1}\right\}}} \tag{3.88}$$

In order to maximize the received signal power, we jointly formulate the RF precoder design and the RAS problems to maximize the precoder gain such as

$$(\mathrm{P2})\begin{cases} \min\limits_{\mathbf{B}_{\mathrm{RF}},\mathbf{H}_a\subseteq\mathbf{H}} & \mathrm{Tr}\left\{\left(\mathbf{H}_a\mathbf{B}_{\mathrm{RF}}\mathbf{B}_{\mathrm{RF}}^H\mathbf{H}_a^H\right)^{-1}\right\} \\ \text{s.t.} & \mathbf{B}_{\mathrm{RF}}(n,m) = e^{j\theta_{n,m}},\ \forall n,m. \end{cases} \tag{3.89}$$

where $j=\sqrt{-1}$. The first step to solve (P2) is to derive a closed form solution to $\mathbf{B}_{\mathrm{RF}}$ assuming $\mathbf{H}_a$ is given. This is difficult because the objective function of (P2) is non-convex, moreover, the constant amplitude of $\mathbf{B}_{\mathrm{RF}}$ is non-convex constraint. We propose to solve (P2) by selecting the ARA at first assuming FD precoder and then we consider those antennas to design the RF precoder.

3.3.2.1 RAS based convex optimization

Problem (P1) can be reformulated in terms of eigenvalues of $\left(\mathbf{H}_a\mathbf{H}_a^H\right)$ as

$$(\mathrm{P3})\begin{cases} \min\limits_{\mathbf{H}_a\subseteq\mathbf{H}} & \sum\limits_{i=1}^{N_a}\frac{1}{\lambda_i} \\ \text{s.t.} & \lambda_i \in \boldsymbol{\lambda}\left\{\mathbf{H}_a\mathbf{H}_a^H\right\}, i=1,\cdots,N_a. \end{cases} \tag{3.90}$$

where $\boldsymbol{\lambda}\left\{\mathbf{H}_a\mathbf{H}_a^H\right\}$ is a vector that includes eigenvalues of $\left(\mathbf{H}_a\mathbf{H}_a^H\right)$. Since (P3) is non-convex, we propose two different designs in which we minimize lower bounds on the objective function of (P3). In both cases, we obtain a non-convex problem; however, we relax non-convex constraint to convert into convex program and achieve suboptimal solution.

Max-min eigenvalue

The objective function of (P3) is lower bounded by $\frac{1}{\lambda_{N_a}}$ where λ_{N_a} is the smallest eigenvalue of $\left(\mathbf{H}_a\mathbf{H}_a^H\right)$. We propose to minimize this lower bound that implies maximizing λ_{N_a}. The resulting optimization problem can be expressed as

$$(\mathrm{P4})\begin{cases} \max\limits_{\mathbf{H}_a\subseteq\mathbf{H}} & \lambda_{N_a} \\ \text{s.t.} & \lambda_i \in \boldsymbol{\lambda}\left\{\mathbf{H}_a\mathbf{H}_a^H\right\}, \\ & \lambda_1 \geq \lambda_2 \geq \cdots \geq \lambda_{N_a}. \end{cases} \tag{3.91}$$

Let us define $\mathbf{X} \in \mathbb{R}^{N_r \times N_r}$ as a diagonal matrix and $\mathbf{X}_i$ is the i-th diagonal element that follows

$$\mathbf{X}_i = \begin{cases} 1 & \text{if} \quad i^{\text{th}} \text{ receive antenna is active} \\ 0 & \text{if} \quad i^{\text{th}} \text{ receive antenna is silent} \end{cases} \tag{3.92}$$

Let us assume that matrices $\mathbf{X}$ and $\mathbf{H}_a$ share the same N_a ARA. Thus, the largest N_a eigenvalues of $\left(\mathbf{H}^H\mathbf{X}\mathbf{H}\right)$ are same as the eigenvalues of $\mathbf{H}_a\mathbf{H}_a^H$. Moreover, the smallest $(N_t - N_a)$ eigenvalues of $\left(\mathbf{H}^H\mathbf{X}\mathbf{H}\right)$ are zeros. Therefore, without loss of optimality, problem (P4) can be expressed as

$$(\text{P5}) \begin{cases} \max\limits_{\mathbf{X}} & \sum\limits_{i=N_a}^{N_t} \lambda_i \\ \text{s.t.} & \lambda_i \in \boldsymbol{\lambda}\left\{\mathbf{H}^H\mathbf{X}\mathbf{H}\right\}, \\ & \lambda_1 \geq \lambda_2 \geq \cdots > \lambda_{N_t}. \\ & \mathbf{X} \in \text{diagonal}, \, \mathbf{X}_i \in \{0,1\}. \\ & \text{Tr}\left\{\mathbf{X}\right\} = N_a. \end{cases} \tag{3.93}$$

Although the objective function of (P5) is concave in $\mathbf{X}$, (P5) is non-convex optimization problem because ($\mathbf{X}_i \in \{0,1\}$) is non-convex constraint. We do relaxation to convert (P5) into convex optimization problem where replace the non-convex constraint with linear one ($0 \leq \mathbf{X}_i \leq 1$).

Solution $\mathbf{X}^\star$ of the relaxed problem does not follow equation (3.92). Therefore, we generate another solution $\mathbf{X}_a^\star$ such that has ones in positions of maximum N_a diagonal elements of $\mathbf{X}^\star$ and zeros in the other locations.

Min sum of convex fractions

We propose an alternative formulation of the problem using a tighter bound. The proposed lower bound satisfy the following inequality

$$\frac{1}{\lambda_{N_a}} \leq \sum_{i=1}^{N_a} \frac{1}{\sum_{j=N_a-i+1}^{N_a} \lambda_j} \leq \sum_{i=1}^{N_a} \frac{1}{\lambda_i} \tag{3.94}$$

where $\lambda_i \in \boldsymbol{\lambda}\left\{\mathbf{H}_a\mathbf{H}_a^H\right\}, \lambda_1 \geq \lambda_2 \geq \cdots \geq \lambda_{N_a}$. Consequently, the problem can be expressed as

$$(\text{P6}) \begin{cases} \min\limits_{\mathbf{H}_a \subseteq \mathbf{H}} & \sum\limits_{i=1}^{N_a} \dfrac{1}{\sum_{j=N_a-i+1}^{N_a} \lambda_j} \\ \text{s.t.} & \lambda_i \in \boldsymbol{\lambda}\left\{\mathbf{H}_a\mathbf{H}_a^H\right\}, \\ & \lambda_1 \geq \lambda_2 \geq \cdots \geq \lambda_{N_a}. \end{cases} \tag{3.95}$$

Algorithm 3.1 RAS via Dinkelbach algorithm [92]

1: **Input** : $\epsilon < 0$, $\rho_i = 1$, for all $i = 1, \cdots N_a$.
2: **Output** : $\mathbf{X}_a^\star$
3: **repeat**
4: $\mathbf{X}_a^\star = \begin{cases} \min\limits_{\mathbf{X}} & N_a - \sum\limits_{i=1}^{N_a} \rho_i \sum\limits_{j=N_a-i+1}^{N_t} \lambda_j \\ \text{s.t.} & \lambda_i \in \boldsymbol{\lambda}\left\{\mathbf{H}^H\mathbf{X}\mathbf{H}\right\}, \\ & \lambda_1 \geq \lambda_2 \geq \cdots \geq \lambda_{N_t}. \\ & \mathbf{X} \in \text{diagonal}, 0 \leq \mathbf{X}_i \leq 1. \\ & \text{Tr}\left\{\mathbf{X}\right\} = N_a. \end{cases}$
5: $F\left(\mathbf{X}_a^\star\right) = N_a - \sum_{i=1}^{N_a} \rho_i \sum_{j=N_a-i+1}^{N_t} \lambda_i$
6: $\rho_i = \frac{1}{\sum_{j=N_a-i+1}^{N_t} \lambda_i}, \quad i = 1, \cdots, N_a.$
7: **until** $F\left(\mathbf{X}_a^\star\right) > \epsilon$

The fractional nature of (P6) can be exploited to solve this problem. In optimization theory, fractional programming (FP) [91] provides low computational complexity algorithms such as Dinkelbach algorithm [92] to minimize sum of fractional functions of convex numerator and concave denominator (convex fraction). Problem (P6) can be expressed as sum of convex fractions

$$(\text{P7}) \begin{cases} \min\limits_{\mathbf{X}} & \sum\limits_{i=1}^{N_a} \dfrac{1}{\sum_{j=N_a-i+1}^{N_a} \lambda_j} \\ \text{s.t.} & \lambda_i \in \boldsymbol{\lambda}\left\{\mathbf{H}^H\mathbf{X}\mathbf{H}\right\}, \\ & \lambda_1 \geq \lambda_2 \geq \cdots \geq \lambda_{N_t}. \\ & \mathbf{X} \in \text{diagonal}, 0 \leq \mathbf{X}_i \leq 1. \\ & \text{Tr}\left\{\mathbf{X}\right\} = N_a. \end{cases} \tag{3.96}$$

where each fraction in the objective function of (P7) is convex fraction that has constant numerator and concave denominator. In Algorithm 3.1, we convert the non-convex (P7) into sequence of convex problems. Moreover, Algorithm 3.1 converges in few iterations.

3.3.2.2 Sequential add/remove algorithms

The introduced lower bounds in (P5)-(P7) and the relaxation lead to suboptimal solutions. In this section, we propose RAS designs that approach the optimal selection by using efficient sequential methods to solve (P3). In Algorithms 3.2 and 3.3, we (activate/deactivate) one antenna per iteration that has major (posi-

Algorithm 3.2 Best RAS via empty initialization

Input : $(\mathbf{H}, N_r, N_a)$
Output : $\mathbf{H}_a$
$\mathbf{X} = \mathbf{0}_{N_r}, \mathbf{Y} = \mathbf{0}_{N_r}$
$\mathcal{V} = \{1, \cdots, N_r\}, \mathcal{J} = \{1, \cdots, N_r\}, \mathcal{K} =$ Empty set
for $i = 1 : N_a$
  for $j \in \mathcal{V}$
    $\mathbf{X}(j, j) = 1$
    $\lambda_1, \cdots, \lambda_i$ are largest i eigenvalues of $\mathbf{H}^H\mathbf{X}\mathbf{H}$
    $l_j = \sum_{k=1}^{i} \frac{1}{\lambda_k}$
    $\mathbf{X} = \mathbf{Y}$
  end for
  $\mathcal{K} = \mathcal{K} + \arg\min_{\forall j} \quad l_j$
  $\mathbf{X}(\mathcal{K}) = 1, \mathbf{Y}(\mathcal{K}) = 1, \mathcal{V} = \mathcal{J} - \mathcal{K}$
end for
return $\mathbf{H}_a = \mathbf{H}(\mathcal{K}, :)$

tive/negative) effect on (P3). In Algorithms 3.4 and 3.5, we reduce the complexity of Algorithms 3.2 and 3.3 by replacing eigenvalues computation with simple projection methods. Finally, we compare all proposed algorithms with optimal selection (exhaustive search) in terms of performance and complexity.

Best empty initialization

In Algorithm 3.2, we propose efficient iterative method to solve (P3) where we select one good receive antenna per iteration. Initially, ($\mathbf{X} = \mathbf{0}_{N_r}$) and during the i-th iteration the specific diagonal entry in $\mathbf{X}$ is set to one to minimize $\left(\frac{1}{\lambda_1} + \cdots + \frac{1}{\lambda_i}\right)$ where $(\lambda_1, \cdots, \lambda_i)$ are the largest i eigenvalues of $\mathbf{H}^H\mathbf{X}\mathbf{H}$.

Best full initialization

Algorithm 3.3 shows efficient sequential technique to solve (P3) where we deactivate one bad receive antenna per iteration. Initially, ($\mathbf{X} = \mathbf{I}_{N_r}$) and during the i-th iteration specific diagonal entry in $\mathbf{X}$ be equal to zero to minimize $\left(\frac{1}{\lambda_1} + \cdots + \frac{1}{\lambda_{N_a}}\right)$ where $(\lambda_1, \cdots, \lambda_{N_a})$ are the largest N_a eigenvalues of $\mathbf{H}^H\mathbf{X}\mathbf{H}$.

With the aim of avoiding the complexity resulting from eigenvalues computation in Algorithms 3.2 and 3.3, Algorithms 3.4 and 3.5 show iterative designs to select the ARA based simple projection methods.

Low complexity empty initialization

In Algorithm 3.4, $\mathbf{X} = \mathbf{0}_{N_r}$ at initial. Then, we select the receive antenna that has channel vector with the highest norm. Next, at the i-th iteration we select

Algorithm 3.3 Best RAS via full initialization

Input : $(\mathbf{H}, N_r, N_a)$
Output : $\mathbf{H}_a$
$\mathbf{X} = \mathbf{I}_{N_r}, \mathbf{Y} = \mathbf{I}_{N_r}$
$\mathcal{V} = \{1, \cdots, N_r\}, \mathcal{J} = \{1, \cdots, N_r\}, \mathcal{K} =$ Empty set
for $i = 1 : N_r - N_a$
  for $j \in \mathcal{V}$
    $\mathbf{X}(j, j) = 0$
    $\lambda_1, \cdots, \lambda_{N_a}$ are largest N_a eigenvalues of $\mathbf{H}^H\mathbf{X}\mathbf{H}$
    $l_j = \sum_{k=1}^{N_a} \frac{1}{\lambda_k}$
    $\mathbf{X} = \mathbf{Y}$
  end for
  $\mathcal{K} = \mathcal{K} + \arg\min_{\forall j} \quad l_j$
  $\mathbf{X}(\mathcal{K}) = 0, \mathbf{Y}(\mathcal{K}) = 0, \mathcal{V} = \mathcal{J} - \mathcal{K}$
end for
return $\mathbf{H}_a = \mathbf{H}(\mathcal{V}, :)$

one receive antenna where its channel vector $\mathbf{H}(i, :)^H$ has minimum projection on $\mathbf{H}^H\mathbf{X}\mathbf{H}$.

Low complexity full initialization

In Algorithm 3.5, we start with $\mathbf{X} = \mathbf{I}_{N_r}$. Then, at the i-th iteration we deactivate one receive antenna where its channel vector has maximum projection on $\mathbf{H}^H\mathbf{X}\mathbf{H}$.

In Fig. 3.9, we compare all proposed RAS designs with optimal selection in terms of objective function of (P1). RAS designs based convex optimization have lower performance than those based sequential algorithms because the relaxation of the non-convex constraint ($\mathbf{X}_i \in \{0, 1\}$). The lower bound in (P6) is tighter than the lower bound in (P4). Therefore, Algorithm 3.1 outperforms the design in (P5). Algorithms 3.2 and 3.3 approach optimal selection with much lower computational complexity. Algorithms 3.4 and 3.5 avoid the complexity resulting from eigenvalues computation in exchange for less performance than Algorithms 3.2 and 3.3. Maximum and minimum initialization are approaching in performance. However, each is computationally efficient at certain range of N_a.

Computational complexity analysis

The number of SVD needed for optimal selection (S_o), empty initialization of Algorithm 3.2 (S_e) and full initialization of Algorithm 3.3 (S_f) can be expressed as

$$S_o = \binom{N_r}{N_a},$$

Algorithm 3.4 Low complexity RAS via empty initialization

Input : $(\mathbf{H}, N_r, N_a)$
Output : $\mathbf{H}_a$
$\mathbf{X} = \mathbf{0}_{N_r}, \mathcal{J} = \{1, \cdots, N_r\}, \mathcal{K} =$ Empty set
$k = \arg\max_{\forall j} \operatorname{diag}\left(\mathbf{H}\mathbf{H}^H\right)$
$\mathbf{X}(k,k) = 1, \mathcal{K} = \mathcal{K} + k, \mathcal{V} = \mathcal{J} - \mathcal{K}$
for $i = 2 : N_a$
  for $j \in \mathcal{V}$
    $\mathbf{z} = \mathbf{H}(j,:)^H$
    $l_j = \|\mathbf{H}^H\mathbf{X}\mathbf{H}\mathbf{z}\|_2$
  end for
  $\mathcal{K} = \mathcal{K} + \arg\min_{\forall j} \quad l_j$
  $\mathbf{X}(\mathcal{K}) = 1, \mathcal{V} = \mathcal{J} - \mathcal{K}$
end for
return $\mathbf{H}_a = \mathbf{H}(\mathcal{K},:)$

$$S_e = \sum_{i=0}^{N_a-1} N_r - i = N_a\left(N_r - \frac{1}{2}(N_a-1)\right),$$
$$S_f = \sum_{i=0}^{N_r-N_a-1} N_r - i = (N_r-N_a)\left(N_r - \frac{1}{2}(N_r-N_a-1)\right). \tag{3.97}$$

In terms of computational complexity, equation (3.97) shows that empty initialization is the best when $N_a < \frac{N_r}{2}$ while full initialization is better when $N_a > \frac{N_r}{2}$.

As an illustrative example, Table 3.1 shows numerical values of S_o, S_e and S_f at $N_r = 16$ and different numbers of ARA. Therefore, the proposed algorithms are computationally simpler than optimal selection and closely approach the optimal performance.

3.3.2.3 Mutual Information and Optimal N_a

In this section, we derive the mutual information of the discrete channel implemented in the RSM system. Then, we show that the mutual information as a function of N_a has one global maximum. Subsequently, we propose fast algorithm to find the optimal value of N_a that maximizes the mutual information.

According to equations (3.79)-(3.81)-(3.83), the mutual information between the transmitted and the received symbols can be expressed by applying the chain rule in [85] as

$$I(\mathbf{s}, x; \hat{\mathbf{s}}, y) = I(\mathbf{s}, x; \hat{\mathbf{s}}) + I(\mathbf{s}, x; y|\hat{\mathbf{s}})$$
$$I(\mathbf{s}, x; \hat{\mathbf{s}}) = I(\mathbf{s}; \hat{\mathbf{s}}) + I(x; \hat{\mathbf{s}}|\mathbf{s})$$

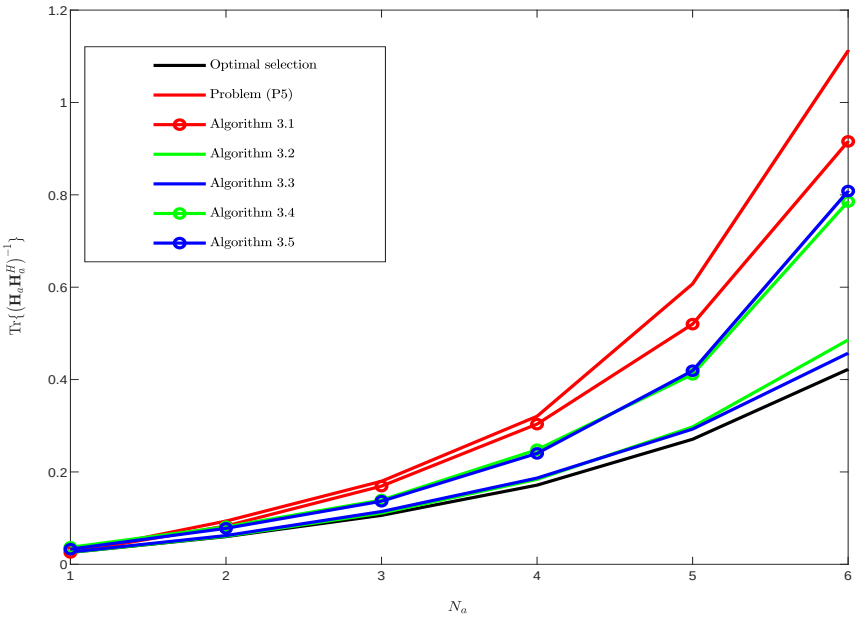

Figure 3.9: Objective function of (P1) versus N_a at 16×32 mmWave channel in (2.12), $L = 16$ and (average over 100 channel realizations).

Algorithm 3.5 Low complexity RAS via full initialization

Input : $(\mathbf{H}, N_r, N_a)$
Output : $\mathbf{H}_a$
$\mathbf{X} = \mathbf{I}_{N_r}, \mathbf{Y} = \mathbf{I}_{N_r}$
$\mathcal{V} = \{1, \cdots, N_r\}, \mathcal{J} = \{1, \cdots, N_r\}, \mathcal{K} =$ Empty set
for $i = 1 : N_r - N_a$
  for $j \in \mathcal{V}$
    $\mathbf{X}(j, j) = 0$
    $\mathbf{z} = \mathbf{H}(j, :)^H$
    $l_j = \|\mathbf{H}^H\mathbf{X}\mathbf{H}\mathbf{z}\|_2$
  end for
  $\mathcal{K} = \mathcal{K} + \arg\max_{\forall j} \quad l_j$
  $\mathbf{X}(\mathcal{K}) = 0, \mathbf{Y}(\mathcal{K}) = 0, \mathcal{V} = \mathcal{J} - \mathcal{K}$
end for
return $\mathbf{H}_a = \mathbf{H}(\mathcal{V}, :)$

$$I(\mathbf{s}, x; y|\hat{\mathbf{s}}) = I(\mathbf{s}; y|\hat{\mathbf{s}}) + I(x; y|\hat{\mathbf{s}}, \mathbf{s}) \tag{3.98}$$

Since $\hat{\mathbf{s}}$ is used only for spatial symbol detection and y for modulation symbol detection, $(I(x; \hat{\mathbf{s}}|\mathbf{s}) = 0, I(\mathbf{s}; y|\hat{\mathbf{s}}) = 0)$. Hence, the mutual information can be expressed as

$$I(\mathbf{s}, x; \hat{\mathbf{s}}, y) = I(\mathbf{s}; \hat{\mathbf{s}}) + I(x; y|\hat{\mathbf{s}}, \mathbf{s}) \triangleq I_s + I_m \tag{3.99}$$

Table 3.1: SVD operations needed at $N_r = 16$

N_a	S_o	S_e	S_f
6	8008	81	115
8	12870	100	100
10	8008	115	81

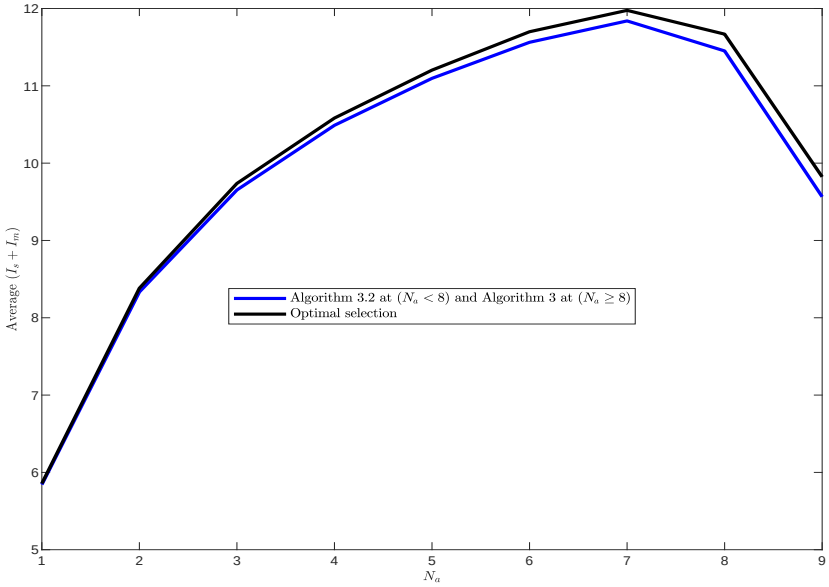

Figure 3.10: Mutual information versus N_a at 16×32 mmWave channel in (2.12), $L = 16$, $\frac{P}{\sigma^2} = 10$dB and (average over 100 channel realizations).

According to equation (3.81), the AD connected to each ARA can receive one of two amplitudes $|n|$ or $|\sqrt{\alpha P} + n|$. Then, the measured amplitude is compared with $\hat{\gamma}$ to detect one spatial bit per antenna. Therefore, spatial mutual information (I_s) can be computed using the BAC [84] as

$$\begin{aligned} I_s &= N_a \left(\mathcal{H}\left(\frac{P_1 + 1 - P_0}{2} \right) - \frac{\mathcal{H}(P_1) + \mathcal{H}(1 - P_0)}{2} \right) \\ P_1 &= \Pr\left(|\sqrt{\alpha P} + n| > \hat{\gamma} \right) = Q_1\left(\frac{1}{\sigma}\sqrt{2\alpha P}, \frac{1}{\sigma}\sqrt{2}\hat{\gamma} \right) \\ P_0 &= \Pr\left(|n| < \hat{\gamma} \right) = 1 - Q_1\left(0, \frac{1}{\sigma}\sqrt{2}\hat{\gamma} \right), \hat{\gamma} \approx \frac{1}{2}\sqrt{\alpha P} \end{aligned} \tag{3.100}$$

where $\mathcal{H}(P) = -P \log_2 P - (1 - P) \log_2 (1 - P)$ and $Q_1(x)$ is first order marcum Q function [77].

Since the BS also transmits one modulation symbol(assume Gaussian), the modulation mutual information (I_m) can be characterized by MISO channel as

$$I_m = \sum_{i=1}^{2^{Na}} \Pr\left(\mathbf{s}_i\right) \sum_{j=1}^{2^{Na}} \Pr\left(\hat{\mathbf{s}}_j|\mathbf{s}_i\right) \log_2\left(1 + \mathrm{SNR}|_{\mathbf{s_i},\hat{\mathbf{s}}_\mathbf{j}}\right) \tag{3.101}$$

$$\mathrm{SNR}|_{\mathbf{s_i},\hat{\mathbf{s}}_\mathbf{j}} = \frac{\left(\sum_{k=1}^{N_a} s_{ik}\hat{s}_{jk}\right)^2}{\max\left(\sum_{k=1}^{N_a} \hat{s}_{jk}, 1\right)} \frac{\alpha P}{\sigma^2} \tag{3.102}$$

$$\Pr\left(\hat{\mathbf{s}}_j|\mathbf{s}_i\right) = \prod_{k=1}^{N_a} \Pr\left(|y_{ik}| \underset{\hat{s}_{jk}=0}{\overset{\hat{s}_{jk}=1}{\gtrless}} \hat{\gamma}\right), \Pr\left(\mathbf{s_i}\right) = \frac{1}{2^{N_a}} \tag{3.103}$$

Fig. 3.10 shows that average mutual information achieved by proposed fast algorithms approach the one obtained by optimal selection. The mutual information increases with N_a until it reaches the maximum then it decreases. Therefore, we can find the optimal N_a by fast iterative algorithm that starts with $N_a = 1$ and stops when mutual information decreases.

3.3.2.4 ZF Hybrid Precoder

After selecting the ARA, we propose novel ZF RF precoder design and we prove that the ZF hybrid precoder is the same as ZF FD precoder at channels with high spatial sparsity. We show that the proposed precoder outperforms the best known in the literature in performance and complexity.

We solve (P2) assuming $\mathbf{H}_a$ is known. We drop the constant amplitude constraint of problem (P2) and replace the quadratic term $\mathbf{B}_{\mathrm{RF}}\mathbf{B}_{\mathrm{RF}}^H$ by the linear term $\mathbf{Y}$ to relax (P2) into a convex problem that can be expressed as

$$(\mathrm{P9}) \begin{cases} \min\limits_{\mathbf{Y}} & \mathrm{Tr}\left\{\left(\mathbf{H}_a\mathbf{Y}\mathbf{H}_a^H\right)^{-1}\right\} \\ \text{s.t.} & \mathrm{Tr}\left\{\mathbf{Y}\right\} = N_t N_f. \\ & \mathbf{Y} \succeq 0 \end{cases} \tag{3.104}$$

Solution $\mathbf{Y}$ has arbitrary rank profile so the RF precoder is designed based the largest N_f eigenvectors of $\mathbf{Y}$ as

$$\mathbf{B}_{\mathrm{RF}} = \mathrm{Arg}\left(\mathbf{V}_{N_f}\{\mathbf{Y}\}\right) \tag{3.105}$$

High spatial sparsity ($L \leq N_f$)

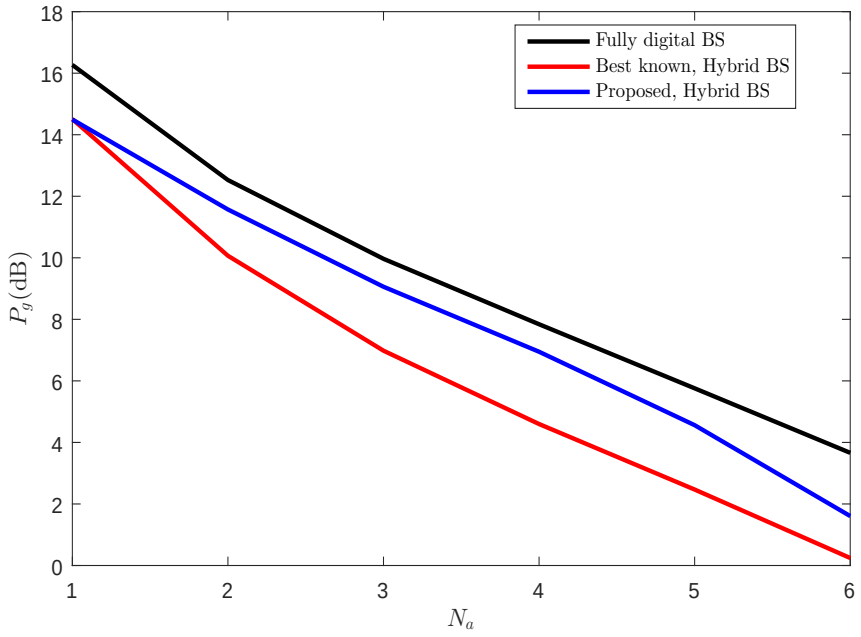

Figure 3.11: Zero forcing precoder gain versus N_a at 16×32 mmWave channel in (2.12), $L = 16$, $N_f = N_a + 1$ and (average over 100 channel realizations).

The channel matrix in equation (2.12) can be expressed as

$$\mathbf{H} = \mathbf{A}_r \mathbf{D} \mathbf{A}_t^H \tag{3.106}$$

where $\mathbf{D} \in \mathbb{C}^{L \times L}$ is the path gain diagonal matrix, $\mathbf{A}_r \in \mathbb{C}^{N_r \times L}$ and $\mathbf{A}_t \in \mathbb{C}^{N_t \times L}$ are matrices containing receive and transmit response vectors, respectively. After RAS, the channel matrix $\mathbf{H}_a$ can be expressed as

$$\mathbf{H}_a = \mathbf{A}_r \left(\mathcal{S}, :\right) \mathbf{D} \mathbf{A}_t^H = \mathbf{A}_{ra} \mathbf{D} \mathbf{A}_t^H \tag{3.107}$$

where $\mathcal{S}$ is set contains indices of ARA.

If $L \leq N_f$, ZF hybrid precoder $\mathbf{B}_h$ becomes exactly the same as ZF digital precoder $\mathbf{B}_d$ because there is a unique RF chain for each scattering path as illustrated in equation (3.108).

$$\begin{aligned} \mathbf{B}_d &= \mathbf{H}_a^H \left(\mathbf{H}_a \mathbf{H}_a^H\right)^{-1} = \left(\mathbf{A}_t\right) \left(\mathbf{D} \mathbf{A}_{ra}^H \left(\mathbf{H}_a \mathbf{H}_a^H\right)^{-1}\right) \\ &= \left(\mathbf{B}_{\mathrm{RF}}\right) \left(\mathbf{B}_{\mathrm{BB}}\right) = \mathbf{B}_h, \quad N_a \leq L \end{aligned} \tag{3.108}$$

Best known ZF RF precoder

In Algorithm 3 in [73], the authors proposed iterative method to solve (P2) assuming $\mathbf{H}_a$ is known. In this algorithm; at first, $\mathbf{B}_{\mathrm{RF}}$ is any feasible matrix. Then, one

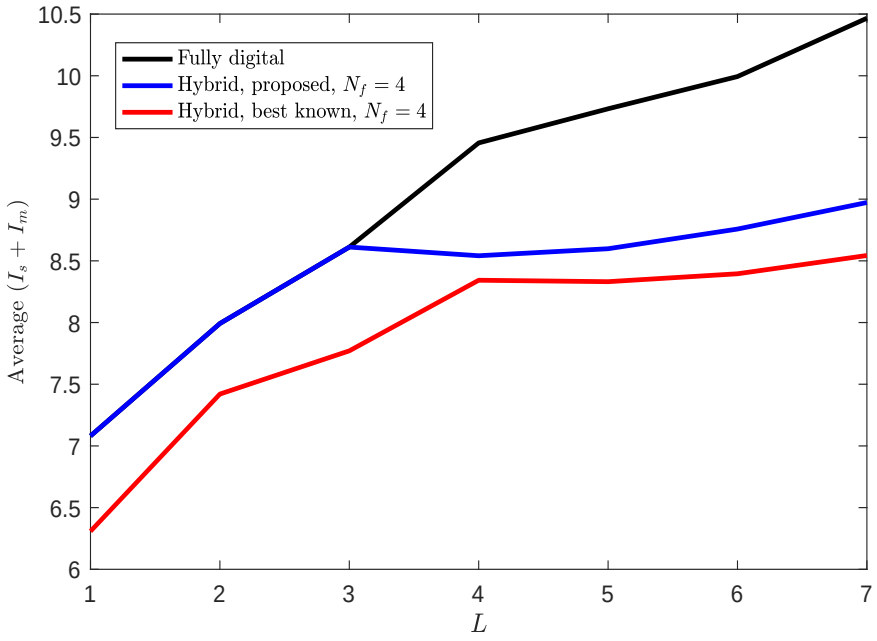

Figure 3.12: Mutual information versus L at 16×32 mmWave channel in (2.12), $\frac{P}{\sigma^2} = 10$dB and (average over 100 channel realizations).

element of $\mathbf{B}_{\text{RF}}$ is updated per iteration. The algorithm stops when $\mathbf{B}_{\text{RF}}$ converges. However, this design is computationally complex because it needs at least $N_t N_f$ iterations to reconstruct $\mathbf{B}_{\text{RF}}$. Moreover, it needs $N_f \geq N_a + 1$; on contrary, the proposed design in (3.105) needs $N_f \geq N_a$. The proposed precoder not only simpler than the design in [73] but also it achieves higher precoding gain as illustrated in Fig. 3.11.

Fig. 3.12 shows the average mutual information of RSM system considering several precoders. For all precoding schemes, N_a is selected to maximize the mutual information. The proposed hybrid precoder is not only superior to that based the design in [73] but also equal to that based FD precoder when $(L \leq N_f)$. The standard deviations of the mutual information over the 100 realizations are close to one for all precoders.

In Fig. 3.13, EE is defined as mutual information per BS power consumption. The proposed hybrid precoding scheme is the most energy efficient architecture when the channel is highly spatially sparse. On the other hand, FD precoding architecture becomes more energy efficient when sparsity level decreases.

3.3.3 Single Radio Frequency Chain UT at Wideband Transmission

Several wideband precoding schemes have been developed based on low complexity MIMO transceiver architectures in the literature. Wideband hybrid precoding was

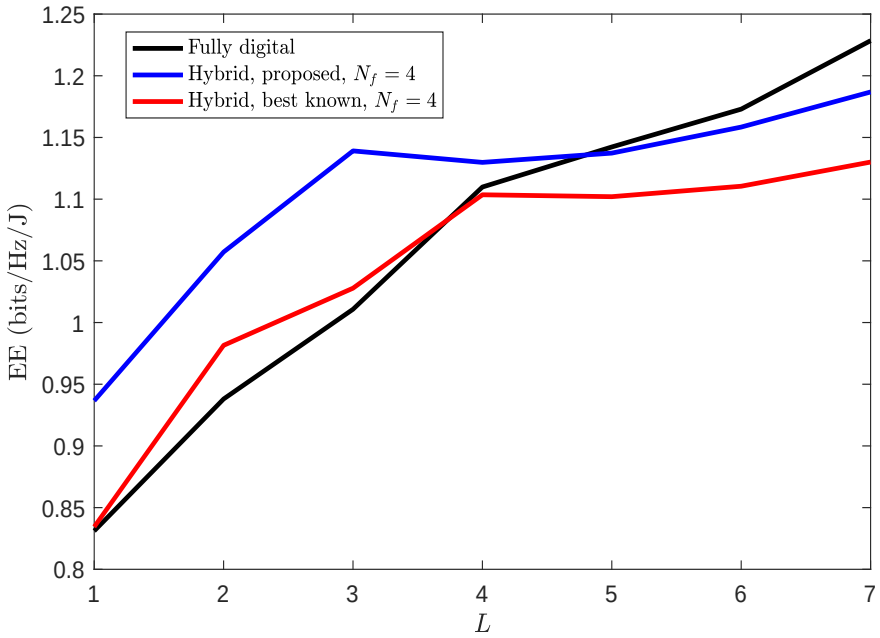

Figure 3.13: Energy efficiency versus L at 16×32 mmWave channel in (2.12), $P_{\text{ref}} = 20\text{mW}$, $\frac{P}{\sigma^2} = 10\text{dB}$ and (average over 100 channel realizations).

developed to reduce the number of the RF chains and high resolution ADCs by adding analog energy efficient devices like PSs, power splitters and power combiners [93]. However, hybrid MIMO transceiver should comprise a large number of analog devices to achieve high SE and hence the hardware power consumption may become significantly large. [28].

RSM schemes exploit the receive antennas as an additional dimension for data transmission [43]-[40] and allow energy efficient hardware design at the UT. An RSM scheme based on a SRF chain and one high resolution ADC is reported in [41] that attains high data rates at outdoor narrowband massive MIMO systems. In this section, we adapt the energy efficient RSM scheme in [41] for outdoor wideband mmWave massive MIMO systems.

Single carrier with channel equalization and OFDM are two methods to combat the frequency selectivity of the wideband transmission. In RSM schemes [43]-[41], it is possible to transmit one spatial symbol per channel use, thus symbols with shorter duration (single carrier) allow transmitting more spatial symbols and attaining higher SE than symbols with longer duration (OFDM). Moreover, the DFT implementation of the OFDM receiver increases the hardware complexity. We therefore propose a wideband single carrier RSM scheme based on a time-domain FIR pre-equalizer [45] and RAS. The contribution of the work presented in this section is published in **[C6]** and can be expressed as follows

- We propose a wideband single carrier RSM scheme based on a low complexity ZF time-domain FIR pre-equalizer with optimized delay for the UT narrowband architecture in [41] and no CSI at the UT and imperfect CSI at the BS.
- We study the impact of the channel angular spread and the number of delay tap channels on the minimum number of FIR taps.
- We show that we can attain high SE by applying RAS and we provide fast and efficient RAS algorithm based on QR decomposition [74].

Bit mapping strategy

For the sake of designing an energy efficient UT architecture, we consider a SRF chain at the UT and thus the BS can transmit one modulation symbol per channel use ($x_j \in (M-\text{PSK})$ constellation, $j = 1, \cdots, \log_2 M$) . For attaining high SE, we exploit the large number of receive antennas by transmitting superimposed spatial symbol ($\mathbf{s}_i \in \mathbb{R}^{N_a \times 1}, i = 1, \cdots, 2^{N_a}, N_a \leq N_r$) that includes N_a data bits, the k-th spatial bit can be one ore zero ($s_{ik} \in \{0, 1\}$) and can be detected using energy efficient hardware. The transmit vector at the precoder input at time n, $\mathbf{z}[n]$, can be expressed as

$$\mathbf{z}[n] = \begin{cases} \mathbf{s}_i[n]x_j[n] & \text{if} \quad \mathbf{s}_i[n] \neq \mathbf{0}_{N_r} \\ \mathbf{s}_i[n] & \text{if} \quad \mathbf{s}_i[n] = \mathbf{0}_{N_r} \end{cases} \tag{3.109}$$

where $\mathrm{E}\big[\mathbf{z}[n]\mathbf{z}[n]^H\big] \approx \frac{1}{2}\mathbf{I}_{N_a}$.

Energy efficient UT circuitry

The UT architecture in Fig. 2.1 comprises one of the power consuming devices (RF chain, high resolution ADC) to detect the modulation symbol and N_r energy efficient devices (AD, 1-bit ADC) to detect the spatial symbol [41]. The AD detects the amplitude of the wideband RF signal with large input impedance and negligible power consumption [61]. The 1-bit ADC compares the received amplitude per antenna with a threshold to detect the binary spatial bit. Then, the detected spatial bit controls a switch to allow the modulation symbol passes through the RF chain and stop the noise. Finally, we detect the modulation symbol in digital domain.

Low complexity FIR pre-equalization at the BS

We consider ZF time-domain FIR pre-equalizer [45] with imperfect CSI at the BS and L_f taps that converts the multiple delay taps channel into single tap chan-

nel to mitigate the intersymbol interference resulting from the delay spread. The proposed pre-equalizer does not require cyclic prefix or zero padding that saves transmission power and enhances the SE. In the sequel, we provide detailed analysis of the ZF pre-equalizer design with optimized delay assuming imperfect CSI.

3.3.3.1 Time Domain ZF Pre-Equalization

We consider pre-equalizer with L_f taps ($\mathbf{F}[k] \in \mathbb{C}^{N_t \times N_a}, k = 0, \cdots, L_f - 1$) such that the transmit precoded vector at time n, $\mathbf{x}[n]$, can be expressed as

$$\mathbf{x}[n] = \sqrt{\alpha P_t} \sum_{k=0}^{L_f-1} \mathbf{F}[k]\mathbf{z}[n-k] \tag{3.110}$$

where the normalization factor $\alpha \approx 2(\sum_{k=0}^{L_f-1} \|\mathbf{F}[k]\|_F^2)^{-1}$, P_t is the transmit power and the $\|.\|_F$ denotes the Frobenius norm operator. The received vector at time n can be expressed as

$$\mathbf{y}[n] = \sum_{i=0}^{N_c-1} \mathbf{H}_a[i]\mathbf{x}[n-i] + \mathbf{n}[n] \tag{3.111}$$

where the generated noise $\mathbf{n}[n] \in \mathbb{C}^{N_a \times 1}$ has independent and identically distributed (i.i.d) $\mathcal{CN}(0, \sigma^2)$ coefficients.

Pre-equalizer design

We design the ZF pre-equalizer to null the intersymbol interference such that the equalized channel ($\mathbf{H}_{eq}[n]$) resulting from the convolution between the pre-equalizer and the time-domain channel taps is identity matrix at time n_d and zero elsewhere as follows

$$\mathbf{H}_{eq}[n] = \sum_{i=0}^{N_c-1} \mathbf{H}_a[i]\mathbf{F}[n-i] = \mathbf{I}_{N_a}\delta[n-n_d] \tag{3.112}$$

From equations (3.110)-(3.111) and (3.112), the received vector at time n can be expressed as

$$\begin{aligned}\mathbf{y}[n] &= \sqrt{\alpha P_t} \sum_{i=0}^{N_c-1} \mathbf{H}_{eq}[i]\mathbf{z}[n-i] + \mathbf{n}[n] \\ &= \sqrt{\alpha P_t}\mathbf{z}[n-n_d] + \mathbf{n}[n]\end{aligned} \tag{3.113}$$

To design the pre-equalizer, we write equation (3.112) as

$$\mathbf{H}_c\mathbf{F}_c = \mathbf{E}_{n_d}$$

$$\begin{bmatrix} \mathbf{H}[0] & \mathbf{0} & \cdots & \cdots & \cdots & \mathbf{0} \\ \mathbf{H}[1] & \mathbf{H}[0] & \ddots & \cdots & \cdots & \vdots \\ \vdots & \mathbf{H}[1] & \ddots & \ddots & \cdots & \vdots \\ \mathbf{H}[N_c-1] & \vdots & \ddots & \mathbf{H}[0] & \ddots & \vdots \\ \mathbf{0} & \mathbf{H}[N_c-1] & \ddots & \mathbf{H}[1] & \ddots & \vdots \\ \vdots & \mathbf{0} & \ddots & \vdots & \ddots & \mathbf{H}[0] \\ \vdots & \vdots & \ddots & \mathbf{H}[N_c-1] & \ddots & \mathbf{H}[1] \\ \vdots & \vdots & \cdots & \mathbf{0} & \ddots & \vdots \\ \vdots & \vdots & \cdots & \cdots & \cdots & \mathbf{H}[N_c-1] \end{bmatrix} \begin{bmatrix} \mathbf{F}[0] \\ \vdots \\ \vdots \\ \vdots \\ \mathbf{F}[L_f-1] \end{bmatrix} = \begin{bmatrix} \mathbf{0} \\ \vdots \\ \vdots \\ \vdots \\ \mathbf{I}_{N_a} \\ \mathbf{0} \\ \vdots \\ \vdots \\ \vdots \end{bmatrix} \tag{3.114}$$

where $\mathbf{H}_c \in \mathbb{C}^{(N_c+L_f-1)N_a \times L_f N_t}$, $\mathbf{F}_c \in \mathbb{C}^{L_f N_t \times N_a}$ and $\mathbf{E}_{n_d} \in \mathbb{C}^{(N_c+L_f-1)N_a \times N_a}$. From equation (3.114), the ZF pre-equalizer can be expressed as

$$\mathbf{F}_c = \mathbf{H}_c^H \left(\mathbf{H}_c \mathbf{H}_c^H\right)^{-1} \mathbf{E}_{n_d} \tag{3.115}$$

where the position of the identity matrix in $\mathbf{E}_{nd}$ means that the signal will be received after $(0 \leq n_d \leq N_c + L_f - 2)$ time lags. We optimise this position so as to maximize the receive power as follows

$$\begin{aligned} n_d = \arg \min_{n_d=i} \sum_{k=0}^{L_f-1} \|\mathbf{F}[k]\|_F^2, \\ i = 0, \cdots, N_c + L_f - 2. \end{aligned} \tag{3.116}$$

Analysis of number of pre-equalizer taps

Realizing the pseudoinverse as in equation (3.115) implies the following necessary and sufficient condition:

$$\text{Rank}\left(\mathbf{H}_c\right) = \left(N_c + L_f - 1\right) N_a \tag{3.117}$$

which can be achieved by ensuring the necessary condition:

$$L_f N_t \geqslant \left(N_c + L_f - 1\right) N_a \tag{3.118}$$

where there is a maximum number of ARA for a given L_f and a minimum number of needed FIR taps for a particular N_a relying on the channel angular and time spreads, respectively as illustrated in the sequel.

In Fig. 3.14, we show the effect of L_f, N_c, N_a and the angular spread on the feasibility of the pseudoinverse in equation (3.115). By increasing L_f, the achievable rank that is, the actual rank of matrix $\mathbf{H}_c$ grows at a faster pace than the Rank-bound $\left(N_c + L_f - 1\right) N_a$ and matches the Rank-bound at the minimum number of needed FIR taps. The time spread N_c leads to boost of the Rank-bound and thus, more FIR taps are needed to allow the Rank $\left(\mathbf{H}_c\right)$ reaching the Rank-bound. Large N_a requires sufficient angular spread to allow ZF of N_a spatial streams spread in

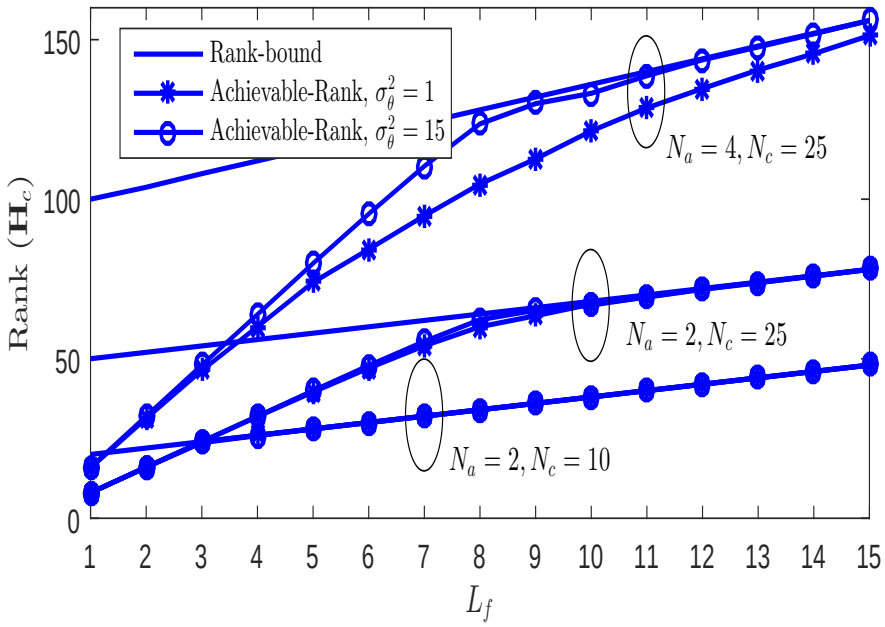

Figure 3.14: Achievable rank and Rank-bound with L_f at $N_r = 16, N_t = 128$ and (average over 1000 channel realizations).

N_c time slots; however, mmWave propagation suffers from narrow angular spread [6]. Thus, the smart reduction of N_a by the RAS is vital to fulfill condition (3.117).

Imperfect CSI at the BS

Let us consider that the channel taps are estimated in error: $\hat{\mathbf{H}}[d] = \mathbf{H}[d] + \underline{\mathbf{H}}_e[d]$ where $\underline{\mathbf{H}}_e[d]$ is error matrix has i.i.d $\mathcal{CN}(0, \sigma_e^2)$ entries. The pre-equalizer design based on imperfect CSI can be expressed as

$$\hat{\mathbf{F}}_c = \left(\mathbf{H}_c + \mathbf{H}_e\right)^\dagger \mathbf{E}_{n_d} = \hat{\mathbf{H}}_c^\dagger \mathbf{E}_{n_d} \tag{3.119}$$

where $\mathbf{H}_e$ is the convolution error matrix. The equalized channel matrix with CSI errors can be expressed as

$$\begin{aligned}\left[\hat{\mathbf{H}}_{eq}[0], \cdots, \hat{\mathbf{H}}_{eq}[N_c + L_f - 2]\right]^T &= \mathbf{H}_c \hat{\mathbf{F}}_c \\ &= \left(\hat{\mathbf{H}}_c - \mathbf{H}_e\right) \hat{\mathbf{F}}_c = \mathbf{E}_{n_d} - \mathbf{H}_e \hat{\mathbf{F}}_c \\ \hat{\mathbf{H}}_{eq}[n] = \mathbf{I}_{N_a} \delta[n - n_d] - \sum_{j=0}^{N_c-1} &\underline{\mathbf{H}}_e[j] \hat{\mathbf{F}} \quad [n - j]\end{aligned} \tag{3.120}$$

Equation (3.120) shows that the equalized channel is not only identity at time n_d as equation (3.112) but it also suffers from several error delay tap channels and thus, we cannot ensure perfect ZF. According to equation (3.120), the received

signal with residual inter-symbol interference can be expressed as

$$\begin{aligned}\mathbf{y}[n] = \sqrt{\hat{\alpha}P_t}\mathbf{z}[n-n_d] + \mathbf{n}[n] - \\ \sqrt{\hat{\alpha}P_t}\sum_{i=0}^{N_c+L_f-2}\left(\sum_{j=0}^{N_c-1}\underline{\underline{\mathbf{H}}}_e[j]\hat{\mathbf{F}}[i-j]\right)\mathbf{z}[n-i]\end{aligned} \tag{3.121}$$

where $\hat{\alpha} = 2/\|\hat{\mathbf{F}}_c\|_F^2$

According to equation (3.121), the covariance matrix ($\mathbf{C}$) of the interference and the generated noise can be expressed as

$$\begin{aligned}\mathbf{C} &= \sigma_n^2\mathbf{I}_{N_a} + \\ &\hat{\alpha}P_t\mathrm{E}\left[\left(\sum_{i=0}^{N_c+L_f-2}\left(\sum_{j=0}^{N_c-1}\underline{\underline{\mathbf{H}}}_e[j]\hat{\mathbf{F}}[i-j]\right)\mathbf{z}[n-i]\right)\right. \\ &\left.\times\left(\sum_{i=0}^{N_c+L_f-2}\left(\sum_{j=0}^{N_c-1}\underline{\underline{\mathbf{H}}}_e[j]\hat{\mathbf{F}}[i-j]\right)\mathbf{z}[n-i]\right)^H\right] \\ &= \left(\sigma_n^2 + \frac{\hat{\alpha}P_t}{2}\mathrm{Tr}\{\mathbf{Q}\}\right)\mathbf{I}_{N_a} = \hat{\sigma}_n^2\mathbf{I}_{N_a}\end{aligned} \tag{3.122}$$

where $\mathbf{Q}$ is a block diagonal matrix with diagonal matrices ($\mathbf{Q}_{ii}, i = 0, \cdots, N_c + L_f - 2$) in the i-th block such that

$$\mathbf{Q}_{ii} = \frac{\sigma_e^2}{N_a}\left(\sum_{j=0}^{N_c-1}\left\|\hat{\mathbf{F}}[i-j]\right\|_F^2\right)\mathbf{I}_{N_a} \tag{3.123}$$

We design n_d so as to maximize the received SINR

$$\begin{aligned}n_d = \arg\max_{n_d=i}\frac{\hat{\alpha}P_t}{\sigma_n^2 + \frac{\hat{\alpha}P_t}{2}\mathrm{Tr}\{\mathbf{Q}\}}, \\ i = 0, \cdots, N_c + L_f - 2.\end{aligned} \tag{3.124}$$

where the optimal n_d can be obtained by exhaustive search over $(N_c + L_f - 1)$ values.

3.3.3.2 Detection

In this section, we illustrate how the energy efficient hardware at the UT can be exploited to recover the spatial and the modulation symbols with no availability of CSI at the UT.

Spatial symbol detection

We consider ML spatial symbol detector that can be implemented using energy efficient devices at the UT (AD, 1-bit ADC) assuming Gaussian intersymbol interference. In [41], the authors show that when applying ZF precoder the (joint or per antenna) ML spatial symbol detectors lead to the same results. The received signal per the k-th ARA at time n assuming imperfect CSI at the BS can be expressed as

$$y_k[n] = \sqrt{\hat{\alpha} P_t} s_{ik}[n - n_d] x_j[n - n_d] + \hat{n}[n] \tag{3.125}$$

where $s_{ik} \in \{0, 1\}$ is the k-th spatial bit and $\hat{n}$ is the noise plus the intersymbol interference. The signal provided by the AD connected to the k-th ARA can be written as

$$a_k[n] = |y_k[n]| \tag{3.126}$$

The ML spatial symbol detector has been developed at equation (16) in [41] and can be expressed as

$$\hat{s}_{ik}[n - n_d] = \begin{cases} 1 & \text{if } a_k[n] > \gamma \\ 0 & \text{if } a_k[n] < \gamma \end{cases}, \quad \gamma \approx \frac{1}{2}\sqrt{\hat{\alpha} P_t} \tag{3.127}$$

The threshold γ is fixed during the channel coherence time and the UT needs to estimate γ to detect the spatial symbol. In [41], the authors show that only one DL pilot symbol is enough to allow the UT estimates γ efficiently.

Modulation symbol detection

We consider limited noise combining scheme to detect the modulation symbol using SRF chain and one high resolution ADC. In order not to accumulate noise, the k-th detected spatial bit $\hat{s}_{ik}[n - n_d]$ controls switch such that $y_k[n]$ is allowed to pass through the RF chain only if $\hat{s}_{ik}[n - n_d] = 1$. The combined signal, $y_c[n]$ (see Fig. 2.1), can be expressed as

$$y_c[n] = \frac{1}{\sum_{k=1}^{N_a} \hat{s}_{ik}[n - n_d]} \sum_{k=1}^{N_a} \hat{s}_{ik}[n - n_d] y_k[n] \tag{3.128}$$

3.3.3.3 Achievable rates and RAS

We consider the mutual information for comparison purposes of the proposed scheme with OFDM FD MIMO. We show that the spatial and modulation symbols mutual information can be modeled using BAC and the MISO channel, respectively. By applying the mutual information chain rule [85] it is shown in [42] that

the RSM mutual information can be written as

$$I_{\text{RSM}} = I_s + I_m \tag{3.129}$$

where I_s and I_m are the achievable rates by the spatial and modulation symbols, respectively.

Spatial symbol achievable rate

The k-th ARA can detect spatial bit $\hat{s}_{ik}[n-n_d] = s_{ik}[n-n_d] = 1$ or 0 with probability p_1 or p_0, respectively. Thus, I_s can be obtained using the binary asymmetric channel assumption [84] as

$$I_s = N_a \left(\mathcal{H}\left(\frac{p_1 + 1 - p_0}{2} \right) - \frac{\mathcal{H}(p_1) + \mathcal{H}(1-p_0)}{2} \right) \tag{3.130}$$

where $\mathcal{H}(p)$ is the entropy function [85] and the probabilities p_1 and p_0 can be expressed as

$$\begin{aligned} p_1 &= \Pr\Big(a_k[n] > \gamma \,|\, s_{ik}[n-n_d] = 1 \Big) \\ &= Q_1\Big(\frac{1}{\hat{\sigma}_n}\sqrt{2\hat{\alpha}P_t}, \frac{1}{\hat{\sigma}_n}\sqrt{2}\gamma \Big) \\ p_0 &= \Pr\Big(a_k[n] < \gamma \,|\, s_{ik}[n-n_d] = 0 \Big) \\ &= 1 - Q_1\Big(0, \frac{1}{\hat{\sigma}_n}\sqrt{2}\gamma \Big) \end{aligned} \tag{3.131}$$

Modulation symbol achievable rate

The combined signal in (3.128) passes through the RF chain and the high resolution ADC and thus, the modulation symbol x_j can be decoded, for simplicity we drop the time notation in this part. In order to obtain received signal amplitude that does not depend on x_j we consider constant amplitude constellation (M-PSK) and thus, I_m with the M-PSK shaping loss [54] can be expressed as

$$I_m = \sum_{i=1}^{2^{N_a}-1} \Pr(\mathbf{s}_i) \sum_{j=1}^{2^{N_a}} \Pr(\hat{\mathbf{s}}_j | \mathbf{s}_i) \times \frac{1}{2}\log_2\left(\frac{4\pi}{e} \text{SINR}|_{\mathbf{s}_\text{i},\hat{\mathbf{s}}_\text{j}} \right) \tag{3.132}$$

$$\text{SINR}|_{\mathbf{s}_\text{i},\hat{\mathbf{s}}_\text{j}} = \frac{\left(\sum_{k=1}^{N_a} s_{ik}\hat{s}_{jk} \right)^2}{\max\left(\sum_{k=1}^{N_a} \hat{s}_{jk}, 1 \right)} \frac{\hat{\alpha}P_t}{\hat{\sigma}^2} \tag{3.133}$$

Algorithm 3.6 RAS via QR decomposition

Input : $\hat{\mathbf{H}}[d], d = 0, \cdots, N_c - 1$
Output : $\mathcal{S}$
$\mathbf{H}_b = \left[\hat{\mathbf{H}}[0], \cdots, \hat{\mathbf{H}}[N_c - 1]\right]$, $I_{\mathrm{RSM}}(0) = 0$
$[\mathbf{Q}\ \mathbf{R}] = \mathrm{QR}\left(\mathbf{H}_b\right)$
$\mathcal{K} = \text{index sort}\left(\mathrm{diag}\left(\mathbf{R}\right), \text{descend}\right)$
for $i = 1 : N_r$
  $\mathbf{H}_x[d] = \hat{\mathbf{H}}[d](\mathcal{K}(1:i), :), \quad d = 0, \cdots, N_c - 1$
  Use $\mathbf{H}_x$[d] to determine $\hat{\mathbf{H}}_c$ as equation (3.114)
  $\hat{\mathbf{F}}_c = \hat{\mathbf{H}}_c \left(\hat{\mathbf{H}}_c \hat{\mathbf{H}}_c^H\right)^{-1} \mathbf{E}_{n_d}$ with optimal n_d
  Use $\hat{\mathbf{F}}_c$ to determine $\hat{\alpha}$ and $\hat{\sigma}_n^2$
  Determine $I_{\mathrm{RSM}}(i)$
  if $(I_{\mathrm{RSM}}(i) < I_{\mathrm{RSM}}(i-1))$, break, **end if**
  $\mathcal{S} = \mathcal{K}(1:i)$
end for
return $\mathcal{S}$

$$\Pr\left(\hat{\mathbf{s}}_j | \mathbf{s}_i\right) = \prod_{k=1}^{N_a} \Pr\left(a_k \underset{\hat{s}_{jk}=0}{\overset{\hat{s}_{jk}=1}{\gtrless}} \gamma\right), \Pr\left(\mathbf{s}_i\right) = \frac{1}{2^{N_a}} \tag{3.134}$$

As mmWave channel is spatially sparse and badly conditioned the channel is rank deficient if all receive antennas are selected, so ZF pre-equalizer is not possible unless we ensure full row rank channel. This can be achieved by the smart removal of the receive antennas. We perform the RAS at the BS to maximize the mutual information and then the BS informs the UT about the selected antennas through control channel. The RAS based exhaustive search is computationally complex especially in large MIMO systems. Thus, we propose fast and efficient RAS algorithm based on the QR decomposition [74] as illustrated in Algorithm 3.6.

In Algorithm 3.6, the QR decomposition is exploited to sort the best antennas in one step. Then, we add one antenna per iteration to the set $\mathcal{S}$ and stop by decreasing the mutual information. Finally, the set $\mathcal{S}$ includes the selected antennas. The RAS decision is performed at the BS and the UT be informed through zero error control channel. Algorithm 3.6 is much faster than the exhaustive search as the maximum number of needed iterations at Algorithm 3.6 is N_r.

3.3.3.4 Fully digital OFDM MIMO

We compare the performance of the proposed energy efficient RSM scheme with the OFDM FD MIMO system. For fair comparison, we assume the CSI is known only at the BS for the FD MIMO system and hence we apply ZF precoder per subcarrier, water-filling power allocation among subcarriers and RAS is performed to maximize the mutual information. We consider M-QAM symbols for the FD system with shaping loss 1.53 dB [94] where the mutual information can be expressed as

$$I_{\text{FD}} = \frac{N_a}{K + C_p} \sum_{k=1}^{K} \log_2 \left(1 + \frac{\frac{P_k}{\sigma^2} / \frac{\pi e}{6}}{\text{Tr}\left\{ (\mathbf{H}_{fa}[k] \mathbf{H}_{fa}[k]^H)^{-1} \right\}} \right) \tag{3.135}$$

where P_k is the subcarrier power, $\sum_{k=1}^{K} P_k = KP_t$, $\mathbf{H}_{fa}[k]$ is the channel after the RAS and C_p is the cyclic prefix.

In FD OFDM MIMO, specific precoder is needed for each subcarrier and the UT needs to know the received power per subcarrier to perform amplitude adjustment before detection that increases the DL training overhead when large number of subcarriers are considered. In contrast, the proposed scheme considers single pre-equalizer and the UT needs one DL training symbol for detection.

3.3.3.5 Simulation Results for wideband RSM scheme

In this section, we compare the SE and the EE of the proposed scheme with FD OFDM system. The EE is defined as the SE per the hardware power consumption at the UT. We use the power consumption model in [28] with $P_{\text{ref}} = 20$ mW. In the simulation environment, we consider $C = 4$, $L = 16$, $N_c = 4$ [11], $K = 4096$, $C_p = 25\%$ as in IEEE 802.11ad, g_{li} are i.i.d $\mathcal{CN}(0, 1)$, $\tau_{li} \in [0, (N_c - 1)T_s]$ is uniformly distributed, $(\tau_{1i} = \tau_{2i} = \cdots = \tau_{Li})$, (ϕ_{li}, θ_{li}) have Laplacian distribution with uniform random means $(\phi_i \in [-\pi/6, \pi/6], \theta_i \in [-\pi, \pi])$ and angular spreads $\sigma_\phi = \sigma_\theta = 3^\circ$ and $\text{SNR} = P_t/\sigma^2$.

Table 3.2: Average N_a over 1000 iterations and $\sigma_e^2 = 0.01$

SNR [dB] / Scheme	-20	-10	0	5
Proposed RSM, $N_r = 8$	1	1.04	2	2.4
FD OFDM, $N_r = 8$	1.09	1.4	2.2	2.6
Proposed RSM, $N_r = 16$	1	1.07	2.2	2.7
FD OFDM, $N_r = 16$	1.13	1.5	2.6	3.1

Fig. 3.15 shows that the SE saturates with the number of the pre-equalizer taps at perfect and imperfect CSI that can be exploited to reduce the hardware

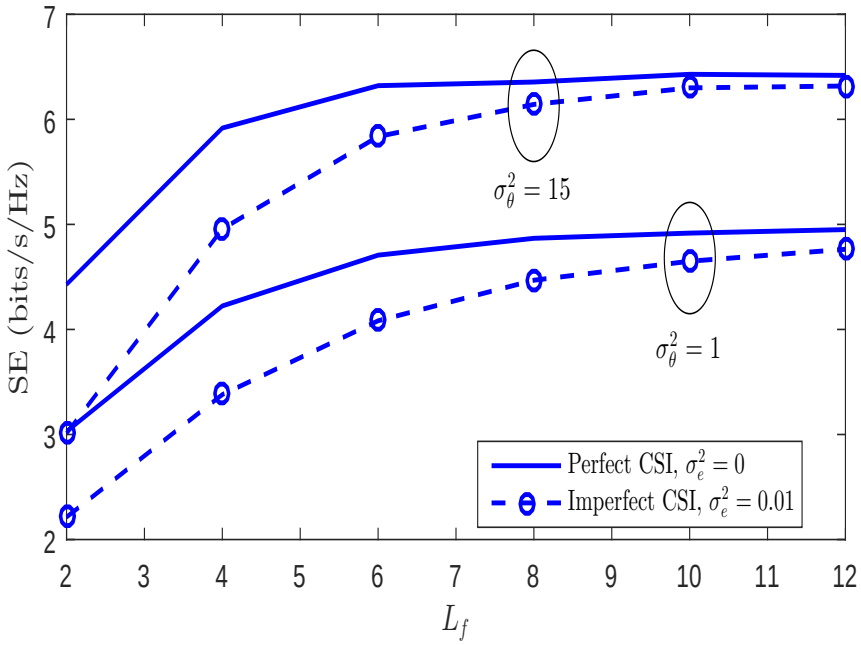

Figure 3.15: Spectral efficiency of the proposed RSM scheme with number of pre-equalizer taps, $N_t = 64$, $N_r = 8$, SNR $= 0$ dB and (average over 1000 realizations).

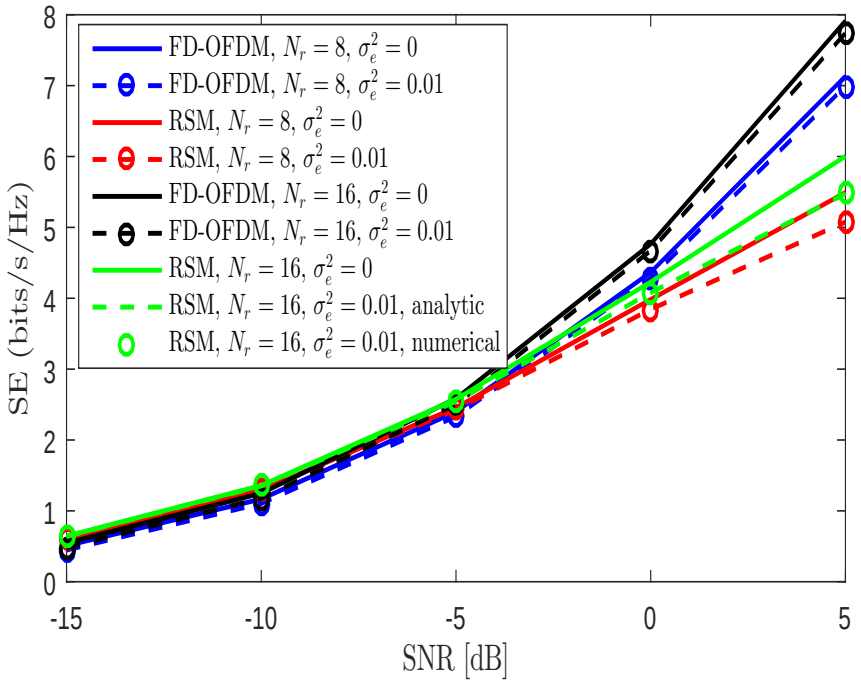

Figure 3.16: Spectral efficiency of the proposed RSM scheme compared to FD OFDM MIMO at $N_t = 32$, $L_f = 10$ and (average over 1000 realizations).

complexity of the BS. Channels with wider angular spread allow more ARA, and thus the spatial symbol can convey more information bits that improves the SE.

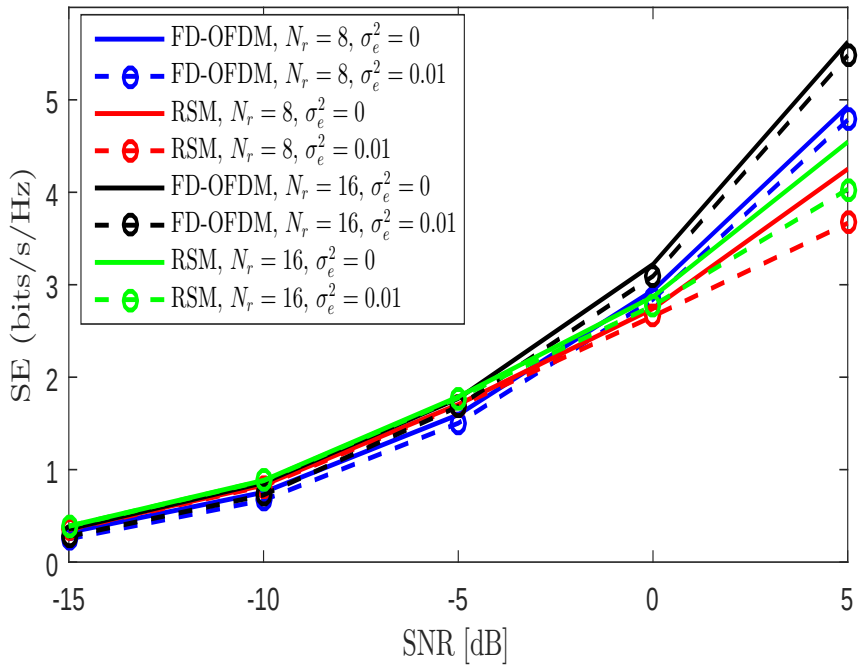

Figure 3.17: 10% Outage spectral efficiency of the proposed RSM scheme compared to FD OFDM MIMO at $N_t = 32$, $L_f = 10$ and (evaluated over 1000 realizations).

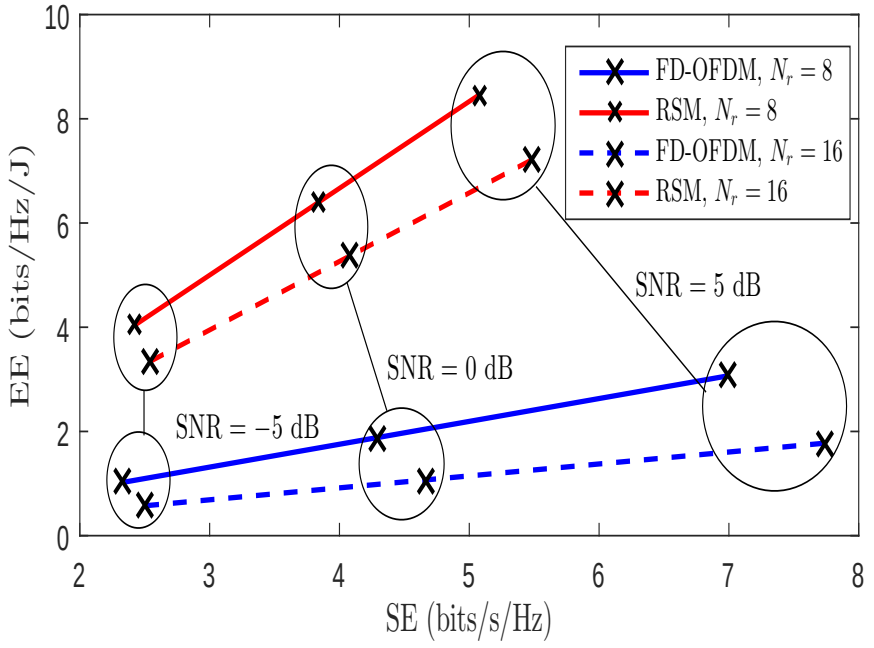

Figure 3.18: Spectral efficiency versus energy efficiency trade-off of the proposed RSM scheme compared to FD OFDM MIMO at $N_t = 32$, $L_f = 10$, $\sigma_e^2 = 0.01$ and (average over 1000 realizations).

Fig. 3.16 and Fig. 3.17 show that the average and outage SE of the proposed scheme (SRF chain) is comparable with the FD OFDM at perfect and imperfect

CSI at the BS. This can be justified as mmWave channels are rank deficient and suffers from severe path loss [68] and thus, the ZF precoder is possible with few number of ARA as depicted in Table 3.2. Therefore, the number of transmit symbols per subcarrier for the FD OFDM is less than number of receive antennas.

Table 3.2 shows that the number of ARA that maximizes the SE is much less than N_r and thus the RAS is substantial with the badly conditioned mmWave channels.

Fig. 3.18 illustrates that the proposed scheme approaches the SE of the FD OFDM and attains superior EE because the proposed UT architecture depends on SRF chain and one high resolution ADC as shown in Fig. 2.1.

3.3.4 Multiple Radio Frequency Chains UT

In this section, we propose novel and low power consuming UT architecture that can work in two modes, RSM or CM by adjusting controlling switches. For the sake of improving the SE, we extend the work in [41] into MRF chains at the UT and we propose a novel combining scheme that achieves high SE assuming single user system.

In Fig. 2.4, for the sake of improving the SE, we propose a novel energy efficient UT circuitry that extends the architecture in Fig. 2.1 into MRF chains. In the proposed architecture, we consider energy efficient control switches. First, the switch $S_k^{''}$ controls the ON/OFF status of the k-th UT antenna. Second, only one of the switches $(S_{i1}^{'}, \cdots, S_{iN_{rf}}^{'})$ is ON to connect the i^{th} received signal to a specific RF chain. Finally, the switch S_{ij} can be always closed (IC scheme) or controlled by the received spatial symbol (DC scheme). The status of switches remains fixed within the channel coherence time.

3.3.4.1 Multiple RF RSM with independent combining (MRF-RSM-IC)

We can transmit multiple modulation symbols and a single spatial symbol per channel use by employing MRF chains at the UT. Therefore, the SE can be more severely affected if transmitting the all-zeroes spatial symbol. This further motivates the IC scheme where the modulation symbols are transmitted even for the all-zeroes spatial symbol. In this case, the transmit signal vector at the precoder input can be expressed as

$$\mathbf{x}_i^j = \mathbf{\Lambda}\left(\mathbf{s}_i\right)\mathbf{F}\mathbf{x}_j \tag{3.136}$$

where $\mathbf{\Lambda}\left(\mathbf{s}_i\right) \in \mathbb{R}^{N_a \times N_a}$ is a diagonal matrix whose entries contain the spatial symbols $\mathbf{\Lambda}_{ii} \in \{\alpha_0, 1-\alpha_0\}$, $\mathbf{x}_j \in \mathbb{C}^{N_m \times 1}$, $N_m \leqslant N_{rf}$ is the number of the transmitted modulation symbols and $\mathbf{F} \in \mathbb{R}^{N_a \times N_m}$ is a matrix that maps from the N_m modu-

lation symbols to N_a active antennas and can be expressed as

$$\mathbf{F}_{nm} = \begin{cases} 1 & \text{if } n-m = lN_m, l = 0, \cdots, \lfloor \frac{N_a-1}{N_m} \rfloor. \\ 0 & \text{else} \end{cases} \tag{3.137}$$

where the n-th ARA receives the m-th modulation symbol if $\mathbf{F}_{nm} = 1$. The covariance matrix $\mathbf{R}_{ss}$ can be expressed as

$$\mathbf{R}_{ss} = \mathrm{E}\Big[\mathbf{\Lambda}\left(\mathbf{s}_i\right)\mathbf{F}\mathbf{F}^H\mathbf{\Lambda}\left(\mathbf{s}_i\right)^H\Big] = \frac{1}{2^{N_a}}\sum_{i=1}^{2^{N_a}}\mathbf{\Lambda}\left(\mathbf{s}_i\right)\mathbf{F}\mathbf{F}^H\mathbf{\Lambda}\left(\mathbf{s}_i\right)^H \tag{3.138}$$

The detection of the spatial symbol and the spatial mutual information ($I_S^{\text{MRF-RSM-IC}}$) are the same as in the SRF case. The combined signal vector $\mathbf{y}_c$ of the modulation symbols and the combined $\text{SNR}_{c,l}$ of the l^{th} modulation symbol can be expressed as

$$\mathbf{y}_c = \mathbf{F}^T\left(\sqrt{\alpha_r P_t}\mathbf{\Lambda}\left(\mathbf{s}_i\right)\mathbf{F}\mathbf{x}_j + \mathbf{n}\right), \quad \text{SNR}_{c,l} = \frac{\left(\left[\mathbf{F}^T\mathbf{\Lambda}\left(\mathbf{s}_i\right)\mathbf{F}\right]_{ll}\right)^2}{\left[\mathbf{F}^T\mathbf{F}\right]_{ll}}\frac{\alpha_r P_t}{\sigma^2}. \tag{3.139}$$

where, at the UT, the matrix $\mathbf{F}^T$ is used to connect N_a received symbols to N_m RF chains: the n-th received symbol goes to the m-th RF chain if $\mathbf{F}_{nm} = 1$ (the switch S'_{nm} in Fig. 2.4 is closed). The modulation symbols mutual information and the SE of the MRF-RSM-IC scheme can be expressed as

$$\begin{aligned} I_M^{\text{MRF-RSM-IC}} &= \sum_{l=1}^{N_m}\sum_{i=1}^{2^{N_a}}\Pr\left(\mathbf{s}_i\right) I_{M-\text{PSK}}\left(\text{SNR}_{c,l}\right), \\ \text{SE}^{\text{MRF-RSM-IC}} &= I_S^{\text{MRF-RSM-IC}} + I_M^{\text{MRF-RSM-IC}}. \end{aligned} \tag{3.140}$$

3.3.4.2 Multiple RF Conventional Modulation (MRF-CM)

In the CM scheme with MRF chains at the UT, it is possible to transmit $N_m \leq N_{rf}$ M-QAM symbols to maximize the SE

$$\text{SE}^{\text{MRF-CM}} = \sum_{l=1}^{N_m}\log_2\left(1 + \frac{\alpha_c P_t}{\sigma^2}/\frac{\pi e}{6}\right). \tag{3.141}$$

by properly selecting the active antennas. In order to be able to apply ZF precoding at the BS, we ensure full-rank channel by activating the set of receive antennas that maximizes the SE.

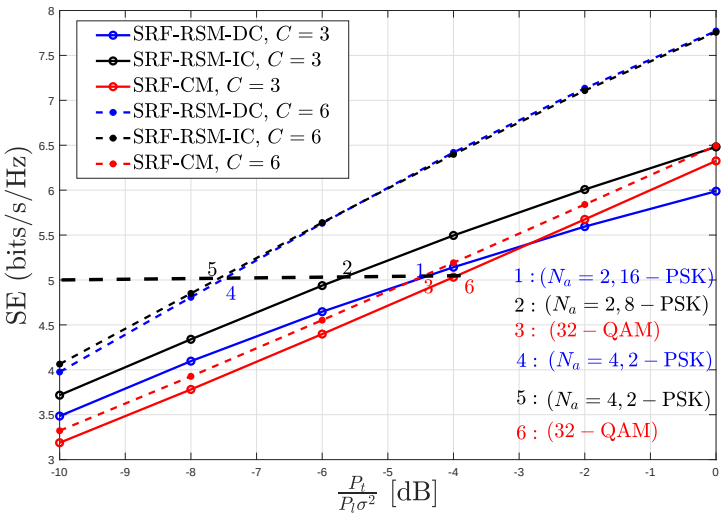

Figure 3.19: Spectral efficiency of the single user RSM-DC, RSM-IC and CM assuming single RF UT, $N_t = 128$ and $N_r = 16$ (average over 1000 channel realizations).

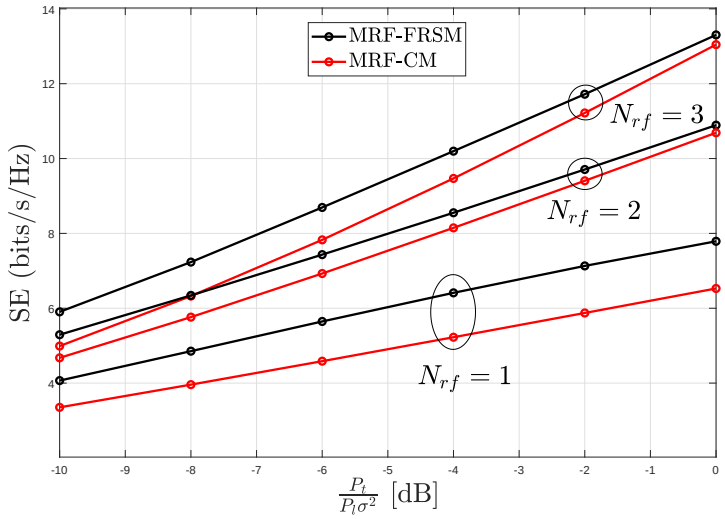

Figure 3.20: Spectral efficiency of the single user flexible RSM compared to CM assuming multiple RF UT, $N_t = 128$, $N_r = 16$ and $C = 6$ (average over 1000 channel realizations).

3.3.4.3 Simulation Results

Fig. 3.19 compares the SE of the RSM-DC, RSM-IC and CM schemes for a single user system assuming a SRF chain at the UT and the RAS method. At low number of scattering clusters C, the IC scheme outperforms the DC but they have similar performance at high C. To understand this behavior, we should keep in mind that a large value of C implies a larger rank channel matrix and hence more active antennas. In the DC scheme, the modulation symbol is not transmitted

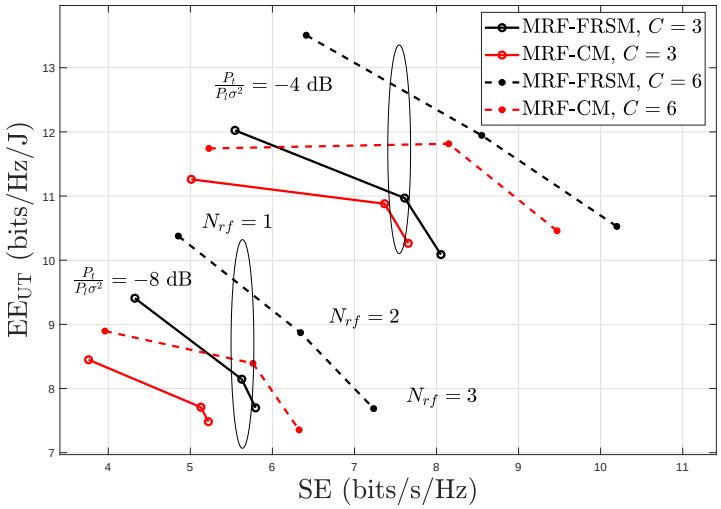

Figure 3.21: Trade-off in spectral efficiency versus energy efficiency at the UT of the single user flexible RSM compared to CM assuming multiple RF UT, $N_t = 128$ and $N_r = 16$ (average over 1000 channel realizations).

with high probability for low C and this degrades the SE. Higher values of C allow transmitting more spatial bits and thus, the SE of the RSM schemes outperform CM transmission considering SRF at the UT.

Fig. 3.20 illustrates the SE of the flexible RSM (FRSM) scheme compared to the simple CM transmission for single user system assuming MRF chains at the UT and applying the RAS procedure. The FRSM scheme outperforms the CM especially at low number of RF chains at the UT. Increasing N_{rf} at the UT allows transmitting more modulation symbols and single spatial symbol. Thus, the SE of FRSM and CM transmissions converge at high N_{rf}.

Fig. 3.21 shows the $\mathrm{SE} - \mathrm{EE_{UT}}$ trade-off of the FRSM scheme compared to CM transmission for the single user system assuming MRF chains at the UT and the RAS method at realistic SNR values of the outdoor mmWave propagation. The FRSM outperforms the CM in SE and EE at low and high SNR regimes. Increasing N_{rf} improves the SE and increases the power consumption at the UT which entails a degradation in the $\mathrm{EE_{UT}}$.

3.4 Spatial Modulation for Joint Uplink and Downlink Massive MIMO System

In this section, first, we study the impact of the UL circuitry on the DL SE. Then, we propose an UL HTSM scheme. After that, we propose a DL HRSM scheme. Finally, we jointly optimizes the UL and DL system parameters considering SM

scheme implemented on novel hybrid hardware at the UT (hybrid means that the precoding and combining are performed in RF and baseband in a similar way to the one in Fig. 1.3). Specifically, thanks to the channel reciprocity assumption, we propose a single optimization algorithm for the UL and the DL design. This joint optimization design has lower computational complexity at the BS than the individual design and attains the same performance as explained in the description of Algorithm 3.11 in page 103.

3.4.1 The Impact of the UL Circuitry on the DL Spectral Efficiency

In this section, we exploit the spatial dimension at the UT to attain high SE in the UL and DL transmissions based on energy efficient UT's circuitry. Specifically, we propose two hybrid UL UT's architectures where each demands specific DL control signals overhead and hence the DL SE is affected by the UL transmission scheme selected. Thus, we design the UL architecture by taking special attention to the UL SE, DL SE, UL hardware power consumption and computational complexity. The contributions and novelties of this section are published in **[C5]** and can be expressed as follows

- We propose energy efficient UL/DL spatial transmission schemes and propose a joint design.
- We develop two novel UL schemes based on novel energy efficient architectures that outperform the state-of-the-art in terms of SE and EE.

3.4.1.1 UL Transmit Spatial Modulation

In this section, we propose three UL transmission schemes based on three UL architectures as shown in Fig. 2.2a, 2.2b and 2.2c. We compare the three UL schemes in terms of SE, EE, computational complexity and the number of DL control symbols overhead.

UL hybrid transmit spatial modulation

In HTSM as proposed in [38], the UT antennas are divided into N groups each contains N_g antennas. Incoming bit stream is divided into two parts where the first $\log_2 N$ bits are used to choose the antenna array index and the remaining $\log_2 M$ bits are modulated according to an M-ary modulation scheme. The UT chooses the analog beamformer for the selected antenna array and transmits the modulated symbol through this antenna array. We assume TDD reciprocity where the UL channel matrix $\mathbf{H}^u$ is the transpose of the DL channel matrix $\mathbf{H}$. The

received symbol at the BS can be written as

$$\mathbf{r} = \sqrt{P_t}\mathbf{H}_n^u \mathbf{f}_n x_j + \mathbf{n}. \tag{3.142}$$

Therein, x_j is the j-th symbol from M-ary constellation diagram, $\mathbf{f}_n \in \mathbb{C}^{N_g \times 1}$ is the analog beamformer vector of n-th antenna array and $\mathbf{H}_n^u \in \mathbb{C}^{N_t \times N_g}$ is the channel between n-th antenna array and the BS. Finally, P_t is the average transmit power of the UT. We consider ULA analog beamformer where its response can be expressed as

$$\mathbf{f}_n = \frac{1}{\sqrt{N_g}}[1, e^{j\pi \sin(\phi_n)}, \ldots, e^{j\pi(N_g-1)\sin(\phi_n)}]^T, \tag{3.143}$$

where ϕ_n is the quantized angle $\frac{2\pi l}{L}$ from a codebook $\mathcal{F} = \{\mathbf{f}_l \in \mathbb{C}^{N_g \times 1} : \mathbf{f}_l^H \mathbf{f}_l = 1,\, l = 1, \ldots, L\}$ with $L = 2^B$ where B represents the resolution of codebook.

The BS decides the best analog beamformer for each antenna array of the UT, so as to steer the power through the strongest path during the UL data transmission phase. This is done based on the acquired CSI as follows

$$\mathbf{f}_n = \arg \max_{\forall \mathbf{f}_l \in \mathcal{F}} ||\mathbf{H}_n^u \mathbf{f}_l||^2. \tag{3.144}$$

The BS informs the UT about the best f_n through DL control channel with low overhead as illustrated in the sequel. In the UL reception, the BS applies a digital combiner as follows

$$\mathbf{y}^u = \mathbf{W}\sqrt{P_t}\mathbf{H}_n^u \mathbf{f}_n x_j + \mathbf{W}\mathbf{n}, \tag{3.145}$$

where the digital combiner $\mathbf{W} \in \mathbb{C}^{N \times N_t}$ is constructed by the help of ZF principles as $\mathbf{W} = [\mathbf{H}_1^u \mathbf{f}_1, \ldots, \mathbf{H}_N^u \mathbf{f}_N]^\dagger = \mathbf{D}^\dagger$. Herein, $\mathbf{y}^u \in \mathbb{C}^{N \times 1}$ contains the information of the selected UT antenna array index and the modulated symbol. Each entry of $\mathbf{y}^u$ has the following values

$$\mathbf{y}^u(l) = \begin{cases} x_j + \mathbf{z}(l) & \text{if} \quad n = l \\ \mathbf{z}(l) & \text{if} \quad n \neq l \end{cases} \tag{3.146}$$

where $\mathbf{z}(l)$ is the l-th entry of $\mathbf{z} = \mathbf{W}\mathbf{n}$. Finally, the transmitted symbol is decoded jointly by applying ML detector as

$$[\hat{n}, \hat{x}_j] = \arg \min_{l,m} \left| \mathbf{y}^u(l) - \sqrt{P_t} x_m \right|^2. \tag{3.147}$$

We evaluate the UL joint spatial and modulation bit error rate P_e numerically by generating spatially modulated symbols, transmitting through the channel, detect-

ing them and then calculating the number of correctly received bits per the total number of transmitted bits. Hence, we determine the UL SE (R_{UL}) as

$$R_{UL} = (\log_2 N + \log_2 M)\,(1 - P_e)^{\log_2 N + \log_2 M}, \tag{3.148}$$

where N and M are designed to maximize the UL SE. A closed form expression of P_e can be obtained from the union bound error probability of the ML detector.

UL hybrid TSM with uniform grouping

In this scheme, the UT antennas are uniformly distributed among the channel groups $(\mathbf{H}_1^u, \ldots, \mathbf{H}_N^u)$ where $\mathbf{H}_1^u$ and $\mathbf{H}_N^u$ include UT antennas indices from 1 to N_g and $N_g(N-1)+1$ to NN_g, respectively. Mapping the UT antennas into groups does not depend on the channel and hence, UG does not require any computational complexity. The BS designs the quantized analog beamforming angles ϕ_n and informs the UT about them during the DL training. Thus, this scheme requires NB/R_{DL} control symbols where R_{DL} is the DL SE. Fig. 2.2a shows that this scheme requires N_g PSs and N_r switches. However, UG could create correlation among the groups. Hence, the BS may be unable to distinguish between similar groups and as a result we could loose spatial data.

For the sake of improving the UL SE, we propose two novel UL SM schemes, each having specific hardware architecture and we compare their SE with the state-of-the-art (UG). Then, we show that the UL transmission scheme affects the DL SE due to the variation in the DL control signals overhead. Hence, the best UL scheme is designed based on UL SE, DL SE and UL EE.

UL hybrid TSM with transmit antenna grouping

In this scheme, and for each channel realization, we select the best N_g transmit antennas in each group to maximize the post processing received SNR. For simplicity, we consider infinite resolution codebook in selecting the best antennas inside each group where the analog beamformer can be expressed as

$$\mathbf{f}_n = \mathbf{v}_1\left(\mathbf{H}_n \mathbf{H}_n^H\right), \tag{3.149}$$

where $\mathbf{v}_1\{.\}$ denotes the maximum eigenvector. The associated post processing received SNR_n can be expressed as

$$\mathrm{SNR}_n = \frac{P_t/\sigma^2}{[\mathbf{W}\mathbf{W}^H]_{n,n}} = \frac{P_t/\sigma^2}{[\mathbf{D}^\dagger(\mathbf{D}^\dagger)^H]_{n,n}} = \frac{P_t/\sigma^2}{[\mathbf{R}^{-2}]_{n,n}}. \tag{3.150}$$

where $[\mathbf{Q}\,\mathbf{R}\,\mathbf{e}] = \mathrm{QR}(\mathbf{D}, 0)$, $\mathbf{R}$ is a square upper triangular matrix and $\mathbf{D}(:, \mathbf{e}) =$

Algorithm 3.7 TAG via QR decomposition

1: **Input** : $\mathbf{H}, N, N_g, K = \binom{N_r}{N_g}$ and tol $= 10^{-5}$
2: **Output** : $\mathcal{S}$
3: Generate all possible groups $\mathbf{H}_a(i), i = 1, \cdots, K$
4: $\mathbf{f}_i = \mathbf{v}_1 \left(\mathbf{H}_a(i)\mathbf{H}_a(i)^H\right), i = 1, \cdots, K$
5: $\mathbf{X} = [\mathbf{H}_a^u(1)\mathbf{f}_1, \ldots, \mathbf{H}_a^u(K)\mathbf{f}_K]$
6: $[\mathbf{Q}\ \mathbf{R}\ \mathbf{e}] = \mathrm{QR}(\mathbf{X}, 0)$ such that $\mathbf{X}(:, \mathbf{e}) = \mathbf{QR}$
7: $N_{\max} = \mathrm{Find}\left(|\mathrm{diag}(\mathbf{R})| \geqslant \mathrm{tol}|\mathbf{R}_{11}|\right)$
8: $\mathcal{S} = \mathbf{e}\left(1 : \min\left(N, 2^{\lfloor \log_2 N_{\max} \rfloor}\right)\right)$
9: **return** $\mathcal{S}$

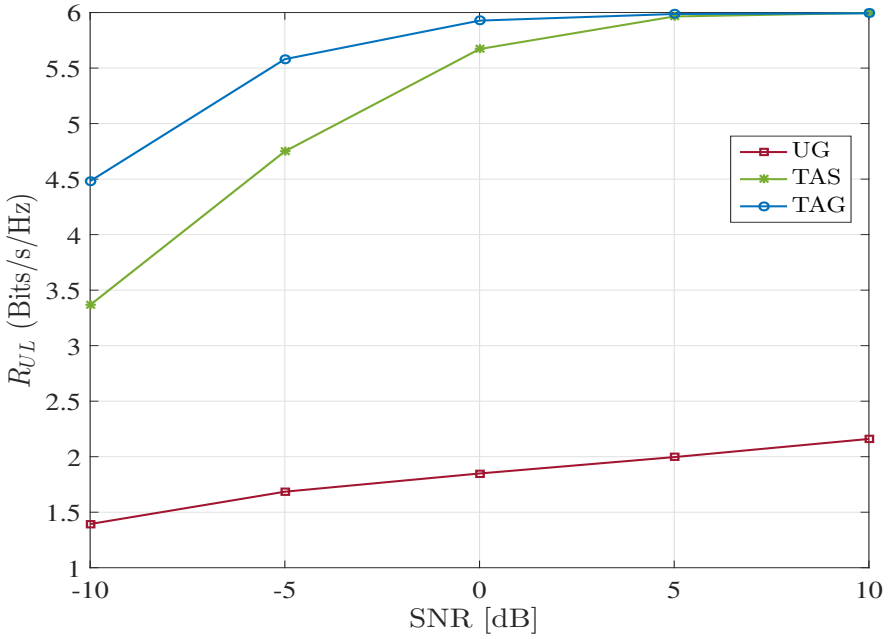

Figure 3.22: UL SE of different UL transmission schemes at $N_t = 128$, $N = 4$, $N_g = 4$, $C = 3$, $\xi = 1$, $\sigma^2 = 1$ and (average over 1000 realizations)

QR. In Algorithm 3.7, we generate all possible channel groups and then, we select the best possible groups to maximize the received SNR shown in equation (3.150) through maximizing the diagonal entries of $\mathbf{R}$ in one step thanks to the QR decomposition. Although this scheme maximizes the received SNR, it demands $\binom{N_r}{N_g}$ maximum eigenvector computations and one QR decomposition that could be computationally complex for massive UT arrays. Moreover, extra DL control symbols are needed to inform the UT about the antennas selected in each group. This scheme requires $N(B + N_r)/R_{DL}$ control symbols. Fig. 2.2b shows that TAG needs N_g PSs and $N_g N_r$ switches.

UL TSM with transmit antenna selection

This scheme is a special case of TAG when each group contains one antenna

Algorithm 3.8 TAS via QR decomposition

1: **Input** : $\mathbf{H}^u, N$ and tol
2: **Output** : $\mathcal{S}$
3: $[\mathbf{Q}\ \mathbf{R}\ \mathbf{e}] = \mathrm{QR}\left(\mathbf{H}^u, 0\right)$ such that $\mathbf{H^u}\left(:, \mathbf{e}\right) = \mathbf{QR}$
4: $N_{\max} = \mathrm{Find}\left(|\mathrm{diag}(\mathbf{R})| \geqslant \mathrm{tol}|\mathbf{R}_{11}|\right)$
5: $\mathcal{S} = \mathbf{e}\left(1 : \min\left(N, 2^{\lfloor \log_2 N_{\max} \rfloor}\right)\right)$
6: **return** $\mathcal{S}$

without analog beamforming. The received SNR can be expressed as

$$\mathrm{SNR}_n = \frac{P_t}{\sigma^2 \left[\left((\mathbf{H}^u)^H \mathbf{H}^u\right)^{-1}\right]_{n,n}}. \tag{3.151}$$

In Algorithm 3.8, we select the best possible antennas to maximize the received SNR by applying the QR decomposition. This scheme requires only one QR decomposition. Therefore, it is much faster than TAG when N_g is large and demands $(NB + N_r)/R_{DL}$ DL control symbols. As shown in Fig. 2.2c, the scheme requires N_r switches and no PSs are needed.

Impact of the selected UL scheme in the DL SE

Assuming N_{DL} is the total number of DL channel uses per frame and $\frac{N_r}{R_{DL}} + 1$ DL control channel uses are needed for all schemes to inform the UT about the DL active antennas and the DL detection threshold shown in Fig. 2.1. Moreover, each UL architecture requires specific number of DL control symbols for the beamforing in the UL data transmission phase and thus the DL SE varies with the UL architecture as

$$\mathrm{SE}_{DL,\mathrm{UG}} = \left(\frac{N_{DL} - \left(\frac{N_r + NB}{R_{DL}} + 1\right)}{N_{DL}}\right) R_{DL}, \tag{3.152}$$

$$\mathrm{SE}_{DL,\mathrm{TAG}} = \left(\frac{N_{DL} - \left(\frac{N_r + NB + NN_r}{R_{DL}} + 1\right)}{N_{DL}}\right) R_{DL}, \tag{3.153}$$

$$\mathrm{SE}_{DL,\mathrm{TAS}} = \left(\frac{N_{DL} - \left(\frac{2N_r}{R_{DL}} + 1\right)}{N_{DL}}\right) R_{DL}. \tag{3.154}$$

Fig. 3.22 shows that TAG achieves the best performance due to its ability to combat the spatial correlation by optimizing the antennas inside each group. TAG outperforms TAS at low SNR due to the beamforing gain provided by TAG algorithm and TAS approaches the performance of TAG at high SNR.

Fig. 3.31a shows the SE-EE trade-off of the three UT architectures. TAS achieves superior EE, since it does not require PSs. The SE achieved by TAS

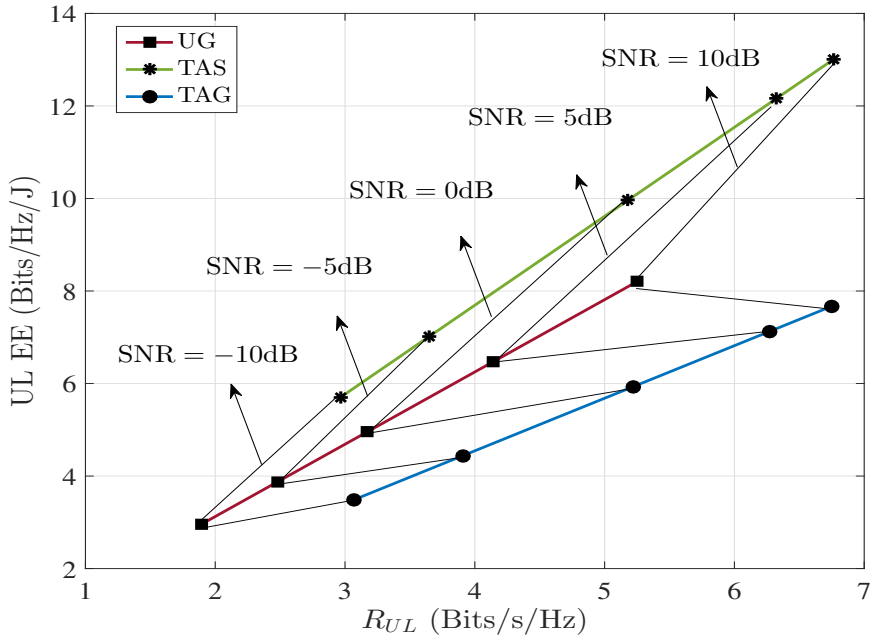

Figure 3.23: UL SE vs EE of different UL transmission schemes at $N_t = 128$, $N = 4$, $N_g = 4$, $C = 5$, $\xi = 1$, $\sigma^2 = 1$ and (average over 1000 realizations)

at $C = 5$ approaches the TAG. Hence, TAS is the best at sufficient SNR or at moderate scattering environment.

3.4.1.2 DL Receive Spatial Modulation

In the DL RSM, the BS transmits data per channel use in the form of two modulated symbols where $N_a \leqslant N_r$ data bits are mapped onto the spatial symbol $\mathbf{s}_i \in \mathbb{R}^{N_a \times 1}, i = 1, \cdots, 2^{N_a}$ and $\log_2 M$ data bits are mapped onto the M-ary constellation diagram modulation symbol x_j. The transmit symbol $\mathbf{x}_i^j$ at the precoder input can be expressed as

$$\mathbf{x}_i^j = \begin{cases} \mathbf{s}_i x_j & \text{if} \quad \mathbf{s}_i \neq \mathbf{0}_{N_r} \\ \mathbf{s}_i & \text{if} \quad \mathbf{s}_i = \mathbf{0}_{N_r} \end{cases} \tag{3.155}$$

where the modulation symbol is not transmitted if the spatial symbol is all zeros. The symbol $\mathbf{x}_i^j$ passes through the precoder and the channel where the received symbol at the UT can be expressed as

$$\mathbf{y} = \mathbf{H}_a \mathbf{P} \mathbf{x}_i^j + \mathbf{n}. \tag{3.156}$$

Herein, $\mathbf{H}_a \in \mathbb{C}^{N_a \times N_t}$ is the channel after receive antennas selection (RAS) that illustrated in Sec. 3.4.1.2, $\mathbf{n} \in \mathbb{C}^{N_a \times 1}$ is the generated noise vector at the UT with i.i.d circularly symmetric complex Gaussian entries, $\mathcal{CN}(0, \sigma^2)$, and $\mathbf{P} \in \mathbb{C}^{N_t \times N_a}$

Algorithm 3.9 RAS via QR decomposition

Input : $\mathbf{H}$
Initial : $R_{\mathrm{DL}}(0) = 0$
Output : $\mathcal{S}$
$[\mathbf{Q}\,\mathbf{R}\,\mathbf{e}] = \mathrm{QR}\left(\mathbf{H}^{u}, 0\right)$ such that $\mathbf{H^u}\left(:, \mathbf{e}\right) = \mathbf{QR}$
for $i = 1 : N_r$
  $\mathbf{H}_x = \mathbf{H}(\mathbf{e}(1:i), :)$
  Determine $R_{\mathrm{DL}}(i) = I_s + I_m$
  if $(R_{\mathrm{DL}}(i) < R_{\mathrm{DL}}(i-1))$, break, **end if**
  $\mathcal{S} = \mathbf{e}(1:i)$
end for
return $\mathcal{S}$

is a ZF precoder, fixed during the coherence time, and satisfies

$$\mathrm{E}\left[\|\mathbf{P}\mathbf{x}_i^j\|_2^2\right] = \mathrm{Tr}\left\{\mathbf{P}\mathbf{R}_{ss}\mathbf{P}^H\right\} = P_t, \tag{3.157}$$

where $\mathbf{R}_{ss} = \mathrm{E}\left[\mathbf{s}_i\mathbf{s}_i^H\right]$ and P_t is the transmit power. The ZF precoder can be expressed as

$$\mathbf{P} = \sqrt{\alpha P_t}\mathbf{H}_a^H\left(\mathbf{H}_a\mathbf{H}_a^H\right)^{-1}, \tag{3.158}$$

where $\alpha = 1/\mathrm{Tr}\left\{\left(\mathbf{H}_a\mathbf{H}_a^H\right)^{-1}\right\}$ is a normalization factor used to fix the transmit power.

The detection of the spatial and modulation symbols for the DL RSM system based on ZF precoding is studied in [41]. In this system, each UT DL antenna is connected to an AD as shown in Fig. 2.1. The signal measured by the k-th AD is compared with a threshold $\hat{\gamma}$ to detect the k-th spatial bit such that $\hat{s}_{ik} \in \{0, 1\}$. Then, the modulation symbol detection is performed on the combined signal

$$y_c = \sum_{k=1}^{N_a} \sqrt{\alpha P_t}\hat{s}_{ik}s_{ik}x_j + \hat{s}_{ik}n_k \tag{3.159}$$

through the RF chain to enable decoding of the modulation symbol x_j. Note that the received signal per antenna is allowed to pass through the RF chain only if the detected spatial bit is one ($s_{ik} = 1$). In this way noise is not enhanced.

DL SE (R_{DL})

In [42], the authors show that the SE of the DL RSM scheme R_{DL} can be computed as spatial rate I_s plus modulation rate I_m. As each DL UT antenna detects

binary spatial bit, I_s can be expressed using the BAC rate expression as

$$I_s = N_a\left(\mathcal{H}\left(\frac{P_1+1-P_0}{2}\right)-\frac{\mathcal{H}(P_1)+\mathcal{H}(1-P_0)}{2}\right),$$

$$P_1 = \Pr\left(|\sqrt{\alpha P_t}+n|>\hat{\gamma}\right) = Q_1\left(\frac{1}{\sigma}\sqrt{2\alpha P_t},\frac{1}{\sigma}\sqrt{2}\hat{\gamma}\right),$$

$$P_0 = \Pr\left(|n|<\hat{\gamma}\right) = 1-Q_1\left(0,\frac{1}{\sigma}\sqrt{2}\hat{\gamma}\right). \tag{3.160}$$

where $\hat{\gamma}\approx\frac{1}{2}\sqrt{\alpha P_t}$, $Q_1(x)$ is first order Marcum Q function and the entropy function $\mathcal{H}(P) = -P\log_2 P-(1-P)\log_2(1-P)$.

In [41], the authors showed that the constant amplitude constellation ($M-$PSK) achieves the best performance for the DL RSM scheme, thus, we consider the shaping loss of the $M-$PSK symbols in evaluating the modulation symbol rate expression. Since we transmit one modulation symbol, I_m can be computed using the MISO channel rate formula as

$$I_m = \sum_{i=1}^{2^{N_a}-1}\Pr(\mathbf{s}_i)\sum_{j=1}^{2^{N_a}}\Pr(\hat{\mathbf{s}}_j|\mathbf{s}_i)\times\frac{1}{2}\log_2\left(\frac{4\pi}{e}\mathrm{SNR}|_{\mathbf{s}_i,\hat{\mathbf{s}}_j}\right),$$

$$\mathrm{SNR}|_{\mathbf{s}_i,\hat{\mathbf{s}}_j} = \frac{\left(\sum_{k=1}^{N_a}s_{ik}\hat{s}_{jk}\right)^2}{\max\left(\sum_{k=1}^{N_a}\hat{s}_{jk},1\right)}\frac{\alpha P_t}{\sigma^2}, \tag{3.161}$$

$$\Pr(\hat{\mathbf{s}}_j|\mathbf{s}_i) = \prod_{k=1}^{N_a}\Pr\left(|y_{ik}|\underset{\hat{s}_{jk}=0}{\overset{\hat{s}_{jk}=1}{\gtrless}}\hat{\gamma}\right), \Pr(\mathbf{s}_i) = \frac{1}{2^{N_a}}.$$

DL receive antenna selection

The spatially sparse nature of mmWave propagation leads to badly conditioned and rank deficient channels if all receive antennas are considered and thus the ZF precoder is unfeasible. Channel full-rank can be ensured by smart selection of receive antennas. A possible criterion is the maximization of the DL SE. The RAS is performed at the BS and then the UT is informed through control channel. For the sake of reducing the computational complexity, we propose an efficient RAS algorithm based on QR decomposition a much faster approach than exhaustive search.

In Algorithm 3.9, we apply QR decomposition to sort the independent antennas in one step. Next, we select the receive antennas sequentially where we select one antenna per iteration and add it to the set $\mathcal{S}$ (the set includes the selected

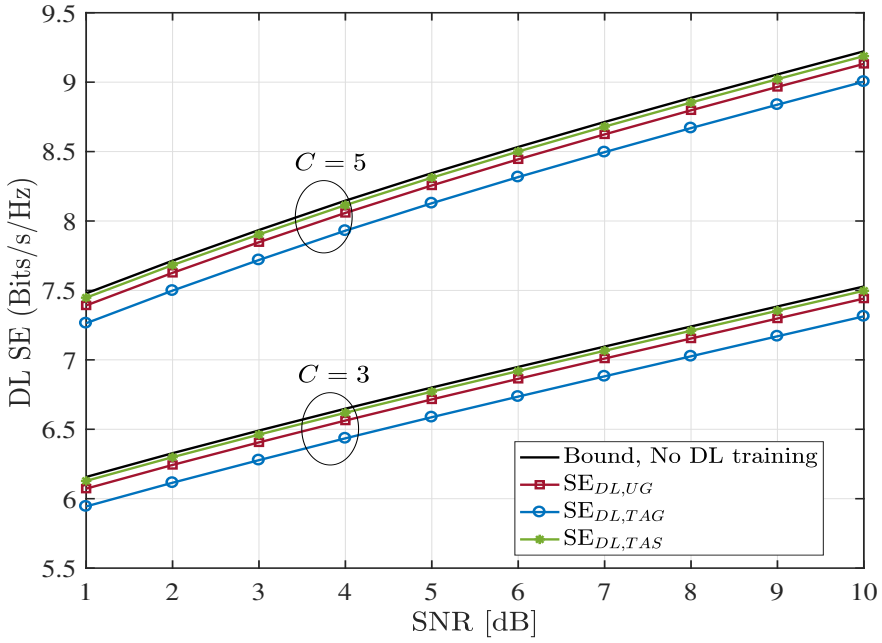

Figure 3.24: DL SE corresponding to different UL transmission schemes at $N_t = 128$, $N = 4$, $N_g = 4$, $\xi = 1$, $\sigma^2 = 1$ and (average over 1000 realizations)

antennas). We stop adding more antennas when the DL SE decreases.

Fig. 3.24 shows the DL SE efficiency for the different UL architectures assuming $N_{DL} = 500$ as in 5G New Radio. The DL SE is not sensitive to the UL architecture as the number of required DL control symbols for all architectures are much smaller than N_{DL}. Therefore, we select the best UL architecture based on UL SE, EE and the computational complexity.

3.4.1.3 Evaluation on deterministic ray-based channels

We validate the results in more realistic channel model assuming one 128 ULA BS and 60 user locations each with 32 ULA distributed inside a 28-GHz small-cell in Manhattan area in New York City. 37 users are in line-of-sight connection with the BS as shown in Fig. 3.25. The antenna elements at the BS have 60° aperture and the antenna elements at the MS are isotropic. The BS is 8 meter above the ground and the UTs are 1.5 meter above the ground. The mmWave massive MIMO channels between the UTs and the BS are predicted from the ray-based Volcano technology by SIRADEL [95]. The Volcano model computes deterministic multiple paths that combine interactions with the buildings, trees and ground. It has been widely used in the last twenty years to assess the multi-path channel and network performance, either in urban, indoor and mixed environments. Afterwards, we compare the results obtained from the stochastic channel with the

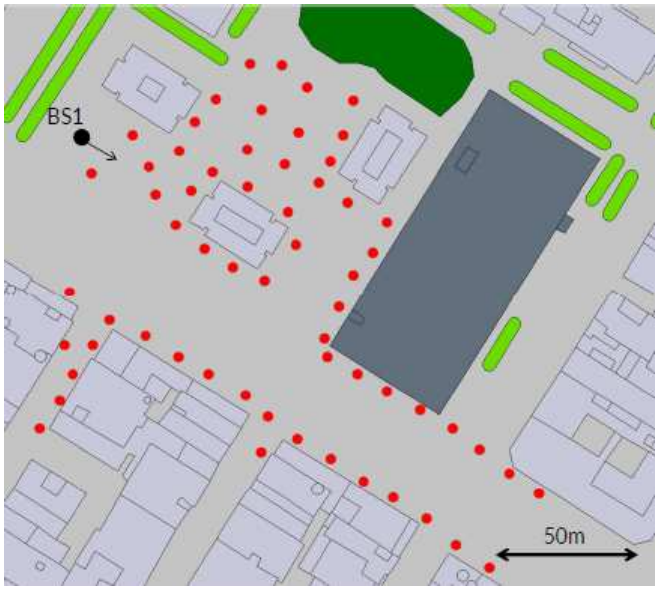

Figure 3.25: Top view of realistic users distribution (red dots) inside mmWave small cell in Manhattan area in New York City.

one obtained from the deterministic assuming the same large scale fading (path-loss (ξ) computed from the deterministic simulator) at $\sigma^2 = -84$dBm.

In Fig. 3.26, it can be seen that the DL SE based on the stochastic and deterministic channels are similar at $C = 3$. We can clearly see the wide SE gap caused by the rich scattering environment when the number of clusters is $C = 10$ that could enhance the spatial multiplexing and lead to unrealistic results.

3.4.2 Uplink Hybrid Transmit Spatial Modulation

We propose a novel two stages analog precoding aided HTSM scheme assuming ZF combiner at the BS and energy efficient UT architecture. The contributions of this section are published in **[J1]**. In order to combat the severe path-loss associated with the mmWave propagation, we apply a transmit beamformer stage that consists of linear arrays of PSs. As the application of the ZF combiner at the BS requires a full-rank MIMO channel, we use at the UT analog switches stage to perform antenna selection and grouping that reduces the correlation among the UT antennas and ensures the rank condition. Antenna selection is needed even if with MMSE combiner, as illustrated in [96]. The design of the UL transmitter is done in the following steps. First, the PSs stage consists of N_g^{UL} transmit analog beamformers that are employed to boost the transmit beamforming gain. Each analog beamformer contains N_a^{UL} active PSs. Next, the switches stage is used to combat the spatial correlation among the UT antennas and as a result the received power at the BS is maximized. This is achieved by selecting the best number and the best set of the UT antennas to be connected to each transmit analog

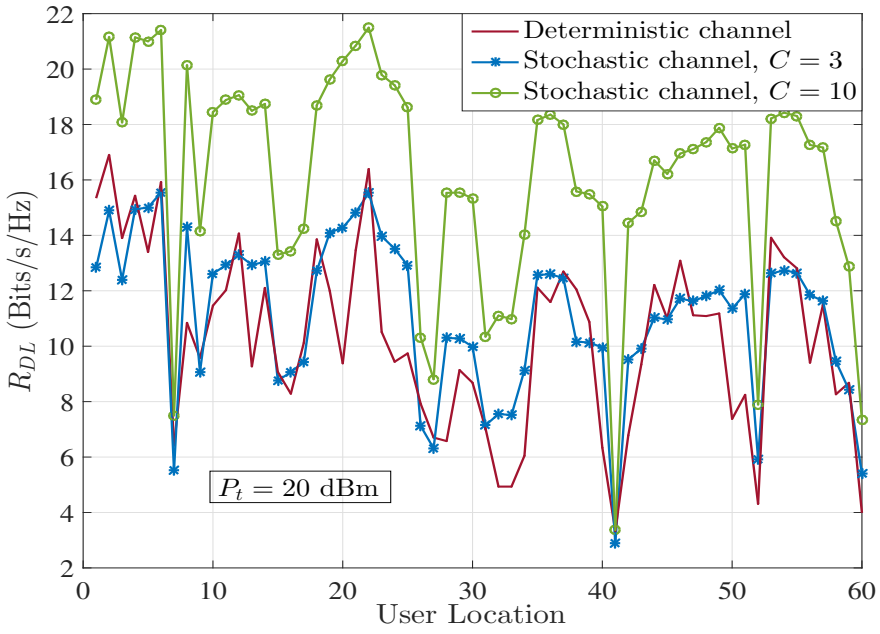

Figure 3.26: DL SE vs users locations based on stochastic channels (average over 1000 realizations) and deterministic ray based channels at $N_t = 128$, $N_r = 32$, $C = \{3, 10\}$, $P_t = 20$dBm and $\sigma^2 = -84$dBm.

beamformer. Mapping the incoming UL bit stream to symbols is performed in two parts, the first N_g^{UL} bits (spatially modulated bits) are mapped into transmit power levels of the N_g^{UL} transmit analog beamformers such that the i-th beamformer transmits high or low power if the i-th spatial bit is 1 or 0, respectively. The remaining $\log_2 M^{\mathrm{UL}}$ bits (modulation bits) are modulated using standard M^{UL}-ary modulation schemes. As a result, the signal transmitted to the BS can be expressed as

$$\begin{aligned} \mathbf{x}_t^{\mathrm{UL}} &= \sqrt{\alpha^{\mathrm{UL}} P_t}\mathbf{A}_{\mathrm{SW}}^{\mathrm{UL}}\mathbf{A}_{\mathrm{PS}}^{\mathrm{UL}}\mathbf{t}_i^{\mathrm{UL}}x^{\mathrm{UL}} \ \text{ with} \\ \mathbf{t}_i^{\mathrm{UL}} &= (1-2a_0^{\mathrm{UL}})\mathbf{s}_i^{\mathrm{UL}} + a_0^{\mathrm{UL}}\mathbf{1}_{N_g^{\mathrm{UL}}}, \end{aligned} \tag{3.162}$$

where the details of the parameters are given in Table 3.3. Moreover, $\mathbf{f}_l^{\mathrm{UL}}$ is the PSs response vector so it has constant amplitude and satisfies $|\mathbf{f}_l^{\mathrm{UL}(i)}| = |\mathbf{f}_l^{\mathrm{UL}(j)}| \ \forall \ i, j, \ l = 1, \cdots, N_g^{\mathrm{UL}}$, $\mathbf{A}_{\mathrm{SW}}^{\mathrm{UL}}$ connects the PSs to the UT antennas in such a way that $\mathbf{A}_{\mathrm{SW}}^{\mathrm{UL}\ (i,j)} = 1$ when the j-th PS represented by the j-th column of $\mathbf{A}_{\mathrm{SW}}^{\mathrm{UL}}$ is connected to the i-th UT antenna represented by the i-th row of $\mathbf{A}_{\mathrm{SW}}^{\mathrm{UL}}$ and hence, $\|\mathbf{A}_{\mathrm{SW}}^{\mathrm{UL}(j)}\|_0 = 1, j = 1, \cdots, N_a^{\mathrm{UL}} N_g^{\mathrm{UL}}$. The PS inside a specific beamformer is connected to distinct UT antenna and thus $\mathbf{A}_{\mathrm{SW}}^{\mathrm{UL}}$ satisfies $\|\mathbf{A}_{\mathrm{SW}}^{\mathrm{UL}(i,(k-1)N_a^{\mathrm{UL}}+1:kN_a^{\mathrm{UL}})}\|_0 \in \{0, 1\}, i = 1, \cdots, N_U, k = 1, \cdots, N_g^{\mathrm{UL}}$. Finally, α^{UL} is the coefficient that ensures the constant average transmit power and can be

Table 3.3: Elements of the uplink signal model

x^{UL}	UL modulation symbol $\in \mathbb{C}^{1\times 1}$ with $\mathrm{E}\left[x^{\mathrm{UL}}x^{\mathrm{UL}H}\right]=1$
$\mathbf{s}_i^{\mathrm{UL}}$	UL spatial symbol $\in \mathbb{R}^{N_g^{\mathrm{UL}}\times 1}, i=1,\cdots,2^{N_g^{\mathrm{UL}}}$ mapped from N_g^{UL} bits from the incoming data bits with $\Pr(\mathbf{s}_i^{\mathrm{UL}})=1/2^{N_g^{\mathrm{UL}}}$
$\mathbf{t}_i^{\mathrm{UL}}$	the mapped version of the spatial symbol $\mathbf{s}_i^{\mathrm{UL}}$ to high and low amplitudes $\{a_H^{\mathrm{UL}}=1-a_0^{\mathrm{UL}}, a_L^{\mathrm{UL}}=a_0^{\mathrm{UL}}\}$; respectively and $\{0\leqslant a_0^{\mathrm{UL}}\leqslant \frac{1}{2}\}$
$\mathbf{A}_{\mathrm{PS}}^{\mathrm{UL}}$	UL analog phase shifters matrix $\in \mathbb{C}^{N_a^{\mathrm{UL}}N_g^{\mathrm{UL}}\times N_g^{\mathrm{UL}}}$, $\mathbf{A}_{\mathrm{PS}}^{\mathrm{UL}}=$ blockdiag$\{\mathbf{f}_1^{\mathrm{UL}},\cdots,\mathbf{f}_{N_g^{\mathrm{UL}}}^{\mathrm{UL}}\}$
$\mathbf{f}_l^{\mathrm{UL}}$	UL analog beamformer response vector $\in\mathbb{C}^{N_a^{\mathrm{UL}}\times 1}$
$\mathbf{A}_{\mathrm{SW}}^{\mathrm{UL}}$	UL analog switches matrix $\in \mathbb{R}^{N_{\mathrm{U}}\times N_a^{\mathrm{UL}}N_g^{\mathrm{UL}}}, \mathbf{A}_{\mathrm{SW}}^{\mathrm{UL}\ (i,j)} \in \{0,1\}, i=1,\cdots,N_U, j=1,\cdots,N_a^{\mathrm{UL}}N_g^{\mathrm{UL}},$

expressed as

$$\begin{aligned}\alpha^{\mathrm{UL}} &= \frac{1}{\mathrm{E}[\|\mathbf{A}_{\mathrm{SW}}^{\mathrm{UL}}\mathbf{A}_{\mathrm{PS}}^{\mathrm{UL}}\mathbf{t}_i^{\mathrm{UL}}x^{\mathrm{UL}}\|_2^2]}\\ &= \frac{1}{\mathrm{Tr}\left\{\mathbf{A}_{\mathrm{SW}}^{\mathrm{UL}}\mathbf{A}_{\mathrm{PS}}^{\mathrm{UL}}\mathbf{R}_{ss}^{\mathrm{UL}}\mathbf{A}_{\mathrm{PS}}^{\mathrm{UL}H}\mathbf{A}_{\mathrm{SW}}^{\mathrm{UL}H}\right\}},\\ \text{with } \mathbf{R}_{ss}^{\mathrm{UL}} &= \frac{1}{2^{N_g^{\mathrm{UL}}}}\sum_{i=1}^{2^{N_g^{\mathrm{UL}}}}\mathbf{t}_i^{\mathrm{UL}}\mathbf{t}_i^{\mathrm{UL}H}.\end{aligned} \tag{3.163}$$

As an illustrative example to link matrix $\mathbf{A}_{\mathrm{SW}}^{\mathrm{UL}}$ and the proposed architecture in Fig. 2.3, let us consider $N_U=4$, $N_g^{\mathrm{UL}}=2$, $N_a^{\mathrm{UL}}=2$ and the UL switching matrix is

$$\mathbf{A}_{\mathrm{SW}}^{\mathrm{UL}}=\begin{bmatrix}1&0&0&0\\0&0&0&0\\0&0&1&0\\0&1&0&1\end{bmatrix}, \tag{3.164}$$

The first row of $\mathbf{A}_{\mathrm{SW}}^{\mathrm{UL}}$ in Eq. (3.164) shows that the first antenna is connected to the first PS of the first group. The third row of $\mathbf{A}_{\mathrm{SW}}^{\mathrm{UL}}$ shows that the third antenna is connected to the first PS of the second group. Similarly, the fourth row of $\mathbf{A}_{\mathrm{SW}}^{\mathrm{UL}}$ describes that the fourth antenna combines the signals coming from second PS of the first group and second PS of the second group. We jointly optimise a_0^{UL}, $\mathbf{A}_{\mathrm{PS}}^{\mathrm{UL}}$ and $\mathbf{A}_{\mathrm{SW}}^{\mathrm{UL}}$ to maximize the EE under SE requirements. The received symbol at the BS is

$$\mathbf{r}^{\mathrm{UL}}=\sqrt{\alpha^{\mathrm{UL}}P_t}\mathbf{H}^{\mathrm{UL}}\mathbf{A}_{\mathrm{SW}}^{\mathrm{UL}}\mathbf{A}_{\mathrm{PS}}^{\mathrm{UL}}\mathbf{t}_i^{\mathrm{UL}}x^{\mathrm{UL}}+\mathbf{n}^{\mathrm{UL}}. \tag{3.165}$$

Therein, $\mathbf{r}^{\mathrm{UL}} \in \mathbb{C}^{N_{\mathrm{BS}} \times 1}$ is the received signal vector at the BS and $\mathbf{n}^{\mathrm{UL}} \in \mathbb{C}^{N_{\mathrm{BS}} \times 1}$ is the noise vector with i.i.d circularly symmetric complex Gaussian elements $\mathcal{CN}(0,\, \sigma^2)$. Furthermore, the effective UL channel matrix can be indicated as $\mathbf{H}_e^{\mathrm{UL}} = \mathbf{H}^{\mathrm{UL}} \mathbf{A}_{\mathrm{SW}}^{\mathrm{UL}} \mathbf{A}_{\mathrm{PS}}^{\mathrm{UL}} = \left[\mathbf{H}_1^{\mathrm{UL}} \mathbf{f}_1^{\mathrm{UL}}, \cdots, \mathbf{H}_{N_g^{\mathrm{UL}}}^{\mathrm{UL}} \mathbf{f}_{N_g^{\mathrm{UL}}} \right] \in \mathbb{C}^{N_{\mathrm{BS}} \times N_g^{\mathrm{UL}}}$ where $\mathbf{H}_k^{\mathrm{UL}} = \mathbf{H}^{\mathrm{UL}} \mathbf{A}_{\mathrm{SW}}^{\mathrm{UL}((k-1)N_a^{\mathrm{UL}}+1:kN_a^{\mathrm{UL}})} \in \mathbb{C}^{N_{\mathrm{BS}} \times N_a^{\mathrm{UL}}}$ is the effective sub-channel matrix of the k-th beamforming group. In the UL reception, the BS applies a ZF combiner to enable the spatial and modulation symbols detection as follows

$$\mathbf{y}^{\mathrm{UL}} = \mathbf{W} \mathbf{r}^{\mathrm{UL}}, \tag{3.166}$$

where the ZF combiner matrix is computed as $\mathbf{W} = \left(\mathbf{H}_e^{\mathrm{UL}H} \mathbf{H}_e^{\mathrm{UL}} \right)^{-1} \mathbf{H}_e^{\mathrm{UL}H}$ and can be implemented using the hybrid architecture proposed in [67]. We select the beamforming groups and the antennas per group to ensure full rank effective channel $\mathbf{H}_e^{\mathrm{UL}}$. The post-processed signal $\mathbf{y}^{\mathrm{UL}} \in \mathbb{C}^{N_g^{\mathrm{UL}} \times 1}$ comprises the spatial and modulation symbols. Hence, the k-th entry of $\mathbf{y}^{\mathrm{UL}}$ takes the following values

$$y_k^{\mathrm{UL}} = \begin{cases} \sqrt{\alpha^{\mathrm{UL}} P_t} a_H^{\mathrm{UL}} x^{\mathrm{UL}} + n_k^{'} & \text{if} \quad s_{ik}^{\mathrm{UL}} = 1 \\ \sqrt{\alpha^{\mathrm{UL}} P_t} a_L^{\mathrm{UL}} x^{\mathrm{UL}} + n_k^{'} & \text{if} \quad s_{ik}^{\mathrm{UL}} = 0 \end{cases} \tag{3.167}$$

where $n_k^{'} \in \mathcal{CN}(0,\, \sigma_k^{'2})$ is the k-th entry of the post-processed noise variable $\mathbf{n}^{'} = \mathbf{W}\mathbf{n}^{\mathrm{UL}}$ with variance $\sigma_k^{'2} = \left[\mathbf{W}\mathbf{W}^H \right]^{(k,k)} \sigma^2$.

3.4.2.1 Uplink maximum likelihood detector

Since we assume that the number of RF chains at the BS is at least C, we can jointly detect the spatial and the modulation symbols using an ML approach as:

$$\begin{aligned} \left[\hat{\mathbf{s}}^{\mathrm{UL}}, \hat{x}^{\mathrm{UL}} \right] &= \underset{s_i^{\mathrm{UL}}, x_j^{\mathrm{UL}}}{max} \; f\left(\mathbf{y}^{\mathrm{UL}} | \mathbf{s}_i^{\mathrm{UL}}, x_j^{\mathrm{UL}} \right) \\ &= \underset{s_i^{\mathrm{UL}}, x_j^{\mathrm{UL}}}{min} \; \left\| \mathbf{R}_{n'n'}^{-\frac{1}{2}} \left(\mathbf{y}^{\mathrm{UL}} - \sqrt{\alpha^{\mathrm{UL}}} \mathbf{t}_i^{\mathrm{UL}} x_j^{\mathrm{UL}} \right) \right\|_2^2, \end{aligned} \tag{3.168}$$

where $\mathbf{R}_{n'n'} = \sigma^2 \mathbf{W}\mathbf{W}^H$. Although the ML detector provides optimal performance, exhaustive search in Eq. (3.168) is computationally complex if a large number of bits per spatial symbol is being transmitted. Since our goal is to maximize the EE under SE constraint, we prove in the sequel an expression for the SE of the ML detector assuming Gaussian x^{UL}, and propose a low-complexity detector assuming M-PSK x^{UL}. Finally, we show that the SE of the reduced complexity detector achieves a tight lower bound on the mutual information.

3.4.2.2 Spectral efficiency of the maximum likelihood detector with Gaussian x^{UL}

We consider the SE as a performance metric to evaluate the proposed scheme. By applying the mutual information chain rule, the SE can be defined as

$$\begin{aligned} I\left(\mathbf{s}^{\mathrm{UL}}, x^{\mathrm{UL}}; \mathbf{y}^{\mathrm{UL}}\right) &= I\left(\mathbf{s}^{\mathrm{UL}}; \mathbf{y}^{\mathrm{UL}}\right) + I\left(x^{\mathrm{UL}}; \mathbf{y}^{\mathrm{UL}} | \mathbf{s}^{\mathrm{UL}}\right), \\ I\left(\mathbf{s}^{\mathrm{UL}}; \mathbf{y}^{\mathrm{UL}}\right) &= h\left(\mathbf{y}^{\mathrm{UL}}\right) - h\left(\mathbf{y}^{\mathrm{UL}} | \mathbf{s}^{\mathrm{UL}}\right) \triangleq I_S^{\mathrm{UL}}, \\ I\left(x^{\mathrm{UL}}; \mathbf{y}^{\mathrm{UL}} | \mathbf{s}^{\mathrm{UL}}\right) &= h(\mathbf{y}^{\mathrm{UL}} | \mathbf{s}^{\mathrm{UL}}) - h(\mathbf{y}^{\mathrm{UL}} | \mathbf{s}^{\mathrm{UL}}, x^{\mathrm{UL}}) \triangleq I_M^{\mathrm{UL}}. \end{aligned} \tag{3.169}$$

Assuming Gaussian-distributed x^{UL}, the differential entropies in Eq. (3.169) can be computed from

$$h(\mathbf{y}^{\mathrm{UL}}) = -\int_{\mathcal{C}^{N_g^{\mathrm{UL}}}} f(\mathbf{y}^{\mathrm{UL}}) \log_2 f(\mathbf{y}^{\mathrm{UL}}) \mathrm{d}\mathbf{y}^{\mathrm{UL}} \tag{3.170}$$

where $f(\mathbf{y}^{\mathrm{UL}})$ is the PDF of the complex Gaussian mixture random vector

$$\begin{aligned} f(\mathbf{y}^{\mathrm{UL}}) &= \sum_{i=1}^{2^{N_g^{\mathrm{UL}}}} \Pr\left(\mathbf{s}_i^{\mathrm{UL}}\right) f(\mathbf{y}^{\mathrm{UL}} | \mathbf{s}_i^{\mathrm{UL}}) \\ &= \frac{1}{2^{N_g^{\mathrm{UL}}}} \sum_{i=1}^{2^{N_g^{\mathrm{UL}}}} \frac{1}{\pi^{N_g^{\mathrm{UL}}} |\mathbf{\Sigma}_i|} e^{-\mathbf{y}^{\mathrm{UL}H} \mathbf{\Sigma}_i^{-1} \mathbf{y}^{\mathrm{UL}}} \text{ with} \\ \mathbf{\Sigma}_i &= \alpha^{\mathrm{UL}} P_t \mathbf{t}_i^{\mathrm{UL}H} \mathbf{t}_i^{\mathrm{UL}} + \mathbf{R}_{n'n'}. \end{aligned} \tag{3.171}$$

The closed form expression of the differential entropy of a Gaussian mixture $h(\mathbf{y}^{\mathrm{UL}})$ is unknown [97]. Moreover, the numerical evaluation of $h(\mathbf{y}^{\mathrm{UL}})$ is computationally complex especially in large-scale MIMO systems when the size of $\mathbf{y}^{\mathrm{UL}}$ can be large. In the sequel, we propose a novel and reduced complexity method to evaluate $h(\mathbf{y}^{\mathrm{UL}})$. In this method, we apply the conditional entropy chain rule on $h(\mathbf{y}^{\mathrm{UL}})$ and we prove a closed form expression for the conditional probability density function $f(y_k^{\mathrm{UL}} | y_{k-1}^{\mathrm{UL}}, \cdots, y_1^{\mathrm{UL}})$. Finally, we reduce the computational complexity by simplifying the integral in Eq. (3.170) to be sum of double integrals as follows

$$\begin{aligned} h(\mathbf{y}^{\mathrm{UL}}) &= h(y_1^{\mathrm{UL}}) + \sum_{k=2}^{N_g^{\mathrm{UL}}} h(y_k^{\mathrm{UL}} | y_{k-1}^{\mathrm{UL}}, \cdots, y_1^{\mathrm{UL}}) \text{ with} \\ &f(y_k^{\mathrm{UL}} | y_{k-1}^{\mathrm{UL}}, \cdots, y_1^{\mathrm{UL}}) = \\ &\frac{1}{2^k} \sum_{i=1}^{2^k} f(y_k^{\mathrm{UL}} | y_{k-1}^{\mathrm{UL}}, \cdots, y_1^{\mathrm{UL}}, \mathbf{t}_i^{\mathrm{UL}}(1:k)). \end{aligned} \tag{3.172}$$

Lemma 3.1. *The conditional density function of the random variable* $(y_k^{UL}|y_{k-1}^{UL},\cdots,y_1^{UL},\mathbf{t}_i^{UL}(1:k))$ *is distributed as a zero-mean complex Gaussian :*

$$f(y_k^{UL}|y_{k-1}^{UL},\cdots,y_1^{UL},\mathbf{t}_i^{UL}(1:k))=\mathcal{CN}(0,\,\sigma_K^2+P_{i,K}).$$

Proof.

$$h\Big(y_k^{\mathrm{UL}}|y_{k-1}^{\mathrm{UL}},\cdots,y_1^{\mathrm{UL}},\mathbf{t}_i^{\mathrm{UL}(1:k)}\Big)\overset{(a)}{=}h\Big(y_1^{\mathrm{UL}},\cdots,y_k^{\mathrm{UL}}|\mathbf{t}_i^{\mathrm{UL}(1:k)}\Big)-$$
$$h\Big(y_1^{\mathrm{UL}},\cdots,y_{k-1}^{\mathrm{UL}}|\mathbf{t}_i^{\mathrm{UL}(1:k)}\Big)$$
$$\overset{(b)}{=}\log_2\pi e\frac{\Big|\alpha^{\mathrm{UL}}P_t\mathbf{t}_i^{\mathrm{UL}(1:k)}\mathbf{t}_i^{\mathrm{UL}(1:k)^H}+\mathbf{R}_{n'n'}^{(1:k,1:k)}\Big|}{\Big|\alpha^{\mathrm{UL}}P_t\mathbf{t}_i^{\mathrm{UL}(1:k-1)}\mathbf{t}_i^{\mathrm{UL}(1:k-1)^H}+\mathbf{R}_{n'n'}^{(1:k-1,1:k-1)}\Big|}$$
$$\overset{(c)}{=}\log_2\pi e\frac{\Big|\mathbf{R}_{n'n'}^{(1:k,1:k)}\Big|}{\Big|\mathbf{R}_{n'n'}^{(1:k-1,1:k-1)}\Big|}\frac{1+\alpha^{\mathrm{UL}}P_t\mathbf{t}_i^{\mathrm{UL}(1:k)T}\mathbf{R}_{n'n'}^{(1:k,1:k)^{-1}}\mathbf{t}_i^{\mathrm{UL}(1:k)}}{1+\alpha^{\mathrm{UL}}P_t\mathbf{t}_i^{\mathrm{UL}(1:k-1)^T}\mathbf{R}_{n'n'}^{(1:k-1,1:k-1)^{-1}}\mathbf{t}_i^{\mathrm{UL}(1:k-1)}}$$
$$\overset{(d)}{=}\log_2\pi e\Big(\sigma_K^2+P_{i,K}\Big),\ \text{ where }\ \sigma_K^2=\frac{\Big|\mathbf{R}_{n'n'}^{(1:k,1:k)}\Big|}{\Big|\mathbf{R}_{n'n'}^{(1:k-1,1:k-1)}\Big|}\ \text{ and}$$
$$P_{i,K}=\sigma_K^2\alpha^{\mathrm{UL}}P_t\frac{\mathbf{t}_i^{\mathrm{UL}(1:k)^T}\mathbf{R}_{n'n'}^{(1:k,1:k)^{-1}}\mathbf{t}_i^{\mathrm{UL}(1:k)}-\mathbf{t}_i^{\mathrm{UL}(1:k-1)^T}\mathbf{R}_{n'n'}^{(1:k-1,1:k-1)^{-1}}\mathbf{t}_i^{\mathrm{UL}(1:k-1)}}{1+\alpha^{\mathrm{UL}}P_t\mathbf{t}_i^{\mathrm{UL}(1:k-1)^T}\mathbf{R}_{n'n'}^{(1:k-1,1:k-1)^{-1}}\mathbf{t}_i^{\mathrm{UL}(1:k-1)}}$$

Step $\overset{(a)}{=}$ follows from chain rule of entropy, step $\overset{(b)}{=}$ follows from Gaussian distributions, step $\overset{(c)}{=}$ follows from applying the identity $|\mathbf{A}+\mathbf{t}\mathbf{t}^H|=|\mathbf{A}|\big(1+\mathbf{t}^H\mathbf{A}^{-1}\mathbf{t}\big)$ and step $\overset{(d)}{=}$ follows from noise and signal powers separation. Therefore,

$$f\Big(y_k^{\mathrm{UL}}|y_{k-1}^{\mathrm{UL}},\cdots,y_1^{\mathrm{UL}},\mathbf{t}_i^{\mathrm{UL}(1:k)}\Big)=\mathcal{CN}\Big(0,\,\sigma_K^2+P_{i,K}\Big)$$

■

Therefore, we can determine the k-th differential entropy $h(y_k^{\mathrm{UL}}|y_{k-1}^{\mathrm{UL}},\cdots,y_1^{\mathrm{UL}})$ by evaluating the double integral numerically regardless the size of $\mathbf{y}^{\mathrm{UL}}$. Thus, we significantly reduce the computational complexity. As an illustrative example that highlights the proposed reduced complexity method of evaluating $h\left(\mathbf{y}^{\mathrm{UL}}\right)$, let us

consider $N_g^{\mathrm{UL}} = 3$. The proposed 2-D integral method achieves the same exact values of $h\left(\mathbf{y}^{\mathrm{UL}}\right)$ as the 16-D integral in Eq. (3.170). The differential entropy $h(\mathbf{y}^{\mathrm{UL}}|\mathbf{s}^{\mathrm{UL}})$ can be expressed in closed form as

$$\begin{aligned} h(\mathbf{y}^{\mathrm{UL}}|\mathbf{s}^{\mathrm{UL}}) &= \sum_{i=1}^{2^{N_g^{\mathrm{UL}}}} \Pr\left(\mathbf{s}_i^{\mathrm{UL}}\right) h(\mathbf{y}^{\mathrm{UL}}|\mathbf{s}^{\mathrm{UL}} = \mathbf{s}_i^{\mathrm{UL}}) \\ &= \frac{1}{2^{N_g^{\mathrm{UL}}}} \sum_{i=1}^{2^{N_g^{\mathrm{UL}}}} \log_2(\pi e)^{N_g^{\mathrm{UL}}} \left| \alpha^{\mathrm{UL}} P_t \mathbf{t}_i^{\mathrm{UL}} \mathbf{t}_i^{\mathrm{UL}H} + \mathbf{R}_{n'n'} \right| \\ &= \frac{1}{2^{N_g^{\mathrm{UL}}}} \sum_{i=1}^{2^{N_g^{\mathrm{UL}}}} \Bigg(N_g^{\mathrm{UL}} \log_2(\pi e) \\ &+ \log_2 |\mathbf{R}_{n'n'}| \left(1 + \alpha^{\mathrm{UL}} P_t \mathbf{t}_i^{\mathrm{UL}H} \mathbf{R}_{n'n'}^{-1} \mathbf{t}_i^{\mathrm{UL}}\right) \Bigg). \end{aligned} \tag{3.173}$$

Based on the low computational complexity method of evaluating $h(\mathbf{y}^{\mathrm{UL}})$ and the closed from of $h(\mathbf{y}^{\mathrm{UL}}|\mathbf{s}^{\mathrm{UL}})$, we can evaluate the spatial rate I_S^{UL} in Eq. (3.169) efficiently. Moreover, the differential entropy $h(\mathbf{y}^{\mathrm{UL}}|\mathbf{s}^{\mathrm{UL}}, x)$ can be expressed as

$$h(\mathbf{y}^{\mathrm{UL}}|\mathbf{s}^{\mathrm{UL}}, x) = h(\mathbf{n}^{'}) = \log_2(\pi e)^{N_g^{\mathrm{UL}}} |\mathbf{R}_{n'n'}|. \tag{3.174}$$

According to Eq. (3.173) and Eq. (3.174), I_M^{UL} in Eq. (3.169) can be expressed in closed form as

$$I_M^{\mathrm{UL}} = \frac{1}{2^{N_g^{\mathrm{UL}}}} \sum_{i=1}^{2^{N_g^{\mathrm{UL}}}} \log_2\left(1 + \alpha^{\mathrm{UL}} P_t \mathbf{t}_i^{\mathrm{UL}H} \mathbf{R}_{n'n'}^{-1} \mathbf{t}_i^{\mathrm{UL}}\right). \tag{3.175}$$

Finally, according to Eq. (3.169), the UL SE can be evaluated as $\mathrm{SE}^{\mathrm{UL}} = I_S^{\mathrm{UL}} + I_M^{\mathrm{UL}}$.

3.4.2.3 Uplink reduced complexity detection with M-PSK x^{UL}

Let us propose a low complexity detection method whereby the spatial and the modulation symbols are detected separately. The size of the search space for the reduced complexity detector is $N_a^{\mathrm{UL}} + M$ which is much smaller than that of the ML detector ($2^{N_a^{\mathrm{UL}}} \times M$). In Fig. 2 in [41], the authors showed that constant amplitude constellations (M-PSK) achieves the best performance with the reduced complexity SM detector.

From Eq. (3.168), the ML spatial symbol detector is $\hat{\mathbf{t}}^{\mathrm{UL}} = x^{\mathrm{UL}} \mathbf{y}^{\mathrm{UL}} / \sqrt{\alpha^{\mathrm{UL}} P_t}$. However, x^{UL} is unknown so we exploit the fact that M-PSK modulation symbols have constant amplitude and hence, $|x^{\mathrm{UL}}| = 1$. Then, in order to detect the k-

th binary spatially modulated bit, we compare the absolute value of y_k^{UL} with a threshold γ^{UL} as follows

$$\hat{s}_{ik}^{\mathrm{UL}} = \begin{cases} 1 & \text{if} \quad |y_k^{\mathrm{UL}}| \geqslant \gamma^{\mathrm{UL}} \\ 0 & \text{if} \quad |y_k^{\mathrm{UL}}| < \gamma^{\mathrm{UL}} \end{cases} \quad \text{with}$$
$$\gamma^{\mathrm{UL}} = \frac{1}{2}\sqrt{\alpha^{\mathrm{UL}} P_t}\left(a_H^{\mathrm{UL}} + a_L^{\mathrm{UL}}\right). \tag{3.176}$$

According to Eq. (3.168), the optimal modulation symbol detector can be expressed as

$$\begin{aligned} x_j^{\mathrm{UL}\star} &= \underset{x_j^{\mathrm{UL}} \in M-\mathrm{PSK}}{max} \Re\left\{ x_j^{\mathrm{UL}H} \mathbf{t}_i^{\mathrm{UL}H} \mathbf{R}_{n'n'}^{-1} \mathbf{y}^{\mathrm{UL}} \right\} \\ &= \underset{x_j^{\mathrm{UL}} \in M-\mathrm{PSK}}{min} \left| x_j^{\mathrm{UL}} - \mathbf{v}_i^{\mathrm{OC}H} \mathbf{y}^{\mathrm{UL}} \right|_2 \quad \text{with} \\ \mathbf{v}_i^{\mathrm{OC}} &= \mathbf{R}_{n'n'}^{-1} \mathbf{t}_i^{\mathrm{UL}} = \mathbf{H}_e^{\mathrm{UL}H} \mathbf{H}_e^{\mathrm{UL}} \mathbf{t}_i^{\mathrm{UL}}, \end{aligned} \tag{3.177}$$

where $\mathbf{v}_i^{\mathrm{OC}}$ is the optimal modulation symbol combiner. Since $\mathbf{t}_i^{\mathrm{UL}}$ is unknown at the UT. We propose to use the detected spatial symbol in Eq. (3.176). Therefore, the combined signal can be expressed as

$$y_c^{\mathrm{UL,OC}} = \sqrt{\alpha^{\mathrm{UL}} P_t} \hat{\mathbf{t}}_l^{\mathrm{UL}T} \mathbf{H}_e^{\mathrm{UL}H} \mathbf{H}_e^{\mathrm{UL}} \mathbf{t}_i^{\mathrm{UL}} x^{\mathrm{UL}} + \hat{\mathbf{t}}_l^{\mathrm{UL}T} \mathbf{H}_e^{\mathrm{UL}H} \mathbf{n}^{\mathrm{UL}}. \tag{3.178}$$

Eq. (3.178) shows that the SNR perceived for the spatial symbol detection affects the modulation symbol detection. Thus, we propose the use of an equal ratio combiner (ERC) combined signal that is independent from the detected spatial symbol as

$$y_c^{\mathrm{UL,ERC}} = \mathbf{1}_{N_g^{\mathrm{UL}}}^T \mathbf{y}^{\mathrm{UL}} = \sqrt{\alpha^{\mathrm{UL}} P_t} \mathbf{1}_{N_g^{\mathrm{UL}}}^T \mathbf{t}_i^{\mathrm{UL}} x^{\mathrm{UL}} + \mathbf{1}_{N_g^{\mathrm{UL}}}^T \mathbf{W} \mathbf{n}^{\mathrm{UL}}. \tag{3.179}$$

After that, we apply minimum distance detector on the combined signal to detect the M-PSK symbol. In the sequel, we provide closed form expressions for the UL SE for both combiners.

3.4.2.4 Spectral efficiency of the reduced complexity detector with M-PSK x^{UL}

As we detect the spatial and the modulation symbols independently, the SE of the proposed reduced complexity detection UL HTSM scheme can be expressed as

$$\mathrm{SE}_r^{\mathrm{UL}} = I_{S,r}^{\mathrm{UL}} + I_{M,r}^{\mathrm{UL}}. \tag{3.180}$$

We transmit binary spatial symbol with input $s_{ik}^{\mathrm{UL}} \in \{0,1\}, k = 1, \cdots, N_g^{\mathrm{UL}}$ and output $\hat{s}_{ik}^{\mathrm{UL}} \in \{0,1\}$ as in Eq. (3.176) and thus, the wireless channel between s_{ik}^{UL} and $\hat{s}_{ik}^{\mathrm{UL}}$ can be characterized by the BAC [84]. Hence, the UL spatial rate (defined as $I_{S,r}^{\mathrm{UL}}$) can be expressed as a contribution of N_g^{UL} parallel BACs as

$$\begin{aligned} I_{S,r}^{\mathrm{UL}} &= I\left(\mathbf{s}^{\mathrm{UL}}, \hat{\mathbf{s}}^{\mathrm{UL}}\right) = \sum_{k=1}^{N_g^{\mathrm{UL}}} I\left(s^{\mathrm{UL}}, \hat{s}^{\mathrm{UL}}\right) \\ &= \sum_{k=1}^{N_g^{\mathrm{UL}}} \mathcal{H}\left(\frac{P_{0k} + 1 - P_{1k}}{2}\right) - \frac{\mathcal{H}(P_{0k}) + \mathcal{H}(1 - P_{1k})}{2}. \end{aligned} \tag{3.181}$$

Herein, the entropy function is $\mathcal{H}(p) = -p\log_2(p) - (1-p)\log_2(1-p)$ and the probabilities of the false detection of the spatially modulated bits 1 and 0 are

$$\begin{aligned} P_{1k} &= \Pr\left(\hat{s}_{ik}^{\mathrm{UL}} = 1 | s_{ik}^{\mathrm{UL}} = 0\right) = \Pr\left(|y_k^{\mathrm{UL}}| > \gamma^{\mathrm{UL}} | s_{ik}^{\mathrm{UL}} = 0\right) \\ &= 1 - Q_1\left(\sqrt{2\alpha^{\mathrm{UL}} P_t} a_H^{\mathrm{UL}} / \sigma_k^{'}, \sqrt{2}\gamma^{\mathrm{UL}} / \sigma_k^{'}\right), \end{aligned} \tag{3.182}$$

$$\begin{aligned} P_{0k} &= \Pr\left(\hat{s}_{ik}^{\mathrm{UL}} = 0 | s_{ik}^{\mathrm{UL}} = 1\right) = \Pr\left(|y_k^{\mathrm{UL}}| < \gamma^{\mathrm{UL}} | s_{ik}^{\mathrm{UL}} = 1\right) \\ &= Q_1\left(\sqrt{2\alpha^{\mathrm{UL}} P_t} a_L^{\mathrm{UL}} / \sigma_k^{'}, \sqrt{2}\gamma^{\mathrm{UL}} / \sigma_k^{'}\right), \end{aligned} \tag{3.183}$$

where $|y_k^{\mathrm{UL}}|$ is Ricean distributed and $Q_1(.)$ is the first order Marcum-Q-function.

The combined signals in Eq. (3.178) and in Eq. (3.179) include one M-PSK symbol. Thus, the UL modulation rate with OC ($I_{M,r}^{\mathrm{UL,OC}}$) and with ERC ($I_{M,r}^{\mathrm{UL,ERC}}$) can be expressed by the MISO rate expression with the asymptotic M-PSK shaping loss approximation [54], [98]

$$\begin{aligned} &I_{M,r}^{\mathrm{UL,OC}} = I(x^{\mathrm{UL}}; y_c^{\mathrm{UL,OC}} | \hat{\mathbf{s}}^{\mathrm{UL}}, \mathbf{s}^{\mathrm{UL}}) \\ &= \sum_{i=1}^{2^{N_g^{\mathrm{UL}}}} \Pr\left(\mathbf{s}_i^{\mathrm{UL}}\right) \sum_{l=1}^{2^{N_g^{\mathrm{UL}}}} \Pr\left(\hat{\mathbf{s}}_l^{\mathrm{UL}} | \mathbf{s}_i^{\mathrm{UL}}\right) \frac{1}{2} \log_2\left(\frac{4\pi}{e} \mathrm{SNR}_{i,l}^{\mathrm{UL}}\right) \\ &\text{where } \ \mathrm{SNR}_{i,l}^{\mathrm{UL}} = \frac{|\hat{\mathbf{t}}_l^{\mathrm{UL}T} \mathbf{H}_e^{\mathrm{UL}H} \mathbf{H}_e^{\mathrm{UL}} \mathbf{t}_i^{\mathrm{UL}}|^2}{\|\hat{\mathbf{t}}_l^{\mathrm{UL}T} \mathbf{H}_e^{\mathrm{UL}H}\|_2^2} \frac{\alpha^{\mathrm{UL}} P_t}{\sigma^2}, \\ &\Pr\left(\hat{\mathbf{s}}_l^{\mathrm{UL}} | \mathbf{s}_i^{\mathrm{UL}}\right) = \prod_{k=1}^{N_g^{\mathrm{UL}}} \Pr\left(|y_k^{\mathrm{UL}}| \underset{\hat{s}_{lk}^{\mathrm{UL}}=0}{\overset{\hat{s}_{lk}^{\mathrm{UL}}=1}{\gtrless}} \gamma_k^{\mathrm{UL}} \mid s_{ik}^{\mathrm{UL}}\right), \\ &\text{and } \ \Pr\left(\mathbf{s}_i^{\mathrm{UL}}\right) = \frac{1}{2^{N_g^{\mathrm{UL}}}}. \end{aligned} \tag{3.184}$$

$$I_{M,r}^{\mathrm{UL,ERC}} = I(x^{\mathrm{UL}}; y_c^{\mathrm{UL,ERC}} | \mathbf{s}^{\mathrm{UL}})$$

$$= \sum_{i=1}^{2^{N_g^{\mathrm{UL}}}} \Pr\left(\mathbf{s}_i^{\mathrm{UL}}\right) \frac{1}{2} \log_2\left(\frac{4\pi}{e}\mathrm{SNR}_i^{\mathrm{UL}}\right) \quad \text{where}$$

$$\mathrm{SNR}_i^{\mathrm{UL}} = \frac{|\mathbf{1}_{N_g^{\mathrm{UL}}}^{\mathrm{UL}T} \mathbf{t}_i^{\mathrm{UL}}|^2}{\|\mathbf{1}_{N_g^{\mathrm{UL}}}^{\mathrm{UL}T} \mathbf{W}\|_2^2} \frac{\alpha^{\mathrm{UL}} P_t}{\sigma^2}. \tag{3.185}$$

According to Eq. (3.181), for higher spatial rates, the difference between the amplitude levels $\left(a_H^{\mathrm{UL}}, a_L^{\mathrm{UL}}\right)$ should be maximized. In contrast, the SNR of the modulation symbol shown in Eq. (3.184) and in Eq. (3.185) increases with both a_H^{UL} and a_L^{UL}. Thus, we optimise the values of a_H^{UL} and a_L^{UL} to maximize the sum of spatial plus modulation rates. To conclude the evaluation of performance for the UL, let us compute the mutual information between inputs $(\mathbf{s}^{\mathrm{UL}}, x^{\mathrm{UL}})$ and the outputs $(\hat{\mathbf{s}}^{\mathrm{UL}}, y_c^{\mathrm{UL,ERC}})$ and show that the proposed low complexity detection scheme with ERC achieves a tight lower bound on the mutual information as follows

$$\begin{aligned}
I(\mathbf{s}^{\mathrm{UL}}, x^{\mathrm{UL}}; \hat{\mathbf{s}}^{\mathrm{UL}}, y_c^{\mathrm{UL,ERC}}) &= I(\mathbf{s}^{\mathrm{UL}}, x^{\mathrm{UL}}; \hat{\mathbf{s}}^{\mathrm{UL}}) \\
&\quad + I(\mathbf{s}^{\mathrm{UL}}, x^{\mathrm{UL}}; y_c^{\mathrm{UL,ERC}} | \hat{\mathbf{s}}^{\mathrm{UL}}) \text{ with} \\
I(\mathbf{s}^{\mathrm{UL}}, x^{\mathrm{UL}}; \hat{\mathbf{s}}^{\mathrm{UL}}) &= I(\mathbf{s}^{\mathrm{UL}}; \hat{\mathbf{s}}^{\mathrm{UL}}) + I(x^{\mathrm{UL}}; \hat{\mathbf{s}}^{\mathrm{UL}} | \mathbf{s}^{\mathrm{UL}}), \\
I(\mathbf{s}^{\mathrm{UL}}, x^{\mathrm{UL}}; y_c^{\mathrm{UL,ERC}} | \hat{\mathbf{s}}^{\mathrm{UL}}) &= I(\mathbf{s}^{\mathrm{UL}}; y_c^{\mathrm{UL,ERC}} | \hat{\mathbf{s}}^{\mathrm{UL}}) \\
&\quad + I(x^{\mathrm{UL}}; y_c^{\mathrm{UL,ERC}} | \hat{\mathbf{s}}^{\mathrm{UL}}, \mathbf{s}^{\mathrm{UL}}).
\end{aligned} \tag{3.186}$$

Note that, since x^{UL} belongs to the constant amplitude constellation (M-PSK), the received power levels do not depend on x^{UL}. Thus, the detected spatial symbol $\hat{\mathbf{s}}^{\mathrm{UL}}$ and x^{UL} are independent and they are also independent given $\mathbf{s}^{\mathrm{UL}}$, this implies $I(x^{\mathrm{UL}}; \hat{\mathbf{s}}^{\mathrm{UL}} | \mathbf{s}^{\mathrm{UL}}) = 0$. Eq. (3.179) shows that $y_c^{\mathrm{UL,ERC}}$ does not depend on $\hat{\mathbf{s}}^{\mathrm{UL}}$ and therefore, $I(x^{\mathrm{UL}}; y_c^{\mathrm{UL,ERC}} | \hat{\mathbf{s}}^{\mathrm{UL}}, \mathbf{s}^{\mathrm{UL}}) = I(x^{\mathrm{UL}}; y_c^{\mathrm{UL,ERC}} | \mathbf{s}^{\mathrm{UL}})$ and $I(\mathbf{s}^{\mathrm{UL}}; y_c^{\mathrm{UL,ERC}} | \hat{\mathbf{s}}^{\mathrm{UL}}) = I(\mathbf{s}^{\mathrm{UL}}; y_c^{\mathrm{UL,ERC}})$. Finally, Eq. (3.186) can be simplified as follows

$$\begin{aligned}
I(\mathbf{s}^{\mathrm{UL}}, x^{\mathrm{UL}}; \hat{\mathbf{s}}^{\mathrm{UL}}, y_c^{\mathrm{UL,ERC}}) &= I(x^{\mathrm{UL}}; y_c^{\mathrm{UL,ERC}} | \mathbf{s}^{\mathrm{UL}}) \\
&\quad + I(\mathbf{s}^{\mathrm{UL}}; \hat{\mathbf{s}}^{\mathrm{UL}}) + I(\mathbf{s}^{\mathrm{UL}}; y_c^{\mathrm{UL,ERC}}), \\
&= \mathrm{SE}_r^{\mathrm{UL}} + I(\mathbf{s}^{\mathrm{UL}}; y_c^{\mathrm{UL,ERC}}).
\end{aligned} \tag{3.187}$$

Therefore, the SE in Eq. (3.180) is a lower bound on the mutual information with a gap ratio

$$L_g = I(\mathbf{s}^{\mathrm{UL}}; y_c^{\mathrm{UL,ERC}}) / \mathrm{SE}_r^{\mathrm{UL}}. \tag{3.188}$$

The mutual information $I(\mathbf{s}^{\mathrm{UL}}; y_c^{\mathrm{UL,ERC}})$ can be bounded as

$$\begin{aligned} I(\mathbf{s}^{\mathrm{UL}}; y_c^{\mathrm{UL,ERC}}) &= h\left(y_c^{\mathrm{UL,ERC}}\right) - h\left(y_c^{\mathrm{UL,ERC}}|\mathbf{s}^{\mathrm{UL}}\right) \text{ with} \\ h\left(y_c^{\mathrm{UL,ERC}}\right) &\leqslant h\left(y_c^{\mathrm{UL,ERC}}|\mathbf{s}^{\mathrm{UL}} = \mathbf{1}_{N_g^{\mathrm{UL}}}\right) \\ &\overset{(a)}{=} \frac{1}{2}\log_2\left(4\pi^3 e \max\left(P_i\right)\sigma^2_{c,\mathrm{ERC}}\right) \text{ and} \\ h\left(y_c^{\mathrm{UL,ERC}}|\mathbf{s}^{\mathrm{UL}}\right) &= \frac{1}{2^{N_g^{\mathrm{UL}}}}\sum_{i=1}^{2^{N_g^{\mathrm{UL}}}} h\left(y_c^{\mathrm{UL,ERC}}|\mathbf{s}^{\mathrm{UL}} = \mathbf{s}_i^{\mathrm{UL}}\right) \\ &= \frac{1}{2^{N_g^{\mathrm{UL}}}}\sum_{i=1}^{2^{N_g^{\mathrm{UL}}}} \frac{1}{2}\log_2\left(4\pi^3 e P_i \sigma^2_{c,\mathrm{ERC}}\right) \\ I(\mathbf{s}^{\mathrm{UL}}; y_c^{\mathrm{UL,ERC}}) &\leqslant \frac{1}{2}\log_2 \frac{\max\left(P_i\right)}{\sqrt[2^{N_g^{\mathrm{UL}}}]{\prod_{i=1}^{2^{N_g^{\mathrm{UL}}}} P_i}}. \end{aligned} \tag{3.189}$$

Therein, $P_i = |\mathbf{1}_{N_g^{\mathrm{UL}}}^{\mathrm{UL}T}\mathbf{t}_i^{\mathrm{UL}}|^2\alpha^{\mathrm{UL}}P_t$, $\sigma^2_{c,\mathrm{ERC}} = \|\mathbf{1}_{N_g^{\mathrm{UL}}}^{\mathrm{UL}T}\mathbf{W}\|_2^2\sigma^2$, $\max(\cdot)$ denotes the maximum operator and step $\overset{(a)}{=}$ follows from the shaping loss of the M-PSK symbols [54], [98]. As an illustrative example, let us consider $\sigma^2_{c,\mathrm{ERC}} = 1$, $a_H^{\mathrm{UL}} = 1$ and $a_L^{\mathrm{UL}} = \frac{1}{2}$. Hence, Fig. 3.27 shows that the upper bound of the gap ratio is in range of $0.05\% \leqslant L_g \leqslant 0.4\%$ and decreases with the transmit power at different number of groups and wide range of received powers. Thus, the $\mathrm{SE}_r^{\mathrm{UL}}$ of the reduced complexity detection scheme achieves a tight lower bound on the mutual information.

3.4.3 Downlink Hybrid Receive Spatial Modulation

The contributions of this section are published in [**J1**]. In the DL transmission phase, we propose a novel two stages analog combining aided HRSM scheme at the UT, assuming ZF precoding at the BS. First, a switches stage is used to select the UT antennas and connect them to the PSs arrays to ensure full rank equivalent channel and thus, enable the ZF precoding at the BS. Next, N_g^{DL} receive analog beamformers, each containing N_a^{DL} active PSs, are used to enhance the receive beamforming gain. We apply the ZF precoder at the BS on the effective channel (MIMO channel + DL RF combiner at the UT). Thus, smart design of the analog combiner at the UT boosts the received power at the UT and enhances SE. Similarly to what was done for the UL, the incoming DL bit stream is mapped into two streams. The first N_g^{DL} spatially modulated bits are mapped to the

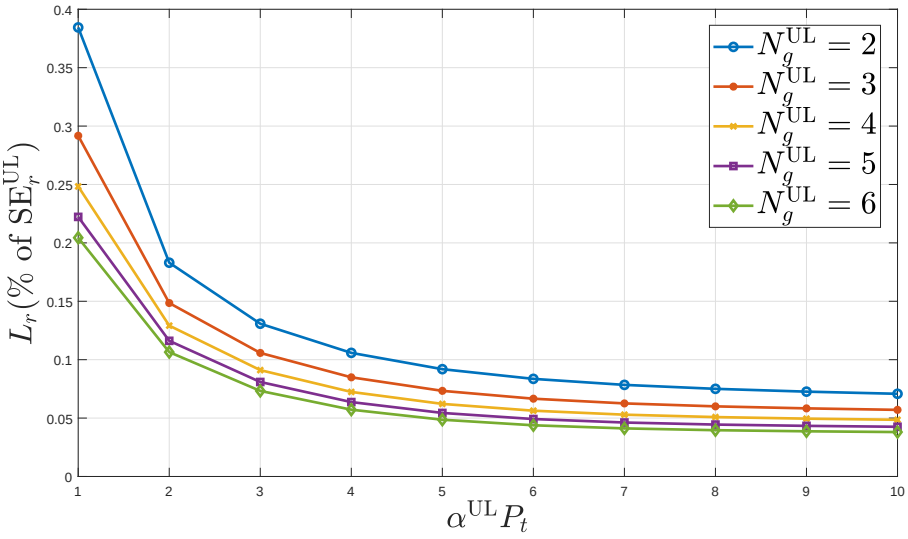

Figure 3.27: Upper bound of the gap ratio of the $\mathrm{SE}_r^{\mathrm{UL}}$ at different values of N_g^{UL}.

received power levels from the N_g^{DL} receive analog combiners such that the i-th combiner receives high or low power if the i-th spatial bit is 1 or 0, respectively. The remaining bits are mapped to an M-ary constellation. In this way, the BS transmits the following signal

$$\begin{aligned}
&\mathbf{x}_t^{\mathrm{DL}} = \sqrt{\alpha^{\mathrm{DL}} P_t}\mathbf{P}\mathbf{t}_i^{\mathrm{DL}} x^{\mathrm{DL}} \quad \text{with} \\
&\mathbf{t}_i^{\mathrm{DL}} = (1 - 2a_0^{\mathrm{DL}})\mathbf{s}_i^{\mathrm{DL}} + a_0^{\mathrm{DL}}\mathbf{1}_{N_g^{\mathrm{DL}}} \text{ and} \\
&t_{ik}^{\mathrm{DL}} = \begin{cases} a_H^{\mathrm{DL}} = 1 - a_0^{\mathrm{DL}} & \text{if} \quad s_{ik}^{\mathrm{DL}} = 1 \\ a_L^{\mathrm{DL}} = a_0^{\mathrm{DL}} & \text{if} \quad s_{ik}^{\mathrm{DL}} = 0 \end{cases}
\end{aligned} \tag{3.190}$$

where $x^{\mathrm{DL}} \in \mathbb{C}^{1\times 1}$ is the DL modulation symbol, $\{\mathbf{s}_i^{\mathrm{DL}} \in \mathbb{R}^{N_g^{\mathrm{DL}}\times 1}, i = 1, \cdots, 2^{N_g^{\mathrm{DL}}}\}$ is the DL spatial symbol that includes N_g^{DL} data bits and $\{\mathbf{t}_i^{\mathrm{DL}} \in \mathbb{R}^{N_g^{\mathrm{DL}}\times 1}, i = 1, \cdots, 2^{N_g^{\mathrm{DL}}}\}$ is the mapped version of the spatial symbol $\mathbf{s}_i^{\mathrm{DL}}$. Moreover, $\mathbf{P} \in \mathbb{R}^{N_t \times N_g^{\mathrm{DL}}}$ is the ZF precoder and α^{DL} is a normalization coefficient that fixes the average transmit power

$$\begin{aligned}
&\alpha^{\mathrm{DL}} = \frac{1}{\mathrm{E}[\|\mathbf{P}\mathbf{t}_i^{\mathrm{DL}} x^{\mathrm{DL}}\|_2^2]} = \frac{1}{\mathrm{Tr}\left\{\mathbf{P}\mathbf{R}_{ss}^{\mathrm{DL}}\mathbf{P}^H\right\}} \quad \text{with} \\
&\mathbf{R}_{ss}^{\mathrm{DL}} = \frac{1}{2^{N_g^{\mathrm{DL}}}} \sum_{i=1}^{2^{N_g^{\mathrm{DL}}}} \mathbf{t}_i^{\mathrm{DL}} \mathbf{t}_i^{\mathrm{DL}H}.
\end{aligned} \tag{3.191}$$

The received vector at the UT can be expressed as

$$\mathbf{r}^{\mathrm{DL}} = \sqrt{\alpha^{\mathrm{DL}} P_t}\mathbf{H}\mathbf{P}\mathbf{t}_i^{\mathrm{DL}} x^{\mathrm{DL}} + \mathbf{n}^{\mathrm{DL}} \tag{3.192}$$

where $\mathbf{H}$ is the DL channel matrix which, assuming channel reciprocity, is the transpose of the UL channel matrix $\mathbf{H} = (\mathbf{H}^{\mathrm{UL}})^T$ and $\mathbf{n}^{\mathrm{DL}} \in \mathbb{C}^{N_u \times 1}$ is the noise vector with i.i.d circularly symmetric complex Gaussian elements $\mathcal{CN}(0, \sigma^2)$. At the UT, we apply a two stages analog combiner on the received vector $\mathbf{r}^{\mathrm{DL}}$ as follows

$$\begin{aligned}\mathbf{y}^{\mathrm{DL}} &= \sqrt{\alpha^{\mathrm{DL}} P_t}\mathbf{A}_{\mathrm{PS}}^{\mathrm{DL}H}\mathbf{A}_{\mathrm{SW}}^{\mathrm{DL}H}\mathbf{H}\mathbf{P}\mathbf{t}_i^{\mathrm{DL}} x^{\mathrm{DL}} \\ &\quad + \mathbf{A}_{\mathrm{PS}}^{\mathrm{DL}H}\mathbf{A}_{\mathrm{SW}}^{\mathrm{DL}H}\mathbf{n}^{\mathrm{DL}}\end{aligned} \tag{3.193}$$

where variables are defined in Table 3.4. Moreover, $\mathbf{f}_l^{\mathrm{DL}}$ has constant amplitude

Table 3.4: Elements of the downlink signal model

$\mathbf{A}_{\mathrm{PS}}^{\mathrm{DL}}$	DL analog phase shifters matrix $\in \mathbb{C}^{N_a^{\mathrm{DL}} N_g^{\mathrm{DL}} \times N_g^{\mathrm{DL}}}$, $\mathbf{A}_{\mathrm{PS}}^{\mathrm{DL}} = \mathrm{blockdiag}\{\mathbf{f}_1^{\mathrm{DL}}, \cdots, \mathbf{f}_{N_g^{\mathrm{DL}}}^{\mathrm{DL}}\}$
$\mathbf{f}_l^{\mathrm{DL}}$	DL analog combining response vector $\in \mathbb{C}^{N_a^{\mathrm{DL}} \times 1}$
$\mathbf{A}_{\mathrm{SW}}^{\mathrm{DL}}$	DL analog switches matrix $\in \mathbb{R}^{N_{\mathrm{U}} \times N_a^{\mathrm{DL}} N_g^{\mathrm{DL}}}$, $\mathbf{A}_{\mathrm{SW}}^{\mathrm{DL}\ (i,j)} \in \{0,1\}, i = 1, \cdots, N_U, j = 1, \cdots, N_a^{\mathrm{DL}} N_g^{\mathrm{DL}}$

and thus $|\mathbf{f}_l^{\mathrm{DL}(i)}| = |\mathbf{f}_l^{\mathrm{DL}(j)}| = 1 \ \forall\ i, j,\ l = 1, \cdots, N_g^{\mathrm{DL}}$, $\mathbf{A}_{\mathrm{SW}}^{\mathrm{DL}}$ connects the PSs to the UT antennas such that $\mathbf{A}_{\mathrm{SW}}^{\mathrm{DL}\ (i,j)} = 1$ means that the j-th PS represented by the j-th column of $\mathbf{A}_{\mathrm{SW}}^{\mathrm{DL}}$ is connected to the i-th UT antenna represented by the i-th row of $\mathbf{A}_{\mathrm{SW}}^{\mathrm{DL}}$ so $\|\mathbf{A}_{\mathrm{SW}}^{\mathrm{DL}(j)}\|_0 = j = 1, \cdots, N_a^{\mathrm{DL}} N_g^{\mathrm{DL}}$, the PS inside certain combiner is connected to specific UT antenna and thus $\|\mathbf{A}_{\mathrm{SW}}^{\mathrm{DL}(i,(k-1)N_a^{\mathrm{DL}}+1:kN_a^{\mathrm{DL}})}\|_0 \in \{0,1\}, i = 1, \cdots, N_U, k = 1, \cdots, N_g^{\mathrm{DL}}$. The received signal after the combining in Eq. (3.193) can be cast as

$$\begin{aligned}\mathbf{y}^{\mathrm{DL}} &= \sqrt{\alpha^{\mathrm{DL}} P_t}\mathbf{H}_e^{\mathrm{DL}}\mathbf{P}\mathbf{t}_i^{\mathrm{DL}} x^{\mathrm{DL}} + \mathbf{n}^{''} \text{ with} \\ \mathbf{H}_e^{\mathrm{DL}} &= \mathbf{A}_{\mathrm{PS}}^{\mathrm{DL}H}\mathbf{A}_{\mathrm{SW}}^{\mathrm{DL}H}\mathbf{H} = \left[\mathbf{f}_1^{\mathrm{DL}H}\mathbf{H}_1^{\mathrm{DL}}; \cdots; \mathbf{f}_{N_g}^{\mathrm{DL}H}\mathbf{H}_{N_g^{\mathrm{DL}}}^{\mathrm{DL}}\right], \\ \mathbf{n}^{''} &= \mathbf{A}_{\mathrm{PS}}^{\mathrm{DL}H}\mathbf{A}_{\mathrm{SW}}^{\mathrm{DL}H}\mathbf{n}^{\mathrm{DL}}, \\ \mathbf{H}_k^{\mathrm{DL}} &= \mathbf{A}_{\mathrm{SW}}^{\mathrm{DL}H((k-1)N_a^{\mathrm{DL}}+1:kN_a^{\mathrm{DL}})}\mathbf{H}.\end{aligned} \tag{3.194}$$

Herein, $\mathbf{H}_e^{\mathrm{DL}} \in \mathbb{C}^{N_g^{\mathrm{DL}} \times N_{\mathrm{BS}}}$ is the effective DL channel matrix. Moreover, the RF combiner satisfies $\|\mathbf{A}_{\mathrm{SW}}^{\mathrm{DL}}\mathbf{A}_{\mathrm{PS}}^{\mathrm{DL}}\|_2 = 1$ and thus, the $\mathbf{n}^{''}$ entries have i.i.d $\mathcal{CN}(0, \sigma^2)$ distribution. We design the precoder $\mathbf{P}$ at the BS to zero force the effective DL

channel as

$$\mathbf{P} = \mathbf{H}_e^{\mathrm{DL}H}\left(\mathbf{H}_e^{\mathrm{DL}}\mathbf{H}_e^{\mathrm{DL}H}\right)^{-1}. \tag{3.195}$$

where $\mathbf{P}$ can be implemented as a fully connected hybrid architecture with no performance penalty, according to [67]. The k-th entry of $\mathbf{y}^{\mathrm{DL}}$ can be expressed as

$$y_k^{\mathrm{DL}} = \begin{cases} \sqrt{\alpha^{\mathrm{DL}}P_t}a_H^{\mathrm{DL}}x^{\mathrm{DL}} + n_k^{''} & \text{if} \quad s_{ik}^{\mathrm{DL}} = 1 \\ \sqrt{\alpha^{\mathrm{DL}}P_t}a_L^{\mathrm{DL}}x^{\mathrm{DL}} + n_k^{''} & \text{if} \quad s_{ik}^{\mathrm{DL}} = 0 \end{cases} \tag{3.196}$$

where $n_k^{''}$ is the k-th entry of $\mathbf{n}^{''}$. Note that, the ZF precoder in Eq (3.195) could increase the received noise power in case of imperfect CSI at the BS as discussed in [66].

3.4.3.1 Downlink detection

For the sake of improving the EE at the UT, we consider energy efficient UT circuitry as depicted in Fig. 2.3 and thus, avoid applying ML detection. Instead, we propose using the reduced complexity detection method with ERC presented in Section 3.4.2.3 : we exploit the analog devices (AD and 1-bit ADCs) to detect the DL spatial symbol and the digital devices (RF chain and high resolution ADC) to detect the DL modulation symbol.

The k-th AD connected to the k-th receive analog combiner in Fig. 2.3 measures the amplitude of the k-th signal $|y_k^{\mathrm{DL}}|$ in the RF domain and next, we detect the k-th DL spatial bit by comparing the measured amplitude to a threshold through the k-th 1-bit ADC

$$\hat{s}_{ik}^{\mathrm{DL}} = \begin{cases} 1 & \text{if} \quad |y_k^{\mathrm{DL}}| \geqslant \gamma^{\mathrm{DL}} \\ 0 & \text{if} \quad |y_k^{\mathrm{DL}}| < \gamma^{\mathrm{DL}} \end{cases} \quad \text{with}$$

$$\gamma^{\mathrm{DL}} = \frac{1}{2}\sqrt{\alpha^{\mathrm{DL}}P_t}\left(a_H^{\mathrm{DL}} + a_L^{\mathrm{DL}}\right). \tag{3.197}$$

Similar to the UL reduced complexity modulation symbol detection, we combine all the signals of $\mathbf{y}_k^{\mathrm{DL}}$. Thereafter, the combined signal passes through the RF chain and the high resolution ADC to detect the DL modulation symbol. The combined signal can be expressed as

$$y_c^{\mathrm{DL,ERC}} = \mathbf{1}_{N_g^{\mathrm{DL}}}^T\mathbf{y}^{\mathrm{DL}} = \sqrt{\alpha^{\mathrm{DL}}P_t}\mathbf{1}_{N_g^{\mathrm{DL}}}^T\mathbf{t}_i^{\mathrm{DL}} + \mathbf{1}_{N_g^{\mathrm{DL}}}^T\mathbf{n}^{''}. \tag{3.198}$$

3.4.3.2 Downlink spectral efficiency

The reduced complexity detection method in the DL given with Eq. (3.197) and Eq. (3.198) and in the UL given with Eq. (3.176) and Eq. (3.179) are similar. Therefore, the SE of the DL transmission $\mathrm{SE}^{\mathrm{DL}} = I_S^{\mathrm{DL}} + I_M^{\mathrm{DL}}$ can be derived in similar way according to Eq. (3.181) and Eq. (3.185)

$$I_S^{\mathrm{DL}} = N_g^{\mathrm{DL}} \left(\mathcal{H}\left(\tfrac{P_0+1-P_1}{2}\right) - \tfrac{\mathcal{H}(P_0)+\mathcal{H}(1-P_1)}{2} \right), \tag{3.199}$$

where the sum in Eq. (3.181) is not needed as the noise power is the same for all groups and

$$\begin{aligned}
P_1 &= \Pr\left(\hat{s}_{ik}^{\mathrm{DL}} = 1 | s_{ik}^{\mathrm{DL}} = 0\right) \\
&= 1 - Q_1\left(\sqrt{2\alpha^{\mathrm{DL}} P_t} a_H^{\mathrm{DL}}/\sigma, \sqrt{2}\gamma^{\mathrm{DL}}/\sigma\right), \\
P_0 &= \Pr\left(\hat{s}_{ik}^{\mathrm{DL}} = 0 | s_{ik}^{\mathrm{DL}} = 1\right) \\
&= Q_1\left(\sqrt{2\alpha^{\mathrm{DL}} P_t} a_L^{\mathrm{DL}}/\sigma, \sqrt{2}\gamma^{\mathrm{DL}}/\sigma\right), \\
I_M^{\mathrm{DL}} &= \frac{1}{2^{N_g^{\mathrm{UL}}}} \sum_{i=1}^{2^{N_g^{\mathrm{DL}}}} \frac{1}{2} \log_2\left(\frac{4\pi}{e} \mathrm{SNR}_i^{\mathrm{DL}}\right) \quad \text{with} \\
\mathrm{SNR}_i^{\mathrm{DL}} &= \frac{|\mathbf{1}_{N_g^{\mathrm{DL}}}^{\mathrm{DL}T} \mathbf{t}_i^{\mathrm{DL}}|^2}{N_g^{\mathrm{DL}}} \frac{\alpha^{\mathrm{UL}} P_t}{\sigma^2}.
\end{aligned} \tag{3.200}$$

Similar to the UL case, we select the amplitude levels $\left(a_H^{\mathrm{DL}}, a_L^{\mathrm{DL}}\right)$ to maximize the $\mathrm{SE}^{\mathrm{DL}}$.

3.4.4 Joint Uplink and Downlink Design

The contributions of this section are published in **[J1]**.

3.4.4.1 Low complexity uplink/downlink optimization algorithm

In HTSM/HRSM systems, we consider to include an analog phase shifting stage to achieve high gain. On the other side, employing many PSs increases the power consumption and could degrade the EE. Thus, we design a hybrid system to maximize the EE such that the attained SE is equal or larger than quality of service threshold achieved by (generalized TSM (GTSM)/generalized RSM (GRSM), same architecture as in Fig. 2.3 but without PSs [41]). In Algorithm 3.10, we evaluate the SE of the GTSM/GRSM systems for comparison with the proposed hybrid systems and as an input to Algorithm 3.11. We apply the QR decomposition [74]

Algorithm 3.10 UL and DL system parameters optimization of generalized SM

1: **Input** : $\mathbf{H}$ and $N_{g,\max}$
2: **Output** : $\mathrm{SE}^{\mathrm{UL}}_{\mathrm{GTSM}}$ and $\mathrm{SE}^{\mathrm{DL}}_{\mathrm{GRSM}}$
3: $[\mathbf{Q}\ \mathbf{R}\ \mathcal{A}] = \mathrm{QR}\left(\mathbf{H}^H, 0\right)$ such that $\mathbf{H}^H(:, \mathcal{A}) = \mathbf{QR}$
4: **for** $N_g = 1 : N_{g,\max}$
5: $\quad \mathbf{H}^{\mathrm{DL}}_e = [\mathbf{H}^{(\mathcal{A}(1),:)}; \ldots; \mathbf{H}^{(\mathcal{A}(N_g),:)}], \mathbf{H}^{\mathrm{UL}}_e = \mathbf{H}^{\mathrm{DL}H}_e$
6: $\quad \mathcal{SE}^{\mathrm{UL}}_{\mathrm{GTSM}}(N_g) = \underset{a_0^{\mathrm{UL}}}{\text{maximize}} \left(I^{\mathrm{UL}}_S + I^{\mathrm{UL}}_M\right), \quad s.t. \ \ 0 \leqslant a_0^{\mathrm{UL}} \leqslant \frac{1}{2}$
7: $\quad \mathcal{SE}^{\mathrm{DL}}_{\mathrm{GRSM}}(N_g) = \underset{a_0^{\mathrm{DL}}}{\text{maximize}} \left(I^{\mathrm{DL}}_S + I^{\mathrm{DL}}_M\right), \quad s.t. \ \ 0 \leqslant a_0^{\mathrm{DL}} \leqslant \frac{1}{2}$
8: **end for**
9: **return** $\mathrm{SE}^{\mathrm{UL}}_{\mathrm{GTSM}} = \max\left(\mathcal{SE}^{\mathrm{UL}}_{\mathrm{GTSM}}\right)$
$\mathrm{SE}^{\mathrm{DL}}_{\mathrm{GRSM}} = \max\left(\mathcal{SE}^{\mathrm{DL}}_{\mathrm{GRSM}}\right)$

Algorithm 3.11 UL and DL system parameters optimization of the hybrid SM

1: **Input** : $\mathbf{H} = \mathbf{A}_R \mathbf{D} \mathbf{A}^H_t$, $\mathrm{SE}^{\mathrm{UL}}_{\mathrm{GTSM}}$, $\mathrm{SE}^{\mathrm{DL}}_{\mathrm{GRSM}}$ and P_t
2: **Output** : $\mathbf{A}^{\mathrm{UL}^\star}_{\mathrm{SW}}$, $\mathbf{A}^{\mathrm{UL}^\star}_{\mathrm{PS}}$, $\mathbf{A}^{\mathrm{DL}^\star}_{\mathrm{SW}}$, $\mathbf{A}^{\mathrm{DL}^\star}_{\mathrm{PS}}$, $\alpha_0^{\mathrm{UL}^\star}$ and $\alpha_0^{\mathrm{DL}^\star}$.
3: $\theta_{max} = \theta_i : i = \arg\max_j |\mathbf{D}_{j,j}|, \quad j = 1, \cdots, L$
4: **for** $N_a = 1 : N_{\mathrm{U}}$
5: $\quad$ Generate all possible antennas arrays sub-channels $\mathbf{H}_i = \mathbf{A}_{\mathrm{SW},i}\mathbf{H}, \quad i = 1, \cdots, K = \binom{N_{\mathrm{U}}}{N_a}$, $\mathbf{A}^{(l,m)}_{\mathrm{SW},i} \in \{0, 1\}, \|\mathbf{A}^{(k)}_{\mathrm{SW},i}\|_0 = 1, k = 1, \cdots, N_a, \ \|\mathbf{A}^{(i,:)}_{\mathrm{SW},i}\|_0 \in \{0, 1\}, i = 1, \cdots, N_U$.
6: $\quad \mathbf{f}_i = \sqrt{\frac{N_r}{N_a}} \mathbf{A}_{R,i}(:, \theta_{max}), \quad i = 1, \cdots, K$
7: $\quad \mathbf{H}_e = [\mathbf{f}^H_1 \mathbf{H}_1; \ldots; \mathbf{f}^H_K \mathbf{H}_K]$
8: $\quad [\mathbf{Q}\ \mathbf{R}\ \mathcal{A}] = \mathrm{QR}\left(\mathbf{H}^H_e, 0\right)$ such that $\mathbf{H}^H_e(:, \mathcal{A}) = \mathbf{QR}$
9: $\quad$ **for** $N_g = 1 : N_{g,\max}$
10: $\quad\quad \mathbf{A}_{\mathrm{SW}}(N_a, N_g) = \left[\mathbf{A}_{SW,\mathcal{A}(1)}, \cdots, \mathbf{A}_{SW,\mathcal{A}(N_g)}\right]$
11: $\quad\quad \mathbf{A}_{\mathrm{PS}}(N_a, N_g) = \mathrm{blockdiag}\left(\mathbf{f}_{\mathcal{A}(1)}, \cdots, \mathbf{f}_{\mathcal{A}(N_g)}\right)$
12: $\quad\quad \mathbf{H}^{\mathrm{UL}}_e = [\mathbf{H}^H_{\mathcal{A}(1)}\mathbf{f}_{\mathcal{A}(1)}, \ldots, \mathbf{H}^H_{\mathcal{A}(N_g)}\mathbf{f}_{\mathcal{A}(N_g)}]$
13: $\quad\quad \mathcal{SE}^{\mathrm{UL}}(N_a, N_g) = \underset{a_0^{\mathrm{UL}}}{\text{maximize}} \left(I^{\mathrm{UL}}_S + I^{\mathrm{UL}}_M\right) \quad s.t. \ \ 0 \leqslant a_0^{\mathrm{UL}} \leqslant \frac{1}{2}$
14: $\quad\quad \Omega^{\mathrm{UL}}(N_a, N_g) = a_0^{\mathrm{UL}}$
15: $\quad\quad \mathbf{H}^{\mathrm{DL}}_e = [\mathbf{f}^H_{\mathcal{A}(1)}\mathbf{H}_{\mathcal{A}(1)}; \ldots; \mathbf{f}^H_{\mathcal{A}(N_g)}\mathbf{H}_{\mathcal{A}(N_g)}]$
16: $\quad\quad \mathcal{SE}^{\mathrm{DL}}(N_a, N_g) = \underset{a_0^{\mathrm{DL}}}{\text{maximize}} \left(I^{\mathrm{DL}}_S + I^{\mathrm{DL}}_M\right) \quad s.t. \ \ 0 \leqslant a_0^{\mathrm{DL}} \leqslant \frac{1}{2}$
17: $\quad\quad \Omega^{\mathrm{DL}}(N_a, N_g) = a_0^{\mathrm{DL}}$
18: $\quad$ **end for**
19: **end for**
20: Solve the optimization problem in Eq. 3.201 to obtain the operating points $\left(N^\star_a, N^\star_g\right)$ for the UL and the DL transmissions
21: **return** $\mathbf{A}^{\mathrm{UL}^\star}_{\mathrm{SW}} = \mathbf{A}_{\mathrm{SW}}\left(N^{\mathrm{UL}^\star}_a, N^{\mathrm{UL}^\star}_g\right)$, $\mathbf{A}^{\mathrm{UL}^\star}_{\mathrm{PS}} = \mathbf{A}_{\mathrm{PS}}\left(N^{\mathrm{UL}^\star}_a, N^{\mathrm{UL}^\star}_g\right)$, $a_0^{\mathrm{UL}^\star} = \Omega\left(N^{\mathrm{UL}^\star}_a, N^{\mathrm{UL}^\star}_g\right)$, $\mathbf{A}^{\mathrm{DL}^\star}_{\mathrm{SW}} = \mathbf{A}_{\mathrm{SW}}\left(N^{\mathrm{DL}^\star}_a, N^{\mathrm{DL}^\star}_g\right)$, $\mathbf{A}^{\mathrm{DL}^\star}_{\mathrm{PS}} = \mathbf{A}_{\mathrm{PS}}\left(N^{\mathrm{DL}^\star}_a, N^{\mathrm{DL}^\star}_g\right)$, $a_0^{\mathrm{DL}^\star} = \Omega\left(N^{\mathrm{DL}^\star}_a, N^{\mathrm{DL}^\star}_g\right)$.

to sort the channel matrix rows. Specifically, the set $\mathcal{A}$ in step 3 of Algorithm 3.10 includes the most uncorrelated UT antennas sorted in descending order according to the strength of the path between the UT antenna and the BS and $N_{g,\max}$ represents the maximum number of groups, a value that is upper bounded by the maximum number of clusters that describe the channel. Next, we select the best

sub-channel matrix that maximizes the SE[1]. In Algorithm 3.11, we optimize the analog beamforming and combining matrices and the spatial amplitude levels in UL and DL at a given P_t. Specifically, for a given number of PSs (N_a) inside the group, we have $\binom{N_U}{N_a}$ possible ways of connecting the N_a PSs to the N_U antennas of the UT and this leads to $\binom{N_U}{N_a}$ possible different groups of PSs. Each PSs group is designed to steer the beam in the direction of the strongest path. Next, we generate a large effective channel matrix that includes all of the possible antenna arrays groups. Thanks to the QR decomposition [74], we can sort the linearly independent groups in one step[2]. To evaluate the computational complexity of Algorithm 3.11, we should consider the matrix multiplications operations in steps 7, 12 and 15 and the QR decomposition in step 8 (main source of the computational complexity). Note that, thanks to the joint optimization in Algorithm 3.11, we perform the steps from 5 to 8 only once for the UL and the DL optimization. Hence, we save $\sum_{N_a=1}^{N_U}\binom{N_\mathrm{U}}{N_a}$ matrix multiplications to generate the effective channel in step 7. Moreover, we apply the QR decomposition in step 8 only once for the UL and the DL that reduces the complexity with order of $\mathrm{O}\left(\sum_{N_a=1}^{N_U}\binom{N_\mathrm{U}}{N_a}N_t^2\right)$ flops. In steps 12 and 15, we perform $\sum_{N_a=1}^{N_U}\sum_{N_g=1}^{C} N_a N_g$ matrix multiplications. As an illustrative example, let us consider $N_t = 32$ and $N_u = 16$ and $C = 4$, and hence, we need 65535 matrix multiplications for step 7, 2720 matrix multiplications for steps 12 and 15 and 67×10^6 add/multiply operations to perform the QR decomposition. The computational of complexity of the separate UL and DL optimization is 133790 matrix multiplications and 134×10^6 add/multiply operations. Thanks to the joint optimization in Algorithm 3.11, we reduce the complexity to 68255 matrix multiplications (51% reduction) and 67×10^6 add/multiply operations (50% reduction).

Thereafter, we evaluate the UL and DL SE and the EE (defined as the SE divided by the UT hardware power consumption) with optimized amplitude levels for number of groups starts from one to $N_{g,\max}$. We repeat the procedure for every number of active antennas in a group ($N_a = 1 : N_U$) until we complete $N_U \times N_{g,\max}$ grids for the $\mathrm{SE}^{\mathrm{UL}}$, $\mathrm{SE}^{\mathrm{DL}}$, $\mathrm{EE}^{\mathrm{UL}}$ and $\mathrm{EE}^{\mathrm{DL}}$. Finally, the BS selects the UL and DL operating points in the grids that maximize the EE such that the SE is better than that of systems without PSs (GTSM/GRSM) evaluated in Algorithm 3.10.

[1]We cannot consider the full channel matrix when the matrix is rank deficient as the ZF precoding/combining does not exist.

[2]Note that we need linearly independent groups to perform ZF precoding/combining matrices.

Algorithm 3.12 Transmit power optimization using bisection method

1: **Input** : lower bound, upper bound and ϵ
2: **if** |lower bound − upper bound| $> \epsilon$ **then**
3: Apply Algorithm 3.11 at $P_t = \frac{\text{lower bound+upper bound}}{2}$
4: **if** optimization condition is satisfied, problem (3.201) is infeasible for step 1 or the EE resulting from solving problem (3.201) at $P_t = \frac{\text{lower bound+upper bound}}{2}$ is greater than or equals to the EE at $P_t =$ lower bound for step 2 **then**
5: lower bound $= P_t$, else, upper bound $= P_t$
6: **end if**
7: **end if**

This is formulated as:

$$\begin{aligned} &\left(N_a^\star, N_g^\star\right) = \\ &\underset{N_a \in \{1,\cdots,N_U\}, N_g \in \{1,\cdots,N_{g,\max}\}}{\text{maximize}} \quad \text{EE} = \frac{\text{SE}(N_a, N_g, P_t)}{P_C(N_a, N_g, P_t)} \\ &\text{subject to} \quad \text{SE} \geqslant t \end{aligned} \tag{3.201}$$

where problem (3.201) is solved for the UL considering SE $= \mathcal{SE}^{\text{UL}}$, $P_C = P_C^{\text{UL}}$, $t = \text{SE}_{\text{GTSM}}^{\text{UL}}$ and for the DL considering SE $= \mathcal{SE}^{\text{DL}}$, $P_C = P_C^{\text{DL}}$ and $t = \text{SE}_{\text{GRSM}}^{\text{DL}}$. The optimization of the amplitude levels in steps 13 and 17 of Algorithm 3.11 leads to non linear objective function in one unknown and one linear constraint that can be efficiently evaluated using bisection method. Algorithm 3.11 maximizes the EE at a given transmit power, but the optimal transmit power still needs to be computed. This can be done in two steps. First, evaluating the the minimum transmit power that ensures the SE constraint of problem (3.201). Second, determine the transmit power within the evaluated feasible interval that maximizes the EE. In step 1, we apply the bisection method in Algorithm 3.12 with initial lower bound ($P_t = 0$) and upper bound ($P_t =$ maximum transmit power $P_{t,\max}$). At each iteration, we apply Algorithm 2 using the value of P_t in the middle of the upper and lower bounds. The updated lower bound is P_t if problem (3.201) is infeasible, otherwise, the updated upper bound is P_t. The bisection iterations stop when the gap between the bounds satisfies specific accuracy. The output of step 1 is the minimum transmit power $P_{t,\min}$ that ensures the SE constraint of problem (3.201). In step 2, we apply another bisection method as illustrated in Algorithm 3.12 with initial lower bound ($P_t = 0$) and upper bound ($P_t = P_{t,\min}$). At each iteration, we solve Algorithm 3.11 at P_t in the middle of the bounds. The updated lower bound is P_t if the optimized EE at P_t is greater than or equals to the optimized EE at the lower bound, otherwise, the updated upper bound is P_t. The iterations stop when the gap between the bounds satisfies a given accuracy level. The output of step 2 is the optimal transmit power that maximizes the EE under SE constraint. In

exhaustive search based design, line 8 in Algorithm 3.11 should be replaced with exhaustive search selection of N_g groups out of $\binom{N_u}{N_a}$ possible groups for all values of N_g.

The number of grid points of the proposed algorithm $N_{g,p}$ and the exhaustive search $N_{g,es}$ can be expressed as

$$\begin{aligned} N_{g,p} &= N_U \times N_{g,\max}, \\ N_{g,es} &= 1 + \sum_{N_a=1}^{N_U-1} \sum_{N_g=1}^{N_{g,\max}} \left(\binom{N_U}{N_a} \atop N_g \right), \forall \binom{N_U}{N_a} \geqslant N_g. \end{aligned} \tag{3.202}$$

As an illustrative example, consider $N_U = 16$ and $N_{g,\max} = C = 4$. The corresponding number of grid points are $N_{g,p} = 64$ and $N_{g,es} = 2.9 \times 10^{15}$ and thus, the proposed algorithm significantly reduces the computational complexity.

3.4.4.2 Simulation results

In this section, we evaluate the performance of the proposed HTSM/HRSM schemes compared to the GTSM/GRSM schemes in terms of SE and EE. We show the achievable SE, EE, SE-EE trade-off and illustrate the optimal numbers of needed groups and PSs per group for the UL and the DL systems. In order to validate the efficiency of the proposed algorithm, we compare the EE obtained from the reduced complexity algorithm with the one obtained from the exhaustive search. We evaluate the system performance in both stochastic and deterministic channel environments.

Performance evaluation in stochastic channel

In the stochastic simulation environment, we consider $\sigma^2 = -84$ dBm and $P_l = 90$ dB.

Fig. 3.28 shows the EE comparison of the UL HTSM and the DL HRSM schemes when we apply the proposed fast Algorithm 3.11 compared to the exhaustive search. Thanks to the QR decomposition in Algorithm 3.11, we obtain the same performance as the exhaustive search with significant reduction in the computational complexity as explained in Eq. (3.202).

Fig. 3.29 shows the proposed system behavior in terms of the optimized number of groups and antennas per groups of the HTSM/HRSM designs. The number of groups and antennas per group are obtained from Algorithm 2 and are designed to ensure full rank effective channel matrix and enable the ZF combining and precoding in the UL and DL, respectively. As we maximize the EE, we keep the total number of the PSs small. Therefore, the increase in number of groups is necessarily associated to the decrease in the number of PSs per group. At low SNR, we need high beamforming/combining gains. Hence, the number of PSs

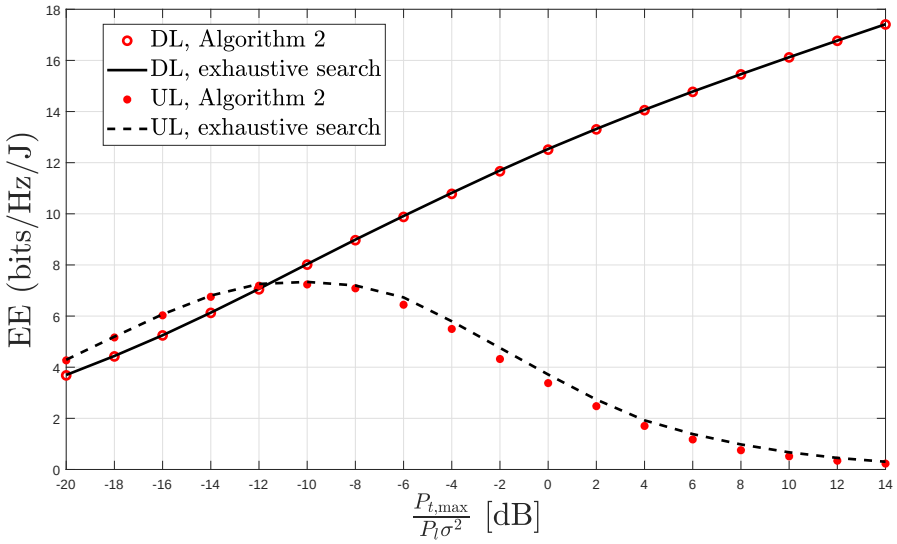

Figure 3.28: EE of the proposed schemes evaluated by Algorithm 3.11 and by exhaustive search vs. received SNR at $N_{\mathrm{BS}} = 128$, $N_U = 4$, $N_{g,\max} = C = 3$ (average over 1000 channel realizations).

per group is high and thus, the number of groups is small. Increasing the SNR reduces the required beamforming/combining gains. As a result, the number of PSs per group decreases and the number of groups increases to attain high spatial multiplexing gain.

Fig. 3.30a shows the SE of the proposed UL HTSM and DL HRSM designs compared to the UL GTSM and the DL GRSM schemes. At low SNR regime (common assumption associated with outdoor mmWave propagation), the proposed hybrid designs achieve superior SE as the PSs stages in the HTSM and HRSM schemes provide high beamforming and combining gains; respectively and combat the severe path-loss. At high SNR, each group may contain one or two PSs as explained in Fig. 3.29. Since the small number of antennas at an array is not sufficient to provide high beamforming gains, the GTSM approaches the SE of the HTSM. On the other hand, the HRSM still outperforms GRSM at high SNR even with the small number of phase shifters per group. The SE of the HRSM is higher than HTSM as the ZF combiner in the HTSM system could amplify the UL noise power. In contrast, the RF combiner of the HRSM does not affect the DL noise power.

Fig. 3.30b shows the SE of the UL HTSM scheme when we apply Algorithm 3.11 with (Gaussian input distribution and optimum detector) shown in Eq. (3.169) and Eq. (3.175) and (M-PSK modulated input and reduced complexity detector) as in Eq. (3.181) and Eq. (3.185). The reduced complexity scheme approaches the optimal performance specifically at low SNR.

Fig. 3.31a shows the UL EE of the proposed HTSM scheme when the transmit

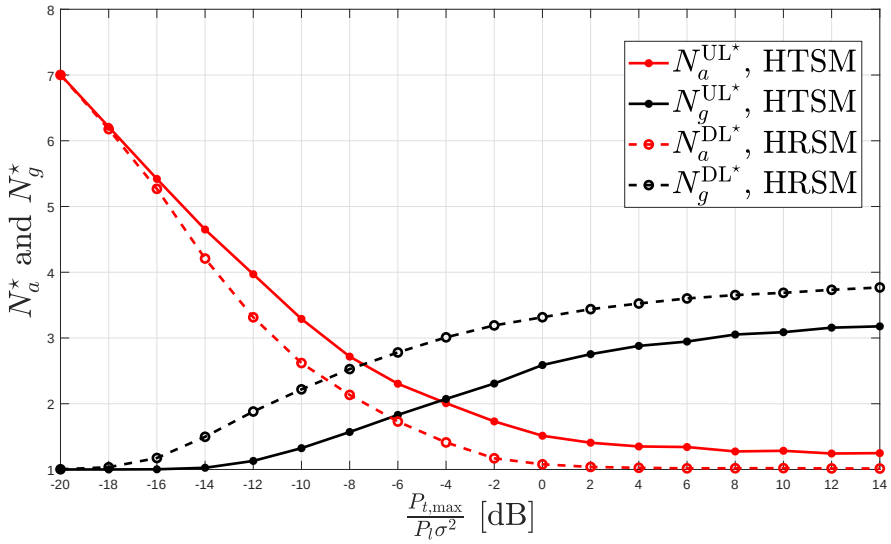

Figure 3.29: Optimum number of antennas per group and number of groups of the HTSM/HRSM schemes vs. received SNR at $N_{\mathrm{BS}} = 128$, $N_U = 16$, $N_{g,\max} = C = 4$ (average over 1000 channel realizations).

power is optimized, or the maximum available transmit power is used. We compare it to the UL EE of the GTSM system. The proposed scheme outperforms the GTSM system especially at low SNR when the beamforming gain is needed. Optimizing the transmit power slightly improves the EE due to the SE constraint shown in Eq. (3.201). Fig. 3.31b represents the DL EE-SE trade-off of the proposed HRSM design compared to the GRSM scheme. At low SNR, the proposed hybrid design achieves superior SE and EE due to the high gain of the PSs stage. At high SNR regime, generalized system achieves slightly higher EE as the number of groups tends to be one and the SE gap of the two systems reduces.

Fig. 3.32 shows the UL and DL EE at the UT of the proposed scheme compared to hybrid SM in [38] and hybrid MIMO in [30] assuming SRF chain at the UT. Transmitting M-PSK modulation symbols and applying reduced complexity detector, the proposed hybrid SM with optimized grouping explained in Algorithm 3.11 attains higher EE than hybrid SM with UG proposed in [38] in UL and DL. Moreover, in DL, it outperforms the the hybrid MIMO in [30]. Considering M-QAM symbols and applying ML detector, the proposed UL HTSM achieves superior EE than the hybrid MIMO in [30].

Performance evaluation for a ray-trace model

With the aim of evaluating the performance of the proposed system in typical small-cell scenario at 28 GHz, we consider a realistic user distribution and generate deterministic channels per user, and then compare the system performance with the stochastic and deterministic channels. Several outdoor small-cell mmWave channel samples have been predicted from the ray-based propagation model Vol-

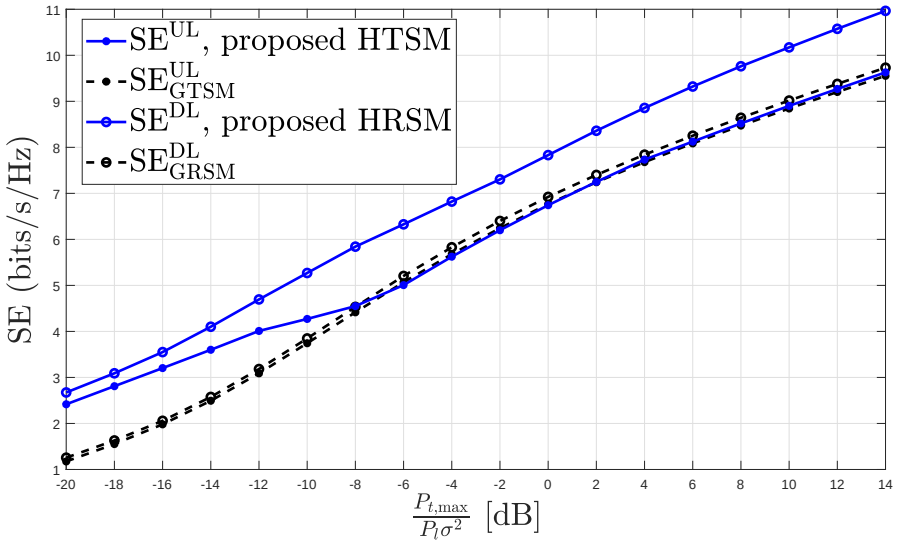

(a) HTSM-HRSM compared to GTSM-GRSM

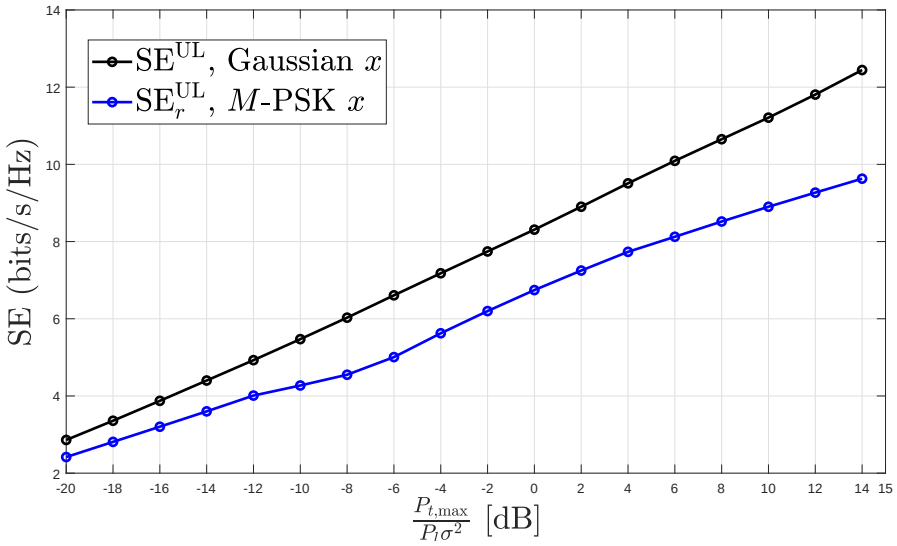

(b) Optimal and reduced complexity detectors

Figure 3.30: SE of the proposed HTSM-HRSM compared to GTSM-GRSM schemes and SE of HTSM with Gaussian modulation symbol and optimal detector compared to the scheme with M-PSK modulation symbol and reduced complexity detector at $N_{\mathrm{BS}} = 128$, $N_U = 16$, $N_{g,\max} = C = 4$ (average over 1000 channel realizations).

canoUrban [95]. Those samples are the result of physical interactions between the electromagnetic wave and the real representation of a dense urban environment, more precisely, a district in New York Manhattan. A small-cell is positioned at 8 meters above the ground, at a typical location for a lamppost. Three sectors are installed at the small-cell. Each sector is feeding a linear antenna array with boresight direction oriented towards azimuth 0°, 120° and 240°, as depicted in Fig. 3.33. Each linear antenna array is formed of 128° vertically-polarized antenna

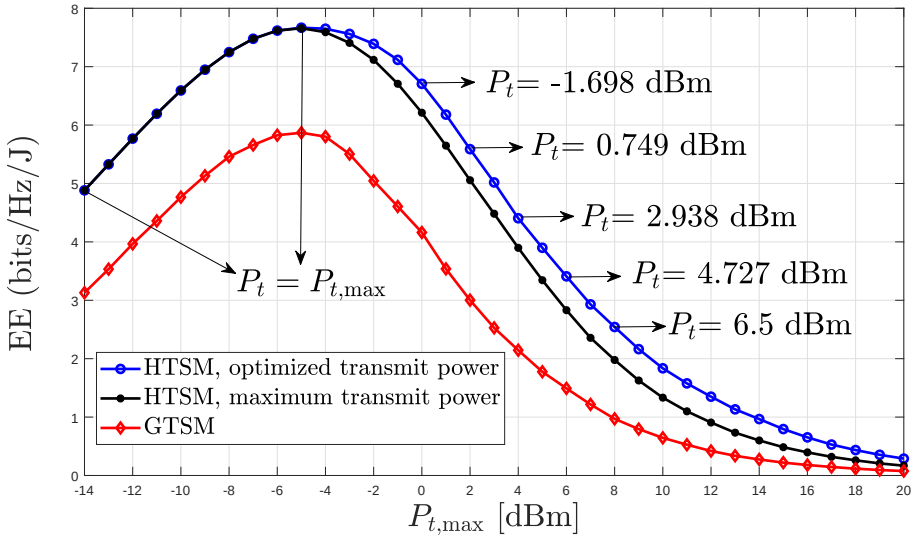

(a) UL EE

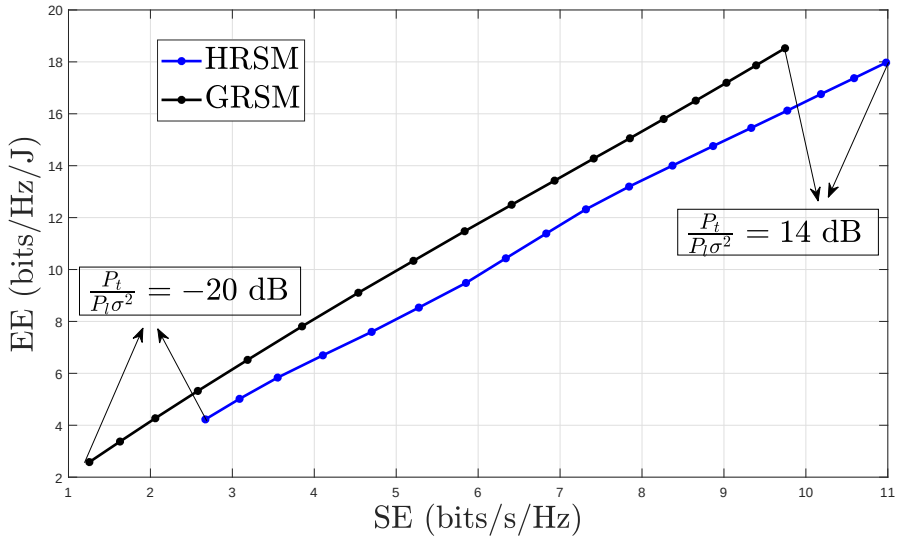

(b) DL EE-SE trade-off

Figure 3.31: UL EE and DL EE-SE trade-off of the proposed HTSM and HRSM schemes compared to GTSM and GRSM methods at $N_{\text{BS}} = 128$, $N_U = 16$, $N_{g,\max} = C = 4$ (average over 1000 channel realizations).

elements, which are uniformly distributed in the horizontal plane, at frequency 28 GHz, and with half-wavelength separation. All antenna elements have same radiation pattern with 60° half-power horizontal beamwidth.

The users are assumed to be pedestrians distributed on the surrounding pavements at a maximum 220 meters range from the small-cell. The user equipment is located at 1.5 meter above the ground. Its antenna is a ULA with 16 vertically-polarized isotropic elements positioned in the horizontal plane. The channel sam-

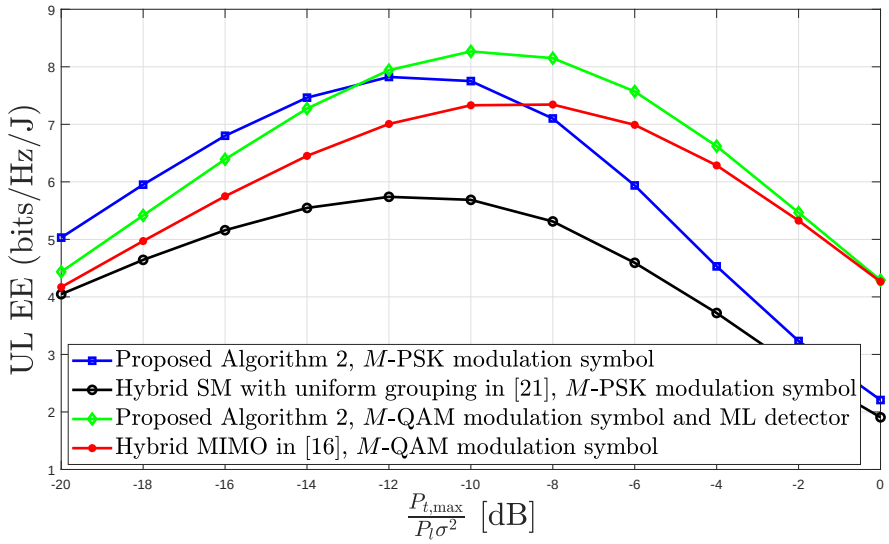

(a) UL EE

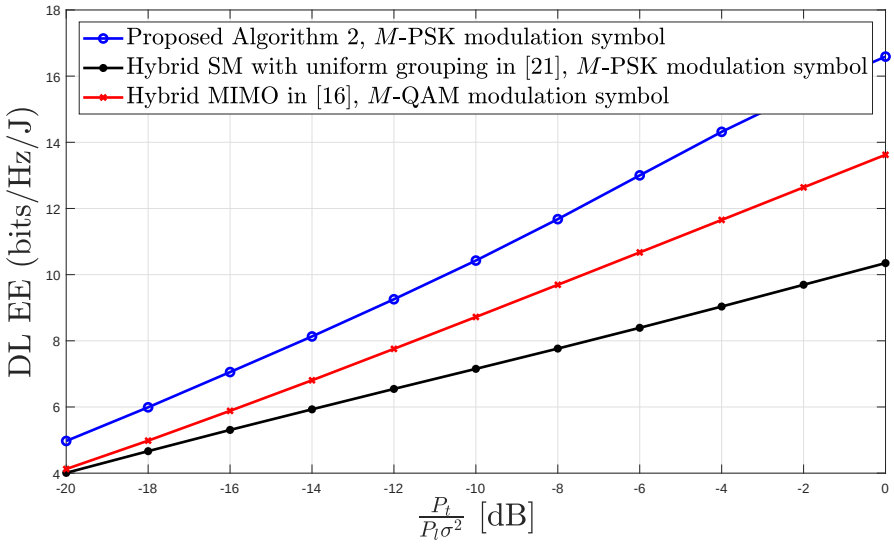

(b) DL EE

Figure 3.32: UL and DL energy efficiency at the UT of the proposed scheme compared to hybrid SM in [38] and hybrid MIMO in [30] assuming single RF chain, $N_{\text{BS}} = 128$, $N_U = 16$, $N_{g,\max} = C = 6$ (average over 1000 channel realizations).

ples are produced from 142 different user positions. Users are positioned either in a wide or a narrow street, or even in a small square. Few of them are in NLoS situation. Finally, a total number of 180 channel samples are created: 50, 69 and 61 for respectively sector 0, 1 and 2 with 37 NLoS samples.

The SE of the proposed UL HTSM and DL HRSM designs evaluated on the stochastic channel model with $C = 2$ and $C = 6$ scatterers and the deterministic channel model for the scenario proposed in Fig. 3.33 assuming the same path-loss

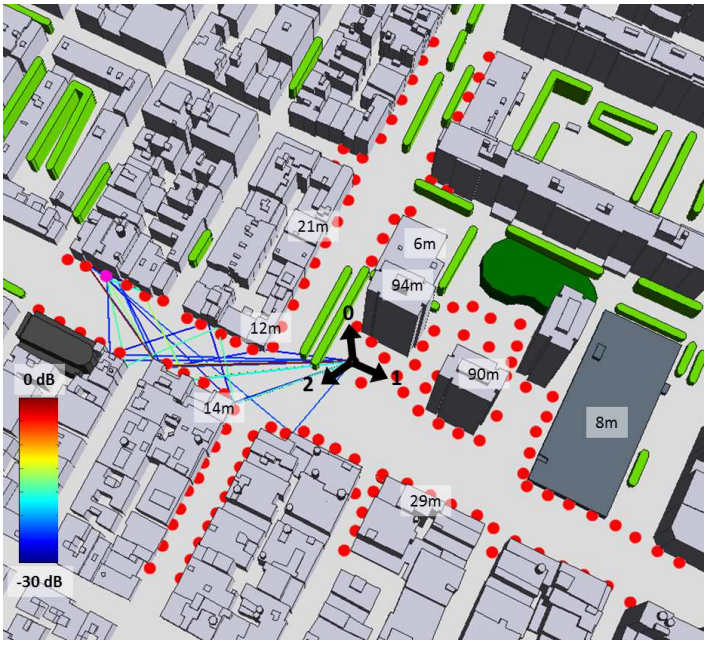

Figure 3.33: Top view of realistic users distribution (red dots) served by three sectors mMIMO BSs inside mmWave small-cell in Manhattan area in New York City where the farthest user at 220 metre distance from the small-cell.

for the two models is depicted in Fig. 3.36. The noise level is $\sigma^2 = -84$ dBm, the transmit power is $P_t = 20$ dBm, the carrier frequency is $f_c = 28$ GHz, BW $= 10$ MHz and 76% of the users have delay spread smaller than the symbol time for the simulation setup so that we can consider non-frequency selective channel. Sector 0 has the lowest scattering environment due to the LoS users and the vegetation. Sector 1 has more NLoS users and thus, the users achieve high SE. Sector 2 users are farther away than the users in the other sectors and thus, its users have greater path-loss and lower SE. From this experiment, we show that the proposed design not only attains high performance with the theoretical stochastic channel model in Eq. (2.12) but it also achieves similar performance with the realistic channel model. Moreover, the performance evaluation of the 28 GHz channels at BW $= 10$ MHz based on stochastic channel model gives a realistic assessment if the number of clusters is in the range of $C = 2$ and $C = 6$.

3.5 Conclusions

In Sec. 3.3.1.1, we have considered the DL of a massive MIMO single user operating in the mmWave outdoor narrowband channel environment. We developed a novel RSM architecture aimed to reduce the power consumption at the UT and achieve high throughput. We proposed ZF precoding scheme and derived the required decoder, providing expressions for the ABEP. A performance comparison is per-

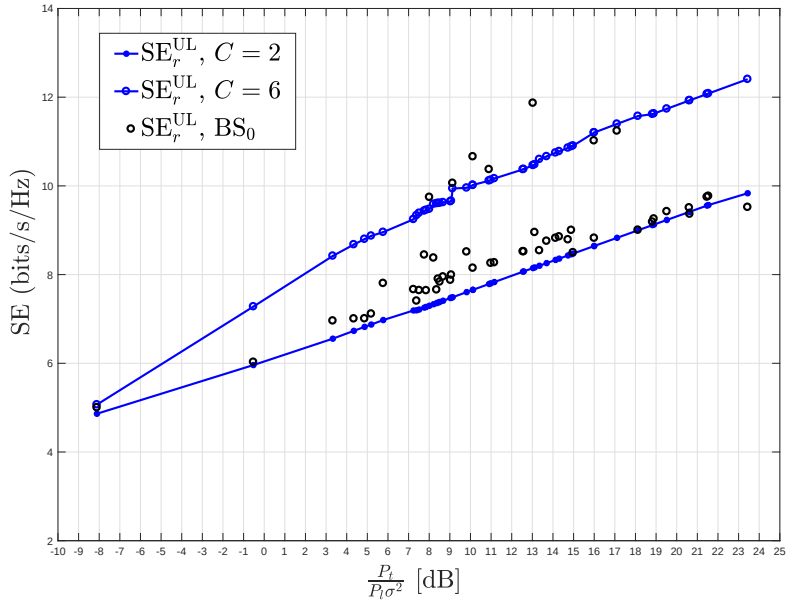

(a) UL SE of sector 0

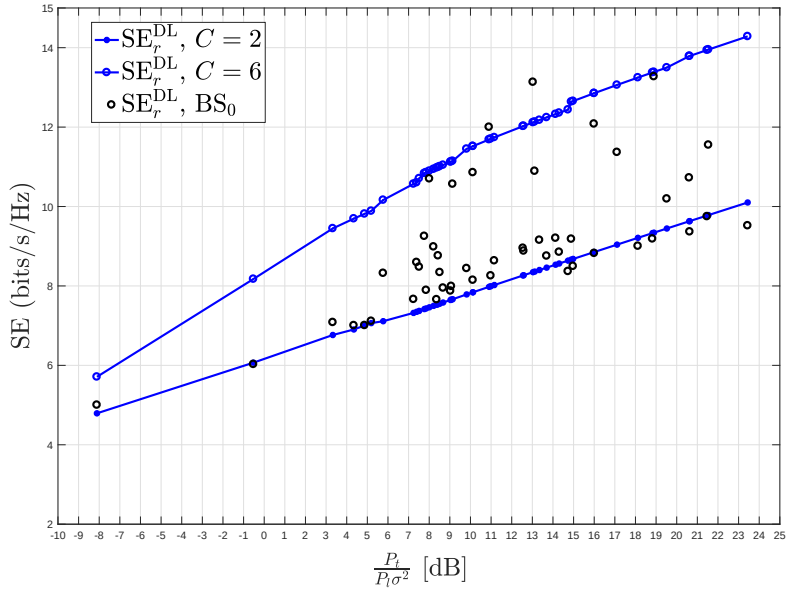

(b) DL SE of sector 0

Figure 3.34: Sector 0 SE of the proposed UL and DL hybrid design evaluated on stochastic (in blue, for $C = 2$, $C = 6$ and average over 100 realizations) and deterministic channel samples (in dots) assuming the same path-loss for the two models, $\sigma^2 = -84$ dBm, $P_t = 20$ dBm, $f_c = 28$ GHz and BW = 10 MHz.

formed between the proposed system and FD MIMO showing that an appropriate constellation selection can reduce the performance gap.

In Sec. 3.3.1.6, the proposed MMSE RSM scheme outperforms the ZF RSM

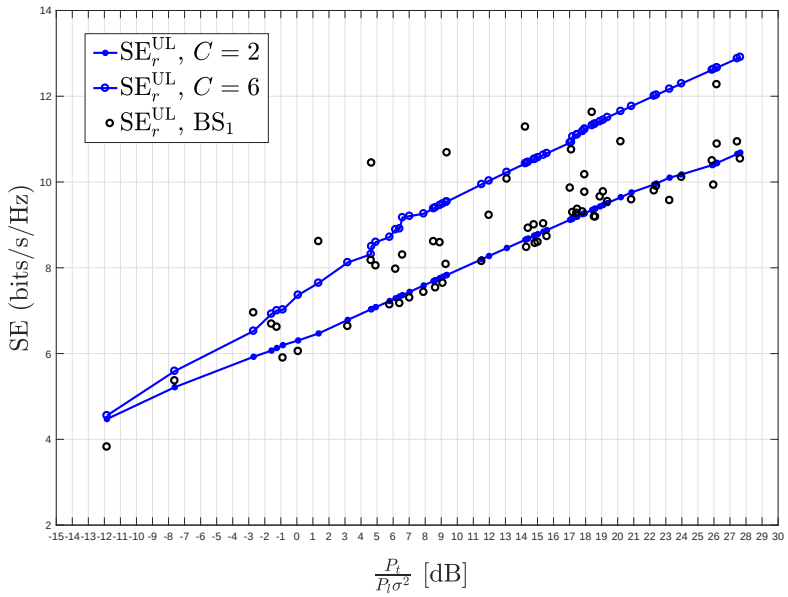

(a) UL SE of sector 1

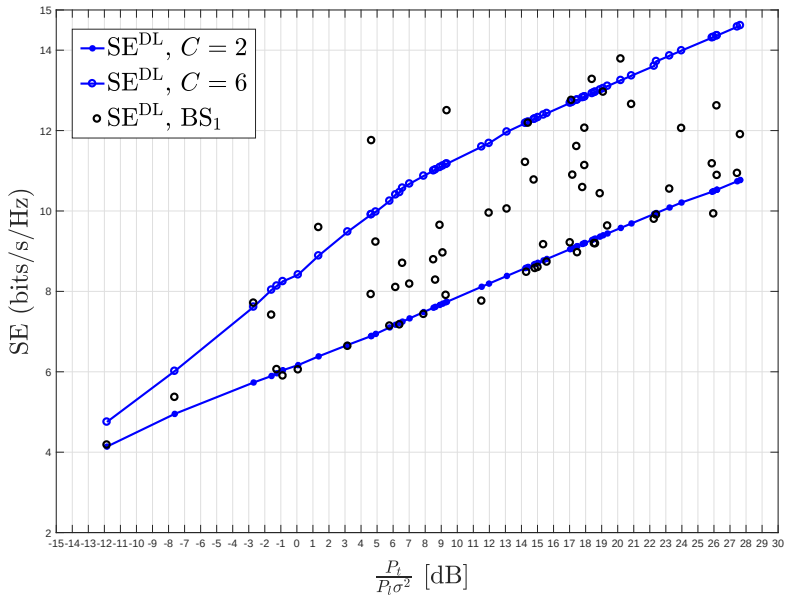

(b) DL SE of sector 1

Figure 3.35: Sector 1 SE of the proposed UL and DL hybrid design evaluated on stochastic (in blue, for $C = 2$, $C = 6$ and average over 100 realizations) and deterministic channel samples (in dots) assuming the same path-loss for the two models, $\sigma^2 = -84$ dBm, $P_t = 20$ dBm, $f_c = 28$ GHz and BW $= 10$ MHz.

because forcing some antennas to receive zero signals could reduce the high level signals received by other antennas which leads to degradation in the mutual information specifically in spatially correlated channels. Simulation results show that

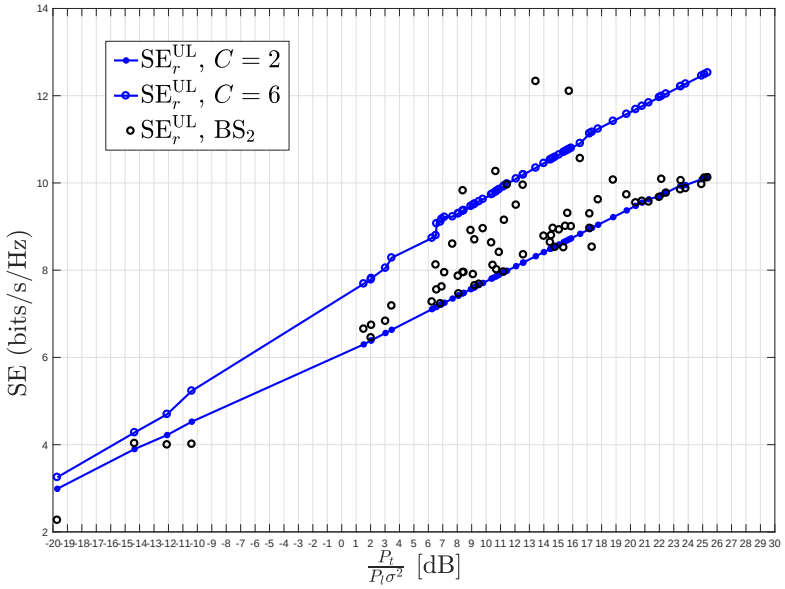

(a) UL SE of sector 2

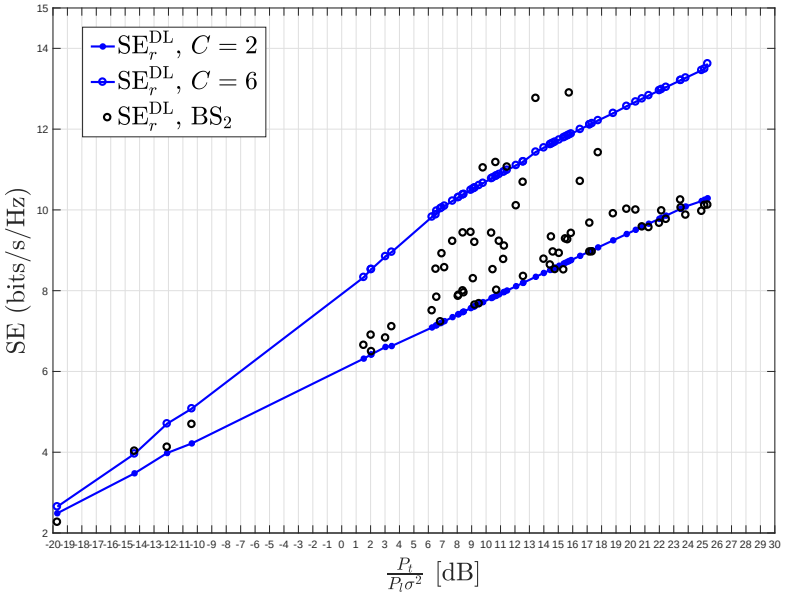

(b) DL SE of sector 2

Figure 3.36: Sector 2 SE of the proposed UL and DL hybrid design evaluated on stochastic (in blue, for $C = 2$, $C = 6$ and average over 100 realizations) and deterministic channel samples (in dots) assuming the same path-loss for the two models, $\sigma^2 = -84$ dBm, $P_t = 20$ dBm, $f_c = 28$ GHz and BW $= 10$ MHz.

there is an optimal number of receive antennas that maximizes the mutual information at given SNR. Thus, we apply RAS method based exhaustive search (computationally complex) to maximize the mutual information. It is better to consider the HSA threshold when N_t is large to get the same performance as the

exact threshold but with much lower computational complexity. A low number of DL training symbols are needed to estimate the detection thresholds that could be useful for channels with small coherence time.

In Sec. 3.3.2, the proposed RAS based convex optimization are suboptimal due to relaxing non-convex constraints. Therefore, performance of proposed RAS sequential algorithms are superior to that based convex optimization. For low computational complexity, its useful to start with empty initialization when $\left(N_a < \frac{N_r}{2}\right)$ and full initialization at $\left(N_a \geq \frac{N_r}{2}\right)$. We also developed fast algorithm to determine the optimal number of ARA that maximizes the mutual information. The proposed ZF hybrid precoder outperforms the best known design and becomes optimal when the channel is very spatially sparse. Hybrid precoder is the most energy efficient when the channel is limited by few number of scattering paths; otherwise, FD is better.

In Sec. 3.3.3, the proposed wideband single carrier RSM architecture provides an interesting trade-off between EE and SE at the UT. The proposed RSM scheme outperforms the FD MIMO in EE and approaches the SE. Not surprisingly, it has been observed that the SE saturates with the number of FIR taps and the minimum number of taps increases with the time spread N_c. Optimizing the FIR delay n_d based on the channel errors is necessary to both combat the intersymbol interference and maximize the received signal power. The BS just requires the channel error and receive noise variances to optimize the FIR delay. The RAS is vital for single carrier RSM schemes to make the pre-equalizer possible in rank deficient MIMO channels.

With the purpose of improving the SE, Sec. 3.3.4 shows that the proposed RSM scheme can be extended to more general case where the UT circuitry consists of MRF chains.

In Sec. 3.4, we proposed novel and energy efficient hybrid transceiver architecture based on two stages analog beamformer in the UL and combiner in the DL, respectively. The analog switches stage smartly allocate the UT antennas on the PSs groups to minimize the spatial correlation. Moreover, the analog PSs stage maximizes the beamforming/combining gains to combat the path-loss. We proposed a novel and computationally efficient optimization algorithm to design the analog stages. The proposed design achieves the same performance as the exhaustive search method but with much lower computational complexity. The flexibility of the architecture allows optimising the hybrid transceiver at any SNR regime: At low SNR regime, we activate only one group of PSs and maximize the number of PSs inside the group to attain high post processing SNR. At high SNR regime, the number of groups increases and as a result the spatial rate increases. Moreover,

the number of PSs per group decreases as optimizing the EE implies reducing the total number of PSs. We validated the performance of the proposed design on a realistic deployment in Manhattan area in New York City. The performance evaluation for mmWave small-cell at 28 GHz shows that the stochastic channel models provides results close to those obtained with the deterministic channel if the number of clusters is chosen to emulate the real-world scenario.

Chapter 4

Multiple Users Spatial Modulation

4.1 Contribution

In this chapter, we address challenge 6. Part of the research contributions presented in this chapter are accepted with minor revision in IEEE Transactions on Wireless Communications **[J2]**.

4.2 Introduction

A major advantage of massive antenna systems is to multiplex multiple users at the same time and the same frequency in DL and in UL to enhance the network SE. Extending SM schemes to multiple users is not straightforward due to the complicated joint power allocation and antenna selection problem. Moreover, the transceiver hardware limitations add more constraints. Several work have been developed for multiple user SM schemes. In [60], the authors evaluated the performance of the RSM scheme assuming MIMO BC and FD transceivers; however, they did not consider power control and the transmit power is equally split among the users. In [59], a DL multi-user RSM scheme has been proposed; however, a high energy consuming FD UT architecture is considered. In [99], the authors study the needed number of UT antennas for UL MU SM systems.

In this chapter, we consider DL RSM scheme and UL TSM scheme for a multi-user MIMO system operating at mmWave outdoor environment. In the single user scenario in Sec. 3.4, thanks to the channel reciprocity and that both BS and UT have continues power constraint, we proposed joint design for the UL and the DL schemes in Algorithm 3.11. The joint design of the UL and the DL is challenging

because they have different power control mechanisms. The UL power control is limited to ON/OFF users scenario as the CSI is not available at the UTs. This limitation is not applied to the DL power control as the CSI is known at the BS. Hence, in this chapter, we propose separate design for the DL and UL systems. The main novelty and contributions are submitted at [**J2**] and can be expressed as follows

- We extend the single user RSM scheme to multiple users scenario in the DL. Specifically, we propose novel fast and efficient algorithm to jointly optimize number of users, set of antennas and the transmit power allocated to each user so as to maximize the sum SE.

- We propose two options for the optimization of the MAC system parameters. First, using the same parameters as in the BC based on reciprocity and the assumption that the same users are being served that entailing lower computation requirements. Second is proposing new algorithm for optimizing the parameters of the MAC system. In this algorithm, we jointly optimize number of users, set of active antennas at each user and we decide the ON/OFF status of each user to maximize the sum SE as illustrated in Algorithm 4.4. The new MAC algorithm is less complex than the BC algorithm due to using binary power allocation scheme in the MAC transmission.

4.3 Multi-user RSM for Broadcast Channel

In this section, we consider that a single BS serves N_U users each having N_r antennas in the DL by applying ZF precoding and assuming RSM with the IC method illustrated in Sec. 3.3.4. We consider FD BS and the UT architecture in Fig. 2.4. We provide a novel algorithm that jointly optimizes the number of users, the set of active antennas and the transmit power allocated for each user with the goal of maximizing the sum SE. At a given number of users and set of antennas per user, we formulate the power allocation as a non-convex optimization problem. Next, we propose an alternating optimization algorithm that converts the non-convex problem into a series of convex problems. Finally, we compare the performance and the convergence of the proposed alternating optimization with the successive convex approximation framework, which is also a popular approach to solve non-convex problems [100], [101].

For simplicity, let us consider the system model that assumes a SRF chain at each UT; however, the analysis can be straightforward extended to MRF chains thanks to the use of the mapping matrix $\mathbf{F}$ shown in Eq. (3.137). In the DL, the

BS broadcasts different SM symbol to each user such that the transmit signal after precoding can be expressed as

$$\begin{aligned}
\mathbf{x}_t &= \sum_{k=1}^{N_U} \sqrt{b_k}\mathbf{P}_k\mathbf{s}_{i,k}x_{j,k}, \quad \text{with} \\
\mathrm{E}\left[\mathbf{x}_t^H\mathbf{x}_t\right] &= \sum_{k=1}^{N_U} b_k \,\mathrm{Tr}\left\{\mathbf{P}_k\mathbf{R}_{s_k,s_k}\mathbf{P}_k^H\right\} = \sum_{k=1}^{N_U} b_k\mu_k = P_t, \\
\mathbf{R}_{s_k,s_k} &= \frac{1}{2^{N_{a,k}}}\sum_{i=1}^{2^{N_{a,k}}} \mathbf{s}_{i,k},\mathbf{s}_{i,k}^H, \\
\mathbf{P} &= \mathbf{H}_a^H\left(\mathbf{H}_a\mathbf{H}_a^H\right)^{-1}, \quad \mathbf{P}_k = \mathbf{P}\left(:, 1+\sum_{i=0}^{k-1} N_{a,i} : \sum_{i=1}^{k} N_{a,i}\right),
\end{aligned} \tag{4.1}$$

where, per the k-th user, $x_{j,k}$ is M-PSK modulation symbol, $\mathbf{s}_{i,k} \in \mathbb{R}^{N_{a,k}\times 1}$ is the spatial symbol and its entries $s_{i,k}(n) \in \{0 < \alpha_{0,k} < 0.5, 1-\alpha_{0,k}\}$, $\forall\, n = 1, \cdots, N_{a,k}$ (number of active antennas at the k-th UT), $\mathbf{P}_k \in \mathbb{C}^{N_t\times N_{a,k}}$ is the precoding matrix associated to user k, b_k is power allocation factor, $\mathbf{R}_{s_k,s_k}$ represents the spatial symbol covariance matrix, $\mathbf{H}_a = [\mathbf{H}_{a,1}, \cdots, \mathbf{H}_{a,N_U},]^T \in \mathbb{C}^{\sum_{k=1}^{N_U} N_{a,k}\times N_t}$ is the channel matrix of all the users after having applied the antenna selection, $\mathbf{H}_{a,k}$ represents the user channel matrix after antenna selection from the matrix $\mathbf{H}_k$ and $\mathbf{P} \in \mathbb{C}^{N_t\times\sum_{k=1}^{N_U} N_{a,k}}$ is the multi-user ZF precoding matrix. The signal received by the k-th user can be expressed as

$$\mathbf{y}_k = \mathbf{H}_{a,k}\left(\sum_{k=1}^{N_U}\sqrt{b_k}\mathbf{P}_k\mathbf{s}_{i,k}x_{j,k}\right) + \mathbf{n}_k, \quad \mathbf{y}_k = \sqrt{b_k}\mathbf{s}_{i,k}x_{j,k} + \mathbf{n}_k \tag{4.2}$$

where the combined SNR at the k-th user is

$$\mathrm{SNR}_{i,k} = \frac{\left(\mathbf{1}_{N_{a,k}}^T\mathbf{s}_{i,k}\right)^2}{N_{a,k}}\frac{b_k}{\sigma^2}. \tag{4.3}$$

The received signal in Eq. (4.2) is similar to that of the single user case that is mentioned in Eq. 3.4. Thus, the mutual information for the spatial symbol ($I_{S,k}$) and for the modulation symbol ($I_{M,k}$) of the k-th user can be expressed in a similar way as follows

$$I_{S,k} = N_{a,k} \times \left(\mathcal{H}\left(\frac{P_{0,k}+1-P_{1,k}}{2}\right) - \frac{\mathcal{H}\left(P_{0,k}\right)+\mathcal{H}\left(1-P_{1,k}\right)}{2}\right),$$

Algorithm 4.1 Joint user, antenna selection and power allocation

1: **Input** : $\mathbf{H}_1, \cdots, \mathbf{H}_{N_U}$
2: **Initialization** : $R(0) = 0$ and $n = 0$
3: **Output** : $b_k^\star$ and $\alpha_{0,k}^\star$, $\forall\ k = 1, \cdots, N_U$
4: $[\mathbf{Q}\ \mathbf{R}\ \mathcal{A}] = \mathrm{QR}\left(\mathbf{H}^H, 0\right)$ such that $\mathbf{H}^H(:, \mathcal{A}) = \mathbf{QR}$, $\mathbf{H} = [\mathbf{H}_1, \cdots, \mathbf{H}_{N_U}]^T$
5: **for** $i = 1 : \mathrm{length}(\mathcal{A})$
6: $n = n + 1$
7: $\mathbf{H}_a = \mathbf{H}([\mathcal{A}(1), \cdots, \mathcal{A}(n)], :)$
8: Solve (P1) using $\mathbf{H}_a$ to obtain $\alpha_{0,k}(n)$, $b_k(n)$ and $R(n) = \sum_{k=1}^{N_U} \mathrm{SE}_k$, $\forall\ k = 1, \cdots, N_U$
9: **if** $R(n) < R(n-1)$ **then**
10: $\mathcal{A} = \mathcal{A} - \mathcal{A}(n)$
11: $n = n - 1$
12: **end if**
13: **end for**
14: **return** $b_k^\star = b_k(n)$ and $\alpha_{0,k}^\star = \mu_k(n)$, $\forall\ k = 1, \cdots, N_U$

$$I_{M,k} = \sum_{i=1}^{2^{N_{a,k}}} \Pr\left(\mathbf{s}_{i,k}\right) I_{M-\mathrm{PSK}}\left(\mathrm{SNR}_{i,k}\right). \tag{4.4}$$

where the error probabilities can be expressed as

$$\begin{aligned} &P_{1,k} = 1 - \mathcal{Q}_1\left(\frac{1}{\sigma}\sqrt{2}a_{h,k}, \frac{1}{\sigma}\sqrt{2}\gamma_k\right), \quad P_{0,k} = \mathcal{Q}_1\left(\frac{1}{\sigma}\sqrt{2}a_{l.k}, \frac{1}{\sigma}\sqrt{2}\gamma_k\right), \\ &a_{h,k} = (1-\alpha_{0,k})\sqrt{b_k}, \quad a_{l,k} = \alpha_{0,k}\sqrt{b_k} \text{ and } \quad \gamma_k = \frac{a_{h,k} + a_{l,k}}{2}, \end{aligned} \tag{4.5}$$

and the SE of the k-th user can be expressed as

$$\mathrm{SE}_k = I_{S,k} + I_{M,k}. \tag{4.6}$$

In multiple users scenario, the joint power allocation, user and antenna selection is the main challenge compared to the single user scenario. In Algorithm 4.1, we jointly optimize the number of users, the set of active antennas, the high and low spatial amplitude levels and the power allocated for each user to maximize the sum SE. At first, we apply the QR decomposition on $\mathbf{H} = [\mathbf{H}_1, \cdots, \mathbf{H}_{N_U}]^T$ to sort the UT antennas indices. The set $\mathcal{A}$, in line 4 of Algorithm 4.1, includes the sorted all users antennas indices such that $\mathcal{A}(1)$ refers to the antenna index with maximum $\mathbf{R}_{ii}$ value. Next, we add one antenna per iteration from set $\mathcal{A}$. For the resulting user distribution and active antennas per user, we allocate the transmit power $P_{t,k} = b_k\mu_k$ and design the spatial levels $\alpha_{0,k}$ to maximize the sum SE. Hence, the

Algorithm 4.2 Power allocation using the proposed alternating optimization

1: Initialization: Consider any value of $\alpha_{0,k}$ such that $0 \leq \alpha_{0,k} \leq 0.5 \ \forall \ k = 1, \cdots, N_U$ and $i = 0$
2: $i = i + 1$
3: Problem (P2) takes $\alpha_{0,k}$ as input and gives the transmit power per user $P_{t,k}(i)$ as an output
4: Problem (P3) takes $P_{t,k}(i)$ as an input and gives $\alpha_{0,k}$ and b_k as an output
5: Go to step 2 until $|P_{t,k}(i) - P_{t,k}(i-1)| \leq \epsilon$

power allocation optimization problem can be expressed as

$$(\text{P1}) \begin{cases} \underset{b_1,\cdots,b_{N_U},\alpha_{0,1},\cdots,\alpha_{0,N_U}}{\text{maximize}} & \sum_{k=1}^{N_U} I_{M,k} + I_{S,k} \\ \text{subject to} & \sum_{k=1}^{N_U} b_k \mu_k = P_t, \quad 0 \leqslant \alpha_{0,k} \leqslant 0.5, \quad \forall \ k = 1, \cdots, N_U, \end{cases} \tag{4.7}$$

where μ_k can be expressed as

$$\mu_k = \left(\frac{\alpha_{0,k}^2 + (1 - \alpha_{0,k})^2}{2} - \frac{1}{4} \right) \text{Tr} \left\{ \mathbf{P}_k^H \mathbf{P}_k \right\} \quad + \frac{1}{4} \text{Tr} \left\{ \mathbf{1}_{N_{a,k}} \mathbf{P}_k^H \mathbf{P}_k \right\}. \tag{4.8}$$

At each iteration in Algorithm 4.1, we determine the sum SE resulting from the solution of (P1) and if it degrades, we discard the antenna added at this iteration. We repeat the above procedure with all antennas in the set $\mathcal{A}$.

From Eq. (4.4), the spatial and modulation symbols mutual information are not convex functions in the power allocation variables b_k and the spatial level factors $\alpha_{0,k}$ and thus, the objective function of problem (P1) is non-convex. Moreover, problem (P1) has a non-convex joint power constraint. The multi-user TAS are performed after RAS where we deactivate one weak transmit antenna per iteration, in a similar way to full initialization Algorithm 3.3, to enhance the EE under sum SE constraints. In the sequel, we propose an alternating optimization algorithm as a solution to problem (P1) based on a sequence of convex optimization problems. After that, we compare the performance and the convergence of the proposed algorithm with successive convex approximation scheme.

4.3.1 Alternating Optimization

In Algorithm 4.2, we propose an alternating optimization method to solve problem (P1). First, we fix the values of the spatial levels $\alpha_{0,k}$ and thus, the power constraint of problem (P1) becomes linear in b_k. However, the objective function is still expressed by not convex mutual information expressions. Therefore, we propose a linear piecewise approximation for the modulation and the spatial symbols mutual

information as follows

$$\tilde{I}_{M,k} = \min_{q_n}\left\{ I_{M,k|_{b_k=q_n}} + \frac{d}{db_k} I_{M,k|_{b_k=q_n}} (b_k - q_n)\right\},$$
$$q_0 = 0,\ q_{n+1} = q_n + \frac{1}{\left|\frac{d^2}{db_k^2} I_{M,k|_{b_k=q_n}}\right|},\ n = 0, \cdots, N. \tag{4.9}$$

where the derivative in Eq. (4.9) can be determined numerically, K is a constant and N is the number of piecewise linear functions whose spacing is chosen as the inverse of the variation of the slope of $I_{M,k}$. Large N leads to better approximation of the function. Finally,

$$\tilde{I}_{S,k} = N_{a,k} \min\{1, I_{S,1k}, I_{S,2k}\}, \tag{4.10}$$

where $I_{S,1k}$ and $I_{S,2k}$ are tangents to $I_{S,k}$ and passes through $I_{S,k} = \beta_1$ and $I_{S,k} = \beta_2$, respectively. [1] At given spatial levels $\alpha_{0,k}$ and thanks to the approximations in Eq. (4.9) and Eq. (4.10), we can reformulate problem (P1) as a convex program

$$\text{(P2)} \begin{cases} \underset{b_1,\cdots,b_{N_U}}{\text{maximize}} & \sum_{k=1}^{N_U} \tilde{I}_{M,k} + \tilde{I}_{S,k} \\ \text{subject to} & \sum_{k=1}^{N_U} b_k \mu_k = P_t, \end{cases} \tag{4.11}$$

that can be efficiently solved to determine the transmit power allocated to the k-th user $P_{t,k} = b_k \mu_k$ as illustrated in step 3 of Algorithm 4.2. After that, we solve problem (P1) using the obtained $P_{t,k}$ from step 3 to determine updated values of b_k and $\alpha_{0,k}$ as

$$\text{(P3)} \begin{cases} \underset{b_1,\cdots,b_{N_U},\alpha_{0,1},\cdots,\alpha_{0,N_U}}{\text{maximize}} & \sum_{k=1}^{N_U} I_{M,k} + I_{S,k} \\ \text{subject to} & b_k \mu_k = P_{t,k},\ \ 0 \leqslant \alpha_{0,k} \leqslant 0.5,\ \ \forall\ k = 1, \cdots, N_U. \end{cases} \tag{4.12}$$

Problem (P3) has individual power constraints and the objective function is the sum of independent mutual information per user. Thus, we can reformulate problem (P3) as N_U sub-problems, each can be expressed as

$$\text{(P4)} \begin{cases} \underset{b_k,\alpha_{0,k}}{\text{maximize}} & I_{M,k} + I_{S,k} \\ \text{subject to} & b_k = \frac{P_{t,k}}{\mu_k},\ \ 0 \leqslant \alpha_{0,k} \leqslant 0.5, \end{cases} , k = 1, \cdots, N_U \tag{4.13}$$

[1] We consider binary spatial transmission per the UT antenna and thus, the spatial mutual information reaches saturation value and does not further improve with increasing SNR. Therefore, we consider three lines to approximate the spatial mutual information as depicted in Eq. (4.10).

where the optimal value of $\alpha_{0,k}$ can be obtained using the bisection methods [102] and $b_k = P_{t,k}/\mu_k$. Finally, we repeat steps 3 and 4 of Algorithm 4.2 until convergence.

4.3.2 Successive Convex Approximation

Another popular approach to the solution of non-convex problems is successive convex approximation. In order to apply the framework of the successive convex approximation [101], the constrains of the power allocation must define a convex set. Thus, we modify the system model in Eq. (4.1) by replacing the power allocation variables b_k and the spatial levels $0 \leqslant \alpha_{0,k} \leqslant 1$ with high level amplitudes $a_{h,k}$ and low level amplitudes $a_{l,k}$ as follows

$$\begin{aligned}
\mathbf{x}_t^{\mathrm{SCA}} &= \sum_{k=1}^{N_U} \mathbf{P}_k \mathbf{s}_{i,k} x_{j,k},\ s_{i,k}(n) \in \{a_{l,k}, a_{h,k}\}, \\
\mathrm{E}\big[\mathbf{x}_t^H \mathbf{x}_t\big] &= \sum_{k=1}^{N_U} \mathrm{Tr}\left\{\mathbf{P}_k \mathbf{R}_{s_k,s_k} \mathbf{P}_k^H\right\} = \sum_{k=1}^{N_U} \mathbf{a}_k^T \mathbf{A}_k \mathbf{a}_k = P_t, \quad \mathbf{A}_k = \begin{bmatrix} c_k & d_k/2 \\ d_k/2 & c_k \end{bmatrix}, \\
\mathbf{a}_k &= \begin{bmatrix} a_{l,k} & a_{h,k} \end{bmatrix}^T, \quad c_k = \frac{1}{4}\mathrm{Tr}\left\{\mathbf{P}_k^H \mathbf{P}_k\right\} + \frac{1}{4}\mathrm{Tr}\left\{\mathbf{1}_{N_{a,k}} \mathbf{P}_k^H \mathbf{P}_k\right\}, \\
d_k &= \frac{1}{2}\mathrm{Tr}\left\{\mathbf{1}_{N_{a,k}} \mathbf{P}_k^H \mathbf{P}_k\right\} - \frac{1}{2}\mathrm{Tr}\left\{\mathbf{P}_k^H \mathbf{P}_k\right\}.
\end{aligned} \tag{4.14}$$

Accordingly, the received signal and the combined SNR of the k-th user can be expressed as

$$\mathbf{y}_k^{\mathrm{SCA}} = \mathbf{s}_{i,k} x_{j,k} + \mathbf{n}_k, \quad \mathrm{SNR}_{i,k}^{\mathrm{SCA}} = \frac{\left(n_{1,ik} a_{h,k} + n_{0,ik} a_{l,k}\right)^2}{\left(n_{1,ik} + n_{0,ik}\right)\sigma^2}. \tag{4.15}$$

where $n_{1,ik}$ and $n_{0,ik}$ denote number of ones and zeros in $\mathbf{s}_{i,k}$, respectively. The mutual information of the spatial ($I_{S,k}^{\mathrm{SCA}}$) and the modulation ($I_{M,k}^{\mathrm{SCA}}$) symbols can be expressed in a similar way to that in Eq. (4.4). The high and low amplitude levels are designed to maximize the sum SE as

$$\text{(P5)} \begin{cases} \underset{a_1,\cdots,a_{N_U}}{\text{maximize}} & U\left(\mathbf{a}_1, \cdots, \mathbf{a}_{N_U}\right) = \sum_{k=1}^{N_U} I_{M,k}^{\mathrm{SCA}} + I_{S,k}^{\mathrm{SCA}} \\ \text{subject to} & \sum_{k=1}^{N_U} \mathbf{a}_k^T \mathbf{A}_k \mathbf{a}_k \leqslant P_t. \end{cases} \tag{4.16}$$

In Algorithm 4.3, we illustrate how the successive convex approximation method solves problem (P5). First, the objective function is approximated using convex

Algorithm 4.3 Power allocation using successive convex approximation

1: Initialization: $\gamma^{(0)} = 1$, $\tau = 1$, $\epsilon = 0.1$ and $\mathbf{a}_k^{(0)}$ is a feasible point satisfies $\sum_{k=1}^{N_U} \mathbf{a}_k^T \mathbf{A}_k \mathbf{a}_k = P_t$
2: Solve problem (P6) to determine $\hat{\mathbf{a}}_k^{(n)}$, $\forall k = 1, \cdots, N_U$
3: $\mathbf{a}_k^{(n+1)} = \mathbf{a}_k^{(n)} + \gamma^{(n)} \left(\hat{\mathbf{a}}_k^{(n)} - \mathbf{a}_k^{(n)} \right)$
4: $\gamma^{(n+1)} = \gamma^{(n)} \left(1 - \epsilon \gamma^{(n)} \right)$
5: Go to step 2 until $\|\mathbf{a}_k^{(n+1)} - \mathbf{a}_k^{(n)}\|_2 \leq \epsilon$

expansion at any feasible point as

$$\text{(P6)} \begin{cases} \underset{a_1, \cdots, a_{N_U}}{\text{maximize}} \sum_{k=1}^{N_U} \nabla_{\mathbf{a}_k^n} U(\mathbf{a})^T_{|_{\mathbf{a}=\mathbf{a}^n}} (\mathbf{a}_k - \mathbf{a}_k^n) + \dfrac{\tau}{2} \|\mathbf{a}_k - \mathbf{a}_k^n\|_2^2 \\ \text{subject to } \sum_{k=1}^{N_U} \mathbf{a}_k^T \mathbf{A}_k \mathbf{a}_k \leqslant P_t. \end{cases} \tag{4.17}$$

and hence, we solve the convex problem (P6) to obtain $\hat{\mathbf{a}}_k^{(n)}$ as shown in step 2 of Algorithm 4.3. At step 3, we use the determined $\hat{\mathbf{a}}_k^{(n)}$ to update the solution $\mathbf{a}_k^{(n+1)}$. The above procedure is repeated until convergence.

In the sequel, we evaluate the system performance of the proposed RSM schemes compared to CM methods (water filling power allocation+M-QAM symbols) for multiple users transmissions. In the simulations scenario, we consider the stochastic channel model in Eq. (2.12) with $g_i \sim \mathcal{CN}(0, 1)$, and $\phi_i \in [-\pi/6, \pi/6], \theta_i \in [-\pi, \pi]$ are uniformly distributed, $\eta = 0.9$, $\beta_1 = 0$, $\beta_2 = 0.9$, BW = 100MHz and $\sigma^2 = -94$ dBm and $N = 10$. The proposed UT architecture in Fig. 2.1 can accommodate either with RSM or CM transmissions through adjusting controlling switches. Thus, this FRSM scheme is able to capture the best performance of RSM and CM methods.

Fig. 4.1 illustrates the sum SE of four users by allocating the available power using the alternating optimization method proposed in Algorithm 4.2 compared to that of successive convex approximation illustrated in Algorithm 4.3. We take the best result after optimization using ten different initial points. The proposed alternating optimization converges at a much faster rate than the successive convex approximation.

Fig. 4.2 shows the per user spatial and modulation symbols mutual information. We allocate the power to four users by applying the proposed alternating optimization algorithm. Users with high SNR, achieve higher values of modulation symbol mutual information while the spatial mutual information saturates at low SNR as we transmit as many spatial bits as number of active antennas at the UT (less than or equal to number of scattering clusters C).

Fig. 4.3 shows the sum SE of the proposed joint user, antenna and power alloca-

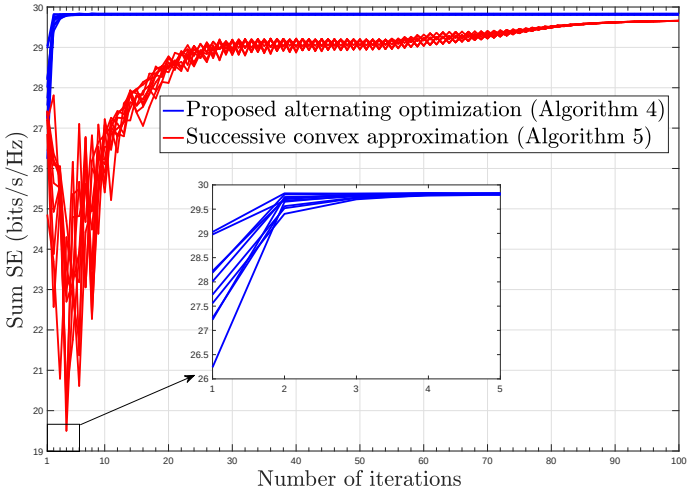

Figure 4.1: Sum SE of the proposed alternating optimization scheme compared to the successive convex approximation technique assuming 10 random initial points, $N_U = 4$, $C = 3$, $P_t/P_l\sigma^2 = 14, 13, 12$ and 11 dB for the four users, $N_t = 128$ and $N_r = 16$ (average over 1000 channel realizations).

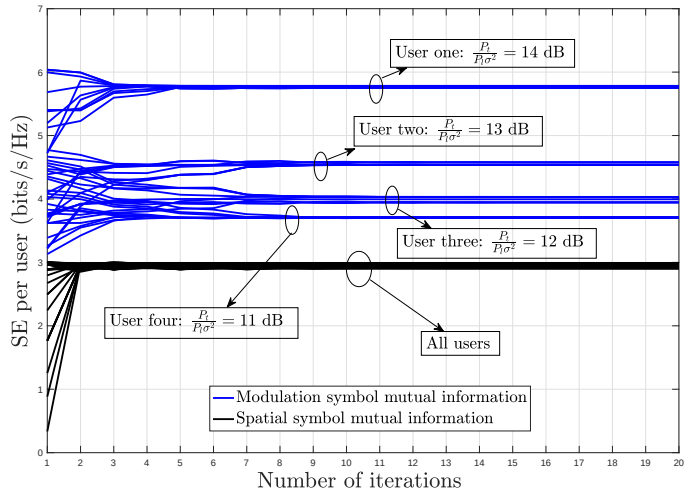

Figure 4.2: Per user spatial and modulation symbols mutual information of the proposed alternating optimization scheme assuming 10 random initial points, $N_U = 4$, $C = 3$, $P_t/P_l\sigma^2 = 14, 13, 12, 11$ dB for the four users, $N_t = 128$ and $N_r = 16$ (average over 1000 channel realizations).

tion Algorithm 4.1 compared to that of exhaustive search based antenna selection over all the users. The proposed algorithm tightly approaches the performance of the exhaustive search but with significantly lower search complexity.

Fig. 4.4 illustrates the sum SE of the proposed RSM scheme in Algorithm 4.1 with alternating optimization power allocation compared to CM (M-QAM transmission+ water filling power allocation [103]). The RSM scheme achieves higher SE than CM as the spatial mutual information requires low SNR to reach

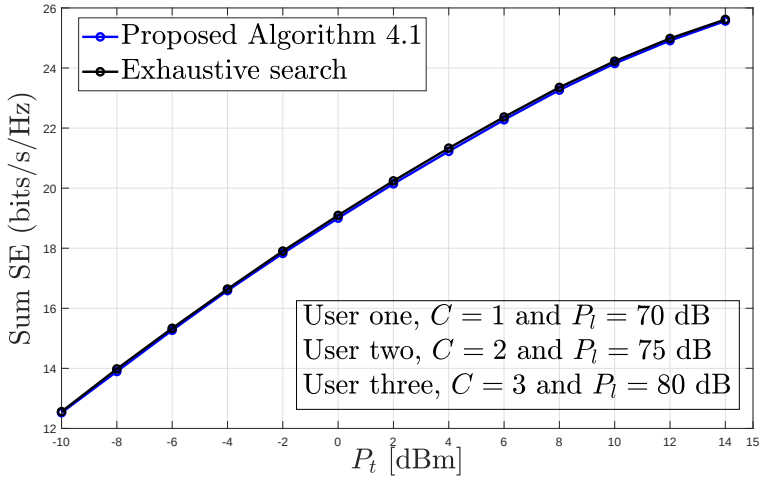

Figure 4.3: Sum SE of the proposed joint user, antenna selection and power allocation Algorithm 4.1 compared to the exhaustive search over all the UTs antennas combinations at $N_U = 3$, $C = 1, 2, 3$, $P_l = 70, 75, 80$ dB, $N_t = 128$ and $N_r = 3$ (average over 1000 channel realizations).

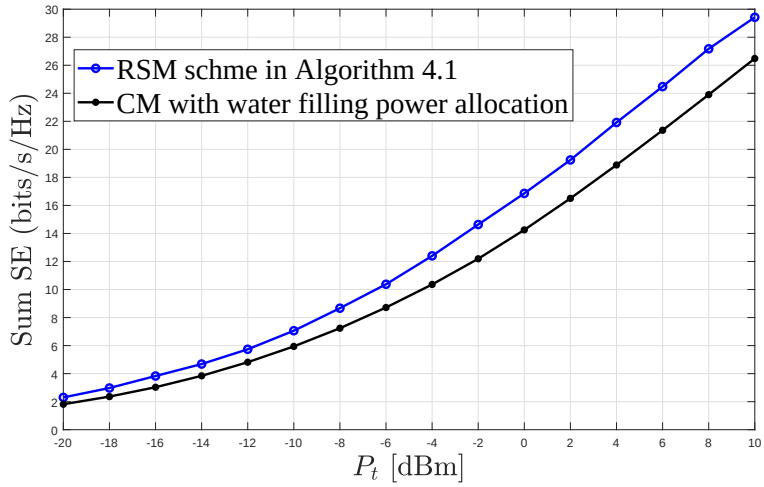

Figure 4.4: Sum SE of the proposed RSM in Algorithm 4.1 compared to CM with water filling power allocation at $N_U = 4$, $N_{rf} = 1$, $C = 6$, $P_l = 80, 85, 90, 95$ dB, $N_t = 128$ and $N_r = 16$ (average over 1000 channel realizations).

saturation, as depicted in Fig. 4.2.

4.4 Multi-user TSM for UL multiple access channel

In the UL, the users transmit different SM symbols to the BS where the transmit signal by the k-th user can be expressed as

$$\mathbf{x}_k = \sqrt{P_t/N_U}\mathbf{s}_{i,k}x_{j,k} \tag{4.18}$$

and the received signal at the BS from all the users can be expressed as

$$\mathbf{r} = \sum_{k=1}^{N_U} \sqrt{P_t/N_U}\mathbf{H}_k \mathbf{s}_{i,k} x_{j,k} + \mathbf{n} \tag{4.19}$$

where $\mathbf{H}_k \in \mathbb{C}^{N_t \times N_{a,k}}$. The BS applies ZF linear receiver such as $\mathbf{y} = \mathbf{Pr}$ where

$$\mathbf{P} = \left(\mathbf{H}_a^H \mathbf{H}_a\right)^{-1} \mathbf{H}_a^H, \quad \mathbf{H}_a = [\mathbf{H}_1, \cdots, \mathbf{H}_{\mathbf{N_U}}].$$

The received signal from the k-th user can be expressed as

$$\mathbf{y}_k = \sqrt{P_t/N_U}\mathbf{s}_{i,k} x_{j,k} + \mathbf{P}_k \mathbf{n} \tag{4.20}$$

where $\mathbf{P}_k \in \mathbb{C}^{N_{a,k} \times N_t}$. The combined SNR per the k-th user can be expressed as

$$\mathrm{SNR}_{c,k} = \frac{\left(\sum_{n=1}^{N_U} \mathbf{s}_{i,k}(n)\right)^2}{\mathrm{Tr}\left\{\mathbf{P}_k \mathbf{P}_k^H\right\}} \frac{P_t/N_U}{\sigma^2} \tag{4.21}$$

We use the $\mathrm{SNR}_{c,k}$ to evaluate the mutual information of the spatial symbol and the conventionally modulated symbol in the same way as Eq. (4.4).

Each user transmits signal either with full power or be silent with zero transmit power. In Algorithm 4.4, we jointly optimize the number of active users, the set of active antennas per user, and the high and low spatial amplitude levels for each user to maximize the sum SE. At first, we apply the QR decomposition on $\mathbf{H} = [\mathbf{H}_1, \cdots, \mathbf{H}_{N_U}]^T$ to sort the UT antennas indices. The set $\mathcal{A}$, in line 4 of Algorithm 4.4, includes the sorted UTs antenna indices such that $\mathcal{A}(1)$ refers to the antenna index with maximum $\mathbf{R}_{ii}$ value. Next, we add one antenna per iteration from set $\mathcal{A}$. For the resulting user distribution and active antennas per user, we and design the spatial levels $\alpha_{0,k}$ to maximize the sum SE using bisection method.

In Fig. 4.5, we present the sum SE of four users transmitting simultaneously in the UL using TSM scheme. We optimise number of active users, set of active antennas per user and the spatial levels. We compare the performance of the MAC system operating with proposed UL optimization algorithm (we call it UL optimization in Fig. 4.5) to the MAC operating with the parameters obtained from the BC optimization (we call it DL optimization in Fig. 4.5). The results show that UL-specific optimization achieves significant throughput gain.

Algorithm 4.4 Joint UL user, antenna selection and on/off power allocation

Input : $\mathbf{H}_1, \cdots, \mathbf{H}_{N_U}$
Initialization : $R(0) = 0$ and $n = 0$
Output : $\alpha^{\star}_{0,k}, \quad \forall\ k = 1, \cdots, N_U$
$[\mathbf{Q}\ \mathbf{R}\ \mathcal{A}] = \mathrm{QR}\left(\mathbf{H}^H, 0\right)$ such that $\mathbf{H}^H\left(:, \mathcal{A}\right) = \mathbf{QR}$, $\mathbf{H} = [\mathbf{H}_1, \cdots, \mathbf{H}_{N_U}]^T$
for $i = 1 : \mathrm{length}(\mathcal{A})$
    $n = n + 1$
    $\mathbf{H}_a = \mathbf{H}\left([\mathcal{A}(1), \cdots, \mathcal{A}(n)], :\right)$
    Find $\alpha_{0,k}(n)$ that maximizes the mutual information of each user and evaluate $R(n) = \sum_{k=1}^{N_U} \mathrm{SE}_k, \quad \forall\ k = 1, \cdots, N_U$
    if $R(n) < R(n-1)$ **then**
        $\mathcal{A} = \mathcal{A} - \mathcal{A}(n)$
        $n = n - 1$
    end if
end for
return $\alpha^{\star}_{0,k}, \quad \forall\ k = 1, \cdots, N_U$

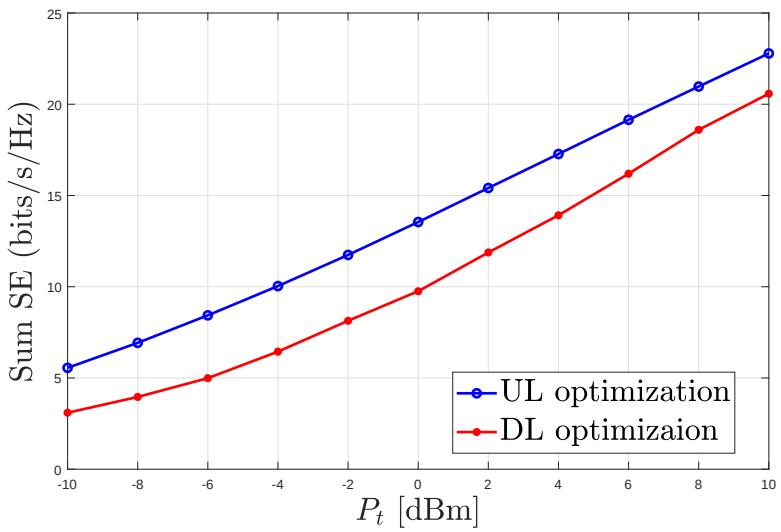

Figure 4.5: Sum SE of the proposed UL optimization in Algorithm 4.4 compared to using the DL optimization results in Algorithm 4.1 at $N_U = 4$, $N_{rf} = 1$, $C = 6$, $P_l = 80, 85, 90, 95$ dB, $N_t = 128$ and $N_r = 16$ (average over 1000 channel realizations).

4.5 Conclusion

In this chapter, we proposed DL RSM scheme for BC and UL TSM for MAC of MU MIMO system operating in mmWave outdoor environment. In the DL multi-user scheme, the proposed algorithm, jointly optimizes number of users, set of active antennas and the power allocated for each user, approaches the performance of exhaustive search but with significant computational complexity reduction. For a given set of users and antennas per each user, the proposed alternating optimization power allocation algorithm outperforms the successive convex approximation

method in terms of performance and convergence. In the UL multi-user scheme, the proposed UL optimization algorithm, jointly optimizes number of users, set of active antennas and the power transmitted from each user, is less complex than the one proposed for the DL scheme due to the ON/OFF power constrains of the MAC transmission. Moreover, the UL multiple users Algorithm outperforms the MAC system that operating with the BC optimization results and thus, separate design is needed for the multiple users case to attain high performance.

Chapter 5

Conclusions and Future Research Directions

5.1 General conclusions

In Sec. 3.3.1.1, we have considered the DL of a massive MIMO single user operating in the mmWave outdoor narrowband channel environment. We developed a novel RSM architecture based on ZF precoding aimed to reduce the power consumption at the UT and achieve high SE. A performance comparison is performed between the proposed system and FD MIMO showing that an appropriate constellation selection can reduce the performance gap.

In Sec. 3.3.1.6, we showed that the proposed MMSE RSM scheme outperforms the ZF RSM in spatially correlated channels. This is because forcing some antennas to receive zero signals could reduce the high level signals received by other antennas. We showed through simulation results that there is an optimal number of receive antennas that maximizes the mutual information at given SNR. Therefore, we applied RAS method based exhaustive search (computationally complex) to maximize the mutual information.

In Sec. 3.3.2, to avoid the computational complexity of the RAS based exhaustive search, we proposed several RAS techniques. We showed that the RAS based on sequential algorithms are superior to that based on convex optimization. In Sec. 3.3.2.4, we learned that the ZF hybrid precoder becomes optimal when the channel is very spatially sparse.

In Sec. 3.3.3, we explained that single carrier systems with FIR pre-equalizer outperforms the multi-carrier for RSM schemes. Moreover, the proposed RSM scheme outperforms the FD MIMO in EE and approaches the SE. We showed that optimizing the FIR delay n_d based on the channel errors is necessary to

both combat the intersymbol interference and maximize the received signal power. We learned that RAS is needed for single carrier RSM schemes to make the pre-equalizer possible in rank deficient MIMO channels. In Sec. 3.3.4, the SE is improved by extending the energy efficient UT architecture to multiple RF chains.

In Sec. 3.4, we proposed novel and energy efficient hybrid transceiver architecture based on two stages analog beamformer in the UL and combiner in the DL, respectively. The analog switches stage smartly allocate the UT antennas on the PSs groups to minimize the spatial correlation. Moreover, the analog PSs stage maximizes the beamforming/combining gains to combat the path-loss. The proposed design attains superior SE-EE trade-off compared to the sate of the art.

In chapter 4, we proposed DL RSM scheme for BC and UL TSM for MAC of MU MIMO system operating in mmWave outdoor environment. We proposed two optimization algorithms, one for the DL multi-user scheme and the other for UL multi-user scheme. The proposed designs outperforms the best known methods in performance and in convergence.

5.2 Future Research Directions

- Recently, machine learning techniques have been developed to tackle the antenna selection problem in MIMO systems. In [104], the authors developed machine learning algorithms for antenna selection on SM. In [105], the authors applied a neural network-based approach to select subset of antennas that maximizes the received SNR. Developing antenna selection algorithms for mmWave SM schemes based on deep neural networks considering the architectures proposed in this work is an interesting research topic.

- Reconfigurable Intelligent Surface (RIS) is a promising candidate for future MIMO systems due to their ability in attaining configurable wireless reflections. Recently, in [106], RIS based SM schemes have been developed showing superior performance compared to the conventional MIMO systems. Extending these RIS based SM schemes for mmWave systems with reduced complexity UT architecture is promising direction that deserves further investigation.

- Massive MIMO transceivers based RF lens antennas have been developed to reduce the cost and the power consumption while attaining high SE [107]. The lens antenna can transmit and receive several spatial beams using lower number of RF chains. Considering lens antennas at the BS for mmWave SM schemes is a novel research topic.

Bibliography

[1] M. Joham, W. Utschick, and J. A. Nossek, "Linear transmit processing in MIMO communications systems", *IEEE Trans. on signal Processing*, vol. 53, no. 8, pp. 2700–2712, Jul. 2005.

[2] *International Telecommunication Union (ITU). IMT traffic estimates for the years 2020 to 2030*, Report ITU-R M.2370-0, Jul. 2015.

[3] L. Ericsson, "More than 50 billion connected devices", *White Paper*, vol. 14, p. 124, Feb. 2011.

[4] T. S. Rappaport *et al.*, *Millimeter wave wireless communications*. Englewood Cliffs, NJ, USA: Prentice-Hall, Sep. 2014.

[5] Z. Pi and F. Khan, "An introduction to millimeter-wave mobile broadband systems", *IEEE Communications Magazine*, vol. 49, no. 6, pp. 101–107, Jun. 2011.

[6] T. S. Rappaport *et al.*, "Millimeter wave mobile communications for 5G cellular: It will work!", *IEEE Access*, vol. 1, pp. 335–349, May 2013.

[7] F. Boccardi *et al.*, "Five disruptive technology directions for 5G", *IEEE Communications Magazine*, vol. 52, no. 2, pp. 74–80, Feb. 2014.

[8] W. Roh *et al.*, "Millimeter-wave beamforming as an enabling technology for 5G cellular communications: Theoretical feasibility and prototype results", *IEEE Communications Magazine*, vol. 52, no. 2, pp. 106–113, Feb. 2014.

[9] S. Rangan *et al.*, "Millimeter-wave cellular wireless networks: Potentials and challenges", *Proceedings of the IEEE*, vol. 102, no. 3, pp. 366–385, Mar. 2014.

[10] A. I. Sulyman *et al.*, "Radio propagation path loss models for 5g cellular networks in the 28 ghz and 38 ghz millimeter-wave bands", *IEEE Communications Magazine*, vol. 52, no. 9, pp. 78–86, Sep. 2014.

[11] K. Venugopal *et al.*, "Time-domain channel estimation for wideband millimeter wave systems with hybrid architecture", *in IEEE International Conference on Acoustics, Speech and Signal Processing (ICASSP)*, pp. 6493–6497, Mar. 2017.

[12] H. Zhao et al., "28 GHz millimeter wave cellular communication measurements for reflection and penetration loss in and around buildings in New York City", *IEEE International Conference on Communications (ICC)*, pp. 5163–5167, Jun. 2013.

[13] L. H. Gonsioroski and L. da Silva Mello, "Preliminary results of measurements of penetration losses through buildings at 2.5 GHz", *in IEEE International Microwave & Optoelectronics Conference (IMOC)*, pp. 1–5, Aug. 2013.

[14] C. R. Anderson and T. S. Rappaport, "In-building wideband partition loss measurements at 2.5 and 60 ghz", *IEEE Trans. on Wireless Communications*, vol. 3, no. 3, pp. 922–928, May 2004.

[15] M. Gapeyenko *et al.*, "Analysis of human-body blockage in urban millimeter-wave cellular communications", *IEEE International Conference on Communications (ICC)*, pp. 1–7, May 2016.

[16] J. G. Andrews *et al.*, "What will 5G be?", *IEEE Journal on Selected Areas in Communications*, vol. 32, no. 6, pp. 1065–1082, Jun. 2014.

[17] T. L. Marzetta, "Massive MIMO: An introduction", *Bell Labs Technical Journal*, vol. 20, pp. 11–22, Mar. 2015.

[18] F. Rusek *et al.*, "Scaling up MIMO: Opportunities and challenges with very large arrays", *IEEE Signal Processing Magazine*, vol. 30, no. 1, pp. 40–60, 2013.

[19] L. Sanguinetti *et al.*, "Optimal linear precoding in multi-user MIMO systems: A large system analysis", *in IEEE Global Communications Conference (GLOBECOM)*, pp. 3922–3927, Dec. 2014.

[20] N. Shariati *et al.*, "Low-complexity channel estimation in large-scale MIMO using polynomial expansion", *in 24th IEEE International Symposium on Personal, Indoor, and Mobile Radio Communications (PIMRC)*, pp. 1157–1162, Sep. 2013.

[21] A. Alkhateeb *et al.*, "Channel estimation and hybrid precoding for millimeter wave cellular systems", *IEEE Journal of Selected Topics in Signal Processing*, vol. 8, no. 5, pp. 831–846, 2014.

[22] Q. H. Spencer, A. L. Swindlehurst, and M. Haardt, "Zero-forcing methods for downlink spatial multiplexing in multiuser MIMO channels", *IEEE Trans. on Signal Processing*, vol. 52, no. 2, pp. 461–471, Feb. 2004.

[23] R. W. Heath, N. Gonzalez-Prelcic, S. Rangan, W. Roh, and A. M. Sayeed, "An overview of signal processing techniques for millimeter wave MIMO systems", *IEEE Journal of Selected Topics in Signal Processing*, vol. 10, no. 3, pp. 436–453, Feb. 2016.

[24] J. Wang et al., "Beam codebook based beamforming protocol for multi-Gbps millimeter-wave WPAN systems", *IEEE Journal on Selected Areas in Communications*, vol. 27, no. 8, Sep. 2009.

[25] V. Venkateswaran and A. van der Veen, "Analog beamforming in MIMO communications with phase shift networks and online channel estimation", *IEEE Trans. on Signal Processing*, vol. 58, no. 8, pp. 4131–4143, Apr. 2010.

[26] X. Zhang et al., "Variable-phase-shift-based RF-baseband codesign for MIMO antenna selection", *IEEE Trans. on Signal Processing*, vol. 53, no. 11, pp. 4091–4103, Oct. 2005.

[27] O. El Ayach et al., "Spatially sparse precoding in millimeter wave MIMO systems", *IEEE Trans. on Wireless Communications*, vol. 13, no. 3, pp. 1499–1513, Mar. 2014.

[28] R. Mendez-Rial *et al.*, "Hybrid MIMO architectures for millimeter wave communications: Phase shifters or switches?", *IEEE Access*, vol. 4, pp. 247–267, Jan. 2016.

[29] X. Gao *et al.*, "Energy-efficient hybrid analog and digital precoding for mmwave MIMO systems with large antenna arrays", *IEEE Journal on Selected Areas in Communications*, vol. 34, no. 4, pp. 998–1009, Apr. 2016.

[30] X. Yu *et al.*, "Alternating minimization algorithms for hybrid precoding in millimeter wave MIMO systems", *IEEE Journal of Selected Topics in Signal Processing*, vol. 10, no. 3, pp. 485–500, Apr. 2016.

[31] S. He *et al.*, "Energy-efficient transceiver design for hybrid sub-array architecture MIMO systems", *IEEE Access*, vol. 4, pp. 9895–9905, 2016.

[32] G. Fettweis, "Hetnet wireless fronthaul: The challenge missed", *in IEEE Communications Theory Workshop*, 2014.

[33] K. J. Kim *et al.*, "Guest editorial spatial modulation in emerging wireless systems", *IEEE Journal on Selected Areas in Communications*, vol. 37, no. 9, pp. 1945–1948, Aug. 2019.

[34] R. Mesleh et al., "Spatial modulation", *IEEE Trans. on Vehicular Technology*, vol. 57, no. 4, pp. 2228–2241, 2008.

[35] R. Zhang, L. Yang, and L. Hanzo, "Generalised pre-coding aided spatial modulation", *IEEE Trans. on Wireless Communications*, vol. 12, no. 11, pp. 5434–5443, Nov. 2013.

[36] M. D. Renzo, "Spatial modulation for generalized MIMO: Challenges, opportunities and implementation", *Proceedings of the IEEE*, vol. 102, no. 1, pp. 56–103, Jan. 2014.

[37] Y. Cui, X. Fang, and L. Yan, "Hybrid spatial modulation beamforming for mmwave railway communication systems", *IEEE Trans. on Vehicular Technology*, vol. 65, no. 12, pp. 9597–9606, Dec. 2016.

[38] M. Yüzgeçcioğlu and E. Jorswieck, "Hybrid beamforming with spatial modulation in multi-user massive MIMO mmwave networks", *in 28th IEEE International Symposium on Personal, Indoor, and Mobile Radio Communications (PIMRC)*, pp. 1–6, Oct. 2017.

[39] M. R. Akdeniz *et al.*, "Millimeter wave channel modeling and cellular capacity evaluation", *IEEE Journal on Selected Areas in Communications*, vol. 32, no. 6, pp. 1164–1179, Jun. 2014.

[40] N. S. Perovic *et al.*, "Receive spatial modulation for los mmwave communications based on TX beamforming", *IEEE Communications Letters*, Dec. 2016.

[41] A. Raafat, A. Agustin, and J. Vidal, "Receive spatial modulation for massive MIMO systems", *in IEEE Global Communications Conference (GLOBECOM)*, pp. 1–6, Dec. 2017.

[42] A. Raafat, A. Agustin, and J. Vidal, "Receive antenna selection and hybrid precoding for receive spatial modulation in massive MIMO systems", *in the 22nd International ITG Workshop on Smart Antennas (WSA)*, pp. 1–8, Mar. 2018.

[43] L.-L. Yang, "Transmitter preprocessing aided spatial modulation for multiple-input multiple-output systems", *in 73rd IEEE Vehicular Technology Conference (VTC Spring)*, pp. 1–5, May 2011.

[44] A. Raafat, A. Agustin, and J. Vidal, "Wideband receive spatial modulation with time domain pre-equalizer for large MIMO systems", *in IEEE Globecom Workshops (GC Wkshps)*, pp. 1–7, 2018-12.

[45] H. Sampath, H. Bolcskei, and A. J. Paulraj, "Pre-equalization for MIMO wireless channels with delay spread", *in 52nd IEEE Vehicular Technology Conference (VTC)*, vol. 3, pp. 1175–1178, Sep. 2000.

[46] A. Raafat *et al.*, "Energy efficient transmit-receive spatial modulation for uplink-downlink large-scale MIMO systems", *in the proceedings of IEEE Global Communications Conference (GLOBECOM)*, pp. 1–6, Dec. 2018.

[47] A. Raafat *et al.*, "Energy efficient transmit-receive hybrid spatial modulation for large-scale MIMO systems", *Accepted, IEEE Trans. on Communications*,

[48] A. Raafat, A. Agustin, and J. Vidal, "Downlink multi-user massive MIMO transmission using receive spatial modulation", *Under Review in IEEE Trans. on Wireless Communications*,

[49] G. H. Golub and C. Reinsch, "Singular value decomposition and least squares solutions", in *Linear Algebra*, Springer, 1971, pp. 134–151.

[50] W. Gander, "Algorithms for the QR decomposition", *Res. Rep*, vol. 80, no. 02, pp. 1251–1268, 1980.

[51] H. L. Van Trees, *Optimum Array Processing, Detection, Estimation, and Modulation Theory*. John Wiley & Sons, 2004.

[52] H. Zhang *et al.*, "A 1-v heterogeneous reconfigurable DSP IC for wireless baseband digital signal processing", *IEEE Journal of Solid-State Circuits*, vol. 35, no. 11, pp. 1697–1704, 2000.

[53] B. Sklar and F. J. Harris, *Digital communications: fundamentals and applications*. Prentice-hall Englewood Cliffs, NJ, 1988, vol. 2001.

[54] R. E. Blahut, *Principles and practice of information theory*. Addison-Wesley Longman Publishing Co., Inc., 1987.

[55] S. Boyd and L. Vandenberghe, *Convex optimization*. Cambridge university press, 2004.

[56] M. Grant and S. Boyd, "Cvx: Matlab software for disciplined convex programming", Sep. 2012.

[57] L. He, J. Wang, and J. Song, "On generalized spatial modulation aided millimeter wave MIMO: Spectral efficiency analysis and hybrid precoder design", *IEEE Trans. on Wireless Communications*, vol. 16, no. 11, pp. 7658–7671, Nov. 2017.

[58] L. He, J. Wang, and J. Song, "Spatial modulation for more spatial multiplexing: Rf-chain-limited generalized spatial modulation aided MM-Wave MIMO with hybrid precoding", *IEEE Trans. on Communications*, vol. 66, no. 3, pp. 986–998, Mar. 2018.

[59] A. Duarte and R. Sampaio-Neto, "Precoding and spatial modulation in the downlink of MU-MIMO systems", *ArXiv Preprint ArXiv:1803.01895*, 2018.

[60] A. Stavridis *et al.*, "Performance analysis of multistream receive spatial modulation in the MIMO broadcast channel", *IEEE Trans. on Wireless Communications*, vol. 15, no. 3, pp. 1808–1820, Mar. 2016.

[61] S. Rami, W. Tuni, and W. R. Eisenstadt, "Millimeter wave MOSFET amplitude detector", *Topical Meeting on Silicon Monolithic Integrated Circuits in RF Systems (SiRF)*, pp. 84–87, Jan. 2010.

[62] A. Serhan, E. Lauga-Larroze, and J. Fournier, "Common-base/common-gate millimeter-wave power detectors", *IEEE Trans. on Microwave Theory and Techniques*, vol. 63, no. 12, pp. 4483–4491, 2015.

[63] S. Shakib *et al.*, "A highly efficient and linear power amplifier for 28-GHz 5G phased array radios in 28-nm CMOS", *IEEE Journal of Solid-State Circuit*, vol. 51, no. 12, pp. 3020–3036, Dec. 2016.

[64] J. Lagos *et al.*, "A single-channel, 600-MS/s, 12-b, ringamp-based pipelined ADC in 28-nm cmos", *IEEE Journal of Solid-State Circuits*, vol. 54, no. 2, pp. 403–416, Feb. 2018.

[65] N. Rostomyan, M. Özen, and P. Asbeck, "28 GHz doherty power amplifier in CMOS soi with 28% back-off pae", *IEEE Microwave and Wireless Components Letters*, vol. 28, no. 5, pp. 446–448, May 2018.

[66] C. Wang *et al.*, "On the performance of the MIMO zero-forcing receiver in the presence of channel estimation error", *IEEE Trans. on Wireless Communications*, vol. 6, no. 3, pp. 805–810, Mar. 2007.

[67] O. El Ayach *et al.*, "Low complexity precoding for large millimeter wave MIMO systems", *in IEEE International Conference on Communications (ICC)*, pp. 3724–3729, Jun. 2012.

[68] T. S. Rappaport and e. al. et, "Wideband millimeter-wave propagation measurements and channel models for future wireless communication system design", *IEEE Trans. on Communications*, vol. 63, no. 9, pp. 3029–3056, Sep. 2015.

[69] V. Raghavan *et al.*, "Millimeter wave channel measurements and implications for PHY layer design", *IEEE Trans. on Antennas and Propagation*, vol. 65, no. 12, pp. 6521–6533, Dec. 2017.

[70] N. S. Alagha and P. Kabal, "Generalized raised-cosine filters", *IEEE Trans. on Communications*, vol. 47, no. 7, pp. 989–997, Jul. 1999.

[71] J. Mo and R. W. Heath, "Capacity analysis of one-bit quantized MIMO systems with transmitter channel state information", *IEEE Trans. on Signal Processing*, vol. 63, no. 20, pp. 5498–5512, Oct. 2015.

[72] A. Younis *et al.* ., "Generalised spatial modulation", *44rd Asilomar Conference on Signals, Systems and Computers*, pp. 1498–1502, Nov. 2010.

[73] F. Sohrabi and W. Yu, "Hybrid digital and analog beamforming design for large-scale antenna arrays", *IEEE Journal of Selected Topics in Signal Processing*, vol. 10, no. 3, pp. 501–513, Apr. 2016.

[74] Y. Wu *et al.*, "Receive antenna selection in the downlink of multiuser MIMO systems", *62nd Vehicular Technology Conference*, vol. 1, pp. 477–481, Sep. 2005.

[75] M. Biguesh and A. B. Gershman, "Training-based MIMO channel estimation: A study of estimator tradeoffs and optimal training signals", *IEEE Trans. on Signal Processing*, vol. 54, no. 3, pp. 884–893, Mar. 2006.

[76] L. Dai, S. Sfar, and K. B. Letaief, "Receive antenna selection for MIMO systems in correlated channels", *IEEE International Conference on Communications*, vol. 5, pp. 2944–2948, Jun. 2004.

[77] M. K. Simon, *Probability distributions involving Gaussian random variables: A handbook for engineers and scientists*. Springer, May 2007.

[78] D. Barry *et al.*, "Analytical approximations for real values of theLambert W-function", *Mathematics and Computers in Simulation*, vol. 53, no. 1, pp. 95–103, Aug. 2000.

[79] J. W. Craig, "A new, simple and exact result for calculating the probability of error for two-dimensional signal constellations", *IEEE Military Communications Conference*, pp. 571–575, Nov. 1991.

[80] C. Walck, *Handbook on statistical distributions for experimentalists*. University of Stockholm Internal Report, 2007.

[81] B. Vrigneau *et al.*, "Extension of the MIMO precoder based on the minimum Euclidean distance: A cross-form matrix", *IEEE Journal of Selected Topics in Signal Processing*, vol. 2, no. 2, pp. 135–146, Apr. 2008.

[82] M. Joham, W. Utschick, and J. A. Nossek, "Linear transmit processing in MIMO communications systems", *IEEE Trans. on Signal Processing*, vol. 53, no. 8, pp. 2700–2712, Aug. 2005.

[83] D. J. Tylavsky and G. R. Sohie, "Generalization of the matrix inversion lemma", *Proceedings of the IEEE*, vol. 74, no. 7, pp. 1050–1052, Jul. 1986.

[84] F. Chapeau-Blondeau, "Noise-enhanced capacity via stochastic resonance in an asymmetric binary channel", *Physical Review E*, vol. 55, no. 2, p. 2016, Feb. 1997.

[85] T. M. Cover and J. A. Thomas, *Elements of information theory*. John Wiley & Sons, 2012.

[86] P. E. McIllree, "Channel capacity calculations for M-ary N-dimensional signal sets", PhD thesis, University of South Australia, Feb. 1995.

[87] A. Wiesel, Y. C. Eldar, and S. Shamai, "Zero-forcing precoding and generalized inverses", *IEEE Trans. on Signal Processing*, vol. 56, no. 9, pp. 4409–4418, Sep. 2008.

[88] M. Gharavi-Alkhansari and A. B. Gershman, "Fast antenna subset selection in MIMO systems", *IEEE transactions on signal processing*, vol. 52, no. 2, pp. 339–347, Feb. 2004.

[89] A. Dua, K. Medepalli, and A. J. Paulraj, "Receive antenna selection in MIMO systems using convex optimization", *IEEE Trans. on Wireless Communications*, vol. 5, no. 9, pp. 2353–2357, Sep. 2006.

[90] L. Liang, W. Xu, and X. Dong, "Low-complexity hybrid precoding in massive multiuser MIMO systems", *IEEE Wireless Communications Letters*, vol. 3, no. 6, pp. 653–656, Dec. 2014.

[91] S. Schaible and T. Ibaraki, "Fractional programming", *European Journal of Operational Research*, vol. 12, no. 4, pp. 325–338, Apr. 1983.

[92] Y. Almogy and O. Levin, "A class of fractional programming problems", *Operations Research*, vol. 19, no. 1, pp. 57–67, Feb. 1971.

[93] S. Park, A. Alkhateeb, and R. W. Heath, "Dynamic subarrays for hybrid precoding in wideband mmwave MIMO systems", *IEEE Transactions on Wireless Communications*, vol. 16, no. 5, pp. 2907–2920, May 2017.

[94] G. D. Forney and G. Ungerboeck, "Modulation and coding for linear Gaussian channels", *IEEE Trans. on Information Theory*, vol. 44, no. 6, pp. 2384–2415, Oct. 1998.

[95] Y. Corre and Y. Lostanlen, "Three-dimensional urban EM wave propagation model for radio network planning and optimization over large areas", *IEEE Trans. on Vehicular Technology*, vol. 58, no. 7, pp. 3112–3123, Sep. 2009.

[96] A. Raafat, A. Agustin, and J. Vidal, "MMSE precoding for receive spatial modulation in large MIMO systems", *in IEEE International Workshop on Signal Processing Advances in Wireless Communications (SPAWC)*, pp. 1–5, Jun. 2018.

[97] M. F. Huber *et al.*, "On entropy approximation for Gaussian mixture random vectors", *in IEEE International Conference on Multisensor Fusion and Integration for Intelligent Systems*, pp. 181–188, Aug. 2008.

[98] B. Goebel *et al.*, "Calculation of mutual information for partially coherent Gaussian channels with applications to fiber optics", *IEEE Trans. on Information Theory*, vol. 57, no. 9, pp. 5720–5736, Sep. 2011.

[99] L. He *et al.*, "On the multi-user multi-cell massive spatial modulation uplink: How many antennas for each user?", *IEEE Trans. on Wireless Communications*, vol. 16, no. 3, pp. 1437–1451, Dec. 2016.

[100] G. Scutari, F. Facchinei, and L. Lampariello, "Parallel and distributed methods for constrained nonconvex optimization—Part I:Theory", *IEEE Trans. on Signal Processing*, vol. 65, no. 8, pp. 1929–1944, Apr. 2016.

[101] G. Scutari *et al.*, "Decomposition by partial linearization: Parallel optimization of multi-agent systems", *IEEE Trans. on Signal Processing*, vol. 62, no. 3, pp. 641–656, Feb. 2013.

[102] P. B. Stark and R. L. Parker, "Bounded-variable least-squares: An algorithm and applications", *Computational Statistics*, vol. 10, pp. 129–129, 1995.

[103] N. Jindal *et al.*, "Sum power iterative water-filling for multi-antenna Gaussian broadcast channels", *in the 36th Asilomar Conference on Signals, Systems and Computers.*, vol. 2, pp. 1518–1522, Nov. 2002.

[104] S. Gecgel *et al.*, "Antenna selection on spatial modulation: A machine learning approach", *in 27th Signal Processing and Communications Applications Conference (SIU)*, pp. 1–4, Apr. 2019.

[105] M. S. Ibrahim *et al.*, "Learning-based antenna selection for multicasting", *in IEEE 19th International Workshop on Signal Processing Advances in Wireless Communications (SPAWC)*, pp. 1–5, Jun. 2018.

[106] E. Basar, "Reconfigurable intelligent surface-based index modulation: A new beyond MIMO paradigm for 6G", *IEEE Trans. on Communications*, Feb. 2020.

[107] Y. J. Cho *et al.*, "Rf lens-embedded antenna array for mmwave MIMO: Design and performance", *IEEE Communications Magazine*, vol. 56, no. 7, pp. 42–48, Jul. 2018.